Tampere University

LAURA KOIVUSALO

# Biomaterial Scaffolds for Corneal Regeneration

## Combining human stem cells and biomaterials for tissue engineering of the corneal epithelium and stroma

Tampere University Dissertations 289

Tampere University Dissertations 289

LAURA KOIVUSALO

# Biomaterial Scaffolds for Corneal Regeneration

*Combining human stem cells and biomaterials for tissue engineering of the corneal epithelium and stroma*

ACADEMIC DISSERTATION
To be presented, with the permission of
the Faculty of Medicine and Health Technology
of Tampere University,
for public discussion in the auditorium F114
of the Arvo-building, Arvo Ylpön katu 34, Tampere,
on 4 September 2020, at 12 o'clock.

ACADEMIC DISSERTATION
Tampere University, Faculty of Medicine and Health Technology
Finland

| | | |
|---|---|---|
| *Responsible supervisor or/and Custos* | Prof Heli Skottman, PhD<br>Tampere University<br>Finland | |
| *Supervisor* | Tanja Ilmarinen, PhD<br>Tampere University<br>Finland | |
| *Pre-examiners* | Prof Neil Lagali, PhD<br>Linköping University<br>Sweden | Asst Prof Mark Ahearne, PhD<br>Trinity College Dublin<br>Ireland |
| *Opponent* | Prof Che Connon, PhD<br>Newcastle University<br>United Kingdom | |

The originality of this thesis has been checked using the Turnitin OriginalityCheck service.



Cover design: Roihu Inc.

ISBN 978-952-03-1646-4 (print)
ISBN 978-952-03-1647-1 (pdf)
ISSN 2489-9860 (print)
ISSN 2490-0028 (pdf)
http://urn.fi/URN:ISBN:978-952-03-1647-1

PunaMusta Oy – Yliopistopaino
Vantaa 2020

"It looked insanely complicated, and this was one of the reasons why the snug plastic cover -- had the words DON'T PANIC printed on it in large friendly letters."

Douglas Adams: *The Hitchhiker's Guide to the Galaxy*

# ACKNOWLEDGEMENTS

This dissertation research was carried out in the Eye Group, currently of Tampere University Faculty of Medicine and Life Science, during the years 2015-2020. Universities, faculties and laboratories have changed along the way, but the Eye Group remains. Although the road here has been winding, but the goal has largely stayed the same throughout the years. Without all those little "side projects" I wouldn't have learned all the things I have, nor built my professional identity. One such side project, currently known as StemSight, will hopefully evolve further in the future, a new journey which I am excited to take.

For funding my dissertation research, I would like to thank Business Finland (Human Spare Parts Project), the Doctoral Programme in Medicine and Life Sciences at Tampere University and the Academy of Finland (Healthy Cornea Project), and all the foundations that have supported my research and travels over the years: Intrumentarium Science Foundation, Alfred Kordelin Foundation, Emil Aaltonen Foundation, the Finnish Foundation for Technology Promotion, The Finnish Concordia Fund and the Foundation Supporting Research in Tampere. I am also grateful to the European COST Action BM1302: Joining Forces in Corneal Regeneration Research, for the travel grants and an excellent summer school.

A huge thanks to my supervisors Professor Heli Skottman and Docent Tanja Ilmarinen, who trusted in me to take on this project in the first place and since then have pretty much given me the freedom to choose my own path. Heli, you are a true visionary (pun intended), and I have been proud to work with you. Thank you for your constant support and trust. Tanja, you are simply amazing. You always find time for a quick pep talk, although you're constantly juggling at least two different manuscripts and managing ten different projects in the lab.

My thesis committee members, Professor Hannu Uusitalo, Professor Minna Kellomäki and Associate Professor Susanna Miettinen, thank you for the discussions during our annual meetings, for your thoughts and insights. I also want to thank the pre-examiners of my thesis, Professor Neil Lagali and Assistant Professor Mark Ahearne, for your kind feedback and valuable comments. Of course, none of the results of this dissertation would be possible without teamwork. So, thank you to all my co-authors, who contributed to its realization: Jennika Karvinen, Eetu Sorsa, Ilari

Jönkkäri, Jari Väliaho, Pasi Kallio, Sumanta Samanta, Vijay Parihar, Oommen Oommen, Lothar Koch, Andrea Deiwick and Boris Chichkov. Thank you also to the staff at Regea Tissue Bank, especially Minna Sjöblom, for offering the discarded human donor corneas for this research. Also, I big thanks to Paijan Tilateurastamo in Urjala for keeping us in a steady supply of pig corneas for the *ex vivo* work.

I want to thank the old BioMediTech people for all the fun we've had during the pre-Christmas parties, seminars and cruises. Our academic environment needs precisely this interdisciplinary crosstalk for creation of new ideas. My colleagues on the 4th floor in Neuro Group, Heart Group and Mese Group, thank you for the crayfish parties and the coffee room conversations, and exchanging ideas in the corridors.

To all the past and present members of the Eye Group, thank you for bearing with me all my engineer-talk, the wild visions and the academic arts-and-crafts. A huge thank you to the pair behind all our work, our beloved lab technicians Outi Melin and Hanna Pekkanen. My fellow PhD students Taina Viheriälä, Meri Vattulainen, Maija Kauppila and Pyry Grönroos, keep the spirits high in the "juniors' office". Maija, it's up to you to take the mantle of the crazy biomaterials engineer, carry it with pride. Special thanks to Anni Mörö and Meri for all the hard work and meaningful conversations during the creation of StemSight, in the process you have become more friends than colleagues.

Lastly, my sincerest thanks to my "pigeon pals", my family and my husband Eero. All of you have always supported me, patiently listened to my ranting and provided great distractions when I have needed it. Eero, words cannot describe my gratitude and my love for you. You are the wind in my sails that pushes me forwards.

Kangasala, 14 July 2020

Laura

# ABSTRACT

Cornea is the transparent tissue in the front of the eye essential for our vision. Its normal function requires a constant turnover of new epithelial cells to maintain a healthy ocular surface. Limbal stem cell deficiency (LSCD) is a severe type of corneal blindness where the normal healing capacity of the corneal epithelium is destroyed, for example due to burns or chemical trauma. This painful and debilitating condition cannot be treated with conventional transplantation of donor corneal tissue but requires the introduction of new therapeutic cells to regain the function of the cornea. In addition to the corneal epithelium, the underlying stromal layer is often also affected in LSCD, and the simultaneous delivery of regenerative cells for both corneal layers would be beneficial for treatment of these patients.

Human pluripotent stem cells (hPSCs) have the capacity to differentiate with high efficacy to limbal epithelial stem cells (LESCs), that could provide the therapeutic cells to restore the function of the corneal epithelium. To regenerate the corneal stromal layer, human adipose stem cells (hASCs) provide an attractive cell source because of their immunomodulatory and antiangiogenic properties, relative abundance and ease of isolation, and their capacity to differentiate towards corneal keratocytes. However, for realizing their full therapeutic potential, clinically relevant biomaterial scaffolds are needed for the delivery of these two stem cell types to the cornea.

This dissertation explored the production of hydrogel-based scaffolds for hASCs and hPSC-LESCs in a corneal tissue-mimicking organization and studied their applicability for implantation to corneal wounds in an *ex vivo* cornea organ culture model. First, hyaluronic acid-based hydrogels were evaluated as suitable cell-encapsulation materials for hASCs. With further modification of the hyaluronic acid with dopamine moieties, tissue adhesive hydrogel implants with encapsulated hASCs and a layer of hPSC-LESCs on the surface were successfully fabricated. Lastly, laser-assisted 3D bioprinting with clinically relevant hydrogel bioinks was used to create

corneal structures accurately mimicking the properties of both the stroma and the epithelium.

In conclusion, this dissertation describes innovative methods to produce functional tissue-engineered structures for the regeneration of both the epithelium and stromal layers of the cornea. With the aim of treating patients with stem cell-based therapies in the future, the clinical applicability of both the raw materials and the ready-made structures were considered throughout this work.

# TIIVISTELMÄ

Sarveiskalvo on silmän etuosan läpinäkyvä kudos, joka on ensisijaisen tärkeä näkökyvyllemme. Terveen silmän pinnan toiminta perustuu epiteelisolujen jatkuvaan uusiutumiseen. Limbaalinen kantasolupuutos (engl. limbal stem cell deficiency, LSCD) on vakava sarveiskalvosokeuden muoto, jossa silmän pinnan epiteelisolukon uusiutumiskyky on menetetty, esimerkiksi palo- tai kemikaalivammojen seurauksena. Kivuliasta ja toimintakykyä heikentävää LSCD:tä ei voida hoitaa perinteisillä, kuolleilta luovuttajalta saatavilla sarveiskalvosiirteillä, vaan sen hoito vaatii uusien kudosta uusivien solujen tuomisen sarveiskalvolle. Epiteelisolujen lisäksi LSCD vaurioittaa usein myös syvempää sarveiskalvon stroomakerrosta. Tästä syystä uusien solujen siirtäminen samanaikaisesti molempien solukerrosten parantamiseksi mahdollistaisi näiden potilaiden paremman hoidon.

Ihmisen erittäin monikykyisistä kantasoluista (eng. human pluripotent stem cells, hPSC) saadaan erilaistettua tehokkaasti limbaalisia epiteelin kantasoluja (eng. limbal epithelial stem cells, LESC), jotka toimivat sarveiskalvon epiteeliä uusivina soluina. Sarveiskalvon strooman hoitoon sopivista soluista ihmisen rasvan kantasolut (engl. human adipose stem cells, hASC) ovat yksi houkuttelevimmista vaihtoehdoista. Rasvan kantasoluilla on kyky muokata kehon immuunireaktioita sekä estää verisuonten uudismuodostumista, niiden saatavuus on hyvä ja eristäminen suhteellisen vaivatonta, minkä lisäksi ne pystyvät erilaistumaan sarveiskalvon strooman keratosyyteiksi. Näiden kantasolujen lääkinnällistä käyttöä varten tarvitaan kuitenkin kliiniseen käyttöön soveltuvia biomateriaaleja ja niistä tehtyjä uudenlaisia tukirakenteita molempien solutyyppien samanaikaiseen siirtämiseen sarveiskalvolle.

Tämän väitöskirjan tavoitteena oli tuottaa hydrogeelipohjaisia tukirakenteita sekä hASC- että hPSC-LESC-soluille matkien sarveiskalvon solujen järjestäytymistä ja tutkia niiden käytännön soveltuvuutta siirteiksi sarveiskalvon kudosviljelymallissa. Väitöskirjan ensimmäisessä osatyössä tutkittiin hyaluronihappopohjaisten hydrogeelien soveltuvuutta hASC-solujen viljelyyn ja siirtoon. Seuraavassa osatyössä hyaluronihappomateriaaliin lisättiin dopamiiniryhmiä, joiden avulla saatiin valmistettua kudokseen tarttuvia geelirakenteita ja pystyttiin kasvattamaan hASC-

soluja sisältävän geelin pinnalle myös hPSC-LESC-solukerros. Kolmannessa osatyössä hASC ja hPSC-LESC -soluista tuotettiin sarveiskalvon stroomaa ja epiteeliä ominaisuuksiltaan muistuttavia rakenteita laseravusteisen 3D biotulostuksen avulla käyttäen kliinisiin käyttötarkoituksiin soveltuvia hydrogeeliraaka-aineita biomusteena.

Kaiken kaikkiaan tässä väitöskirjassa on kuvattu uudenlaisia menetelmiä toiminnallisten kudosteknologisten sarveiskalvosiirteiden valmistukseen epiteeli- ja stroomakerrosten korjaamiseksi. Jotta kantasolupohjaisia hoitomuotoja saataisiin tulevaisuudessa potilaskäyttöön, työssä on kiinnitetty erityistä huomiota sekä lähtömateriaalien että tuotettujen rakenteiden kliiniseen soveltuvuuteen.

# CONTENTS

# ABBREVIATIONS

| | |
|---|---|
| 2D | Two-dimensional |
| 3D | Three-dimensional |
| ABCB5 | ATP-binding cassette, sub family B, member 5 |
| ABCG2 | ATP-binding cassette, sub family G, member 2 |
| ALDH3A1 | Aldehyde dehydrogenase family 3, member A1 |
| ALK | Anterior lamellar keratoplasty |
| αSMA | Alpha smooth muscle actin |
| bFGF | Basic fibroblast growth factor |
| BM40 | Basement membrane protein 40 |
| BM-MSC | Bone marrow-derived mesenchymal stem cells |
| BMP4 | Bone morphogenetic protein 4 |
| C/EBPδ | CCAAT-enhancer binding protein delta |
| CD44 | Cluster of differentiation 44 |
| CEC | Corneal epithelial cell |
| CiRA | Center for iPS Cell Research and Application |
| CLAU | Conjunctival limbal autograft |
| CLET | Cultivated limbal epithelium transplantation |
| Col I | Collagen type I |
| Col IV | Collagen type IV |
| COMET | Cultivated oral mucosal epithelium transplantation |
| CK3 | Cytokeratin 3 |
| CK12 | Cytokeratin 12 |
| CK15 | Cytokeratin 15 |
| CSSC | Corneal stromal stem cell |
| CT | Computed tomography |
| DAPI | 4',6-diamidino-2-phenylindole |
| DMEK | Descemet's membrane endothelial keratoplasty |
| DMEM | Dulbecco's modified Eagle's medium |
| DMEM/F-12 | Dulbecco's modified Eagle's medium/Ham's nutrient mixture F-12 |

| | |
|---|---|
| DPBS | Dulbecco's phosphate buffered saline |
| DS% | Degree of substitution |
| DTNB | 5,5-dithiobis(2-nitrobenzoic acid), Ellman's reagent |
| EB | Embryoid body |
| ECM | Extracellular matrix |
| EDC | 1-[3-(Dimethylamino)propyl]-3-ethylcarbodiimide |
| EV | Extracellular vesicle |
| FDA | Food and Drug Administration |
| FGF | Fibroblast growth factor |
| FRESH | Freeform reversible embedding of suspended hydrogels |
| FTIR | Fourier transform infrared |
| GAPDH | Glyceraldehyde 3-phosphate dehydrogenase |
| GelMA | Methacrylated gelatin |
| GMP | Good manufacturing practice |
| HA | Hyaluronic acid, or hyaluronan |
| HA-ADH | Adipic acid dihydrazide-modified hyaluronic acid |
| HA-Ald | Aldehyde-modified hyaluronic acid |
| HA-CDH | Carbodihydrazide-modified hyaluronic acid |
| HA-DA-CDH | Carbodihydrazide-modified hyaluronic acid with dopamine units |
| hAM | Human amniotic membrane |
| hASC | Human adipose stem cell |
| HE | Haematoxylin and eosin |
| hESC | Human embryonic stem cell |
| hiPSC | Human induced pluripotent stem cell |
| HLA | Human leukocyte antigen |
| ICAM1 | Intercellular adhesion molecule 1 |
| KERA | Keratocan |
| KLAL | Keratolimbal allograft |
| KPro | Keratoprosthetics device |
| LaBP | Laser-assisted bioprinting |
| LESC | Limbal epithelial stem cell |
| LIFT | Laser-induced forward transfer |
| Ln-521 | Laminin-521, human recombinant |
| LUM | Lumican |
| LSCD | Limbal stem cell deficiency |

| | |
|---|---|
| MET | Mesenchymal-to-epithelial transition |
| MSC | Mesenchymal stem cell |
| NHS | N-hydroxysuccinimide |
| NMR | Nuclear magnetic resonance |
| PA | Peptide amphiphile |
| PFA | Paraformaldehyde |
| PK | Penetrating keratoplasty |
| PLGA | Poly-lactide-*co*-glycolide |
| PMMA | Poly(methyl methacrylate) |
| PNIPAAm | Poly(N-isopropylacrylamide) |
| PSC | Pluripotent stem cell |
| qPCR | Quantitative polymerase chain reaction |
| RAFT | Real architecture for 3D tissue |
| RHAMM | Receptor for hyaluronic acid-mediated motility |
| RM | Residual mass |
| ROCK | Rho-associated protein kinase |
| SEAM | Self-formed ectodermal multizone |
| SLET | Simple limbal epithelial transplantation |
| SPARC | Secreted protein, acidic and rich in cysteine |
| SR | Swelling ratio |
| TAC | Transient amplifying cell |
| TNBS | 2,4,6-Trinitrobenzenesulfonic acid |
| UV | Ultraviolet |
| VWF | von Willebrand factor |

# ORIGINAL PUBLICATIONS

This dissertation is based on the following original peer-reviewed publications, referred to as **Study I-III** in the text. The original publications are reproduced at the end of this thesis with permission of the copyright holders.

I **Koivusalo L***, Karvinen J*, Sorsa E, Jönkkäri I, Väliaho J, Kallio P, Ilmarinen T, Miettinen S, Skottman H, Kellomäki M. Hydrazone-crosslinked hyaluronan-based hydrogels for therapeutic delivery of adipose stem cells to treat corneal defects. *Materials Science and Engineering C,* 2018, 85:68-78.**

II **Koivusalo L**, Kauppila M, Samanta S, Parihar VS, Ilmarinen T, Miettinen S, Oommen OP*, Skottman H*. Tissue adhesive hyaluronic acid hydrogels for sutureless stem cell delivery and regeneration of corneal epithelium and stroma. *Biomaterials*, 2019, 225:119156

III Sorkio A, Koch L, **Koivusalo L**, Deiwick A, Miettinen S, Chichkov B*, Skottman H*. Human stem cell based corneal tissue mimicking structures using laser-assisted bioprinting and functional bioinks. *Biomaterials*, 2018, 171:57-71.

* Authors contributed equally

** Publication was included in the doctoral dissertation "Hydrazone Crosslinked Polysaccharide-based Hydrogels for Soft Tissue Engineering" by Jennika Karvinen at the Faculty of Biomedical Sciences and Engineering, Tampere University of Technology, Finland, in November 2018.

# AUTHOR'S CONTRIBUTION

| | |
|---|---|
| I | The study was designed by L. Koivusalo and J. Karvinen. L. Koivusalo designed, performed and analyzed all cell culture experiments and the *ex vivo* proof-of-concept studies. The manuscript was written together by the shared first authors L. Koivusalo and J. Karvinen. |
| II | L. Koivusalo designed the study with the help of O.P. Oommen. L. Koivusalo designed and performed the cell culture and *ex vivo* proof-of-concept studies, and the hydrogel swelling and degradation studies. L. Koivusalo wrote the manuscript as first author. |
| III | L. Koivusalo designed and performed the *ex vivo* proof-of-concept studies and participated in producing figures and critical data analysis. L. Koivusalo co-wrote the manuscript with A. Sorkio and H. Skottman and was responsible for the revisions of the manuscript, including all additional work and writing of the final manuscript. |

# 1 INTRODUCTION

Cornea is the transparent front of the eye, essential for transmittance and refraction of incoming light to the light-sensing retina. The cornea is composed of three cellular layers: epithelium, stroma and endothelium. The stratified corneal epithelium is constantly shed and replenished by new epithelial cells produced by tissue resident stem cells of the cornea called limbal epithelial stem cells (LESCs). If the limbal stem cell niche is destroyed, the normal regenerative function of the corneal epithelium is disrupted, and opaque conjunctival tissue can breach the broken limbal barrier and grow over the cornea (Deng et al., 2019). This severe type of corneal blindness is termed limbal stem cell deficiency (LSCD). LSCD is typically caused by burns and chemical injuries, that do not merely affect the epithelium, but cause also scarring of the underlying corneal stroma (Deng et al., 2019; Dua et al., 2000). As LSCD cannot be treated using conventional transplanted corneal tissue, cell therapies are needed to restore vision in these patients.

Cell therapies for restoring the LESC function to the cornea have previously relied on using isolated primary cells, either from the contralateral healthy eye, a living related donor, or from cadaveric corneas (Fernandez-Buenaga et al., 2018). However, these isolated cells are only available in small quantities and have a limited capacity for self-renewal. Using directed differentiation of human pluripotent stem cells (hPSCs), it is possible to obtain vast amounts of LESCs with clinically appropriate production methods (Hongisto et al., 2017; Mikhailova et al., 2014). As therapeutic cells for corneal stromal regeneration, human adipose stem cells (hASCs) have shown great potential due to their abundant availability, immunomodulatory and anti-angiogenic properties, as well as their capacity to differentiate towards corneal stromal keratocytes both *in vitro* and *in vivo* (Arnalich-Montiel et al., 2008; Du et al., 2010).

In addition to the cellular component, restoration of corneal function also requires suitable biomaterial scaffolds for the transplantation of these cells to the eye. These scaffolds should be non-immunogenic, support the growth of cells both inside and on top of the materials, be transparent and have adequate mechanical properties to allow transplantation (Ahearne et al., 2020; Brunette et al., 2017). For

full regeneration, the biomaterial should degrade after transplantation, allowing the transplanted cells to remodel their surroundings and integrate to the cornea. Finally, the clinical applicability of the biomaterial scaffold should be considered, taking into account the origin of biological raw materials, and suitable transplantation techniques of the final cell-laden scaffold (Brunette et al., 2017).

The aim of this dissertation was to develop suitable biomaterial scaffolds for the transplantation of hASCs to the corneal stroma and the hPSC-derived LESCs for corneal epithelial regeneration and study their transplantation strategies and biological function in a corneal *ex vivo* model using excised porcine corneas.

# 2 LITERATURE REVIEW

## 2.1 The human cornea

The cornea is the transparent front of the eye (Figure 1), which acts as a protective barrier against pathogens and small mechanical damage and is our window to the surrounding world. The cornea and its overlying mucinous tear film also provide two thirds of the refractive power of the eye (DelMonte & Kim, 2011; Meek & Knupp, 2015). This uniquely transparent tissue is comprised of three cellular layers; epithelium, stroma and endothelium, separated by two acellular layers at their interfaces; Bowman's layer and Descemet's membrane. Although the cornea lacks blood vessels, it is one of the most innervated tissues of the body (DelMonte & Kim, 2011). Nutrients to the cornea are supplied by the small vessels on the edges of the cornea, through the anterior chamber and by the tear film. (DelMonte & Kim, 2011)

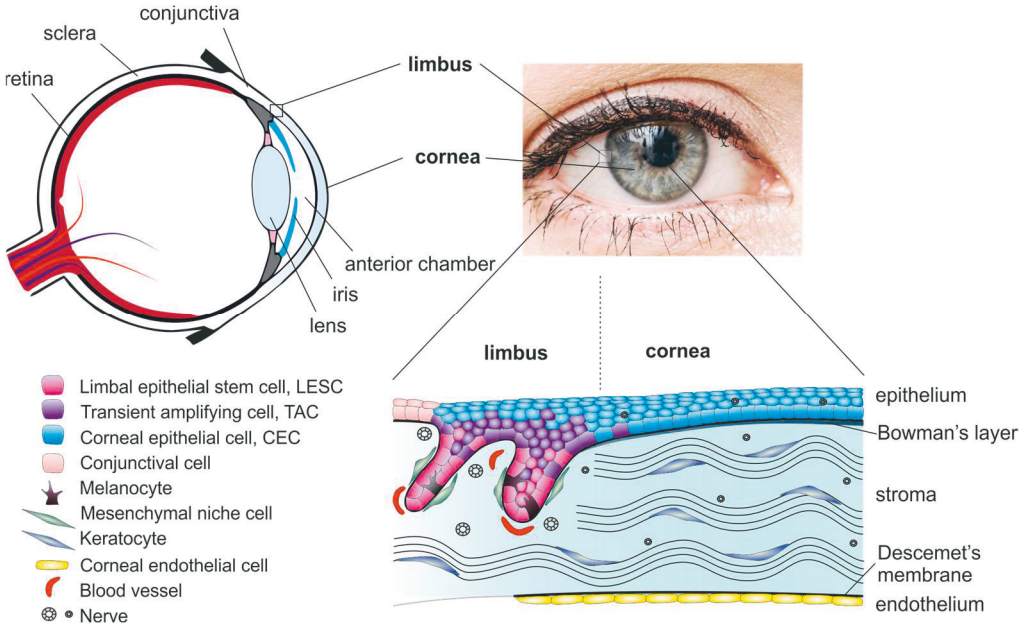


**Figure 1.** Structures of the human eye, cornea and limbus.

The stratified corneal epithelium renews constantly, through shedding of dead cells from the surface and replenishing the epithelium through cell division and migration (Richardson et al., 2016). This renewal capacity is maintained by the tissue resident stem cells of the corneal epithelium, the limbal epithelial stem cells (LESCs), which reside in the periphery of the cornea, in a an area known as the limbus (DelMonte & Kim, 2011; Di Girolamo, 2015; Li et al., 2017; Richardson et al., 2016). The LESCs in the limbus produce migratory daughter cells with a limited potential for cell division, known as transient amplifying cells (TACs) (West et al., 2015). It has been estimated that only 2.5–3% of cells in the limbal epithelium are true slow-cycling LESCs (de Paiva et al., 2005).

The stroma constitutes the bulk of the cornea, making up 80–90% of its thickness (DelMonte & Kim, 2011; Meek & Knupp, 2015). It comprises a densely packed extracellular matrix (ECM) of collagens and proteoglycans, with sparsely distributed quiescent cells called keratocytes. The collagen in the stroma is highly organized in very specific patterns, constituting to both the transparency and mechanical strength of the cornea (Meek & Knupp, 2015; Petsche et al., 2012). In case of injury to the stroma, the normally quiescent keratocytes activate into a migratory and proliferative fibroblast phenotype to repair small wounds (Fini, 1999). At the wound site, these cells are transformed further to alpha smooth muscle actin (αSMA)-expressing myofibroblasts, that contract to close the wound (Fini, 1999). This wound healing response can induce the production of fibrous scar tissue, which leads to the disruption of the regular arrangement of the stroma and a loss of transparency.

The endothelium is a uniform monolayer of hexagonal cells, which actively pump water out of the stroma to maintain its transparency (DelMonte & Kim, 2011). Corneal endothelial cells are non-mitotic *in vivo*, and their density has been shown to decrease with age (Bourne et al., 1997; Hollingsworth et al., 2001). Despite being an integral part of a healthy cornea, the endothelium was left out of the scope of this dissertation.

### 2.1.1 The limbal niche

In the human cornea, the limbus constitutes a physical barrier between the transparent corneal epithelium and the opaque conjunctiva. It also provides a protective microenvironment, a "niche", to the LESCs. The limbal stem cell niche consists of palisades of Vogt, which are upward stromal protrusions, and their complementary epithelial counterparts called the limbal crypts (Shortt et al., 2007a;

Yazdanpanah et al., 2017). Usually, the limbal crypts are mostly concentrated in the superior and inferior limbus, where they are protected by the eye lids, but their size and location varies considerably between individuals (Grieve et al., 2015; Shortt et al., 2007a). The specific environment within these crypts consists of a fenestrated basement membrane with a signature distribution of ECM proteins, allowing a complex interplay between different cell types on both sides. In addition to the LESCs, the limbal niche also houses melanocytes to protect the LESCs from ultraviolet (UV) light, mesenchymal cells for supporting LESCs, and immune cells, blood vessels and nerves (Yazdanpanah et al., 2017). The mesenchymal niche cells, which are located on the stromal side of the basement membrane, have also shown stem cell properties, giving rise to the term corneal stromal stem cells (CSSCs) (Funderburgh et al., 2016; Pinnamaneni & Funderburgh, 2012). The LESCs themselves have been identified morphologically based on their small size and high nucleus to cytoplasm ratio, capability to retain labelled DNA precursors due to slow cell cycling, as well as a panel of protein markers (Dziasko & Daniels, 2016; Schlötzer-Schrehardt & Kruse, 2005). Especially the transcription factor p63, and its specific isoform ΔNp63α, have been shown to be of clinical relevance for determining the success of transplanted LESCs (Rama et al., 2010). Some of the most commonly used markers for identifying LESCs are listed in Table 1.

**Table 1.** Putative stem cell markers commonly used to identify limbal epithelial stem cells.

| Marker | Biological function | Selected references |
|---|---|---|
| **ΔNp63α** | transcription factor, specific isoform of p63 | (Di Iorio et al., 2005; Kawasaki et al., 2006) |
| **C/EBPδ** | transcription factor | (Barbaro et al., 2007) |
| **BMI-1** | transcription factor | (Barbaro et al., 2007) |
| **ABCG2** | membrane transporter | (Budak et al., 2005; de Paiva et al., 2005) |
| **ABCB5** | membrane transporter | (Ksander et al., 2014) |
| **CK15** | cytokeratin | (Hayashi et al., 2007) |
| **CK14** | cytokeratin | (Figueira et al., 2007) |
| **CK19** | cytokeratin | (Chen et al., 2004; Schlötzer-Schrehardt & Kruse, 2005) |
| **N-cadherin** | cell adhesion molecule | (Hayashi et al., 2007) |
| **integrin α9** | cell adhesion molecule | (Chen et al., 2004; Stepp et al., 1995) |

Abbreviations: ABCB5: ATP-binding cassette sub family B member 5; ABCG2: ATP-binding cassette sub family G member 2; C/EBPδ: CCAAT-enhancer binding protein δ; CK: cytokeratin

The components of the limbal basement membrane are important regulators of stem cell proliferation, migration and differentiation (Schlötzer-Schrehardt et al., 2007). The protein composition of the limbal basement membrane differs from the corneal basement membrane especially in laminin subchains and the α chain of collagen type IV (Fukuda et al., 1999; Mei et al., 2012; Schlötzer-Schrehardt et al., 2007). Unique ECM components found only in the limbal basement membrane include laminin α1 and γ3, BM40/SPARC (basement membrane protein 40 or secreted protein acidic and rich in cysteine), and the glycoproteins tenascin-C and vitronectin (Mei et al., 2012; Schlötzer-Schrehardt et al., 2007). Fibronectin is also more highly expressed in the limbal basement membrane than the central cornea or the conjunctiva (Schlötzer-Schrehardt et al., 2007). Both fibronectin and tenascin-C have been found to be upregulated during wound healing also in other parts of the cornea (Mei et al., 2012).

In addition to the unique molecular composition, the limbal niche has a distinct mechanical microenvironment (Eberwein & Reinhard, 2015). The limbal niche has a lower elastic modulus than the central cornea, and this stiffness gradient from the softer limbus to the stiffer central cornea has been shown to drive the differentiation and migration of corneal epithelial cells (Foster et al., 2014; Gouveia et al., 2019b; Jones et al., 2012). Moreover, the cellular stiffness of LESCs themselves has been shown to be lower compared their more differentiated progeny (Bongiorno et al., 2016).

### 2.1.2 Corneal transparency and biomechanics

What makes corneal tissue exceptional, is its combination of transparency and high mechanical strength. Corneal transparency arises from the specific molecular arrangement of the densely packed ECM of the stroma, as well as the transparent corneal cells themselves. The highly organized stromal ECM is rich in collagen, predominantly of type I, with smaller amounts of types III, V, VI and XII (Meek & Boote, 2009). Collagen type I molecules are triple helices, which assemble in a staggered manner to form microfibrils and further into uniformly sized collagen fibrils (Meek & Knupp, 2015). These regularly spaced collagen fibrils are then bundled into approximately 2 μm thick and 200 μm wide lamellae (Meek & Knupp, 2015). This hierarchical assembly of collagen in the stroma is illustrated in Figure 2. Adjacent lamellae are preferentially aligned orthogonally to each other in the central cornea, with a more isotropic arrangement closer to the periphery (Abahussin et al.,

2009; Meek & Knupp, 2015). Moreover, the organization of the lamellae changes throughout the thickness of the cornea, resulting in differing mechanical strength across its depth (Abahussin et al., 2009; Petsche et al., 2012). The lamellar arrangement of the stroma is crucial in maintaining the curved shape of the cornea, whereas the regular fibril arrangement is responsible for its transparency (Meek & Knupp, 2015).

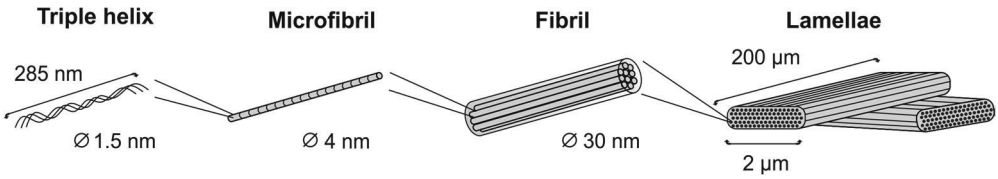


**Figure 2.** Collagen type I hierarchy and organization in the corneal stroma, as described in (Meek & Knupp, 2015).

Proteoglycans between the collagen fibrils regulate matrix assembly and interfibrillar spacing. Proteoglycans contain a protein core decorated with highly sulphated glycosaminoglycans, which bind large amounts of water due to their high negative charge. Specific proteoglycans of the cornea are keratan sulphate-containing lumican, keratocan and mimecan, and dermatan sulphate-containing decorin (Massoudi et al., 2016; Meek & Boote, 2009). Due to their high affinity to water, the interfibrillar proteoglycans can also drive corneal swelling if the pumping action of the endothelium is compromised. Upon swelling, the interfibrillar spacing increases, resulting in increased light scattering and loss of corneal transparency (Meek & Knupp, 2015; Meek et al., 2003).

Uniform refractive index of the cells in the cornea is also crucial for corneal transparency (Meek & Knupp, 2015). Keratocytes in the stroma have a very compact cell body to minimize light scattering and their cytoplasms are packed with crystalline proteins, such as aldehyde dehydrogenases and transketolases (Hassell & Birk, 2010; Jester et al., 1999). The expression of these crystalline proteins has been found to decrease upon injury to the corneal stroma, and is also associated with scar formation (Jester et al., 1999).

The structure of the stroma gives rise to the unique biomechanics of corneal tissue. The cornea is constantly subjected to intraocular pressure, and the precise organization of collagen lamellae within the stroma exists to carry this mechanical load (Abahussin et al., 2009; Dupps & Wilson, 2006). The aligned collagen lamellae can withstand large deformations in the direction of the fibres, whereas the interweaving of collagen bundles can transfer tensile loads between neighbouring

lamellae, contributing to the resilience of the stroma (Dupps & Wilson, 2006; Meek & Boote, 2009). With 78% of stromal weight consisting of water, the cornea can be considered as a complex anisotropic composite, where the collagen lamellae and proteoglycans exist in a matrix of water molecules (Dupps & Wilson, 2006).

## 2.2 Corneal blindness

Corneal opacities are a major cause of blindness worldwide and constitute a great socioeconomic burden, as they primarily affect people at a younger age (Mathews et al., 2018). Global estimates of the number of people suffering from blindness or visual impairment due to corneal opacities range from 4.5 to 5.7 million individuals (Flaxman et al., 2017; Pascolini & Mariotti, 2012). While these numbers mostly reflect the total loss of visual acuity, opacities affecting only one eye are often underreported in these surveys. These unilateral cases of corneal blindness, typically due to ocular trauma or corneal ulceration, are estimated to constitute to 1.52 million new cases every year (Whitcher et al., 2001). Corneal blindness is most common in developing countries, where the infectious disease trachoma causes significant amount of corneal vision loss (Whitcher et al., 2001).

Forms of corneal blindness where the renewal capacity of the epithelium is compromised due to partial or complete loss of LESC function, are classified collectively as limbal stem cell deficiency (LSCD). LSCD is characterized by invasion of blood vessels and the surrounding conjunctiva to the cornea, and it causes ocular discomfort, persistent inflammation, pain and photophobia (Deng et al., 2019). There are a variety of causes for LSCD, ranging from traumatic (e.g. burns or chemical injuries), to acquired diseases (e.g. Stevens-Johnson syndrome or keratoconjunctivitis) and genetic conditions (e.g. aniridia) (Bobba et al., 2017; Vazirani et al., 2018). Also, prolonged contact lens wear has been shown to induce symptoms of LSCD (Bobba et al., 2017; Rossen et al., 2016). LSCD can affect one eye (unilateral) or both eyes (bilateral), and varies in severity (Deng et al., 2019). In the UK, chemical injury-related LSCD has been estimated to affect 148 patients yearly (Ghosh et al., 2019), whereas 240 new cases have been predicted based on the incidence of all LSCD causes (Shortt et al., 2011). In Australia and New Zealand, a one-year surveillance study estimated an incidence of 63 new cases of severe LSCD (Bobba et al., 2017). By extrapolating the estimates of Ghosh et al. (2019) and Bobba et al. (2017) to a population incidence based on statistics of the respective countries, these numbers roughly translate to an incidence of 0.23 per 100 000 people.

### 2.2.1 Corneal transplantation and artificial corneas

Most patients with corneal blindness are treated with cadaveric corneal transplants. Although corneal tissue represents the most common organ transplant worldwide, there is a constant global shortage of donor tissue, with only 1 in every 70 patients receiving a transplant (Gain et al., 2016). With the advancement in surgical techniques, full thickness corneal transplantation (penetrating keratoplasty, PK) can often be replaced by partial thickness corneal grafts aimed to replace only the damaged layers of the cornea. For example, anterior lamellar keratoplasty (ALK) can be performed to replace only the dysfunctional outermost part of the cornea, without disturbing the endothelium. Conversely, Descemet's membrane endothelial keratoplasty (DMEK) can be used to replace only the dysfunctional endothelium layer. These different types of corneal transplantations are illustrated in Figure 3.

Typically, corneal transplants are not immunophenotype matched as the cornea is considered immune-privileged because of its avascular nature (Panda et al., 2007). However, in LSCD this immune privilege is compromised due to the invasion of new blood vessels, which increases the risk of transplant rejection. This high risk of rejection and the low functionality of LESCs in cadaveric grafts make traditional corneal transplantation unsuitable for the treatment of LSCD (Kethiri et al., 2017; Vemuganti et al., 2004). Keratolimbal allografts (KLAL), a transplantation of corneal rims from freshly obtained donor tissue, are considered a possible option for LSCD patients, but a strict immunosuppression regimen is required to combat transplant rejection (Cheung & Holland, 2017; Eslani et al., 2017).

In severe cases of corneal blindness, where previous corneal transplants have failed, prosthetic artificial corneas can be considered as an alternative treatment. Two keratoprosthetics devices (KPros) have gained market approval by the American Food and Drug Administration (FDA); the Boston KPro and the AlphaCor (Lee et al., 2015). They are non-biodegradable synthetic implants designed to replace the optical element of the central cornea. The Boston KPro consists of a rigid poly(methyl methacrylate) (PMMA) optic core, a titanium or PMMA back plate and a rim of donor corneal tissue (Khan, 2015). The AlphaCor is a softer core-and-skirt type device, with a hydrated poly(2-hydroxyethyl methacrylate) (PHEMA) central optic and an opaque porous rim for the fixation of the implant (Myung et al., 2008). However, lack of integration to the host tissue and the risk of severe complications, such as extrusion of the device, anterior chamber inflammation or glaucoma have hindered the widespread use of artificial KPros (Aravena et al., 2018; Jiraskova et al., 2011; Lee et al., 2015).


**Figure 3.** Different types of corneal transplantations are used to replace either the whole cornea (penetrating keratoplasty, PK), the affected parts (anterior lamellar keratoplasty, ALK and Descemet's membrane endothelial keratoplasty, DMEK) or aim to restore the function of the cornea (keratolimbal allograft, KLAL and keratoprosthetics device, KPro).

### 2.2.2 Epithelial reconstruction for treating LSCD

In LSCD, the renewal capacity of the corneal epithelium is compromised. In minor epithelial defects, topical therapeutics such as lubricating eye drops, autologous serum eye drops, bandage contact lenses or patches of human amniotic membrane (hAM) can be sufficient to stabilize the corneal surface after ocular injuries (Dua et al., 2010; Shortt et al., 2011). The placenta-derived hAM has been widely used in ophthalmology, because of its anti-inflammatory and anti-angiogenic properties that can promote re-epithelialization of the corneal surface (Azuara-Blanco et al., 1999; Jirsova & Jones, 2017; Lee & Tseng, 1997). Moreover, hAM is still commonly used as a carrier material for many cell-based therapies for the corneal epithelial reconstruction (Fernandez-Buenaga et al., 2018). Despite its many advantages, the use of donated hAM requires careful donor screening to avoid disease transmission, and is subject to large biologic variation (Connon et al., 2010; Jirsova & Jones, 2017).

For the treatment of severe LSCD, different strategies have been developed for transplantation of new LESCs to the diseased eye. In unilateral LSCD, the preferred techniques utilize autologous limbal biopsies obtained from the contralateral healthy eye, such as conjunctival limbal autograft (CLAU), cultivated limbal epithelial transplantation (CLET) or simple limbal epithelial transplantation (SLET) (Fernandez-Buenaga et al., 2018). In CLAU, tissue segments typically representing 2–3 clock hours are taken from the upper and lower limbal areas of the healthy eye, containing also conjunctival epithelium (Cheung et al., 2017). Although recent evidence suggest CLAU to be safe to the healthy donor eye, worries about inducing LSCD to the healthy eye have driven popularity of surgical techniques requiring smaller biopsies (Cheung et al., 2017; Shanbhag et al., 2020). In CLET, cells from a small limbal biopsy are expanded in culture before being transplanted back to the patients affected eye. This technique, originally described by Pellegrini et al. (1997), was later commercialized and gained market approval in Europe as the first tissue

engineered product (Holoclar®; Chiesi Farmaceutici). In a 3-year follow-up, the efficacy of this method was shown to be 68% (Fasolo et al., 2017). More recently, SLET was developed as a simpler alternative for CLET, that does not require the heavy economic or logistic resources (Sangwan et al., 2012). In SLET, a 2 $mm^2$ limbal biopsy is minced and the fragments transplanted onto the affected eye on a piece of hAM. Overall, CLAU and SLET have shown comparable, or even better results than CLET (Basu et al., 2016; Jackson et al., 2019; Shanbhag et al., 2020). In bilateral LSCD, the limbal biopsy-based treatments can also utilize allogeneic tissues from either living related donors or fresh cadaveric corneas. In these cases, the use of immunosuppression medication is required, but the length of treatment can vary (Baylis et al., 2011). Arguably, the immunosuppression for cell-based therapies is not as heavy as when transplanting allogenic limbal tissue (such as KLAL), which contains highly antigenic immune cells and blood vessels (Holland et al., 2012). These different treatment options for LSCD are illustrated in Figure 4.

Other cell sources apart from corneal cells have also been suggested for replacing corneal epithelium in LSCD patients. For example, cultivated oral mucosal epithelium transplantation (COMET) can be used as an autologous alternative to patients with bilateral disease. By taking small biopsies from the oral cavity and culturing these cells on hAM at the air-liquid interface, they can generate a stratified epithelium resembling the corneal epithelium (Fernandez-Buenaga et al., 2018). Long-term success rates ranging from 53% after 3 years (Satake et al., 2011) to 70% after 4 years (Prabhasawat et al., 2016) have been reported for COMET. In addition to oral mucosal cells, other suggested autologous cell sources for replacing corneal epithelium in bilateral LSCD include conjunctival epithelium (Ricardo et al., 2013), dental pulp stem cells (Gomes et al., 2010), nasal mucosa (Chun et al., 2011), hair follicle stem cells (Meyer-Blazejewska et al., 2011), epidermal stem cells (Yang et al., 2008), and mesenchymal stem cells (MSCs) (Calonge et al., 2019; Holan & Javorkova, 2013; Reinshagen et al., 2011).

An interesting cell-free alternative for treatment of LSCD has been recently proposed, where the already clinically approved collagenase enzyme can be topically applied to locally soften the surface of the cornea, and to promote endogenous regeneration of the corneal epithelium (Gouveia et al., 2019a). This simple and low-cost treatment showed promise in a rabbit alkaline burn model in reducing corneal haze and suppressing inflammation and neovascularization (Gouveia et al., 2019a). This investigational therapy has recently entered into a first-in-human clinical trial in India (TrialSite News, 2019).

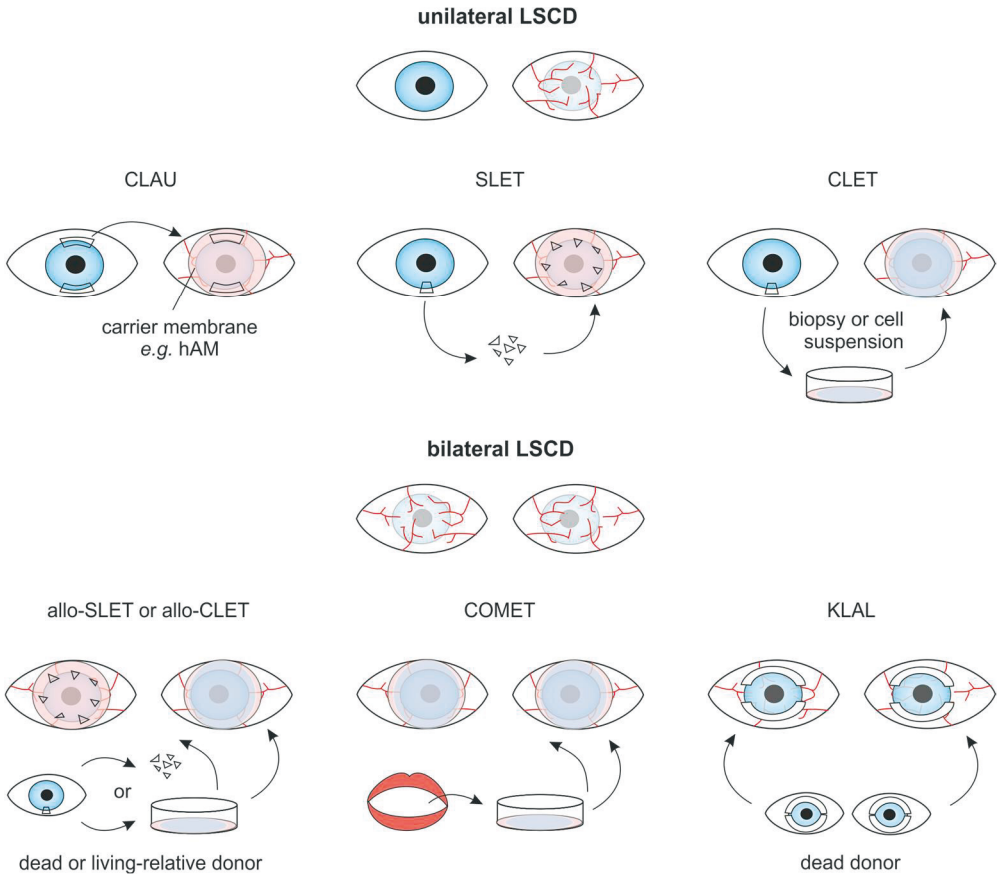


**Figure 4.** Treatment options for unilateral and bilateral LSCD. In unilateral cases, pieces of limbal tissue are taken from the contralateral healthy eye, whereas in bilateral cases an allogeneic donor is needed. Alternatively, autologous oral mucosal epithelium can be used to replace corneal epithelium. CLAU: conjunctival limbal autograft, CLET: cultivated limbal epithelial transplantation, COMET: cultivated oral mucosal epithelium transplantation, hAM: human amniotic membrane, KLAL: keratolimbal allograft, LSCD: limbal stem cell deficiency, SLET: simple limbal epithelial transplantation.

### 2.2.3 Strategies for stromal reconstruction and replacement

To fully restore vision in patients with LSCD, both the regenerative capacity of the epithelium and the transparency of the underlying stroma need to be re-established. Current treatments for LSCD aim to first stabilize the ocular surface using transplantation or reactivation of LESC, after which the scarred stroma is then replaced by corneal transplantation (Baradaran-Rafii et al., 2010; Behaegel et al., 2019; Zakaria et al., 2014). In addition to the inconvenience of a second surgery, the

time between the operations might be long, and the operation still requires suitable corneal donor tissue. The lack of donor corneal tissue has been the main driver for the development of stromal replacements.

In contrast to the cell-based approaches to epithelium regeneration, the approaches for corneal stromal regeneration are mainly aimed at replacing the bulk of the cornea with suitable replacement materials (Matthyssen et al., 2018). Decellularized stromal tissue has been suggested as an alternative for corneal transplantation, with some promising results (Hashimoto et al., 2016; Shafiq et al., 2011). To solve the shortage of corneal donor tissue, mainly decellularized porcine corneas have been suggested, but the use of animal tissue for clinical use still raises concerns with the regulatory authorities regarding traceable manufacturing, consistent quality and possible immune responses (Brunette et al., 2017; Lagali, 2020). *In vitro* approaches for producing corneal stromal equivalents have also been reported, where corneal keratocytes were induced to secrete their own organized ECM in long-term cultures (Gouveia et al., 2017a; Guo et al., 2007).

Biomaterial-based strategies for corneal stromal reconstruction utilize both cell-seeded and acellular methods. Biomaterial implants without cells allow greater freedom in their production methods, for example in using different crosslinking strategies and toxic reagents. These types of implants rely on the recruitment of cells from the corneal stroma for successful integration and regeneration (Ahearne et al., 2020; Griffith et al., 2009). Conversely, stromal regeneration strategies including therapeutic cells within the biomaterial scaffold can provide faster regeneration of the tissue by replacing the lost keratocytes of the slowly regenerating stroma and produce a therapeutic effect through secretion of cytokines and other factors. The different types of biomaterials used as scaffolds for corneal regeneration are described in more detail in Chapter 2.4.

Many different types of cells have been suggested as therapeutic cells for corneal stromal regeneration. Primary human corneal keratocytes isolated from donor corneas have only limited capacity for proliferation *in vitro*, and tend to adopt the activated fibroblast phenotype in culture (Wilson et al., 2012a). Instead, multipotent stem cells of the corneal stroma (CSSCs), have shown better capacity for proliferation and producing native-like stromal ECM (Du et al., 2005; Wu et al., 2014a). The application of CSSCs to the surface of the eye has also been shown to reduce corneal scarring (Basu et al., 2014). Also, MSCs from other sources have shown capacity for producing keratocyte-like cells (Dos Santos et al., 2019).

## 2.3 Stem cells as a treatment modality for the cornea

The eye has historically been at the forefront of stem cell-based therapies, possibly due to the simplicity of visual monitoring of the treatment site *in vivo*. Preclinical studies in animal models are abundant, while some therapies have already advanced to clinical trials. Some of the recent and ongoing clinical trials using stem cells for treating corneal diseases are listed in Table 2.

**Table 2.** Examples of ongoing and recent clinical trials using stem cells for corneal applications.

| Cells | Autologous/ allogeneic | Transplantation vehicle | Indication | Status in July 2020 | Reference/ sponsor |
|---|---|---|---|---|---|
| BM-MSC | Allogeneic | hAM | LSCD | Completed | (Calonge et al., 2019) |
| LESC | Autologous and allogeneic | hAM | LSCD | Ongoing | (Behaegel et al., 2019; Zakaria et al., 2014) |
| LESC | Autologous | Fibrin membrane | LSCD | Phase III Ongoing | (Rama et al., 2010), Chiesi Farmaceutici SpA |
| LESC | Autologous | hAM | LSCD | Recruiting | Massachusetts Eye and Ear Infirmary |
| LESC (ABCB5+) | Allogeneic | Topical suspension | LSCD | Recruiting | RHEACELL GmbH |
| iPSC-CEC | Allogeneic | Cell sheet | LSCD | Ongoing | (Osaka University, 2019) |
| CF + LESC | Allogeneic | Fibrin-agarose | Corneal ulcers | Recruiting | (González-Andrades et al., 2017) |
| LESC + CSSC | Allogeneic | Suspension in fibrin | Corneal scars | Recruiting | (Basu et al., 2014), LV Prasad Eye Institute |
| ASC | Autologous | Injection or decellularized stroma | Keratoconus | Unknown | (Alió del Barrio et al., 2017), Vissum, Instituto Oftalmológico de Alicante |
| ASC | Allogeneic | Injection | Dry Eye | Recruiting | Rigshospitalet, Denmark |
| LESC | Allogeneic | Eye drops | Dry Eye | Recruiting | Rush Eye Associates |

Abbreviations: ASC: adipose stem cells, ABCB5: ATP-binding cassette sub family B member 5, BM-MSC: bone marrow mesenchymal stem cells, CF: corneal fibroblasts, CSSC: corneal stromal stem cells, hAM: human amniotic membrane, iPSC-CEC: induced pluripotent stem cell derived corneal epithelial cells, LESC: limbal epithelial stem cells

Tissue resident stem cells of the cornea, namely LESCs and CSSCs, can be used to treat corneal opacities of the epithelium and the stroma, respectively. However, drawbacks of using isolated primary cells include their limited availability and the variability between donors, which can lead to inconsistent treatment outcomes (O'Callaghan & Daniels, 2011). Moreover, the culture methods used to expand these cells *in vitro* often utilize undefined and xenogeneic components such as serum and feeder cells (O'Callaghan & Daniels, 2011; Shortt et al., 2007b; Sidney et al., 2015). The challenges of using isolated stem cells has led to the investigation of other stem cell sources, such as human pluripotent stem cells (PSCs) or MSCs.

### 2.3.1 Human pluripotent stem cells

PSCs are defined by their capacity for self-renewal and differentiation to all the three different germ layers of an embryo; ectoderm, endoderm and mesoderm. There are two types of PSCs, embryonic stem cells (ESCs) and induced pluripotent stem cells (iPSCs). ESCs are mainly derived from the inner cell mass of early-stage embryos, whereas iPSCs can be reprogrammed from adult somatic cells by inducing the expression of pluripotency genes. Since the discovery of *in vitro* culture methods for human ESCs (Thomson et al., 1998) and iPSCs (Takahashi et al., 2007), hPSCs have provided new means for studying human development, disease modelling, toxicology and cell therapy (Romito & Cobellis, 2016).

Human PSCs have been proposed as an unlimited source of cells for any type of human tissue. Over the years, knowledge of the differentiation methods for obtaining corneal cells from both ESCs and iPSCs has grown vastly, and the culture methods have evolved towards being GMP (good manufacturing practice) compliant and xenobiotic- and feeder cell free, making them more likely to reach clinical use. Although the discovery of iPSC technology has made it possible to use also these cells as autologous cell therapy, the cost of such treatments renders them economically impractical. Minimizing rejections in allogeneic cell therapy with hPSCs requires matching of the human leukocyte antigen (HLA) haplotype between patients and cell lines, and the establishment of clinical grade cell banks with HLA-homozygous cell lines (Wilmut et al., 2015). However, as the frequencies of HLA phenotypes vary between different ethnic groups, population-based cell banks might be needed to cover suitable portion of each population, requiring a coordinated global effort (Gourraud et al., 2012). Initiatives for establishing such HLA haplotype

banks are already underway, for example the Center for iPS Cell Research and Application (CiRA) in Japan (Azuma & Yamanaka, 2016).

Corneal epithelial and progenitor cell differentiation from hPSCs is based on supplying the cells with appropriate growth and differentiation cues from the culture substrate and the culture medium. By mimicking the conditions of the limbal niche, Ahmad et al. produced the first hPSC-derived corneal epithelial cells on collagen type IV (Col IV) coating using limbal fibroblast-conditioned culture medium (Ahmad et al., 2007). Since then, the differentiation methods have improved towards defined and xenobiotic-free culture conditions to improve the efficacy and reliability of corneal differentiation. Drawing inspiration from the early eye development, Mikhailova et al. described an efficient method to obtain corneal epithelial progenitor cells from hPSCs, using human Col IV as culture substrate and small-molecule inhibitors and activators to drive LESC differentiation (Mikhailova et al., 2014). With the implementation of feeder-free hPSC culture techniques, this method was later updated by Hongisto et al. and the ECM substrate was modified to include both human Col IV and human recombinant laminin-521 (Ln-521) (Hongisto et al., 2017). Another approach, also mimicking the development of the eye, for differentiating feeder-free hPSCs to corneal cells was described by Hayashi et al. and named SEAM (self-formed ectodermal autonomous multi-zone) (Hayashi et al., 2016). In the SEAM method, the culture consists of concentric areas of different ocular cells, from which the corneal epithelial cells can be purified by manual pipetting and cell sorting (Hayashi et al., 2016). However, the SEAM method is quite time-consuming, as the full differentiation process to corneal epithelial cells can take 12–16 weeks (Hayashi et al., 2017). Corneal epithelial cell sheets differentiated from allogeneic iPSCs with the SEAM method have recently entered into first-in-human clinical trials in Japan for treatment of bilateral LSCD (Osaka University, 2019).

Keratocyte differentiation using hPSCs has also been reported. Developmentally, keratocytes originate from the neural crest, having a slightly different origin from the surface ectoderm-derived epithelial cells. Thus, keratocyte differentiation from PSCs typically starts with the induction of neural crest cells, followed by 3D culture in cell clusters with fibroblast growth factor (FGF) and ascorbic acid (vitamin C) supplemented medium (Chan et al., 2013; Naylor et al., 2016). With the more readily available cell sources for producing keratocyte-like cells, their differentiation from hPSCs has not attracted considerable attention.

### 2.3.2 Human mesenchymal stem cells

MSCs are multipotent adult stem cells capable of differentiating into various mesenchymal tissues, such as bone, cartilage and adipose tissue. MSCs have been found in various tissues of the human body including bone marrow, adipose tissue and the umbilical cord. Also CSSCs can be classified as MSCs, as they have the potential to differentiate also into other mesenchymal cell types (Funderburgh et al., 2016). Overall, MSCs have been widely studied for applications in regenerative medicine, as they can be relatively easily isolated and display anti-inflammatory and immune-modulatory properties (Dos Santos et al., 2019; Zhang et al., 2015b). Although MSCs are generally known to induce angiogenesis, they have actually been shown to display anti-angiogenetic properties in corneal injuries (Oh et al., 2008).

MSCs have been claimed to differentiate towards both keratocyte and epithelial cells of the cornea (Sánchez-Abarca et al., 2015). As the corneal stroma also represents a mesenchymal tissue, it is not surprising that there is evidence of stromal regeneration using MSCs. *In vivo* animal experiments have shown evidence that human bone marrow derived MSCs (BM-MSCs) and umbilical cord MSCs can assume a keratocyte phenotype in the corneal stroma (Liu et al., 2010; Liu et al., 2012). Furthermore, a comparison of the *in vitro* differentiation capability of four different types of MSCs confirmed that all differentiated towards keratocytes, with CSSCs showing the highest potential (Dos Santos et al., 2019). Although the transdifferentiation of MSCs to corneal epithelial cells has been debated (Harkin et al., 2015), recent evidence suggests that MSCs are capable of undergoing mesenchymal-epithelial transition (MET) and subsequent corneal epithelial lineage commitment *in vitro* (Venugopal et al., 2019). Also, a recent randomized clinical study compared the efficacy of allogeneic BM-MSCs on hAM to allogeneic CLET in treating patients with severe LSCD (Calonge et al., 2019). The study demonstrated improvement of the corneal epithelium in both cases, although the particular mechanism for epithelial restoration (transdifferentiation or paracrine stimulation of remaining LESCs) was not determined (Calonge et al., 2019).

The paracrine effects of MSCs have shown beneficial effects on both epithelium and stromal wound healing. MSCs are known to secrete many anti-inflammatory and anti-angiogenic cytokines, especially in treatment of acute corneal injuries of the epithelium (Oh et al., 2008; Yao et al., 2012). Furthermore, MSC-conditioned medium has been shown to reduce the scar tissue formation of corneal keratocytes *in vitro* (Watson et al., 2010). More recently, the wound healing and anti-fibrotic

property of MSCs has been attributed to paracrine stimulation through secreted extracellular vesicles (EVs) (Samaeekia et al., 2018; Shojaati et al., 2019).

#### 2.3.2.1 Human adipose stem cells

Adipose tissue is an attractive source for MSCs, as human adipose stem cells (hASCs) can be isolated in larger quantities and with better patient compliance compared to BM-MSCs (Lindroos et al., 2011). Because adipose tissue is usually abundant and relatively expendable, autologous hASCs are often available for regenerative therapies. However, their immunomodulatory nature also allows allogeneic hASCs to be a clinically feasible therapeutic option. One such therapy is already on the market, under the trade name Alofisel® (Takeda) for treatment of patients with Crohn's disease (Jones, 2018). The immunomodulatory effects of hASCs has also promoted their use in treatment of immune reactions, such as severe graft-versus-host-disease (Jurado et al., 2017).

For corneal regeneration, hASCs have been applied mainly for regeneration of the stroma through tissue integration and differentiation towards corneal keratocytes (Harkin et al., 2015). Of all MSCs, hASCs have been shown to be second to only the precursor-like CSSCs in their ability to differentiate towards keratocytes (Dos Santos et al., 2019). The *in vitro* differentiation of hASCs towards keratocytes has been demonstrated by several research groups and the differentiation protocols are firmly established (Du et al., 2010; Lynch & Ahearne, 2017; Zhang et al., 2013). Additionally, undifferentiated hASCs have shown to adopt a keratocyte phenotype after implantation to the corneal stroma in animal models (Arnalich-Montiel et al., 2008; Espandar et al., 2012). In a clinical trial, autologous hASCs have been shown to produce new collagen in the corneal stroma of patients with keratoconus, a disease resulting from loosening of stromal collagen and subsequent deformations of the cornea (Alió del Barrio et al., 2017).

Like other types of MSCs, also hASCs have been studied for treatment of corneal epithelium in LSCD. When hASCs on hAM were transplanted into a rabbit LSCD model, they showed moderate suppression of neovascularization, and promotion of healthy corneal epithelium (Galindo et al., 2017). However, the authors explicitly attributed these effects to paracrine factors rather than MET (Galindo et al., 2017). The evidence for *in vivo* transdifferentiation of hASCs to corneal epithelial cells remains poor, but *in vitro* MET with small molecule induction has been demonstrated (Bandeira et al., 2020). In a rat LSCD model, only hASCs with prior *in vitro*

transdifferentiated were capable of reconstructing the corneal epithelium with its typical morphology and marker expression (Bandeira et al., 2020).

## 2.4 Biomaterials for corneal tissue engineering

Biomaterials can be broadly defined as any materials interacting with the body with the purpose of replacing or augmenting tissue function. Although biomaterials encompass a wide variety of hard and soft materials, specific requirements exist for materials for delivering living cells to the cornea. The optimal biomaterial should degrade in the body in a suitable timeframe, display sufficient mechanical toughness to withstand manipulation and implantation, and be transparent to allow unobstructed vision (Chen et al., 2018). The unique combination of transparency and high mechanical strength, which is typical for the cornea is very difficult to replicate by the means of tissue engineering (Matthyssen et al., 2018). To circumvent the challenges of manufacturing such biomaterial scaffolds, many research groups have suggested animal-derived decellularized stromal tissue as a corneal scaffold (Hashimoto et al., 2010; Yoeruek et al., 2012). However, these animal-derived biological scaffolds have a limited clinical translatability and are not considered within the scope of this dissertation.

In the field of corneal tissue engineering, most approaches to date have focused on replacing only one cell layer at a time, with epithelial applications being the most numerous (Chen et al., 2018). The main goal for these studies has been to find more standardisable and risk-free alternatives to the current gold standard transplantation material hAM (O'Callaghan & Daniels, 2011). While scaffolds for corneal epithelium replacements are mostly membranes or films supporting cell growth (i.e. two-dimensional (2D) surfaces), stromal cells require a more three-dimensional (3D) approach for creating relevant biological scaffolds. The underlying principles of manufacturing biomaterial scaffolds for corneal epithelium and stromal tissue engineering are illustrated in Figure 5. Rather than listing all the different biomaterials suggested for corneal applications, this chapter describes the different approaches for producing the various types of corneal scaffolds ranging from hydrogels and fibrous materials to the scaffold-free production methods. Examples are given of each scaffold type, while few materials considered the most relevant within the scope of this dissertation are discussed more thoroughly in the following chapters.

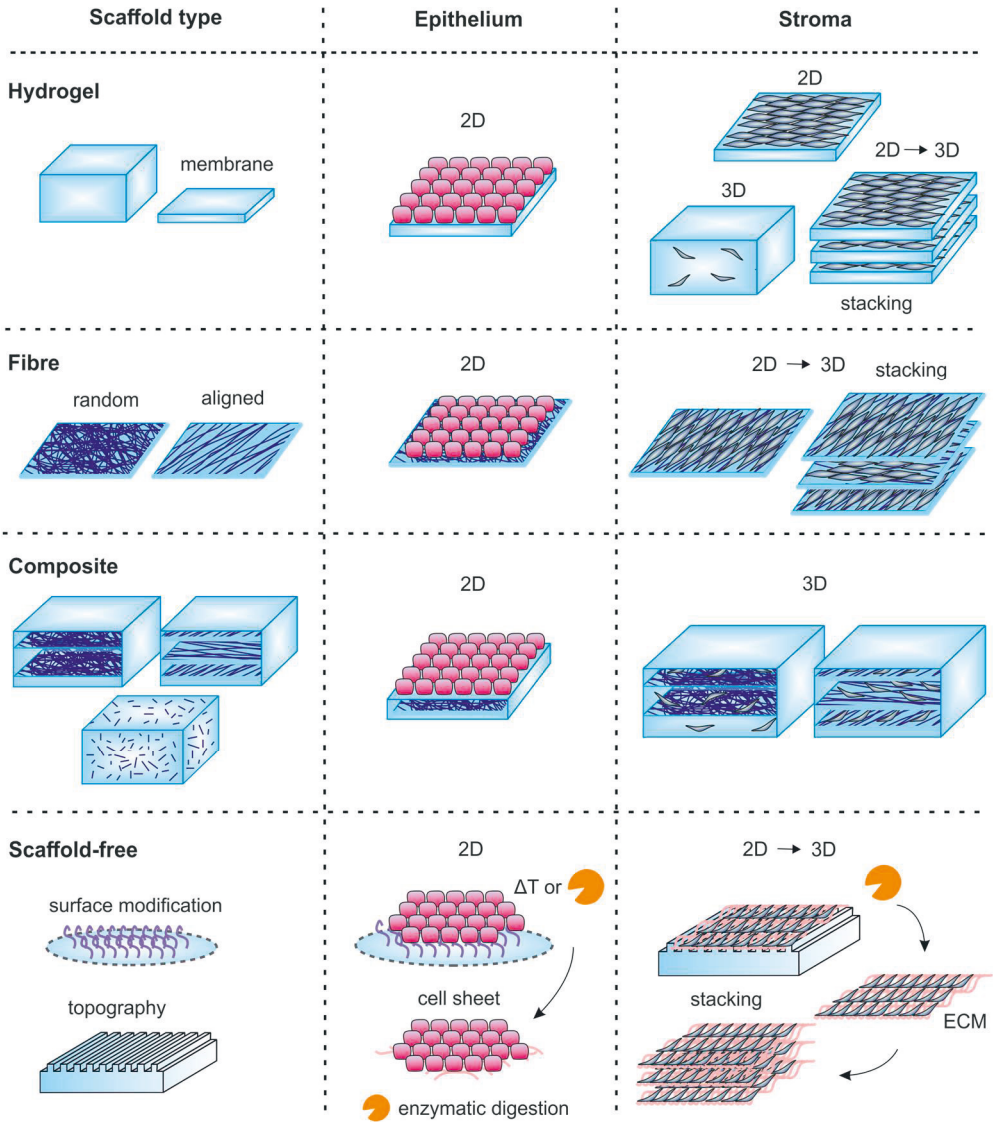


**Figure 5.** Different approaches and scaffold types used for corneal regeneration, and examples of their use for corneal epithelial and stromal tissue engineering. ΔT refers to temperature change.

### 2.4.1 Hydrogels

Hydrogels are crosslinked polymer networks capable of retaining large amounts of water. The crosslinks can be formed through either physical interactions or chemical

bonds. Physical crosslinking can be induced by changes in temperature, causing chain entanglement or hydrogen bonding, by introducing ionic crosslinking agents, or by hydrophobic self-assembly of polymer units (Baroli, 2007). Chemical crosslinking includes the formation of covalent bonds between polymer chains, either via crosslinker molecules or through chemical reactions between functional groups in the hydrogel components (Baroli, 2007). Chemical bonding can also be achieved through photopolymerization, i.e. irradiation with specific wavelengths of light.

In tissue engineering, hydrogels are used as cell culture matrices because they mimic the 3D environment in the body and allow efficient diffusion of nutrients and waste products. Typically, hydrogels have good optical properties, but lack the mechanical properties required in corneal tissue engineering (Oyen, 2014). For corneal applications, hydrogels have been utilized for encapsulation of stromal cells, as culture substrates for epithelial cells and manufacturing of *in vitro* corneal models.

When water is removed from a hydrogel, the result can either lead to the formation of a sponge (lyophilization), or the structure can collapse to form a membrane or a film (evaporation). Sponges can maintain their 3D shape, whereas membranes usually cannot recover their original dimensions after rehydration. For example, collagen and collagen-chondroitin sulphate sponges have been seeded with human primary corneal cells after lyophilization (Orwin & Hubel, 2000; Vrana et al., 2008) and collagen films produced by evaporation, termed vitrigels, have been used as transplantation substrates for human LESCs in a rabbit model (Chae et al., 2015). Due to the drying step, cells cannot be encapsulated in these scaffolds in the manufacturing phase but need to be seeded on their surface afterwards. Since membranes can only be used as 2D culture surfaces, they are used more for corneal epithelial regeneration. However, 3D stromal equivalents can be produced by stacking, for example, collagen or silk fibroin films seeded with corneal stromal cells (Crabb et al., 2006; Gosselin et al., 2018).

Hydrogel materials can either be prefabricated into their final form prior to corneal implantation, or they can be used as injectable, *in situ* -forming scaffolds. Injectable hydrogels are typically precursor solutions that can flow to fill the stromal defect before they are crosslinked, for example, via photopolymerization (Sani et al., 2019), or they can be two-component hydrogels with a suitable gelation time after mixing (Zarembinski et al., 2014). *In situ* -forming hydrogels have been used as cell-free materials to support endogenous stromal regeneration (Sani et al., 2019), and as cell delivery vehicles to the stroma (Lee et al., 2018; Zarembinski et al., 2014).

For successful cell growth, proliferation and maturation, the cells encapsulated inside hydrogels or grown on their surface need to attach to the biomaterial. Some materials, such as collagen and its hydrolysed form gelatin, are inherently conducive for cell attachment and remodelling, while others require some biological functionalization to support cell growth (Zhu & Marchant, 2011). This biological functionalization can be achieved by incorporation of full-length ECM proteins, such as collagen, laminin or fibronectin, or the short peptide sequences that act as binding motifs for the integrin receptors that facilitate cell attachment. Some well-known cell attachment peptides include the fibronectin-derived RGD (arginine-glycine-aspartic acid) sequence and the laminin-derived IKVAV (isoleucine-lysine-valine-alanine-valine) and YIGSR (tyrosine-isoleucine-glycine-serine-arginine) sequences. For example, surface functionalization with the RGD sequence has been used to improve the attachment of LESCs and corneal stromal cells on silk fibroin membranes (Jia et al., 2016; Wu et al., 2014b).

#### 2.4.1.1 Collagen

Collagen has been the most extensively studied scaffold material in corneal tissue engineering due to its role as the principal component in the corneal stroma. A variety of different collagens have been suggested for corneal tissue engineering, including collagen type I from rat, bovine, porcine or equine origin, and plant-based recombinant human collagens type I and III (Crabb et al., 2006; Koulikovska et al., 2015; Levis et al., 2010; Liu et al., 2008; Liu et al., 2009; Petsch et al., 2014). Isolated animal collagens are acid soluble can they typically form gels after neutralization and possible cell incorporation. To improve the mechanical properties of these gels, excess water can be removed from the structure during gelation using plastic compression or capillary fluid flow with a method termed RAFT (Real Architecture For 3D Tissue) (Levis et al., 2015). Removing excess water allows compaction of the collagen fibres to better resemble the dense collagenous ECM in the body. Other methods to mimic the compaction and alignment of collagen in the cornea have included the use of strong magnetic fields or vitrification (Builles et al., 2010; Calderón-Colón et al., 2012).

Improving mechanical properties of collagen hydrogels by increased crosslinking density has been widely explored. Typical crosslinking methods include chemical crosslinking, for example with the EDC/NHS (1-[3-(Dimethylamino)propyl]-3-ethylcarbodiimide and N-hydroxysuccinimide) system, or blending with other polymers to obtain interpenetrating networks (Islam et al., 2015; Koulikovska et al.,

2015; Rafat et al., 2008). However, as these methods can be harmful to cells, they are mostly used to produce only cell-free stromal replacements or films for the culture of corneal epithelial cells. The RAFT method has been the most successful method to produce corneal constructs with tissue-like organization of both stromal and epithelial cells in a suitably robust collagen hydrogel, and its mechanical properties have been further improved by gentle UV-crosslinking (Levis et al., 2015; Mi et al., 2011). Still, the method relies on the use of animal collagen, which can be potentially immunogenic, and poses possible risks of transmitted diseases (Levis et al., 2015; Lynn et al., 2004).

Gelatin, which can be obtained through denaturing and hydrolysis of animal collagen, is considered less immunogenic than its parent molecule, while being cheaper and easier to process (Rose et al., 2014). Without the tertiary structure of native collagen, hydrogel formation of gelatin occurs mainly through chain entanglement in low temperatures, making additional chemical crosslinking necessary for obtaining solid gelatin scaffold for corneal applications. The same chemical crosslinking systems can be used to crosslink collagen and gelatin, but direct chemical functionalization of gelatin is also common (Rose et al., 2014). For example, gelatin modified with methacrylate groups (GelMA) allows UV crosslinking of gelatin-based hydrogels, and the system has been used for keratocytes encapsulation of and their implantation to rabbit corneas *in vivo* (Bektas et al., 2019).

To avoid the use of animal-derived collagen, recombinant human collagens and synthetic collagen peptides have been proposed (Islam et al., 2016; Islam et al., 2015; Liu et al., 2008). Although cell-free recombinant collagen implants have shown excellent biocompatibility in clinical trials as stromal replacements, they degrade very slowly and only rely on recruitment of cells from the surrounding tissue (Fagerholm et al., 2010; Fagerholm et al., 2014). Short collagen-peptide analogues have shown similar cellular recruitment in a pig model with stable corneal regeneration after 1 year (Jangamreddy et al., 2018). However, recombinant collagen or collagen peptide analogues have not yet been used for cell delivery to the cornea, although their suitability as substrates for LESCs has been evaluated *in vitro* (Haagdorens et al., 2019).

#### 2.4.1.2 Fibrin

Fibrin is another protein-based biomaterial commonly used for culture and transplantation of corneal cells. Fibrin can be used either as a 2D membrane or 3D gel for cell encapsulation. Insoluble fibrin gel is formed in the blood clotting cascade

from fibrinogen via enzymatic cleavage by thrombin, and it can be manufactured either from commercially available components, or from isolated blood plasma (Riestra et al., 2017). Fibrin gels produced from the components of a surgical tissue sealant have been used as transplantation substrates for LESCs in the Holoclar® product as well as other experimental work (Bandeira et al., 2020; Pellegrini et al., 1999; Rama et al., 2010). Although fibrin allows cell attachment by itself, the expansion and maturation of human LESCs on fibrin can be further improved by coating the surface with limbus-specific laminin isoforms (Polisetti et al., 2017). The fibrin gel is only translucent upon implantation, but is cleared quite rapidly through degradation in the body (Pellegrini et al., 1999). Blending of agarose to fibrin and subsequent plastic compression of the created scaffold has been shown to increase the transparency and mechanical properties of fibrin scaffolds while slowing down cellular degradation (Ionescu et al., 2011). These plastic-compressed fibrin-agarose scaffolds with encapsulated corneal fibroblasts and LESCs on their surface are being evaluated in a clinical trial for corneal ulcers (González-Andrades et al., 2017).

#### 2.4.1.3 Hyaluronic acid

Hyaluronic acid (HA) is an abundant polysaccharide component of the natural ECM and has been widely used both in clinical applications (*e.g.* dermal fillers and eye drops) and tissue engineering (Burdick & Prestwich, 2011). Chemical modifications of the native HA are well known and aim at tailoring crosslinking strategy, mechanical properties and biological activity (Burdick & Prestwich, 2011). HA has also been identified as a key component of the corneal limbal niche (Gesteira et al., 2017), but its use for corneal tissue engineering is still relatively under-explored (Yazdani et al., 2019). Although cells can interact with endogenous HA using specific cell surface receptors, such as CD44 (cluster of differentiation 44), RHAMM (receptor for HA-mediated motility) and ICAM1 (intercellular adhesion molecule 1), it does not support integrin-mediated cell attachment (Collins & Birkinshaw, 2013; Wang et al., 2010). Possibly, the lack of integrin binding sites in HA has hindered its use as a cell culture material in corneal applications, unless cell detachment is specifically required (Fiorica et al., 2011). This poor cell adhesion to HA can be improved by incorporating other ECM components, with available cell binding motifs. For example, the commercially available HyStem™ system, containing thiol-modified HA and gelatin, heparan sulphate and a crosslinking agent, has been used for transplanting encapsulated hASCs to rabbit corneas *in vivo* and as a culture substrate for LESCs *in vitro* (Chen et al., 2017; Espandar et al., 2012). Moreover, the

HyStem™ hydrogel system has been used as a basis for an injectable hASC delivery system to the eye, where the thiolated HA was crosslinked by disulphide bonds with glutathione disulphide crosslinker, and the gelatin component was replaced with maleimide-tagged RGD sequences while achieving the same beneficial effect on hASC attachment without using animal-derived gelatin (Zarembinski et al., 2014).

### 2.4.2 Fibrous scaffolds

Micro- and nanoscale fibres are another method to mimic the composition of natural ECM. Fibrous scaffolds typically have a high surface area to volume ratio, good porosity and good mechanical properties, but poor optical properties (Kong & Mi, 2016). The fibres in the scaffold can be either random or aligned, which can guide the organization of cells on the scaffolds. In corneal tissue engineering, randomly organized fibrous scaffolds have mainly been used as 2D films or membranes for corneal epithelial cells (Deshpande et al., 2010; Ortega et al., 2013), whereas fibre alignment is typically required for corneal stromal cells, as this resembles the lamellar organization of the stromal ECM (Fernández-Pérez et al., 2020; Phu et al., 2010; Wu et al., 2012b). For stromal tissue engineering, 3D structures can be produced from fibres by stacking them together.

Electrospinning is a well-known method to produce micro- and nanosized fibres of both synthetic and natural polymers. In this method, a charged polymer solution is drawn into fibres using an electric field. The solvent evaporates as polymer fibres are deposited on the oppositely charged collector. By tuning the process parameters, the size and alignment of the electrospun fibres can be controlled. Collector design is a key factor in controlling fibre alignment in electrospinning. Parallel plates and rotating mandrel collectors are the most used for producing uniaxial fibres, whereas switchable perpendicular electrodes have been used to produce orthogonally aligned fibres (Fernández-Pérez et al., 2020; Kong & Mi, 2016). Interestingly, electrospinning collectors have also be designed to produce radially organized fibres and hemispherical fibrous scaffolds for corneal applications (Fernández-Pérez et al., 2020; Kim et al., 2018).

The same natural polymers commonly used in hydrogel scaffolds, such as collagen, gelatin and HA, have been utilized also in fibrous scaffolds, either alone or blended with synthetic polymers (Kim et al., 2018; Wray & Orwin, 2009; Wu et al., 2018; Ye et al., 2014; Zhang et al., 2015a). As the natural polymer fibres tend to be fragile and difficult to handle, blending them with synthetic polymers can increase

their mechanical properties while maintaining their biological functionality (Ahearne et al., 2020). Also, these polymer blends can produce fibrous scaffolds with improved transparency (Kim et al., 2018; Kong & Mi, 2016; Ye et al., 2014).

Another approach for producing more biologically relevant fibre dimensions (tens of nanometres in diameter) takes advantage of the self-assembly process of synthetic molecules, such as peptide amphiphiles (PAs) (Miotto et al., 2015; Wade & Burdick, 2014). These PAs are engineered peptide sequences with hydrophobic alkyl tails, which can organize themselves into fibres in aqueous solutions in response to external stimuli, such as a change in pH or mixing oppositely charged molecules (Miotto et al., 2015; Uzunalli et al., 2014). Rational design of the peptide sequence allows the tailoring of PAs to include specific cell attachment sites for guiding cell proliferation and differentiation, such as laminin or fibronectin –derived sequences (Uzunalli et al., 2014). Although PAs can form hydrogel-like assemblies, they lack the robustness for prolonged cell culture and handling (Gouveia et al., 2014; Miotto et al., 2015). Instead, they can be used to produce fibrous surface patterns or used as injectable solutions (Uzunalli et al., 2014).

### 2.4.3 Composite scaffolds

Composite scaffolds are combinations of two separate materials in the same structure, which give the final product distinct material properties from those of the individual components. For example, incorporating electrospun fibres into a hydrogel matrix gains mechanical strength and contact guidance from the fibres, and a hydrated 3D environment with possible biological factors from the hydrogel (Bosworth et al., 2013). This approach has also been used to create corneal scaffolds (Kong et al., 2017; Tonsomboon & Oyen, 2013; Wilson et al., 2012b). The orthogonal fibre arrangement of the corneal stroma has even been mimicked by stacking layers of aligned polylactide fibres in alternating orientation and encasing the final structure within a collagen gel (Wilson et al., 2012b; Yang et al., 2011).

Although fibre-reinforced composites can achieve the mechanical properties required for corneal scaffolds, the incorporation of fibres compromises their transparency. Creation of transparent fibre-hydrogel composites would require fibre diameters to be below one-tenth of the wavelength of visible light or matching of the refractive indices of the matrix and the fibres (Maranchi et al., 2014). Good attempt at producing a transparent fibre-reinforced composite for corneal applications has been shown by infiltrating a mat of aligned gelatin fibres in an

alginate matrix (Tonsomboon & Oyen, 2013). However, the transparency was ultimately reduced as the gelatin fibres required crosslinking to increase their strength and stability (Tonsomboon & Oyen, 2013). Another attempt at increasing transparency of a composite corneal scaffold used a laser-perforated electrospun mat of poly-lactide-*co*-glycolide (PLGA) sandwiched into plastic compressed collagen matrix (Kong et al., 2017). Furthermore, precise control over fibre alignment and spacing can be used to improve the transparency of a composite, as has been achieved with near-field electrospinning (also called direct writing) of poly(ε-caprolactone)-poly(ethylene glycol) fibres encased into a GelMA hydrogel (Kong et al., 2020).

In addition to electrospun fibres, also PAs have been incorporated into composite scaffolds for corneal stromal cell scaffolds. Incorporating RGD-sequence-containing PAs into collagen hydrogels was shown to increase the cell viability in the scaffold, and decrease their cell-induced shrinkage (Gouveia et al., 2014). This ability to control the shrinkage of the composite material was further utilized to create curved corneal scaffolds. By incorporating PAs only in the central part of collagen gels, encapsulated cells induced contraction of the outer rim of the construct, resulting in cornea-like curvature (Miotto et al., 2019).

Another strategy for creating composite scaffolds for corneal tissue engineering has been to incorporate two different formats of the same material into the same structure. Silk fibroin fibres and films has been combined to create a scaffold with a 3D fibrous matrix for corneal stromal cells and a 2D film surface for LESCs (Bray et al., 2013). Despite its poor transparency, the scaffold could be used as transplantable ring around the limbal area (Bray et al., 2013). Also porcine collagen has been used to create core-and-skirt scaffolds with a translucent plastic compressed collagen skirt for encapsulating cells or drugs and a transparent crosslinked collagen hydrogel core for stromal reconstruction (Rafat et al., 2016).

### 2.4.4 Scaffold-free tissue engineering

One approach for corneal tissue engineering is to transplant cells without any scaffold material, relying only on the ECM production of the cultured cells. From a regulatory perspective, this approach can significantly reduce the regulatory burden for this method, when only cells with their own ECM are transplanted to patients.

For corneal epithelium applications, scaffold-free corneal epithelial sheets have been produced on temperature-responsive surfaces of poly(N-isopropylacrylamide),

PNIPAAm. Cell sheets can be detached from these plates by lowering the temperature to around 20 ºC, which is below the glass transition temperature of PNIPAAm (Nishida et al., 2004). This approach has been used for producing corneal epithelial cell sheets from primary LESCs and hiPSC-CECs, that were lifted and transplanted with the help of PVDF (poly(vinylidene difluoride)) membrane after culturing for 2–3 weeks (Hayashi et al., 2017; Nishida et al., 2004).

Enzymatic release of cell-secreted ECM constructs has been utilized for corneal stromal engineering. As opposed to the traditional cell detachment enzymes trypsin and dispase, a more controlled release of these constructs has been achieved on surfaces with self-assembled PAs containing a matrix metalloprotease (MMP) cleavable site for endogenous protease activity (Gouveia et al., 2015; Gouveia et al., 2017a). The formation of the stromal sheets was controlled by retinoic acid supplementation, which inhibits MMP activity (Gouveia et al., 2015). Removing retinoic acid from the culture medium caused stromal sheets to detach from the culture surfaces (Gouveia et al., 2015; Gouveia et al., 2017a).

Surface patterning has been shown to induce orthogonal lamellar organization of the ECM secreted by corneal stromal cells (Gouveia et al., 2013; Guillemette et al., 2009; Wu et al., 2014b). Interestingly, mere substrate curvature has been shown adequate for inducing corneal stromal cell alignment, and capable of producing enzymatically cleavable curved stromal constructs (Gouveia et al., 2017b). These corneal stromal constructs with lamellar ECM organization have shown increased transparency and mechanical properties (Gouveia et al., 2017b).

The scaffold-free techniques for creating corneal constructs require careful control over the culture conditions and long culture times to achieve adequate amount of transplantable matrix, especially for stromal reconstruction. The procollagen production of corneal stromal cells can be induced using ascorbic acid, and its assembly into ECM can be accelerated by means of macromolecular crowding of the culture medium (Kumar et al., 2015). Commonly, these secreted ECM layers have also been stacked to create thicker constructs (Gouveia et al., 2017a; Guillemette et al., 2009; Proulx et al., 2010).

## 2.5 3D bioprinting

3D bioprinting is the additive manufacturing of tissue-like structures using a living "bioink". The bioink consists of living cells or bioactive compounds dispersed in a biomaterial, which is usually a hydrogel or a hydrogel precursor solution (Malda et

al., 2013). The bioink is then deposited layer-by-layer according to a computer-generated pattern to form the wanted 3D object. Bioprinting facilitates the rapid fabrication of complex tissue architectures with defined spatial organization of cells. There are a variety of different techniques for 3D bioprinting and the field is constantly evolving. The most common methods categorized under this topic are briefly described below and illustrated in Figure 6. The key differences between these 3D bioprinting methods are summarized in Table 3.

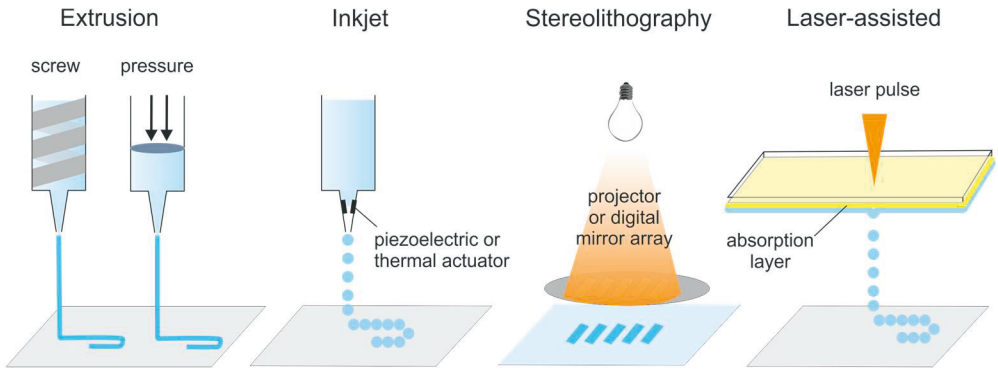


**Figure 6.** Most common approaches in 3D bioprinting, as described in (Malda et al., 2013; Mandrycky et al., 2016).

Extrusion-based bioprinting is the most commonly used method in commercial bioprinters (Angelats Lobo & Ginestra, 2019; Malda et al., 2013). This method utilizes a rotating screw or downward pressure (e.g. piston or compressed air) to force the bioink through a nozzle. Extrusion-based bioprinting requires careful optimization of bioink viscosity and printing parameters to maintain adequate cell viability, as high pressures and shear stresses can damage the cells (Mandrycky et al., 2016). To improve printability of bioinks, shear-thinning materials, such as alginate or nanocellulose are often used in extrusion bioprinting (Axpe & Oyen, 2016; Malda et al., 2013). Despite the widespread use of extrusion bioprinting, one inherent weakness of this nozzle-based approach is the limited printing resolution (Hölzl et al., 2016).

Whereas extrusion-based bioprinting deposits the bioink in a continuous strand, inkjet bioprinting applies the bioink in very small droplets (1–100 picoliters) (Malda et al., 2013). The droplets are pulsed and ejected from the nozzle of the printer head either by means of thermal vaporization or an acoustic wave generated by a piezoelectric actuator (Murphy & Atala, 2014). The bioinks used for this method are typically low viscosity hydrogel precursor solutions with a high surface tension, that

can form solid gels *in situ* after deposition on to the substrate for construction of 3D objects (Hölzl et al., 2016; Murphy & Atala, 2014). Inkjet bioprinting is limited by low cell density (<$10^6$ cells/ml) required to facilitate droplet formation and avoid clogging of the printhead nozzle (Hölzl et al., 2016; Murphy & Atala, 2014).

**Table 3.** Comparison of the four most common 3D bioprinting approaches. Adapted from (Hölzl et al., 2016; Mandrycky et al., 2016; Murphy & Atala, 2014).

| Property | Extrusion | Inkjet | Stereolitho-graphy | Laser-assisted |
|---|---|---|---|---|
| Viscosity range | 30 to > 6 ×$10^7$ mPa/s | <10 mPa/s | No limitations | 1–300 mPa/s |
| Cell density | Nozzle size limiting | <$10^6$ cells/ml | <$10^8$ cells/ml | <$10^8$ cells/ml |
| Cell viability | 40–80% | >85% | >85% | >95% |
| Gelation methods | Chemical, photo-crosslinking, shear thinning, temperature | Chemical, physical, photo-crosslinking | Photo-crosslinking | Chemical, photo-crosslinking |
| Printing speed | Slow | Fast | Fast | Medium |
| Resolution | 200–1000 μm | 10–50 μm | 50–100 μm | 10–100 μm |
| Main advantages | Printing of cell clusters and organoid possible for high cell density | Low cost | Fast, high spatial resolution | No clogging, wide range of viscosities, high cell viability |
| Main challenges | Nozzle clogging, low spatial resolution | Nozzle clogging, low cell density, low viscosity bioinks | Possible phototoxicity to cells, limited bioinks available | High cost, complex system |

Stereolithography can be utilized for 3D bioprinting by selectively solidifying layers in a bath of photopolymerizable bioink. Light is projected through digital micromirror arrays, which control the intensity in each pixel to crosslink the bioink (Mandrycky et al., 2016). As the crosslinking occurs for the entire layer at the same time, this method can produce also very complex shapes without increasing the manufacturing time (Mandrycky et al., 2016). Stereolithography can ether utilize UV or visible light to cure the bioink, depending on the reactive functional groups and possible photoinitiators in the bioink (Wang et al., 2015).

Laser-assisted bioprinting (LaBP) setup consist of two parallel surfaces, the upper donor slide and the lower collector plate. The bioink is applied on top of an energy absorbing layer and suspended above the collector plate. A laser beam is then

focused on a spot of the absorption layer (e.g. gold), causing it to vaporize. The formed high-pressure bubble ejects a droplet of the bioink on to the underlying collector plate. This method allows the use of a large variety of bioink viscosities and does not cause mechanical stress to the cells, resulting in cell viability of over 95% (Mandrycky et al., 2016; Murphy & Atala, 2014). However, the widespread adoption of LaBP technique has been hindered by the high cost and relative complexity of the equipment (Mandrycky et al., 2016).

### 2.5.1 Bioprinting for corneal applications

3D bioprinting has been proposed an effective method to provide alternatives for donor corneal tissues by providing multi-layered, high density cellular constructs with native curved shape (Zhang et al., 2019). The cornea is an appealing target tissue for 3D bioprinting because of its quite simple layered structure and avascular nature (Sommer & Blumenthal, 2019). The digital design allows 3D bioprinting of custom-made implants based on real geometric data of corneal dimensions for individual patients (Zhang. et al., 2019). This approach has been utilized to produce extrusion-printed cornea-mimicking structures using primary corneal keratocytes in alginate-based bioinks (Isaacson et al., 2018). However, alginate alone did not maintain the printed shape in culture, and required addition of methacrylated Col I in the bioink (Isaacson et al., 2018). Collagen and gelatin have also been previously combined with alginate to overcome the poor cell attachment and slow degradability of alginate, and applied to extrusion print corneal epithelial cells (Wu et al., 2016). UV-crosslinking GelMA has also been used to extrusion print human corneal keratocytes, although the bioprinted constructs did not show significant advantages over the bulk GelMA scaffolds (Bektas & Hasirci, 2020).

In another approach to produce 3D bioprinted stromal structures using inkjet printing, the bioink consisted of agarose and Col I (Duarte Campos et al., 2019). Although agarose and alginate are both seaweed-derived polysaccharides, agarose is physically crosslinked via hydrogen bonding, whereas alginate is stabilized through ionic bonds. This makes agarose bioinks thermosensitive and their gelation can be temperature controlled by heating the printing head and cooling the printing substrate (Duarte Campos et al., 2019). This method relied in the initial stabilization of agarose in room temperature, with subsequent gelation of collagen in 37 ºC (Duarte Campos et al., 2019). By incorporating iron nanoparticles in this type of collagen-agarose bioink, it has been possible to magnetically align the collagen fibres

within the bioprinted scaffold, which could be beneficial in corneal applications to mimic the natural collagen organization of the stroma (Betsch et al., 2018).

Another method to produce bioprinted layers of collagen mimicking the 2 μm thick lamellae in the corneal stroma have been described with recombinant human collagen type III (Gibney et al., 2017). In this method, the recombinant collagen was aerosolized and extruded from a nozzle in a pressurized stream of nitrogen gas (Gibney et al., 2017). Human CSSCs were successfully cultured on top of the layered scaffolds crosslinked with EDC/NHS (Gibney et al., 2017). Although the production method of the scaffold constituted as additive manufacturing, the material did not actually function as a true bioink, as the harsh printing conditions did not allow cell incorporation during the production of the scaffold.

Corneal 3D bioprinting is developing a large hype around the world, and many research projects make headlines before realization of peer-reviewed scientific publications. Internet news sites have reported, for example, 3D bioprinted corneas developed using fish collagen in New Zealand (Tuckey, 2017), and plans to make bioprinted stromal replacements from autologous adipose stem cells and collagen (Saunders, 2017). It remains to be seen whether these projects will deliver on their promises to produce alternatives for corneal transplants.

# 3 AIMS OF THE STUDY

The aim of this dissertation was to develop tissue-engineered corneal implants, combining clinically relevant biomaterials and therapeutic stem cells aimed to treat severe corneal blindness involving both scarring of the stroma and LSCD. The therapeutic stem cell types used for the purposes of this study were hASCs for stromal regeneration and hPSC-LESCs to restore the healing capacity of corneal epithelium. The specific aims of this dissertation are outlined below.

1. To investigate suitable hydrogels for hASCs encapsulation and delivery to corneal stromal defects (**Studies I** and **II**).

2. To develop and produce implants with both hASCs and hPSC-LESCs in a tissue-like cell organization (**Studies II** and **III**).

3. To find suitable implantation strategies for the produced scaffolds and study their integration in a porcine *ex vivo* corneal model (**Studies I, II** and **III**).

# 4 MATERIALS AND METHODS

## 4.1 Ethical considerations

The use of human embryos for research purposes at Tampere University has been approved by the national supervisory authority for welfare and health, Valvira (Dnro 1426/32/300/05). The supportive statements of the Ethical Committee of the Pirkanmaa Hospital District allow the derivation, culture, and differentiation of hESC (Skottman/R05116) and hiPCS lines (Uusitalo/R16116) for ophthalmic research, as well as the use hiPSC lines derived in other laboratories (Skottman/R14023). The extraction and use of hASCs for research purposes has also been approved by the Ethical Committee of the Pirkanmaa Hospital District (Miettinen/R15161). No new cell lines were derived for the purposes of this dissertation.

The research use of human donor corneas deemed unsuitable for transplantation has been accepted by the Ethical Committee of the Pirkanmaa Hospital District (Uusitalo/R11134).

## 4.2 Biomaterials for corneal scaffolds

### 4.2.1 Hyaluronic acid hydrogels

In **Studies I-II**, hyaluronic acid (HA, 150 kDa) from Lifecore Biomedical (Chaska, MN) was chemically modified and used to produce hydrazone-crosslinked hydrogel scaffolds. Hydrazone-crosslinking is a mild bio-orthogonal reaction, where a hydrazide group and an aldehyde group react in physiological conditions, producing only water as a by-product. For developing optimal corneal scaffolds from hydrazone-crosslinked hydrogels, we studied different aldehyde- and hydrazide-modified HA components. In **Study I**, HA hydrogels were produced using two different hydrazide-modifications, adipic acid dihydrazide HA (HA-ADH) and carbodihydrazide HA (HA-CDH). In **Study II**, the HA-CDH component was

further modified to include a tissue-adhesive dopamine moiety (HA-DA-CDH). Aldehyde groups were introduced into HA using periodate oxidation, either directly (**Study I**) or through an intermediate product, 2,3-dihydroxypropylamide derivative of HA (**Studies I-II**). Synthesis of aldehyde-modified HA (HA-Ald), HA-ADH, HA-CDH and HA-DA-CDH components are described in detail in the original publications (**Studies I-II**), and the degree of substitution (DS) of reactive groups in the polymer backbone in each study is specified in Table 4.

The freeze-dried hydrogel components were dissolved in either Dulbecco's phosphate buffered saline (DPBS, Lonza, Basel, Switzerland) or 10% sucrose (Sigma-Aldrich, St. Louis, MO) solution, in varying concentrations as specified in Table 4. The components were sterilized either by forcing the dissolved components though a 0.22 μm syringe filter (**Study I**) or subjecting the dry components to UV light for 30 min (**Study II**). The hydrogels were formed by mixing equal volumes of hydrazide-modified HA and aldehyde-modified HA in a suitable mould and allowed to form a gel either in room temperature or in a cell culture incubator (37°C, 5% $CO_2$). In **Study I**, also human collagen type I (Col I) (Sigma-Aldrich) was added to the hydrogel, by first combining it to the HA-Ald, followed by mixing with the hydrazide component.

**Table 4.** Hyaluronic acid hydrogels used in this dissertation.

| Hydrogel | Components | Solvent | Concentration | DS% | Amount of total volume | Study |
|---|---|---|---|---|---|---|
| **H1** | HA-Ald | DPBS | 30 mg/ml | 15% | 50% | **I** |
| | HA-CDH | DPBS | 30 mg/ml | 17% | 50% | |
| **H1C** | HA-Ald | DPBS | 30 mg/ml | 15% | 40% | **I** |
| | HA-CDH | DPBS | 30 mg/ml | 17% | 40% | |
| | Col I | acetic acid | 5 mg/ml | - | 20% | |
| **H2** | HA-Ald | 10% sucrose | 20 mg/ml | 9% | 50% | **I** |
| | HA-ADH | 10% sucrose | 10 mg/ml | 50% | 50% | |
| **HA-HA** | HA-Ald | DPBS | 16 mg/ml | 10% | 50% | **II** |
| | HA-CDH | 10% sucrose | 16 mg/ml | 10% | 50% | |
| **HA-DOPA** | HA-Ald | DPBS | 16 mg/ml | 10% | 50% | **II** |
| | HA-DA-CDH | DPBS | 16 mg/ml | 10% | 50% | |

Abbreviations: ADH: adipic acid dihydrazide, Ald: aldehyde, CDH: carbodihydrazide Col I: human collagen type I, DA: dopamine, DPBS: Dulbecco's phosphate buffered saline, DS: degree of substitution, HA: hyaluronic acid

### 4.2.2 Covalent surface modification of hydrogels

In **Study II**, proteins and peptides were bound on the surface of preformed hydrogels to facilitate cell attachment. In HA-DOPA, the dopamine residue provided a site for Michael addition reaction, which requires free thiol (–SH) groups in the protein and oxidation of the dopamine residues to their reactive quinone form. Primary thiol groups were introduced into native proteins using Traut's reagent (2-iminothiolane) (Thermo Fisher Scientific, Waltham, MA), or alternatively ready-made synthetic peptides with N-terminal cysteine residues were used. Oxidation of the dopamine moieties was achieved by performing the conjugation reaction in pH 10.

The HA-DOPA hydrogels were covalently modified with cysteine-terminated laminin-mimetic peptide CDPGYIGSR (Bachem, Bubendorf, Switzerland, and Calbiochem/Sigma-Aldrich) and Col IV from human placenta (Sigma-Aldrich). Details of the covalent surface modification can be found in the original publication (**Study II**).

### 4.2.3 Bioinks and 3D bioprinting

In **Study III**, hydrogel-based bioinks were used to produce bioprinted cornea-mimicking structures. Different bioinks were developed for epithelial and stromal layers. For the epithelial layer, hPSC-LESCs were printed in a bioink composed of recombinant human laminin 521 (Ln521, BioLamina, Sundbyberg, Sweden) and HA (Sigma-Aldrich) in CnT-30 medium (CELLnTEC, Bern, Switzerland) supplemented with the ROCK (Rho-associated protein kinase) inhibitor RevitaCell™ (Thermo Fisher Scientific). For the stromal structures, hASC were printed in a bioink composed of human Col I (OptiCol™, Cell Guidance Systems, Cambridge, UK), human plasma and thrombin (Sigma-Aldrich) and 10X DPBS. Additionally, HA was added for acellular stromal layers in between cellular layers for production of 3D structures. The different bioinks used for 3D bioprinting of the epithelial and stromal components of the corneal structures are summarized in Table 5. Further details about the bioinks and bioprinting process can be found the original publication (**Study III**).

**Table 5.** Composition of bioinks used for the different layers of the 3D bioprinted corneal structures

| Layer | Cells | Components | Concentration | Amount of total volume |
|---|---|---|---|---|
| **Epithelium** | hPSC-LESC | CnT-30 w/ 1X RevitaCell™ | - | 50% |
| | | Ln521 | 0.1 mg/ml | 33% |
| | | HA | 10 mg/ml | 17% |
| **Stroma** | hASC | Col I | 3 mg/ml | 44,4% |
| | | human plasma | - | 22,2% |
| | | human thrombin | 40 IU/ml | 22,2% |
| | | 10X DPBS | - | 11,1% |
| **Acellular stromal layers** | - | Col I | 3 mg/ml | 40% |
| | | human plasma | - | 20% |
| | | human thrombin | 40 IU/ml | 20% |
| | | HA | 10 mg/ml | 10% |
| | | 10X DPBS | - | 10% |

Abbreviations: Col I: human collagen type I, DPBS: Dulbecco's phosphate buffered saline, HA: hyaluronic acid, hASC: human adipose stem cells, hPSC-LESC: human pluripotent stem cell-derived limbal epithelial stem cells, Ln521: human recombinant laminin-521

The cornea-mimicking structures were bioprinted using LaBP based on laser-induced forward transfer (LIFT). The custom-built setup is described in detail in (Koch et al., 2009). Briefly, the setup consists of a glass slide suspended above a collection surface and a moving laser focusing system. The glass slide contained an energy absorbing material layer and the bioink layer. Focusing of the laser on the absorption layer caused it to evaporate and eject a droplet of the adjacent bioink towards the collection surface underneath. In **Study III**, two different laser setups were used. In the first setup, a Nd:YAG-laser (DIVA II; Thales Laser, Orsay, France) with 1064 nm wavelength was used in conjunction with a 60 nm gold absorption layer. This setup was used for printing both investigated cell types, hPSC-LESCs and hASCs, separately. The second setup consisted of an Er:YAG-laser (DPM-15, Pantec Engineering AG, Ruggell, Liechtenstein) with 2940 nm wavelength, which was used together with Corning® Matrigel® (Thermo Fisher Scientific) as the absorption layer. This setup was used to produce corneal-mimicking structures containing both cell types. The fabrication of the bioprinted corneal structures is illustrated in Figure 7. Details of the 3D bioprinting parameters are described in the original publication (**Study III**).

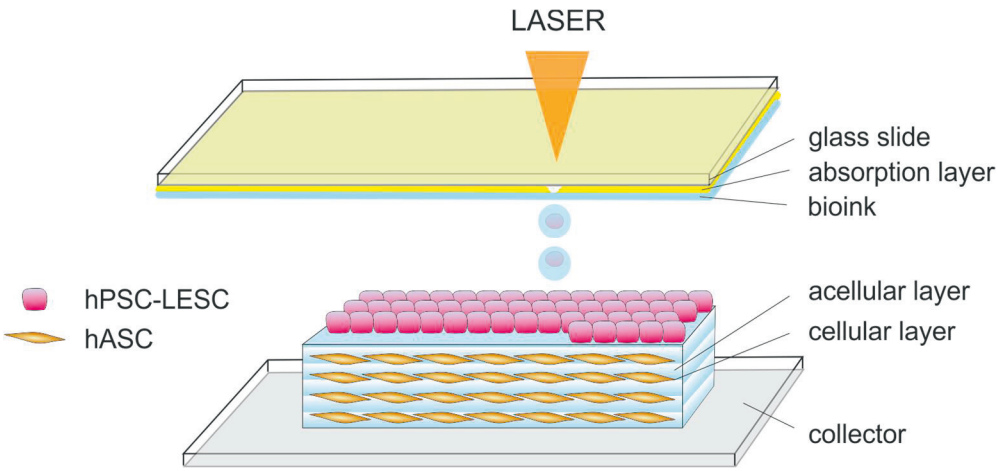


**Figure 7.** The production of cornea-mimicking structures from human pluripotent stem cell-derived limbal epithelial stem cells (hPSC-LESCs) and human adipose stem cells (hASCs) with laser-assisted bioprinting.

## 4.3 Biomaterial characterization methods

### 4.3.1 Spectroscopic methods

The hydrogel components synthesized for the purposes of this work were characterized using different spectroscopic methods. Nuclear magnetic resonance ($^1$H NMR) spectra of the synthesized hydrogel components were used to characterize the HA-components in **Study I** and to estimate the degree of aldehyde and dopamine modifications of HA in **Study II**. In **Study I**, Fourier transform infrared (FTIR) spectroscopy was used to study the chemical structures of the HA components and to verify the presence of hydrazone crosslinks after mixing. Details of the NMR and FTIR measurements are described in the original publications (**Studies I-II**).

UV/Vis spectroscopy was used to determine the amounts of specific chemical entities in the hydrogel components and other reagents. TNBS (2,4,6-trinitrobenzenesulfonic acid) assay was used to study the DS% of HA-Ald and HA-CDH in **Studies I** and **II**, and the primary amine content in Col IV used for surface functionalization in **Study II**. In this assay, TNBS reacts with amines and hydrazides forming a stable trinitrophenyl complex with an absorbance peak at $\lambda$=334 nm. This absorbance was then detected, and the number of reacting groups was determined

from a standard curve. The aldehyde group estimation using TNBS assay was performed indirectly. First, the aldehydes were reacted with an excess of *tert*-butyl carbazate resulting in stable carbazones, analogous to the hydrazone crosslinks. The amount of carbazate consumed from the solution was then determined from a reaction with TNBS based on the absorbance at 334 nm. (Bouhadir et al., 1999)

UV/Vis spectroscopy was also used to quantify the amount of thiol groups in reaction solutions of **Study II**, by measurement of their absorption at λ=412 nm with Ellman's reagent (DTNB, 5,5-dithiobis(2-nitrobenzoic acid)). Ellman's reagent reacts quantitatively with free thiol groups, such as cysteine residues, to form a coloured product. The absorbance values can then be directly translated to concentration using the molar extinction coefficient (14 150 $M^{-1}cm^{-1}$) of Ellman's reagent and Equation (1), where A is the absorbance of the sample at 412 nm, b is the length of the light path, and E is the molar extinction coefficient.

$$. = \frac{A}{bE} \tag{1}$$

### 4.3.2 Rheological and mechanical properties

The physical properties of the produced corneal scaffolds were characterised in **Studies I** and **II** based on the rheological and mechanical properties of the formed HA hydrogels. In **Study I**, the rheological measurements were conducted using a rotational HAAKE RheoStress RS150 rheometer (Thermo Fisher Scientific), whereas in **Study II**, DHR-II rheometer (TA Instruments, New Castle, DE) was used. Amplitude and frequency sweeps were used to determine the storage modulus (G'), loss modulus (G") and loss tangent (tan δ = G"/G') of the hydrogels. In **Study II**, these values were used to calculate the average mesh size (ξ) and average molecular weight between crosslinks ($M_c$), to determine the material properties of the elastic hydrogels based on rubber elastic theory (Oommen et al., 2013). Average mesh size was calculated using Equation 2, where G' is the storage modulus of the hydrogel, N is the Avogadro constant ($6.023\times10^{23}$ /mol), R is the molar gas constant (8.314 J/K mol) and T is the temperature (298 K).

$$\xi = \left(\frac{G'N}{RT}\right)^{-\frac{1}{3}} \tag{2}$$

The molecular weight between crosslinks ($M_c$) was calculated using Equation 3, where c is polymer concentration (1.6%), $\rho$ is the density of water at 298 K (997

kg/m$^3$), R is the molar gas constant, T is the temperature, and $G'_p$ is the peak value of G'.

$$M_c = \frac{c\rho RT}{G'_p} \quad (3)$$

In **Study I**, the mechanical properties of the hydrogels were determined using compression testing with BOSE Electroforce Biodynamic 5100 machine with a 225 N load cell (Bose Corp, Eden Prairie, MN). Compression testing is a valid method for obtaining typical material parameters for fragile hydrogels, since they rarely endure conventional tensile testing (i.e. clamping between two grips). From the obtained stress-strain data, hydrogel bulk stiffness was determined as the derivative of stress with respect to strain, as described in (Karvinen et al., 2017). Moreover, estimates of the second order elastic constants (Young's moduli) were calculated for each hydrogel. Details of the methods and mathematical models can be found in the original publication (**Study I**).

In **Study II**, rheometric tack test was used to measure the tissue adhesion of the hydrogel implants with pig corneal tissue. In the tack test, the cornea was glued to the upper plate, and used to probe the fully cured hydrogel on the bottom plate. After a 2-min holding period, the probe was lifted at a constant rate.

### 4.3.3 Swelling and degradation kinetics

In **Studies I** and **II**, the swelling and enzymatic degradation of the hydrogel scaffolds was studied to estimate the stability of the corneal scaffolds. The swelling ratio (SR) or residual mass (RM) was calculated by weight of the hydrogels according to Equation 4, where $W_i$ denotes the initial weight and $W_t$ the weight of the hydrogel at measurement time point.

$$SR\ or\ RM = \frac{W_t - W_i}{W_i} \times 100\% \quad (4)$$

The hydrogel swelling ratios at 37 °C were examined in cell culture medium in **Study I**, whereas in **Study II**, the hydrogel swelling kinetics were measured in both DPBS and medium. In **Studies I** and **II**, the enzymatic degradation of the HA hydrogels was determined in the presence of hyaluronidase enzyme (20–50 U/ml). Details of the swelling and degradation measurements can be found in the original publications (**Studies I-II**).

### 4.3.4 Optical properties

For corneal scaffolds, transparency and other optical properties are also relevant material properties. The transparency of the hydrogels was evaluated by measuring light transmittance through the hydrogels (**Studies I-II**) and by photography of the scaffolds superimposed on text (**Studies I-III**). Light transmittance across the visible light spectrum was measured using UV/Vis spectrometer, with the hydrogel samples directly prepared into the measuring cuvettes. In **Study I**, the refractive indices of the hydrogels were measured with surface plasmon resonance equipment Navi 210A (BioNavis, Tampere, Finland) using a glass slide with a known refractive index as a reference. The optical properties were only studied for acellular hydrogels. Details of the methods can be found in the original publications (**Studies I-II**).

## 4.4 Cell culture

In this dissertation, two types of human stem cells were used in the produced corneal scaffolds, hASCs and hPSC-LESCs. In **Study I**, only hASCs were used, whereas the biomaterial structures in **Studies II** and **III** contained both cell types.

### 4.4.1 Culture of adipose stem cells

The hASCs used in **Studies I-III** were received from Associate Professor Miettinen's Adult Stem Cell group at Tampere University at passage 2. The hASCs were originally obtained from adipose tissue samples extracted from a female donor during elective plastic surgery, and the cells were isolated mechanically and enzymatically as described in (Lindroos et al., 2009). The surface marker profile of undifferentiated hASCs had been characterized using flow cytometry before cryostorage at passage 1 (Table 6. ). The hASCs were expanded either in Dulbecco's modified Eagle's medium/Ham's nutrient mixture F-12 (DMEM/F-12) medium (Thermo Fisher Scientific) with 5% human serum (BioWest, Nuaillé, France), 1% GlutaMAX™ (Thermo Fisher Scientific) and 1% antibiotics (penicillin-streptomycin, Lonza) (in **Studies I** and **II**) or EBM-2 medium (Lonza) with 2% human serum (**Study III**), and passaged at approximately 80% confluence using TrypLE™ Select (Thermo Fisher Scientific). Cells at passage 3–5 were used in all experiments.

**Table 6.** Cell surface marker profile of the undifferentiated hASCs used in **Studies I-III**.

| Marker | Positive cells (%) |
|---|---|
| **CD75** | 95.8 |
| **CD90** | 99.2 |
| **CD105** | 98.7 |
| **CD14** | 0.7 |
| **CD19** | 0.9 |
| **CD45** | 2.0 |
| **HLA-DR** | 1.1 |
| **CD34** | 47.5 |

Abbreviations: CD: cluster of differentiation, HLA: human leukocyte antigen

### 4.4.2 Culture of pluripotent stem cells

Human ESC line Regea08/017 (XX) was used in **Studies II** and **III**. The cell line has been derived at University of Tampere (Skottman, 2010), and has been later adapted to feeder-free culture conditions (Hongisto et al., 2017). The feeder-free hESCs were cultured on Corning® CellBind (Corning Inc., Corning, NY) culture plates coated with 0.55 μg/cm² of Ln521 (BioLamina) in Essential E8™ Flex medium (Thermo Fisher Scientific) with 0.5% antibiotics. The cells were passaged twice a week using TrypLE™ Select and reseeded at a density of 40 000–50 000 cells/cm². The cell line has been characterized for its pluripotency and karyotype (Skottman, 2010).

### 4.4.3 hPSC-LESC differentiation and culture

The hPSC-LESCs used in **Studies II** and **III** were differentiated from the Regea08/017 hESC line cultured in feeder-free conditions, as previously described (Hongisto et al., 2017). The undifferentiated hESCs were detached and transferred to Corning® Costar® Ultra-Low attachment culture plates in xeno-free basal medium (containing KnockOut™ DMEM) supplemented with 15% KnockOut™ SR XenoFree CTS™, 2 mM GlutaMAX™, 0.1 mM 2-mercaptoethanol, 1% MEM non-essential amino acids (all from Thermo Fisher Scientific) and 0.5% antibiotics) with 5 μM blebbistatin (Sigma-Aldrich) to induce embryoid body (EB) formation. The EBs were cultured in xeno-free basal medium and subjected to 10 μM SB-505124 (Sigma-Aldrich) and 50 ng/ml basic fibroblast growth factor (bFGF;

PeproTech, Rocky Hill, NJ) for 1 day, followed by 2 days in 25 ng/ml bone morphogenetic protein 4 (BMP4; PeproTech). After this induction phase, the EBs were plated onto well plates coated with 0.75 g/cm$^2$ Ln521 and 5 μg/cm$^2$ Col IV in CnT-30 medium. The cells were cultured in CnT-30 for 21–24 days, after which they were detached, counted and frozen in PSC cryopreservation medium (Thermo Fisher Scientific).

For culturing on corneal scaffolds in **Study II**, the hPSC-LESCs were thawed directly onto the hydrogels using a plating density of 0.9–1.5 × 10$^6$ cells/cm$^2$. For bioprinting in **Study III**, the hPSC-LESCs were first thawed onto 0.75 g/cm$^2$ Ln521 and 5 μg/cm$^2$ Col IV –coated well plates in CnT-30 and expanded in culture before being detached and mixed into the bioink for printing.

## 4.5 Cell characterization methods

### 4.5.1 Cell viability and proliferation

The viability and proliferation of the cells within the developed corneal scaffolds was evaluated qualitatively using a LIVE/DEAD™ viability/cytotoxicity kit, and quantitatively using a resazurin-based metabolic assay PrestoBlue™ and the CyQUANT™ cell proliferation kit (all from Thermo Fisher Scientific). The LIVE/DEAD™ staining was performed by incubating the samples in staining solution containing Calcein-AM (2 μM in **Studies I** and **II**, 0.5 μM in **Study III**) and 1 Ethidium homodimer (1 μM in **Studies I** and **II**, 0.25 μM in **Study III**). The diluted PrestoBlue™ reagent, was incubated with the hydrogel samples at 37 ºC for 4 hours (**Studies I** and **II**) or 30 min (**Study III**). The CyQUANT® analysis was performed to determine the DNA content in the hydrogels in **Study II**. The number of cells was estimated using a standard curve of DNA content obtained from 2D-cultured hASCs. Details of the methods can be found in the original publications.

### 4.5.2 Immunofluorescence

In **Studies II** and **III**, indirect immunofluorescence staining was used to evaluate the identity and morphology of the cells in the corneal scaffolds. The primary antibodies used to visualize specific proteins are listed in Table 7. Secondary antibodies anti-rabbit Alexa-488, anti-goat Alexa-568, anti-mouse Alexa-647, anti-

mouse Alexa-488, anti-rabbit Alexa-568 (all from Thermo Fisher Scientific) were diluted 1:800 (**Study II**) or 1:400 (**Study III**). The actin cytoskeleton of the cells was stained with Phalloidin-Atto 550 1:100 (Sigma-Aldrich) in **Study III** together with the secondary antibodies. Cell nuclei were visualized with 4',6-diamidino-2-phenylindole (DAPI) in the mounting medium either with Vecta-Shield (Vector Laboratories, Burlingame, CA) or ProLong™ Gold Antifade mounting medium (Thermo Fisher Scientific). The detailed immunofluorescence staining protocols can be found in the original publications.

**Table 7.** Primary antibodies used to detect specific marker proteins.

| Antibody | Host | Manufacturer | Dilution | Study |
|---|---|---|---|---|
| **CK3** | mouse | Abcam | 1:200 | **III** |
| **CK12** | goat | Santa Cruz Biotechnology | 1:200 | **II** |
| **CK15** | mouse | Thermo Fisher Scientific | 1:200 | **III** |
| **Col I** | mouse | Abcam | 1:200 | **III** |
| **Col IV** | goat | Millipore | 1:200 | **II** |
| **Ki67** | rabbit | Millipore | 1:200 | **III** |
| **p40** | mouse | Biocare Medical | 1:100 | **II** |
| | | | 1:200 | **III** |
| **p63α** | rabbit | Cell Signaling Tech | 1:200 | **III** |
| **VWF** | rabbit | Dako Cytomation | 1:200 | **III** |

Abbreviations: CK: cytokeratin, Col: collagen, VWF: von Willebrand factor

### 4.5.3 Gene expression analysis

In **Study II**, the capability of hASCs to differentiate towards corneal keratocytes was studied using quantitative polymerase chain reaction (qPCR) using specific primers for three keratocyte markers: aldehyde dehydrogenase 3A1 (*ALDH3A1*, Hs00964880_m1), keratocan (*KERA*, Hs00559942_m1) and lumican (*LUM*, Hs00929860_m1). The housekeeping gene glyceraldehyde 3-phosphate dehydrogenase (*GAPDH*, Hs99999905_m1) was used to normalize the data. The TaqMan primers were obtained from Applied Biosystems (Foster City, CA) and the qPCR analysis was run on Applied Biosystems' real-time PCR instrument. The relative fold change of gene expression was analysed using the $2^{-\Delta\Delta Ct}$ method (Schmittgen & Livak, 2008).

In the differentiation experiment, hASCs were cultured for 10 days in keratocyte differentiation medium containing Advanced DMEM (Thermo Fisher Scientific)

supplemented with 10 ng/ml bFGF (PeproTech), 0.1mM ascorbic acid-2-phosphate (Sigma-Aldrich) and 1 μM retinoic acid (Sigma-Aldrich) (Du et al., 2010; Lynch & Ahearne, 2017). For the qPCR analysis, RNA from hASCs cultured in keratocyte differentiation medium in 2D and hASCs encapsulated in hydrogels in *ex vivo* corneal culture were compared to undifferentiated hASCs. Details of the RNA isolation, complementary DNA synthesis and qPCR protocols are described in the original publication (**Study II**).

## 4.6 *Ex vivo* corneal culture

The corneal scaffolds developed in **Studies I-III** were evaluated in a porcine cornea *ex vivo* model to study the interaction of the scaffold with the surrounding corneal tissue, and to evaluate the implantation strategy of each scaffold. Fresh porcine eyes were obtained from an abattoir (Paijan tilateurastamo, Urjala, Finland), and kept in cold AMES buffer (Sigma-Aldrich) (**Study I**) or DPBS (**Studies II** and **III**) containing 2% antibiotics until preparation for culture. The excised corneas were cultured partially submerged in serum-free co-culture medium (CnT-Prime-CC, CELLnTEC) with 1% antibiotics and 0.25 μg/ml amphotericin B (Thermo Fisher Scientific), and optionally 5 μg/ml plasmocin (InvivoGen, Toulouse, France). The corneas were mounted on a Barron artificial anterior chamber (Katena Products, Denville, NJ) where scaffold implantations were performed as shown in Figure 8. After operations were performed, the corneas were returned to fresh culture dishes, covered with contact lenses and cultured partially submerged, so that the surface of the cornea remained at the air-liquid interface under the contact lens. The *ex vivo* corneas with implanted cell-containing scaffolds were cultured in hASC culture medium (**Studies I and III**) or CnT-30 medium (**Study II**).

The *ex vivo* corneas were fixed after 7 days of culture in 4% PFA or acid-formaline/EtOH fixative and either dehydrated and embedded in paraffin (**Studies I** and **III**) or kept overnight in Tissue-Tek® OCT™ (Sakura Finetek Europe, Alphen aan den Rijn, The Netherlands) at 4 ºC followed by snap-freezing in liquid nitrogen (**Study II**).

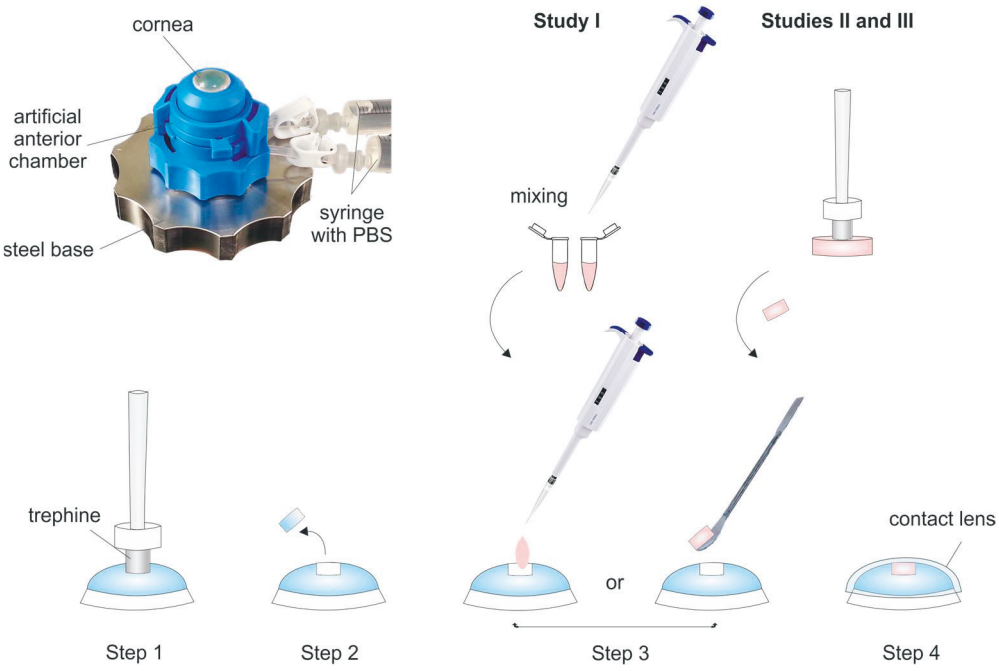


**Figure 8.** Implantation of corneal scaffolds into the porcine cornea *ex vivo* model. A partial depth incision was made to the cornea (Step 1) and the trephined stromal button was removed (Step 2). In Step 3, the scaffold was implanted into the wound site. In **Study I**, the hydrogel mixed with hASCs was made directly into the wound site, whereas in **Studies II** and **III**, the ready-made scaffolds were trephined with the same outer dimensions of the wound and placed in the wound site. After implantation of the scaffolds, the corneas were removed from the artificial anterior chamber and covered with soft contact lenses (Step 4).

## 4.7 Histological evaluation

Immunohistochemical staining against human cell surface marker TRA-1-85 was performed to identify the implanted human cells in the *ex vivo* porcine corneas in **Studies I-III**. Thin sections of the paraffin-embedded (**Studies I** and **III**) or frozen (**Study II**) corneal tissue were captured onto glass slides and stained using anti-TRA-1-85 mouse IgG antibody (courtesy of Peter Andrews, University of Sheffield). Details of the staining procedure can be found in the original publications (**Studies I-III**).

In **Study III**, haematoxylin and eosin (HE) staining was used to observe the structures of normal corneal tissue (human donor cornea deemed unsuitable for transplantation), *ex vivo* cultured porcine corneas and bioprinted corneal structures.

## 4.8 Statistical analyses

In **Study I**, statistical analyses were performed with MATLAB using non-parametric Kruskal-Wallis test and a Mann-Whitney U test were used to test for statistical significance. In **Study II**, the statistical testing was performed with IBT Graph Pad Prism software, version 5.02 using two-way ANOVA. In **Study III**, the statistical analysis was performed with IBM SPSS Statistics software, where significance was determined with Mann-Whitney U test. In all studies, p-values $<0.05$ were considered statistically significant.

# 5 SUMMARY OF THE RESULTS

## 5.1 Hyaluronic acid hydrogels as hASC scaffolds

HA-based hydrogels were studied as scaffolds for hASC encapsulation and cell delivery to the cornea in **Studies I** and **II**. In both studies, the formation of these hydrogels was based on hydrazone crosslinking between an aldehyde-modified and a hydrazide-modified HA component. In **Study I**, comparisons were made between an adipic acid dihydrazide (ADH)-derived hydrazone (denoted as H2) and a carbodihydrazide (CDH)-derived hydrazone (H1). Additionally, human Col I was mixed as the third component with the CDH-hydrazone hydrogel (H1C). In **Study II**, CDH-hydrazone hydrogels (here denoted as HA-HA) were further modified to include dopamine units (DS 14%) (HA-DOPA). The dopamine units were included to facilitate covalent surface modification of the hydrogels and to create hydrogels with tissue-adhesive functionality. The chemical structures of the HA hydrogels are shown in Figure 9. Hydrogel formation occurred rapidly after mixing of the components in all the studied hydrogels. Formation of the hydrazone crosslinks was verified with FTIR (**Study I**/Figure 1).

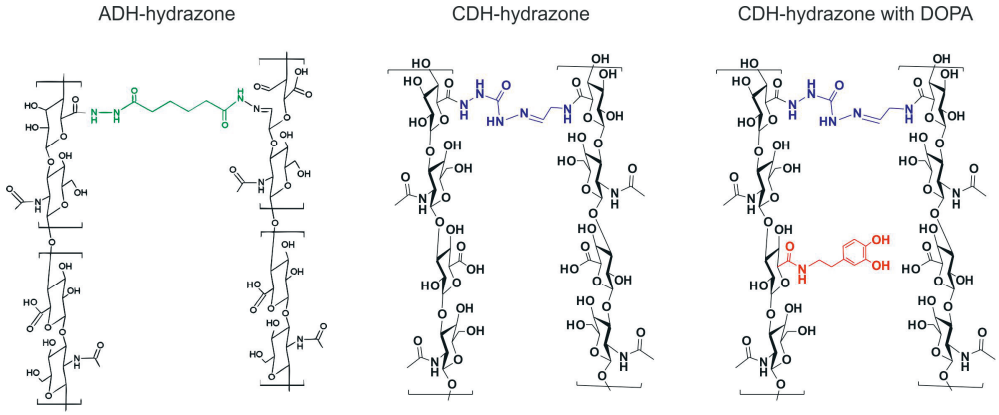


**Figure 9.** Chemical structures of the different HA hydrogels used in this dissertation. In **Study I,** HA hydrogels crosslinked with hydrazone bonds from adipic acid dihydrazide (ADH, in green) and carbodihydrazide (CDH, in blue) were compared. In **Study II**, The CDH-conjugated HA was also modified to include dopamine moieties (in red).

### 5.1.1 Rheological, mechanical and optical properties

The studied HA hydrogels showed typical viscoelastic behaviour of strong gels in rheological measurements. The detailed material characterisations obtained from rheological and compression testing are described in the original publications (**Study I**/Figure 3 and **Study I**/Table 2) and (**Study II**/Figure 2 and **Study II**/Table 2). In **Study I**, compression testing revealed that the hydrogels experienced strain-hardening, meaning that their stiffness was relatively constant at low strains (<20%) but increased at higher strains. The H1 hydrogel was considered the most elastic of the gels in **Study I**, whereas H1C was the stiffest. The stiffness of H1C was attributed to the additional crosslinking of the structure through imine bonds formed between the collagen and the aldehyde groups of HA. In **Study II**, the effect of the encapsulated hASCs on the rheological properties was also evaluated. The presence of cells in the gels affected the rheological measurements considerably. Interestingly, without cells, the HA-HA gel showed higher stiffness than HA-DOPA, whereas with encapsulated hASCs the HA-DOPA gel was stiffer.

To investigate the stability of the hydrogels, their swelling kinetics were studied. It was noted, that an equilibrium swelling state was reached in PBS whereas a steady increase in hydrogel weight was observed in cell culture medium (**Study II**/Figure 2). The swelling ratio measurements in culture medium from both **Studies I** and **II** are shown in Figure 10. The H2 hydrogel with the ADH-derived hydrazone was the least stable, dissolving in medium after 8 hours. Overall, the hydrogels in **Study I** showed much faster and pronounced swelling in 48 hours compared to those in **Study II**, which were measured for 3 weeks. In **Study II**, the comparison of the hydrogel swelling kinetics revealed an almost linear trend in their swelling behaviour, with HA-DOPA gel swelling less than the HA-HA in the later time points. The differences in swelling stability of the hydrogels in **Studies I** and **II** can be attributed to their different initial concentration of the hydrogel components and the resulting final polymer concentration in the hydrogels. Most notably, the polymer content of the H1 hydrogel in **Study I** was almost double to that of HA-HA in **Study II**, and the higher concentration of hygroscopic HA can explain the higher water absorption.

The transparency of the hydrogels was evaluated based on transmittance of light through the hydrogels and photography, as shown in Figure 10. The HA hydrogels showed high light transmittance values, although the measurements were obtained from 10 mm thick samples in micro-cuvettes. In **Study I**, the H1-based hydrogels showed lower transmittance values than H2, which might be caused by their higher polymer concentration and crosslinking degree. Also, the addition of collagen in

H1C gel decreased light transmittance slightly. In **Study II**, both hydrogels showed over 90% transmittance over the entire spectrum, while the lower transmittance in HA-HA might be caused by the minute inhomogeneities of the gel arising from mixing the DPBS and sucrose-dissolved components.

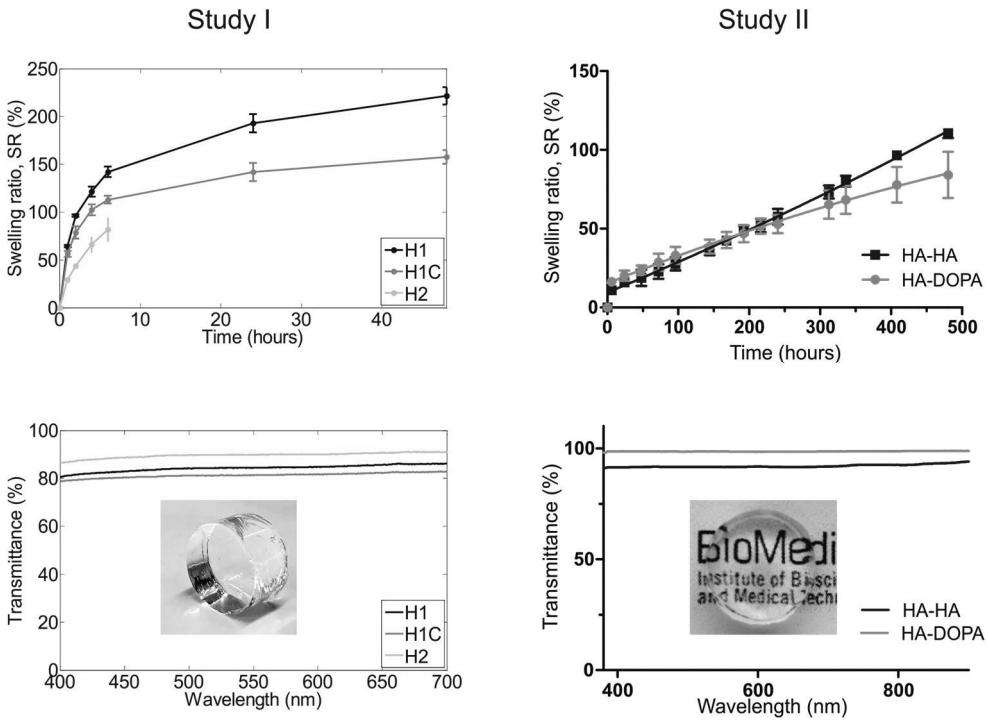


**Figure 10.** Swelling kinetics in cell culture medium and transparency of HA hydrogels. Graphs on the left refer to hydrogels of Study I and graphs on the right to Study II. Transmittance graphs also show an inset of photographed hydrogels, H1 on the left, and HA-DOPA on the right.

## 5.1.2 Cell viability

The viability of encapsulated hASC in the HA hydrogel scaffolds was evaluated qualitatively by LIVE/DEAD™ staining and quantitatively using PrestoBlue™ and CyQUANT™ analyses. The cells remained viable in all the studied hydrogels for 10 days, except for H2, which dissolved and could no longer be evaluated after 3 days in culture. In **Study I**, The PrestoBlue™ analysis of cell metabolic activity showed a drop in the cellular activity after 3 days of cell culture for both H1 and H1C gels, and a significantly higher viability for the H1C in the later timepoints than H1 (**Study I**/Figure 5). In **Study II**, the cell metabolic activity remained quite stable throughout

the culture period, with HA-DOPA showing consistently higher cell viability compared to HA-HA (**Study II**/Figure 6). Also, the number of cells determined by CyQUANT™ was higher in HA-DOPA gels with a significant difference reached on day 10 (**Study II**/Figure 6).

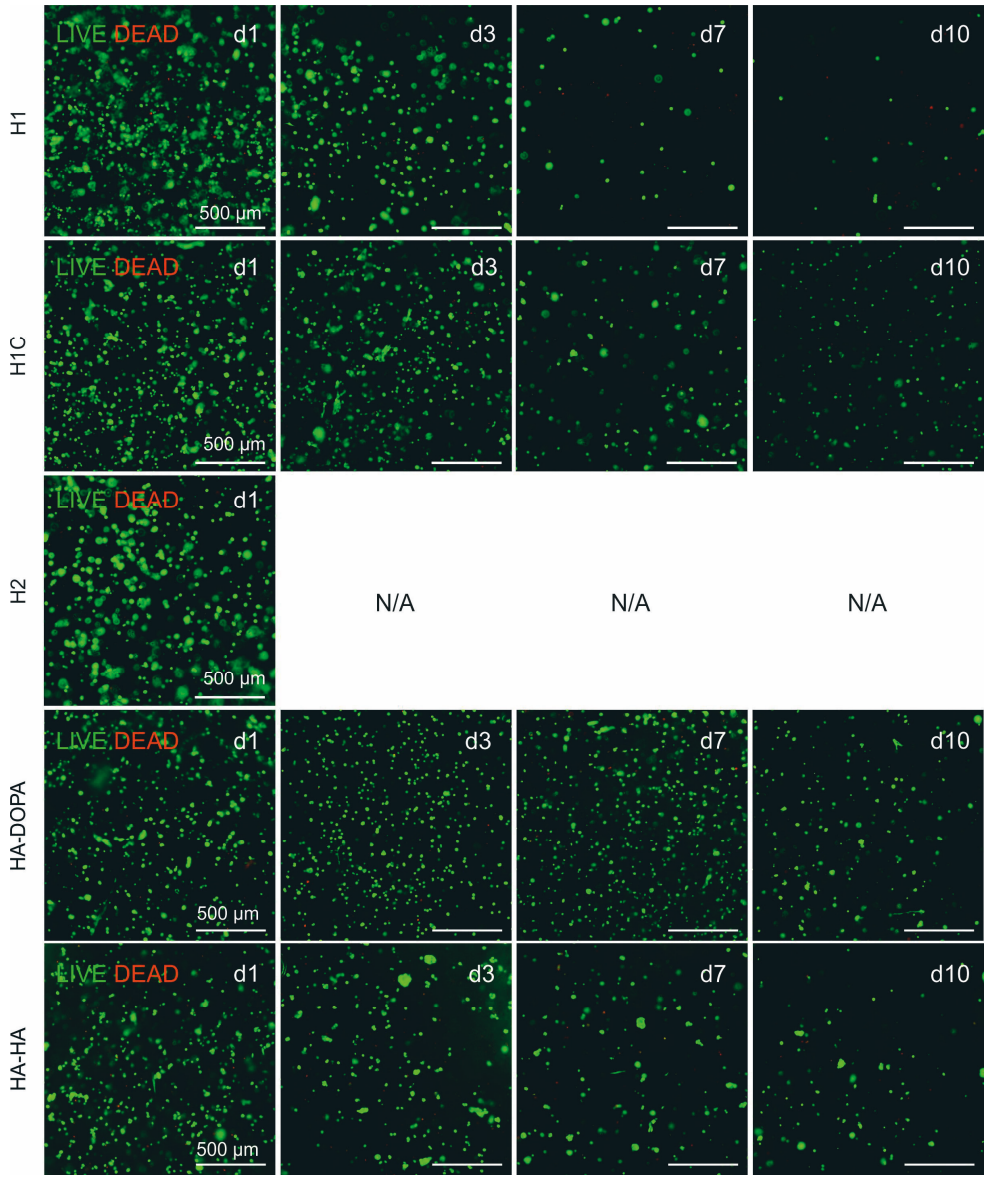


**Figure 11.** Live/dead staining of human adipose stem cells in HA hydrogels used in Studies I and II. Staining could not be performed on H2 hydrogel after the first timepoint because the gel dissolved in culture medium.

The LIVE/DEAD™ staining of the hASC in HA hydrogels (Figure 11) confirmed the high cell viability of these scaffolds. There were very few dead cells visible in the scaffolds. Although the number of live cells seemed to decrease with increased time in culture, this was partly attributed to the strong swelling of the hydrogels in medium. Also, in **Study I**, the cells were observed to escape the gels and grow underneath the surrounding PDMS structures (**Study I**/Figure 5). The LIVE/DEAD™ staining also showed that the hASCs inside the scaffolds were mostly rounded and tended to cluster together. Still, a few elongated cells were observed, especially in H1C and HA-DOPA hydrogels.

## 5.2 Creating tissue-like cellular organization

For creating cornea-mimicking cell organization in the scaffolds, the hASCs needed to be compartmentalized within the structure and the hPSC-LESCs on the surface. Two different approaches were used for achieving this type of cellular organization, surface modification of hASC-encapsulated HA hydrogels (**Study II**) and 3D bioprinting of multi-layered cornea mimicking structures (**Study III**).

### 5.2.1 Surface modification for improving hPSC-LESC attachment

As unmodified HA hydrogels are poor substrates for cell culture, covalent surface modification using extracellular matrix proteins was performed to improve the growth of hPSC-LESCs on the HA scaffolds. The dopamine moiety in the HA-DOPA was used as a modification site, since it can transform to a quinone in high pH, which in turn can react with terminal thiol (–SH) groups. Two different extracellular matrix derivatives were studied for the covalent surface modification, synthetic laminin-derived peptides with a terminal cysteine (CDPGYIGSR) and thiolated Col IV. Although the laminin peptide was effectively conjugated to the hydrogel surface (**Study II**/Figure 4), it did not support the attachment of hPSC-LESCs (**Study II**/Figure 5). However, thiolated Col IV (Col IV-SH) showed clear improvement of hPSC-LESC attachment and maintained their growth for 7 days, compared to both HA-HA gel with Col IV-SH and HA-DOPA with non-thiolated Col IV (Figure 12). The localization of the Col IV on the surface of the hydrogels was verified from cryosections of the hydrogels with encapsulated hASCs and hPSC-LESCs plated on the surface (Figure 12). The hPSC-LESCs cultured on the surface-

modified HA scaffolds also maintained their progenitor marker expression, which was verified by immunofluorescent staining of p63α and p40 (**Study II**/Figure 6).

### 5.2.2 3D bioprinted cornea-mimicking structures

Structures with corneal tissue-like cell organization were manufactured also using laser-assisted 3D bioprinting (**Study III**). The bioinks were optimized separately for both cell types and consisted mainly of human recombinant laminin and CnT-30 medium for hPSC-LESCs and of human Col I, plasma and thrombin for hASCs. Both cell types were bioprinted separately to observe their viability, morphology and marker expression and, finally, cornea-mimicking structures were printed with both cell types in their respective bioinks. The viability of the hPSC-LESCs was high after printing and they maintained their proliferative capacity until day 7 (**Study III**/Figure 2). Also, they showed typical epithelial morphology and progenitor cell marker p63α and p40 expression (Figure 12). Importantly, by day 12 the bioprinted hPSC-LESCs showed maturation with stratification and polarization of the epithelium. The matured epithelium displayed basal expression of p63α and p40 and topical expression of corneal epithelial marker CK3 (**Study III**/Figure 3).

The bioprinted hASCs also showed excellent viability after printing (**Study III**/Figure 4 and Figure 12). The 3D printed stromal structures were created by printing the hASCs in alternating directions, and the cells showed elongated morphology and grew in orthogonally aligned layers similarly as corneal keratocytes in the native stroma (Figure 12). During prolonged culture, the bioprinted stromal structures compacted to a final thickness of 300 μm. Compaction was also observed as shrinkage of the printed structures, which could be avoided by printing the stromal structures onto Matriderm® supportive sheets. However, the Matriderm® supportive sheet was hardly an optimal printing substrate, as it was not transparent and the bioprinted structures could not be separated from it without damaging them.

By bioprinting the hPSC-LESCs on top of the bioprinted stromal structures, 3D cornea-mimicking structures were produced. In production of these structures, substituting Matrigel® as the absorption layer instead of gold, it was possible to get rid of the discoloration caused by embedded gold particles. Although the structures were not fully transparent, text was still discernible beneath them (**Study III**/Figure 8). These hASC and hPSC-LESC -containing structures maintained the layered organization resembling the anterior cornea (Figure 12). However, the cell density especially in the bioprinted stroma was much higher than in the native cornea.

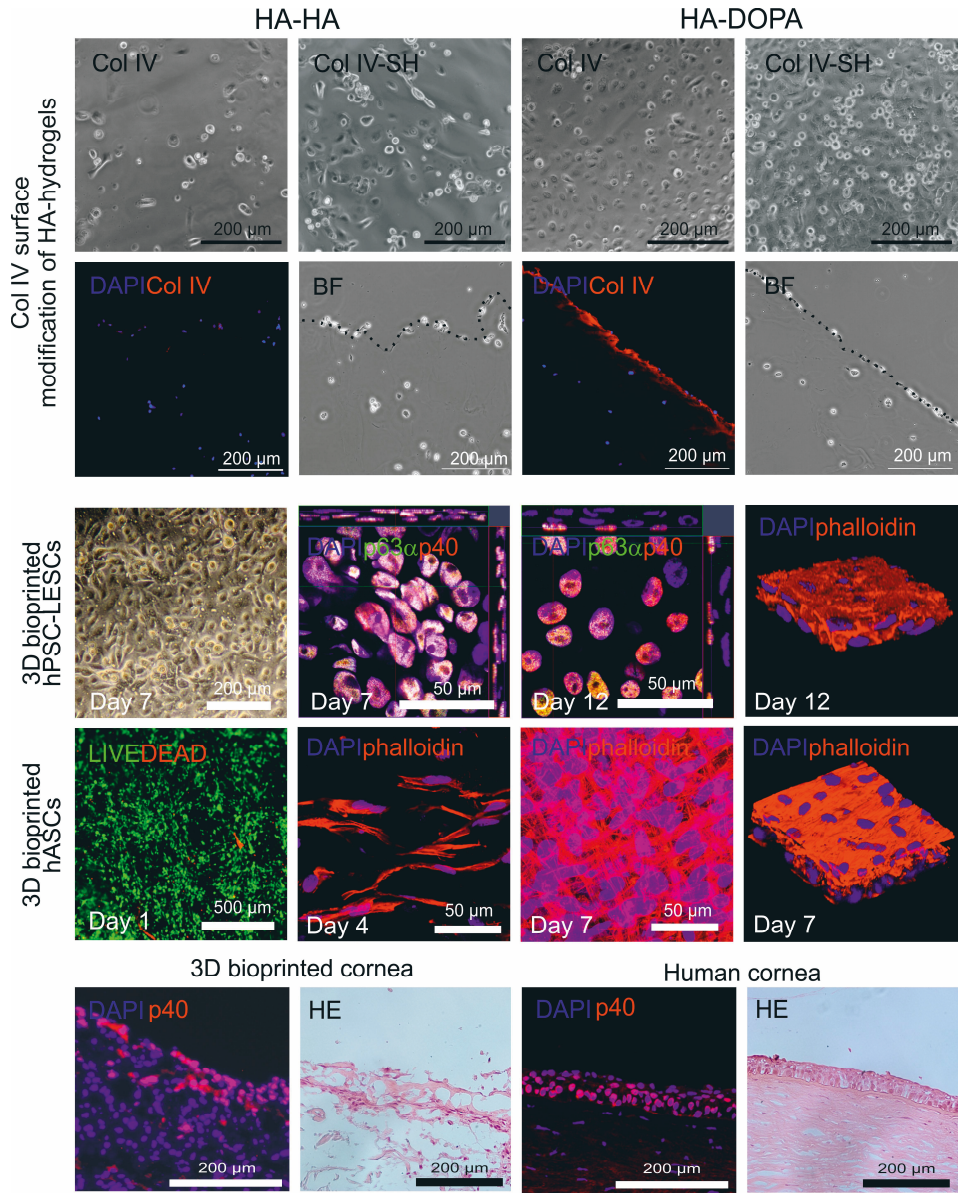


**Figure 12.** Corneal tissue-like cellular organization was achieved by collagen type IV (Col IV) surface modification of HA-based hydrogels (Study II, top panel) and using 3D bioprinting (Study III, middle and bottom panels). In Study II, the thiol-modified Col IV (Col IV-SH) on HA-DOPA gel showed the best hPSC-LESC attachment and the successful covalent binding to HA-DOPA surface was verified by immunofluorescent staining. In Study III, both hPSC-LESCs and hASC remained viable after printing, and the printed structures matured in culture. The bioprinted hPSC-LESCs showed polarized expression of progenitor markers and hASCs produced orthogonally aligned layers. The bioprinted corneal structures with both cell types resembled the architecture of human corneal tissue.

## 5.3 Proof-of-concept in the porcine *ex vivo* model

Each of the produced scaffolds was evaluated for their implantation strategy and tissue integration in a porcine *ex vivo* cornea model (**Studies I-III**). In **Study I**, the hASCs in HA hydrogels were delivered to the stromal defects in the *ex vivo* model as injectable hydrogels, i.e. the hydrogels with hASCs were manufactured directly into cavities made in the corneal stroma. From the histological evaluation, it was apparent, that the hASCs could migrate from the hydrogels into the surrounding stroma, although the hydrogels themselves were lost during tissue processing (**Study I**/Figure 6). Additionally, the histological sections showed that the porcine epithelium had grown over the injected hydrogels.

The proof-of-concept implantation of the hydrogel scaffolds with hASCs and hPSC-LESC proved more successful in **Study II**, where trephined implants from prefabricated scaffolds could simply be placed into the stromal defects. The tissue-adhesive nature of the HA-DOPA implants allowed these implants to remain in tight contact with the surrounding tissue (**Study II**/Figure 7). Human cells were identified both on top of the scaffolds as well as inside them. In **Study II**, we also tested the differentiation capacity of the hASC towards keratocytes after *ex vivo* implantation. After 10 days in culture with a keratocyte differentiation medium, the hASCs showed increased expression of lumican in both HA-HA and HA-DOPA, although other differentiation markers were not detected (**Study II**/Figure 6). The differentiation study was not remotely conclusive but at least provided some validation that the hydrogels would allow hASCs to differentiate similarly as in 2D conditions *in vitro*.

In **Study III**, the 3D bioprinted stromal structures with hASCs were implanted into the *ex vivo* cornea model. As the bioprinted stromal structures also contained the Matriderm® support structure, the structures were placed into the stromal defects with the printed hASCs facing downwards. Cells from the printed structures attached themselves to the defect site and were seen migrating into the surrounding stroma (**Study III**/Figure 7). Furthermore, the implantation was an indication of the robustness of the bioprinted structures, as the bioprinted structures were successfully shipped live from Germany to Finland only two days after their production.

# 6 DISCUSSION

## 6.1 Hydrogels as corneal scaffolds

Hydrogels offer many attractive properties for tissue engineering, such as their good transparency, efficient nutrient diffusion and capacity to encapsulate cells with high viability into a 3D environment resembling the natural ECM (Baroli, 2007). This dissertation explored different methods of applying hydrogel-based materials as tissue-engineered corneal scaffolds for hASCs and hPSC-LESCs. In **Study I**, HA-based hydrogels were studied as scaffolds for hASC encapsulation *in vitro*, and as injectable cell delivery materials *ex vivo*. In **Study II**, dopamine-modified HA hydrogels was used to fabricate hydrogel structures with encapsulated hASCs and a layer of hPSC-LESCs on their surface, that demonstrated improved stability *in vitro* and good transplantation potential *ex vivo*. In **Study III**, hydrogel-based bioinks were used to create layered structures of hASCs and hPSC-LESCs using laser-assisted 3D bioprinting, that accomplished significant structural and biological mimicry of corneal tissue.

The cornea is an exceptionally strong tissue, with complex viscoelastic mechanical properties (Hjortdal, 1996). Although hydrogels are inherently weak materials, many hydrogel-based approaches still aim at replicating the mechanical properties of corneal tissue by utilizing excessive crosslinking or dehydration-driven compaction of the structure, for example via vitrification (Majumdar et al., 2018; Rafat et al., 2008). The biomaterials produced in this manner do not allow cell encapsulation within the hydrogels due to their harsh reaction conditions or toxic crosslinkers but rely only on the recruitment of cells from the surrounding cornea. For example, EDC/NHS crosslinked recombinant human collagen-based acellular stromal replacements have shown capacity to restore transparency of the stroma, with successful infiltration of corneal nerves and keratocytes over a 4-year follow-up (Fagerholm et al., 2014). The slow ECM turnover of native stromal keratocytes makes the integration and degradation of cell-free scaffolds slow, with remnants of the implants still present even 4 years after implantation (Fagerholm et al., 2014). However, this slow remodelling might be advantageous for stable stromal

regeneration, as fast ECM production in the cornea is associated with stromal haze and scar tissue formation (Wilson et al., 2012a).

Cell-based approaches can increase the rate of tissue regeneration but require careful selection of therapeutic cells to obtain the wanted results. MSCs have been shown to suppress corneal scar tissue formation and have the ability to differentiate into functional keratocytes, supporting their use in corneal regeneration (Dos Santos et al., 2019; Mittal et al., 2016). Accordingly, our approach was not to recreate the mechanical strength of the cornea, but rather to use hASCs inside hydrogel scaffolds to support cellular remodelling after implantation to the cornea through direct differentiation towards corneal keratocytes, paracrine stimulation of epithelial and stromal renewal and modulation of the immune response against allogeneic LESCs. Although this was the underlying hypothesis behind the scaffold development, it still lacks validation in the *in vivo* context. Further investigations could be conducted, for example, *in vitro* to study the activation of immune cells in the presence of hASCs or stain for newly synthesized or remodelled ECM in the *ex vivo* model.

Hydrogel scaffolds are typically used for 3D encapsulation and culture of cells. However, engineering the corneal tissue architecture requires combining a 3D matrix for stromal cells and 2D surface for epithelial cells. Only a few methods for obtaining such corneal tissue-like organization with one material have been previously reported, with collagen (Kureshi et al., 2015; Lee et al., 2018), fibrin-agarose (González-Andrades et al., 2017) and a combination of cast silk films and fibrous silk (Bray et al., 2013). In **Study II**, we were able to recreate this tissue-like cell organization by culturing hPSC-LESCs on the surface of hASC-encapsulated HA-DOPA hydrogels, aided by covalent binding of Col IV to the hydrogel surface. The two cell types were also bioprinted into correct tissue-mimicking structures (**Study III**), which hasn't been previously demonstrated.

A general drawback of hydrogels as 3D cell culture scaffolds is their lack of directionality in guiding cell growth. In the native corneal stroma, cells grow in orthogonal layers between the collagen lamellae. This type of cellular alignment could not be achieved by simple encapsulation of hASCs inside HA hydrogels. To increase the layered organization of hASCs, guiding structures, such as fibres could be introduced to the hydrogels (Kong et al., 2020; Wilson et al., 2012b). However, incorporating such orthogonally arranged fibres can compromise the transparency of the hydrogel, and be labour-intensive to manufacture. Alternatively, such orthogonal cell alignment of hASCs resembling the native stromal organization was achieved with laser-assisted 3D bioprinting simply by changing the printing direction between layers (**Study III**).

### 6.1.1 HA-based scaffolds for corneal regeneration

Many of the studied hydrogels and culture substrates for corneal applications to date have been based on collagen, because it is the principal component of the corneal stroma (Ahearne et al., 2020; Chen et al., 2018). Although HA has been identified to play a role in the limbal niche regulation it has not been widely used for corneal tissue engineering due to its poor mechanical properties and low cell adhesion (Fiorica et al., 2011; Gesteira et al., 2017). The HA hydrogels utilized in **Studies I** and **II** were based on the bio-orthogonal hydrazone reaction, which occurs rapidly in mild reaction conditions, without the need for any toxic crosslinking agents and produces only water as a by-product. The hydrazone bond is dynamic by nature, allowing it to reorganize in the presence of proteins. Expectedly, the ADH-derived hydrazone crosslinked HA hydrogels were more susceptible to degradation than the resonance-stabilized CDH-derived hydrazones (Oommen et al., 2013). The stability of the hydrazone-bonded hydrogels was increased by additional crosslinking. In **Study I**, the additional Col I component had the capacity to form imine bonds with the aldehyde groups, whereas in **Study II**, the dopamine moieties could self-polymerize for stabilizing effect.

Despite being a component of the natural ECM, HA does not contain binding sites for integrin receptors, which are required for focal adhesion-mediated signalling for cell survival (Wang et al., 2010). This causes encapsulated cells to remain rounded and inhibits cell growth on their surface. The attachment and elongation of hASCs in 3D scaffolds is essential for their survival and differentiation (Wang et al., 2010). The addition of gelatin or RGD peptides into HA-based hydrogel introduces integrin binding sites and increases cell attachment inside these scaffolds (Chen et al., 2017; Espandar et al., 2012; Zarembinski et al., 2014). In **Study I**, the addition of Col I to the hydrogels produced a similar effect and increased cell elongation in these gels. Encapsulated cells can also secrete their own ECM molecules to create attachment sites for themselves (Loebel et al., 2019). This can drive cell elongation in hydrogels, which do not otherwise contain cell binding sites. In **Study II**, the dopamine moieties seemed to promote the entrapment of secreted endogenous ECM proteins, which would explain the more elongated cell morphology in HA-DOPA hydrogels compared to the HA-HA gels.

## 6.2 Estimating clinical translation of corneal scaffolds

Currently, the treatment of LSCD and its related corneal scarring involves two separate surgeries, first a LESC transplantation (e.g. CLET, SLET or CLAU) later followed by anterior lamellar or penetrating keratoplasty (Behaegel et al., 2019). The aim of this dissertation was to develop methods for simultaneous treatment of both the epithelium and the stromal layers, which would not only reduce the number of surgeries for the patient, but also the need for corneal donor tissue. Ideally, the methods developed in this dissertation could be utilized for providing allogeneic on-demand or off-the-shelf regenerative therapies for patients suffering from LSCD despite a lack of their own LESCs or available donor tissue. With the aim of developing these kinds of regenerative therapies, the clinical suitability of both the therapeutic cells and biomaterial scaffolds should be carefully considered.

An important property of these types of material and cell -based therapies, often overlooked, is their suitability for transplantation in terms of implantation strategies. The translation of research from *in vitro* to *in vivo* can be challenging, and the wasted efforts are costly and time-consuming. As an intermediate step, the *ex vivo* cornea model provides a low-cost and ethical model to evaluate the clinical applicability of cell delivery scaffolds. The porcine corneas, which were obtained as meat processing by-products from a local abattoir, recapitulate the essential physiological characteristics of the human cornea (Notara et al., 2011). However, the excised corneas cannot be used to model the immune responses or inflammation of the LSCD, necessitating the use of whole organism animal models to eventually study the safety and efficacy of cell and biomaterial constructs.

One of the aims of this dissertation was to study the applicability of the developed corneal scaffolds in the *ex vivo* porcine corneal model. This was an important driver for considering suitable transplantation methods for each scaffold. In **Study I**, for example, the excessive swelling of the scaffolds *in vitro* required them to be used as injectable cell delivery vehicles. Interestingly, the *ex vivo* evaluation of these hydrogels showed successful hASC outgrowth to the stroma and overgrowth of porcine epithelium over the wound site, indicating that their clinical potential for cell delivery was considerable despite their lack of *in vitro* stability. The hASC outgrowth observed *ex vivo* in **Study I** was also interesting when comparing to previously studied injectable HyStem™ hydrogels, which did not allow cellular migration from implanted hydrogels *in vivo* even after 10 weeks (Espandar et al., 2012).

The *ex vivo* model was also an appropriate tool to implement the sutureless implantation strategy of the tissue-adhesive hydrogels in **Study II**. Tissue-adhesive

materials are attractive for corneal implantation, because the use of sutures can induce neovascularization and astigmatism (Griffith et al., 2016). Although tissue-adhesive materials based on dopamine have been developed previously (Lee et al., 2010; Shin et al., 2015), this was among the first applications of preformed hydrogels with tissue-adhesive function and encapsulated cells. As an additional advantage, the HA-DOPA hydrogel scaffolds did not exhibit the characteristic brown coloration of polymerized dopamine, which would not be suitable for corneal applications (Dinh et al., 2018; Shin et al., 2015).

The *ex vivo* implantation of the bioprinted stromal structures in **Study III** was also performed without sutures, simply by fitting the trephined structures into corneal wounds with the same dimensions. Because of the underlying Matriderm® sheets used as printing substrates, the bioprinted stromal constructs were placed into the stroma "upside down". For transplantation of the layered stroma-and-epithelium structure, other removable substrates should be considered. The hASCs in the structures adhered to the stromal wound bed, which was enough in the stationary *ex vivo* condition. However, this implantation strategy would not be adequate in a real-life situation, where suturing would likely be needed for fixation of the structure. Alternatively, bioinks utilizing the tissue-adhesive dopamine units could be explored as the next step for manufacturing bioprinted corneal structures.

### 6.2.1 Clinically relevant raw materials

With the aim of producing corneal scaffolds suitable for clinical applications, the use of poorly defined and animal-derived components was avoided. Starting from the cell production, the differentiation process of the hPSC-LESCs has been optimized to be as defined as possible without feeder cells or xenogeneic components (Hongisto et al., 2017). In the LESC production protocol, the only animal-derived component is heparin in the CnT-30 differentiation medium. Although human serum was used in the culture of hASCs, the conditions could be further modified to a more defined serum-free culture (Patrikoski et al., 2013). Only human-based collagens, human plasma and thrombin, and human recombinant laminins were used in the production of the biomaterial scaffolds and the bioinks. Hyaluronic acid, despite being of bacterial origin, is a known and accepted component of many medical products from dermal fillers to eye drops. Although animal-derived materials can also be approved for clinical use, their origin must be well documented and quality controlled (Lagali, 2020). More importantly, the use of any biologically

isolated material, animal or human, is subject to batch-to-batch variation, which can cause unwanted variability in the already complex tissue-engineered constructs.

### 6.2.2 Clinical applications of human stem cells

Another aspect of the clinical significance is functionality of the therapeutic cells. As a non-corneal alternative to regenerative stromal cells, hASCs offer an abundant source of clinically relevant multipotent stem cells. Although they can be easily isolated and expanded for autologous use, their immunomodulatory properties have great benefits in allogeneic therapy, for example in treating graft-vs-host disease (Lindroos et al., 2011). In this dissertation, the rationale of using hASCs without any *in vitro* differentiation prior to their encapsulation, was to rely on their *in vivo* differentiation capability while benefitting from their immunomodulatory properties. This could also be advantageous in transplanting allogeneic hPSC-derived LESCs to patients suffering from LSCD, to hinder possible immune responses. **Study II** also aimed to provide experimental evidence of hASC differentiation of the towards corneal keratocytes in the *ex vivo* model, but their differentiation efficacy remained poor in the study conditions. However, this might have been caused by the short differentiation time, or it might simply be a property of the particular cell line, as the hASCs used in this dissertation were obtained from a single donor. Human ASCs can have significant variability in their differentiation tendency towards certain lineages depending on the donor, which is why differentiation studies should be conducted for more cell lines for more conclusive results (Patrikoski et al., 2013).

The transplantation of autologous LESCs is the current golden standard in treatment of LSCD. For patients suffering from bilateral LSCD, autologous LESCs are not available, and allogeneic primary LESCs or limbal transplants can be an option. Compared to the scarcely available primary LESCs, the hPSC-derived LESCs offer theoretically unlimited amounts of therapeutic cells. Using proteomic profiling, our group has previously shown that the hPSC-LESCs are very similar to primary human LESCs (Mikhailova et al., 2015). With further improvement of the cell production to xenogeneic component and feeder cell -free methods, these cells are consistent in quality and easily ungraded to clinical grade manufacturing (Hongisto et al., 2017).

The hPSC-LESCs used in this dissertation were produced from hESCs. However, LESCs differentiated from iPSCs would more likely to reach clinical

translation in the future, as they face fewer ethical issues than ESCs, and iPSC-donors can be screened for suitable tissue immune phenotypes for matching cell lines to patients (Taylor et al., 2012; Taylor et al., 2005). The need for immunophenotype matching is one of the key questions in allogeneic cell therapies. Although the cornea is typically an immune privileged site due to its avascular nature, severe inflammation and neovascularization characteristic to LSCD can cause adverse reactions to foreign cells. Tapered dosing of immunosuppressive medication, similarly as with non-related donor limbal transplantations, might be required to preserve transplanted cells until full regeneration and normal barrier function of the cornea is re-established (Holland et al., 2012). Hopefully, the first clinical trial using hiPSC-derived corneal epithelial cells for bilateral LSCD will provide more insights on the issues of allogeneic stem cells, immunophenotype matching and immunosuppression (Osaka University, 2019).

## 6.3 3D bioprinting as manufacturing method

Most of the potential of 3D printing technologies lies in the production of complex shapes and rapid manufacturing of individual designs. Using patient-specific digital data, for example from computed tomography (CT) scans, personalized tissues can be produced with 3D bioprinting (Isaacson et al., 2018; Lee et al., 2019). However, printing 3D shapes of organs, such as the heart, with low-viscosity hydrogel materials requires additional support to stabilize the printed strands, such as printing into a gelatine slurry in the FRESH (freeform reversible embedding of suspended hydrogels) method (Lee et al., 2019).

When it comes to the cornea, the layered structure of the native tissue is relatively simple. In **Study III**, this was achieved by printing alternating cellular and acellular layers of bioink, and bioinks with two different cell types. Also, the printing process allowed to recapitulate the orthogonal lamellar alignment of the corneal stroma by changing the printing direction between the layers, which has been difficult to produce using conventional technologies. However, the bioprinted cornea-mimicking structures were produced on a flat surface, missing the curved shape of the actual native cornea. Previously, the bioprinting of curved corneal constructs has been shown with the aid of a hollowed out plastic support (Isaacson et al., 2018). Although curvature was overlooked in the development of the corneal scaffolds in this dissertation, it has been shown to play an important role in keratocyte differentiation (Gouveia et al., 2017b) while correct curvature is important for the

visual acuity of a patient (Brunette et al., 2017), making it important to address this issue in further development of these constructs.

The maturation of 3D bioprinted tissues is a key aspect of manufacturing functional tissues. Maturation includes cellular remodelling of the printed construct, which often remains unstudied in the literature (Malda et al., 2013; Mandrycky et al., 2016). In **Study III**, the maturation of the bioprinted cornea-mimicking structures was observed clearly as compaction of the printed stromal structures and the polarization of the printed epithelium 1–2 weeks after printing. However, upon maturation and cellular remodelling, the constructs also showed some shrinkage unless a supportive sheet was used as a printing substrate.

In the recent years, the field of 3D bioprinting has grown rapidly and commercial players are emerging also in the field of corneal bioprinting. These are mostly research-based spin-offs, such as iFix Medical (Australia), originated from University of Sydney and University of Wollongong, which has developed a handheld "bioprinting" device for directly extruding a transparent bioink into corneal wounds (iFix Medical Pty Ltd., 2019; Sutton et al., 2018). Another university spin-off 3D Biotissues (UK, Newcastle University) aims to manufacture 3D bioprinted curved corneal replacements based on patient corneal dimensions (3D Biotissues Limited, 2019; Isaacson et al., 2018). Whereas the iFix pen is intended for purely biomaterial-based wound closure, 3D Biotissue's approach includes also stromal cells within the bioprinted constructs to produce alternatives to corneal transplants.

With extrusion-based methods dominating the field of commercial 3D bioprinting, the laser-assisted bioprinting has been hindered from large scale adoption by the high-cost equipment, which are usually custom built and laborious to operate (Mandrycky et al., 2016). However, with the evolution of bioprinting field, also new commercial bioprinters utilizing LaBP are becoming available (Listek, 2019). LaBP offers many advantages over other bioprinting techniques, such as high resolution, excellent cell viability, and the possibility to use also high viscosity bioinks. It is likely that the different bioprinting technologies will find their niche areas according to the intended application and specific requirements of the target tissues.

## 6.4 Future of corneal tissue engineering

With the emergence of new stem cell-based therapies on the market, off-the-shelf cell therapies for curing corneal diseases are no longer just science fiction. Because

of their well-documented immunomodulatory properties, allogeneic ASCs are already widely used in clinical trials for various disorders, although their specific mode of function is still poorly understood. However, for the allogeneic cell therapies using hPSC-derived LESCs to reach the clinics, a great deal more experience and knowledge is required of their safety and immunogenic properties. To reach the full potential of allogeneic stem cell therapies in the future, international iPSC banks with different HLA-phenotypes should be established. From these cell banks, suitable cell lines could then be selected for building patient-matched corneal replacements. Alternatively, we could see the successful adoption of the genetically modified iPSCs to generate hypoimmunogenic, or "universal", stem cells, that do not express the HLA molecules on their surface (Deuse et al., 2019).

Creation of full thickness corneal structures, including the third cell layer of the cornea, the endothelium should be developed in the future. Corneal endothelium is also an important part of a functioning cornea, and endothelial cell failure is the most common reason for corneal transplantation in the developed countries (Mathews et al., 2018). Attempts at recreating full thickness corneal structures from immortalized cell lines or isolated primary cells have been reported, but they have yet to show clinical translatability (Griffith et al., 1999; Proulx et al., 2010; Vrana et al., 2008). With the advancements in using hPSCs for corneal regeneration, also corneal endothelial cells could be differentiated from hPSCs (Hayashi et al., 2012) and combined with stromal and epithelial layers.

The evolution of 3D bioprinting methods will allow the manufacturing of increasing complexity of tissue-engineered corneal structures. In the future, the recreation of tissue microstructures, such as the limbal palisades and crypts, may give rise to unforeseen advantages of biomimicry, as the complex cellular interplay in the limbal niche is still relatively poorly understood. The creation of niche-like structures in corneal constructs might also be necessary to maintain the true limbal stem cell population and long-term regenerative capacity of the cornea (Yazdanpanah et al., 2019). Most likely, the advancement of 3D bioprinting techniques and equipment will also make the incorporation of multiple cell types easier. This would allow the addition of also other cell types found in the cornea, such as supporting niche cells, endothelial cells and nerves to make a fully functional 3D bioprinted cornea. While increasing complexity to accurately mimic corneal tissue might be the ultimate goal to push the boundaries of science, the optimal level of complexity should also be considered from the point of view of the patient. At its worst, high cellular complexity might increase the regulatory burden of such a construct and contribute to the price tag of these treatments, without additional therapeutic benefits. To

determine the optimal requirements of tissue-engineered corneal tissue equivalents, we need thorough understanding of the underlying biology of the cornea and its structural and functional components, meriting more basic research in the field.

# 7 CONCLUSIONS

The aim of this dissertation was to produce scaffolds for stem cell delivery to the cornea, providing regenerative therapies to a damaged epithelium as well as the scarred stroma underneath. Human PSC-LESCs were used as the regenerative stem cells of the corneal epithelium and hASCs as the stromal component. Based on the results of these studies, the following conclusions can be drawn:

1. Hydrazone-crosslinked hyaluronic acid hydrogels provided suitable matrices for hASC delivery to the corneal stroma.
    - The addition of collagen or dopamine units promoted cellular elongation within the hydrogels.
    - Hydrogels with poor *in vitro* stability could be used as injectable cell delivery vehicles to corneal stromal defects and allowed hASC outgrowth and corneal epithelial wound healing in an *ex vivo* corneal model.
2. Covalent surface conjugation of collagen IV was necessary for establishing an epithelium layer on top of hyaluronic acid hydrogels.
    - pH-induced quinone formation of dopamine moieties and thiol-modified collagen IV were required for successful covalent surface modification of hydrogels.
    - Cysteine-terminated laminin-mimetic peptide did not support the attachment and growth of hPSC-LESCs.
3. Preformed hydrogel scaffolds with encapsulated hASCs within the hydrogel and hPSC-LESCs on top were successfully implanted into corneal defects in an *ex vivo* corneal model
    - The tissue-adhesive capacity of the preformed hydrogels allowed the implants to stay in tight contact with the surrounding tissue.

4. Laser-assisted 3D bioprinting was successfully used to produce layered cornea-mimicking structures comprising of the two cell types.
    - Orthogonally aligned cell organization was achieved in the 3D bioprinted corneal stromal-mimicking constructs.
    - 3D bioprinted hPSC-LESCs matured into a stratified epithelium with basal expression of limbal progenitor markers p63α and p40 and apical expression of mature epithelium marker CK3.
    - Bioprinted constructs were sufficiently robust to withstand shipment and implantation into an *ex vivo* corneal model.

# REFERENCES


3D Biotissues Limited, 2019 3D Bio-Tissues https://www.3dbiotissues.com/ *Accessed 5 Mar 2020*

Abahussin, M., Hayes, S., Cartwright, N. E. K., Kamma-Lorger, C. S., Khan, Y., Marshall, J. & Meek, K. M. (2009). 3D collagen orientation study of the human cornea using X-ray diffraction and femtosecond laser technology. *Investigative Ophthalmology & Visual Science, 50*(11), 5159-5164.

Ahearne, M., Fernández-Pérez, J., Masterton, S., Madden, P. W. & Bhattacharjee, P. (2020). Designing Scaffolds for Corneal Regeneration. *Advanced Functional Materials, n/a*, 1908996.

Ahmad, S., Stewart, R., Yung, S., Kolli, S., Armstrong, L., Stojkovic, M., Figueiredo, F. & Lako, M. (2007). Differentiation of human embryonic stem cells into corneal epithelial-like cells by in vitro replication of the corneal epithelial stem cell niche. *Stem Cells, 25*(5), 1145-1155.

Alió del Barrio, J., El Zarif, M., De Miguel, M. P., Azaar, A., Makdissy, N., Harb, W., El Achkar, I., Arnalich-Montiel, F. & Alió, J. L. (2017). Cellular therapy with human autologous adipose-derived adult stem cells for advanced keratoconus. *Cornea, 36*(8), 952-960.

Angelats Lobo, D., & Ginestra, P. (2019). Cell Bioprinting: The 3D-Bioplotter™ Case. *Materials, 12*(23), 4005.

Aravena, C., Yu, F. & Aldave, A. J. (2018). Long-term visual outcomes, complications, and retention of the Boston type I keratoprosthesis. *Cornea, 37*(1), 3-10.

Arnalich-Montiel, F., Pastor, S., Blazquez-Martinez, A., Fernandez-Delgado, J., Nistal, M., Alio del Barrio, J. & De Miguel, M. P. (2008). Adipose-Derived Stem Cells Are a Source for Cell Therapy of the Corneal Stroma. *Stem Cells, 26*(2), 570-579.

Axpe, E., & Oyen, M. L. (2016). Applications of alginate-based bioinks in 3D bioprinting. *International Journal of Molecular Sciences, 17*(12), 1976.

Azuara-Blanco, A., Pillai, C. T. & Dua, H. S. (1999). Amniotic membrane transplantation for ocular surface reconstruction. *British Journal of Ophthalmology, 83*(4), 399-402.

Azuma, K., & Yamanaka, S. (2016). Recent policies that support clinical application of induced pluripotent stem cell-based regenerative therapies. *Regenerative Therapy, 4*, 36-47.

Bandeira, F., Goh, T., Setiawan, M., Yam, G. H. & Mehta, J. S. (2020). Cellular therapy of corneal epithelial defect by adipose mesenchymal stem cell-derived epithelial progenitors. *Stem Cell Research & Therapy, 11*(1), 1-13.

Baradaran-Rafii, A., Ebrahimi, M., Kanavi, M. R., Taghi-Abadi, E., Aghdami, N., Eslani, M., Bakhtiari, P., Einollahi, B., Baharvand, H. & Javadi, M. (2010). Midterm outcomes of autologous cultivated limbal stem cell transplantation with or without penetrating keratoplasty. *Cornea, 29*(5), 502-509.

Barbaro, V., Testa, A., Di Iorio, E., Mavilio, F., Pellegrini, G. & De Luca, M. (2007). C/EBPδ regulates cell cycle and self-renewal of human limbal stem cells. *The Journal of Cell Biology, 177*(6), 1037-1049.

Baroli, B. (2007). Hydrogels for tissue engineering and delivery of tissue-inducing substances. *Journal of Pharmaceutical Sciences, 96*(9), 2197-2223.

Basu, S., Sureka, S. P., Shanbhag, S. S., Kethiri, A. R., Singh, V. & Sangwan, V. S. (2016). Simple Limbal Epithelial Transplantation: Long-Term Clinical Outcomes in 125 Cases of Unilateral Chronic Ocular Surface Burns. *Ophthalmology, 123*(5), 1000-1010.

Basu, S., Hertsenberg, A. J., Funderburgh, M. L., Burrow, M. K., Mann, M. M., Du, Y., Lathrop, K. L., Syed-Picard, F. N., Adams, S. M. & Birk, D. E. (2014). Human limbal biopsy–derived stromal stem cells prevent corneal scarring. *Science Translational Medicine, 6*(266), 266ra172.

Baylis, O., Figueiredo, F., Henein, C., Lako, M. & Ahmad, S. (2011). 13 years of cultured limbal epithelial cell therapy: a review of the outcomes. *Journal of Cellular Biochemistry, 112*(4), 993-1002.

Behaegel, J., Zakaria, N., Tassignon, M., Leysen, I., Bock, F., Koppen, C. & Dhubhghaill, S. N. (2019). Short-and Long-Term Results of Xenogeneic-Free Cultivated Autologous and Allogeneic Limbal Epithelial Stem Cell Transplantations. *Cornea, 38*(12), 1543-1549.

Bektas, C. K., & Hasirci, V. (2020). Cell loaded 3D bioprinted GelMA hydrogels for corneal stroma engineering. *Biomaterials Science, 8*(1), 438-449.

Bektas, C. K., Burcu, A., Gedikoglu, G., Telek, H. H., Ornek, F. & Hasirci, V. (2019). Methacrylated gelatin hydrogels as corneal stroma substitutes: in vivo study. *Journal of Biomaterials Science, Polymer Edition, 30*(18), 1803-1821.

Betsch, M., Cristian, C., Lin, Y., Blaeser, A., Schöneberg, J., Vogt, M., Buhl, E. M., Fischer, H. & Duarte Campos, D. F. (2018). Incorporating 4D into bioprinting: Real-time magnetically directed collagen fiber alignment for generating complex multilayered tissues. *Advanced Healthcare Materials, 7*(21), 1800894.

Bobba, S., Di Girolamo, N., Mills, R., Daniell, M., Chan, E., Harkin, D. G., Cronin, B. G., Crawford, G., McGhee, C. & Watson, S. (2017). Nature and incidence of severe limbal stem cell deficiency in Australia and New Zealand. *Clinical & Experimental Ophthalmology, 45*(2), 174-181.

Bongiorno, T., Chojnowski, J., Lauderdale, J. & Sulchek, T. (2016). Cellular Stiffness as a Novel Stemness Marker in the Corneal Limbus. *Biophysical Journal, 111*(8), 1761-1772.

Bosworth, L. A., Turner, L. & Cartmell, S. H. (2013). State of the art composites comprising electrospun fibres coupled with hydrogels: a review. *Nanomedicine: Nanotechnology, Biology and Medicine, 9*(3), 322-335.

Bouhadir, K. H., Hausman, D. S. & Mooney, D. J. (1999). Synthesis of cross-linked poly (aldehyde guluronate) hydrogels. *Polymer, 40*(12), 3575-3584.

Bourne, W. M., Nelson, L. R. & Hodge, D. O. (1997). Central corneal endothelial cell changes over a ten-year period. *Investigative Ophthalmology & Visual Science, 38*(3), 779-782.

Bray, L. J., George, K. A., Suzuki, S., Chirila, T. V., & Harkin, D. G. (2013). Fabrication of a corneal-limbal tissue substitute using silk fibroin. In B. Wright, & C. Connon (Eds.), *Corneal regenerative medicine* (pp. 165-178) Springer.

Brunette, I., Roberts, C. J., Vidal, F., Harissi-Dagher, M., Lachaine, J., Sheardown, H., Durr, G. M., Proulx, S. & Griffith, M. (2017). Alternatives to eye bank native tissue for corneal stromal replacement. *Progress in Retinal and Eye Research, 59*, 97-130.

Budak, M. T., Alpdogan, O. S., Zhou, M., Lavker, R. M., Akinci, M. M. & Wolosin, J. M. (2005). Ocular surface epithelia contain ABCG2-dependent side population cells exhibiting features associated with stem cells. *Journal of Cell Science, 118*(8), 1715-1724.

Builles, N., Janin-Manificat, H., Malbouyres, M., Justin, V., Rovère, M., Pellegrini, G., . . . & Ruggiero, F. (2010). Use of magnetically oriented orthogonal collagen scaffolds for hemi-corneal reconstruction and regeneration. *Biomaterials, 31*(32), 8313-8322.

Burdick, J. A., & Prestwich, G. D. (2011). Hyaluronic acid hydrogels for biomedical applications. *Advanced Materials, 23*(12), H41-H56.

Calderón-Colón, X., Xia, Z., Breidenich, J. L., Mulreany, D. G., Guo, Q., Uy, O. M., . . . & Trexler, M. M. (2012). Structure and properties of collagen vitrigel membranes for ocular repair and regeneration applications. *Biomaterials, 33*(33), 8286-8295.

Calonge, M., Pérez, I., Galindo, S., Nieto-Miguel, T., López-Paniagua, M., Fernández, I., Alberca, M., García-Sancho, J., Sánchez, A. & Herreras, J. M. (2019). A proof-of-concept clinical trial using mesenchymal stem cells for the treatment of corneal epithelial stem cell deficiency. *Translational Research, 206*, 18-40.

Chae, J. J., McIntosh Ambrose, W., Espinoza, F. A., Mulreany, D. G., Ng, S., Takezawa, T., Trexler, M. M., Schein, O. D., Chuck, R. S. & Elisseeff, J. H. (2015). Regeneration of corneal epithelium utilizing a collagen vitrigel membrane in rabbit models for corneal stromal wound and limbal stem cell deficiency. *Acta Ophthalmologica, 93*(1), e57-e66.

Chan, A. A., Hertsenberg, A. J., Funderburgh, M. L., Mann, M. M., Du, Y., Davoli, K. A., Mich-Basso, J. D., Yang, L. & Funderburgh, J. L. (2013). Differentiation of human embryonic stem cells into cells with corneal keratocyte phenotype. *PloS One, 8*(2), e56831.

Chen, D., Qu, Y., Hua, X., Zhang, L., Liu, Z., Pflugfelder, S. C. & Li, D. Q. (2017). A hyaluronan hydrogel scaffold-based xeno-free culture system for ex vivo expansion of human corneal epithelial stem cells. *Eye, 31*(6), 962-971.

Chen, Z., You, J., Liu, X., Cooper, S., Hodge, C., Sutton, G., Crook, J. M. & Wallace, G. G. (2018). Biomaterials for corneal bioengineering. *Biomedical Materials, 13*(3), 032002.

Chen, Z., de Paiva, C. S., Luo, L., Kretzer, F. L., Pflugfelder, S. C. & Li, D. (2004). Characterization of putative stem cell phenotype in human limbal epithelia. *Stem Cells, 22*(3), 355-366.

Cheung, A. Y., & Holland, E. J. (2017). Keratolimbal allograft. *Current Opinion in Ophthalmology, 28*(4), 377-381.

Cheung, A. Y., Sarnicola, E. & Holland, E. J. (2017). Long-term ocular surface stability in conjunctival limbal autograft donor eyes. *Cornea, 36*(9), 1031-1035.

Chun, Y. S., Park, I. K. & Kim, J. C. (2011). Technique for autologous nasal mucosa transplantation in severe ocular surface disease. *European Journal of Ophthalmology, 21*(5), 545-551.

Collins, M. N., & Birkinshaw, C. (2013). Hyaluronic acid based scaffolds for tissue engineering—A review. *Carbohydrate Polymers, 92*(2), 1262-1279.

Connon, C. J., Doutch, J., Chen, B., Hopkinson, A., Mehta, J. S., Nakamura, T., Kinoshita, S. & Meek, K. M. (2010). The variation in transparency of amniotic membrane used in ocular surface regeneration. *British Journal of Ophthalmology, 94*(8), 1057-1061.

Crabb, R. A., Chau, E. P., Evans, M. C., Barocas, V. H. & Hubel, A. (2006). Biomechanical and microstructural characteristics of a collagen film-based corneal stroma equivalent. *Tissue Engineering, 12*(6), 1565-1575.

de Paiva, C. S., Chen, Z., Corrales, R. M., Pflugfelder, S. C. & Li, D. (2005). ABCG2 transporter identifies a population of clonogenic human limbal epithelial cells. *Stem Cells, 23*(1), 63-73.

DelMonte, D. W., & Kim, T. (2011). Anatomy and physiology of the cornea. *Journal of Cataract & Refractive Surgery, 37*(3), 588-598.

Deng, S. X., Borderie, V., Chan, C. C., Dana, R., Figueiredo, F. C., Gomes, J. A., Pellegrini, G., Shimmura, S., Kruse, F. E. & International Limbal Stem Cell Deficiency Working Group. (2019). Global consensus on definition, classification, diagnosis, and staging of limbal stem cell deficiency. *Cornea, 38*(3), 364-375.

Deshpande, P., McKean, R., Blackwood, K. A., Senior, R. A., Ogunbanjo, A., Ryan, A. J. & MacNeil, S. (2010). Using poly (lactide-co-glycolide) electrospun scaffolds to deliver cultured epithelial cells to the cornea. *Regenerative Medicine, 5*(3), 395-401.

Deuse, T., Hu, X., Gravina, A., Wang, D., Tediashvili, G., De, C., Thayer, W. O., Wahl, A., Garcia, J. V. & Reichenspurner, H. (2019). Hypoimmunogenic derivatives of induced pluripotent stem cells evade immune rejection in fully immunocompetent allogeneic recipients. *Nature Biotechnology, 37*(3), 252-258.

Di Girolamo, N. (2015). Moving epithelia: Tracking the fate of mammalian limbal epithelial stem cells. *Progress in Retinal and Eye Research, 48*, 203-225.

Di Iorio, E., Barbaro, V., Ruzza, A., Ponzin, D., Pellegrini, G. & De Luca, M. (2005). Isoforms of ΔNp63 and the migration of ocular limbal cells in human corneal regeneration. *Proceedings of the National Academy of Sciences, 102*(27), 9523-9528.

Dinh, T. N., Hou, S., Park, S., Shalek, B. A. & Jeong, K. J. (2018). Gelatin Hydrogel Combined with Polydopamine Coating To Enhance Tissue Integration of Medical Implants. *ACS Biomaterials Science & Engineering, 4*(10), 3471-3477.

Dos Santos, A., Balayan, A., Funderburgh, M. L., Ngo, J., Funderburgh, J. L. & Deng, S. X. (2019). Differentiation Capacity of Human Mesenchymal Stem Cells into Keratocyte Lineage. *Investigative Ophthalmology & Visual Science, 60*(8), 3013-3023.

Du, Y., Roh, D. S., Funderburgh, M. L., Mann, M. M., Marra, K. G., Rubin, J. P., Li, X. & Funderburgh, J. L. (2010). Adipose-derived stem cells differentiate to keratocytes in vitro. *Molecular Vision, 16*, 2680-2689.

Du, Y., Funderburgh, M. L., Mann, M. M., SundarRaj, N. & Funderburgh, J. L. (2005). Multipotent stem cells in human corneal stroma. *Stem Cells, 23*(9), 1266-1275.

Dua, H. S., Miri, A. & Said, D. G. (2010). Contemporary limbal stem cell transplantation–a review. *Clinical & Experimental Ophthalmology, 38*(2), 104-117.

Dua, H. S., Saini, J. S., Azuara-Blanco, A. & Gupta, P. (2000). Limbal stem cell deficiency: concept, aetiology, clinical presentation, diagnosis and management. *Indian Journal of Ophthalmology, 48*(2), 83.

Duarte Campos, D. F., Rohde, M., Ross, M., Anvari, P., Blaeser, A., Vogt, M., Panfil, C., Yam, G. H., Mehta, J. S. & Fischer, H. (2019). Corneal bioprinting utilizing collagen-based bioinks and primary human keratocytes. *Journal of Biomedical Materials Research Part A, 107*(9), 1945-1953.

Dupps, W. J., & Wilson, S. E. (2006). Biomechanics and wound healing in the cornea. *Experimental Eye Research, 83*(4), 709-720.

Dziasko, M. A., & Daniels, J. T. (2016). Anatomical Features and Cell-Cell Interactions in the Human Limbal Epithelial Stem Cell Niche. *The Ocular Surface, 14*(3), 322-330.

Eberwein, P., & Reinhard, T. (2015). Concise reviews: the role of biomechanics in the limbal stem cell niche: new insights for our understanding of this structure. *Stem Cells, 33*(3), 916-924.

Eslani, M., Haq, Z., Movahedan, A., Moss, A., Baradaran-Rafii, A., Mogilishetty, G., Holland, E. J. & Djalilian, A. R. (2017). Late acute rejection after allograft limbal stem cell transplantation: evidence for long-term donor survival. *Cornea, 36*(1), 26.

Espandar, L., Bunnell, B., Wang, G. Y., Gregory, P., McBride, C. & Moshirfar, M. (2012). Adipose-Derived Stem Cells on Hyaluronic Acid–Derived Scaffold: A New Horizon in Bioengineered Cornea. *Archives of Ophthalmology, 130*(2), 202-208.

Fagerholm, P., Lagali, N. S., Ong, J. A., Merrett, K., Jackson, W. B., Polarek, J. W., Suuronen, E. J., Liu, Y., Brunette, I. & Griffith, M. (2014). Stable corneal regeneration four years after implantation of a cell-free recombinant human collagen scaffold. *Biomaterials, 35*(8), 2420-2427.

Fagerholm, P., Lagali, N. S., Merrett, K., Jackson, W. B., Munger, R., Liu, Y., Polarek, J. W., Söderqvist, M. & Griffith, M. (2010). A biosynthetic alternative to human donor tissue for inducing corneal regeneration: 24-month follow-up of a phase 1 clinical study. *Science Translational Medicine, 2*(46), 46ra61.

Fasolo, A., Pedrotti, E., Passilongo, M., Marchini, G., Monterosso, C., Zampini, R., Bohm, E., Birattari, F., Franch, A. & Barbaro, V. (2017). Safety outcomes and long-term effectiveness of ex vivo autologous cultured limbal epithelial transplantation for limbal stem cell deficiency. *British Journal of Ophthalmology, 101*(5), 640-649.

Fernandez-Buenaga, R., Aiello, F., Zaher, S. S., Grixti, A. & Ahmad, S. (2018). Twenty years of limbal epithelial therapy: an update on managing limbal stem cell deficiency. *BMJ Open Ophthalmology, 3*(1), e000164.

Fernández-Pérez, J., Kador, K. E., Lynch, A. P. & Ahearne, M. (2020). Characterization of extracellular matrix modified poly(ε-caprolactone) electrospun scaffolds with differing fiber orientations for corneal stroma regeneration. *Materials Science and Engineering: C, 108*, 110415.

Figueira, E. C., Di Girolamo, N., Coroneo, M. T. & Wakefield, D. (2007). The phenotype of limbal epithelial stem cells. *Investigative Ophthalmology & Visual Science, 48*(1), 144-156.

Fini, M. E. (1999). Keratocyte and fibroblast phenotypes in the repairing cornea. *Progress in Retinal and Eye Research, 18*(4), 529-551.

Fiorica, C., Senior, R. A., Pitarresi, G., Palumbo, F. S., Giammona, G., Deshpande, P. & MacNeil, S. (2011). Biocompatible hydrogels based on hyaluronic acid cross-linked with a polyaspartamide derivative as delivery systems for epithelial limbal cells. *International Journal of Pharmaceutics, 414*(1–2), 104-111.

Flaxman, S. R., Bourne, R. R. A., Resnikoff, S., Ackland, P., Braithwaite, T., Cicinelli, M. V., . . . & Zheng, Y. (2017). Global causes of blindness and distance vision impairment 1990–2020: a systematic review and meta-analysis. *The Lancet Global Health, 5*(12), e1221-e1234.

Foster, J. W., Jones, R. R., Bippes, C. A., Gouveia, R. M. & Connon, C. J. (2014). Differential nuclear expression of Yap in basal epithelial cells across the cornea and substrates of differing stiffness. *Experimental Eye Research, 127*, 37-41.

Fukuda, K., Chikama, T., Nakamura, M. & Nishida, T. (1999). Differential distribution of subchains of the basement membrane components type IV collagen and laminin among the amniotic membrane, cornea, and conjunctiva. *Cornea, 18*(1), 73-79.

Funderburgh, J. L., Funderburgh, M. L. & Du, Y. (2016). Stem Cells in the Limbal Stroma. *The Ocular Surface, 14*(2), 113-120.

Gain, P., Jullienne, R., He, Z., Aldossary, M., Acquart, S., Cognasse, F. & Thuret, G. (2016). Global survey of corneal transplantation and eye banking. *JAMA Ophthalmology, 134*(2), 167-173.

Galindo, S., Herreras, J. M., López-Paniagua, M., Rey, E., de la Mata, A., Plata-Cordero, M., Calonge, M. & Nieto-Miguel, T. (2017). Therapeutic Effect of Human Adipose Tissueâ€ Derived Mesenchymal Stem Cells in Experimental Corneal Failure Due to Limbal Stem Cell Niche Damage. *Stem Cells, 35*(10), 2160-2174.

Gesteira, T. F., Sun, M., Coulson-Thomas, Y. M., Yamaguchi, Y., Yeh, L., Hascall, V. & Coulson-Thomas, V. J. (2017). Hyaluronan rich microenvironment in the limbal stem cell niche regulates limbal stem cell differentiation. *Investigative Ophthalmology & Visual Science, 58*(11), 4407-4421.

Ghosh, S., Salvador-Culla, B., Kotagiri, A., Pushpoth, S., Tey, A., Johnson, Z. K. & Figueiredo, F. C. (2019). Acute Chemical Eye Injury and Limbal Stem Cell Deficiency—A Prospective Study in the United Kingdom. *Cornea, 38*(1), 8-12.

Gibney, R., Matthyssen, S., Patterson, J., Ferraris, E. & Zakaria, N. (2017). The Human Cornea as a Model Tissue for Additive Biomanufacturing: A Review. *Procedia CIRP, 65*, 56-63.

Gomes, J. Á P., Monteiro, B. G., Melo, G. B., Smith, R. L., da Silva, Marcelo Cavenaghi Pereira, Lizier, N. F., Kerkis, A., Cerruti, H. & Kerkis, I. (2010). Corneal reconstruction with tissue-engineered cell sheets composed of human immature dental pulp stem cells. *Investigative Ophthalmology & Visual Science, 51*(3), 1408-1414.

González-Andrades, M., Mata, R., del Carmen González-Gallardo, M., Medialdea, S., Arias-Santiago, S., Martínez-Atienza, J., Ruiz-García, A., Pérez-Fajardo, L., Lizana-Moreno, A. & Garzón, I. (2017). A study protocol for a multicentre randomised clinical trial evaluating the safety and feasibility of a bioengineered human allogeneic nanostructured anterior cornea in patients with advanced corneal trophic ulcers refractory to conventional treatment. *BMJ Open, 7*(9), e016487.

Gosselin, E. A., Torregrosa, T., Ghezzi, C. E., Mendelsohn, A. C., Gomes, R., Funderburgh, J. L. & Kaplan, D. L. (2018). Multi-layered silk film co-culture system for human corneal epithelial and stromal stem cells. *Journal of Tissue Engineering and Regenerative Medicine, 12*(1), 285-295.

Gourraud, P., Gilson, L., Girard, M. & Peschanski, M. (2012). The role of human leukocyte antigen matching in the development of multiethnic "haplobank" of induced pluripotent stem cell lines. *Stem Cells, 30*(2), 180-186.

Gouveia, R. M., Lepert, G., Gupta, S., Mohan, R. R., Paterson, C. & Connon, C. J. (2019a). Assessment of corneal substrate biomechanics and its effect on epithelial stem cell maintenance and differentiation. *Nature Communications, 10*(1), 1-17.

Gouveia, R. M., Vajda, F., Wibowo, J. A., Figueiredo, F. & Connon, C. J. (2019b). YAP, ΔNp63, and β-catenin signaling pathways are involved in the modulation of corneal epithelial stem cell phenotype induced by substrate stiffness. *Cells, 8*(4), 347.

Gouveia, R. M., González-Andrades, E., Cardona, J. C., González-Gallardo, C., Ionescu, A. M., Garzon, I., Alaminos, M., González-Andrades, M. & Connon, C. J. (2017a). Controlling the 3D architecture of Self-Lifting Auto-generated Tissue Equivalents (SLATEs) for optimized corneal graft composition and stability. *Biomaterials, 121*, 205-219.

Gouveia, R. M., Koudouna, E., Jester, J., Figueiredo, F. & Connon, C. J. (2017b). Template curvature influences cell alignment to create improved human corneal tissue equivalents. *Advanced Biosystems, 1*(12), 1700135.

Gouveia, R. M., Castelletto, V., Hamley, I. W. & Connon, C. J. (2015). New self-assembling multifunctional templates for the biofabrication and controlled self-release of cultured tissue. *Tissue Engineering Part A, 21*(11-12), 1772-1784.

Gouveia, R. M., Jones, R. R., Hamley, I. W. & Connon, C. J. (2014). The bioactivity of composite Fmoc-RGDS-collagen gels. *Biomaterials Science, 2*(9), 1222-1229.

Gouveia, R. M., Castelletto, V., Alcock, S. G., Hamley, I. W. & Connon, C. J. (2013). Bioactive films produced from self-assembling peptide amphiphiles as versatile substrates for tuning cell adhesion and tissue architecture in serum-free conditions. *Journal of Materials Chemistry B, 1*(44), 6157-6169.

Grieve, K., Ghoubay, D., Georgeon, C., Thouvenin, O., Bouheraoua, N., Paques, M. & Borderie, V. M. (2015). Three-dimensional structure of the mammalian limbal stem cell niche. *Experimental Eye Research, 140*, 75-84.

Griffith, M., Alarcon, E. I. & Brunette, I. (2016). Regenerative approaches for the cornea. *Journal of Internal Medicine, 280*(3), 276-286.

Griffith, M., Jackson, W. B., Lagali, N., Merrett, K., Li, F. & Fagerholm, P. (2009). Artificial corneas: a regenerative medicine approach. *Eye, 23*(10), 1985-1989.

Griffith, M., Osborne, R., Munger, R., Xiong, X., Doillon, C. J., Laycock, N. L., Hakim, M., Song, Y. & Watsky, M. A. (1999). Functional human corneal equivalents constructed from cell lines. *Science, 286*(5447), 2169-2172.

Guillemette, M. D., Cui, B., Roy, E., Gauvin, R., Giasson, C. J., Esch, M. B., Carrier, P., Deschambeault, A., Dumoulin, M. & Toner, M. (2009). Surface topography induces 3D self-orientation of cells and extracellular matrix resulting in improved tissue function. *Integrative Biology, 1*(2), 196-204.

Guo, X., Hutcheon, A. E., Melotti, S. A., Zieske, J. D., Trinkaus-Randall, V. & Ruberti, J. W. (2007). Morphologic characterization of organized extracellular matrix deposition by ascorbic acid–stimulated human corneal fibroblasts. *Investigative Ophthalmology & Visual Science, 48*(9), 4050-4060.

Haagdorens, M., Cėpla, V., Melsbach, E., Koivusalo, L., Skottman, H., Griffith, M., Valiokas, R., Zakaria, N., Pintelon, I. & Tassignon, M. (2019). In vitro cultivation

of limbal epithelial stem cells on surface-modified crosslinked collagen scaffolds. *Stem Cells International, 2019*

Harkin, D. G., Foyn, L., Bray, L. J., Sutherland, A. J., Li, F. J. & Cronin, B. G. (2015). Concise reviews: can mesenchymal stromal cells differentiate into corneal cells? A systematic review of published data. *Stem Cells, 33*(3), 785-791.

Hashimoto, Y., Hattori, S., Sasaki, S., Honda, T., Kimura, T., Funamoto, S., Kobayashi, H. & Kishida, A. (2016). Ultrastructural analysis of the decellularized cornea after interlamellar keratoplasty and microkeratome-assisted anterior lamellar keratoplasty in a rabbit model. *Scientific Reports, 6*, 27734.

Hashimoto, Y., Funamoto, S., Sasaki, S., Honda, T., Hattori, S., Nam, K., Kimura, T., Mochizuki, M., Fujisato, T. & Kobayashi, H. (2010). Preparation and characterization of decellularized cornea using high-hydrostatic pressurization for corneal tissue engineering. *Biomaterials, 31*(14), 3941-3948.

Hassell, J. R., & Birk, D. E. (2010). The molecular basis of corneal transparency. *Experimental Eye Research, 91*(3), 326-335.

Hayashi, R., Ishikawa, Y., Katori, R., Sasamoto, Y., Taniwaki, Y., Takayanagi, H., Tsujikawa, M., Sekiguchi, K., Quantock, A. J. & Nishida, K. (2017). Coordinated generation of multiple ocular-like cell lineages and fabrication of functional corneal epithelial cell sheets from human iPS cells. *Nature Protocols, 12*(4), 683.

Hayashi, R., Ishikawa, Y., Sasamoto, Y., Katori, R., Nomura, N., Ichikawa, T., Araki, S., Soma, T., Kawasaki, S. & Sekiguchi, K. (2016). Co-ordinated ocular development from human iPS cells and recovery of corneal function. *Nature, 531*(7594), 376.

Hayashi, R., Ishikawa, Y., Ito, M., Kageyama, T., Takashiba, K., Fujioka, T., Tsujikawa, M., Miyoshi, H., Yamato, M. & Nakamura, Y. (2012). Generation of corneal epithelial cells from induced pluripotent stem cells derived from human dermal fibroblast and corneal limbal epithelium. *PLoS One, 7*(9)

Hayashi, R., Yamato, M., Sugiyama, H., Sumide, T., Yang, J., Okano, T., Tano, Y. & Nishida, K. (2007). N-Cadherin is expressed by putative stem/progenitor cells and melanocytes in the human limbal epithelial stem cell niche. *Stem Cells, 25*(2), 289-296.

Hjortdal, J. Ø. (1996). Regional elastic performance of the human cornea. *Journal of Biomechanics, 29*(7), 931-942.

Holan, V., & Javorkova, E. (2013). Mesenchymal stem cells, nanofiber scaffolds and ocular surface reconstruction. *Stem Cell Reviews and Reports, 9*(5), 609-619.

Holland, E. J., Mogilishetty, G., Skeens, H. M., Hair, D. B., Neff, K. D., Biber, J. M. & Chan, C. C. (2012). Systemic immunosuppression in ocular surface stem cell transplantation: results of a 10-year experience. *Cornea, 31*(6), 655-661.

Hollingsworth, J., Perez-Gomez, I., Mutalib, H. A. & Efron, N. (2001). A population study of the normal cornea using an in vivo, slit-scanning confocal microscope. *Optometry and Vision Science, 78*(10), 706-711.

Hölzl, K., Lin, S., Tytgat, L., Van Vlierberghe, S., Gu, L. & Ovsianikov, A. (2016). Bioink properties before, during and after 3D bioprinting. *Biofabrication, 8*(3), 032002.

Hongisto, H., Ilmarinen, T., Vattulainen, M., Mikhailova, A. & Skottman, H. (2017). Xeno- and feeder-free differentiation of human pluripotent stem cells to two distinct ocular epithelial cell types using simple modifications of one method. *Stem Cell Research & Therapy, 8*(1), 291.

iFix Medical Pty Ltd., 2019 iFix Medical https://www.ifixmedical.com/ *Accessed 5 Mar 2020*

Ionescu, A., Alaminos, M., de la Cruz Cardona, J, de Dios García López-Durán, J, González-Andrades, M., Ghinea, R., Campos, A., Hita, E. & del Mar Pérez, M. (2011). Investigating a novel nanostructured fibrin–agarose biomaterial for human cornea tissue engineering: Rheological properties. *Journal of the Mechanical Behavior of Biomedical Materials, 4*(8), 1963-1973.

Isaacson, A., Swioklo, S. & Connon, C. J. (2018). 3D bioprinting of a corneal stroma equivalent. *Experimental Eye Research, 173*, 188-193.

Islam, M. M., Ravichandran, R., Olsen, D., Ljunggren, M. K., Fagerholm, P., Lee, C., Griffith, M. & Phopase, J. (2016). Self-assembled collagen-like-peptide implants as alternatives to human donor corneal transplantation. *RSC Advances, 6*(61), 55745-55749.

Islam, M. M., Cėpla, V., He, C., Edin, J., Rakickas, T., Kobuch, K., . . . & Griffith, M. (2015). Functional fabrication of recombinant human collagen–phosphorylcholine hydrogels for regenerative medicine applications. *Acta Biomaterialia, 12*, 70-80.

Jackson, C. J., Myklebust Ernø, I. T., Ringstad, H., Tønseth, K. A., Dartt, D. A. & Utheim, T. P. (2019). Simple limbal epithelial transplantation: Current status and future perspectives: Concise review. *Stem Cells Translational Medicine, 9*(3), 316-327.

Jangamreddy, J. R., Haagdorens, M. K., Islam, M. M., Lewis, P., Samanta, A., Fagerholm, P., Liszka, A., Ljunggren, M. K., Buznyk, O. & Alarcon, E. I. (2018). Short peptide analogs as alternatives to collagen in pro-regenerative corneal implants. *Acta Biomaterialia, 69*, 120-130.

Jester, J. V., Moller-Pedersen, T., Huang, J., Sax, C. M., Kays, W. T., Cavangh, H. D., Petroll, W. M. & Piatigorsky, J. (1999). The cellular basis of corneal transparency: evidence for 'corneal crystallins'. *Journal of Cell Science, 112*(5), 613-622.

Jia, L., Ghezzi, C. E. & Kaplan, D. L. (2016). Optimization of silk films as substrate for functional corneal epithelium growth. *Journal of Biomedical Materials Research Part B: Applied Biomaterials, 104*(2), 431-441.

Jiraskova, N., Rozsival, P., Burova, M. & Kalfertova, M. (2011). AlphaCor artificial cornea: clinical outcome. *Eye, 25*(9), 1138.

Jirsova, K., & Jones, G. L. (2017). Amniotic membrane in ophthalmology: properties, preparation, storage and indications for grafting—a review. *Cell and Tissue Banking, 18*(2), 193-204.

Jones, G. (2018, 27 Mar). Takeda's Alofisel becomes Europe's first allogeneic stem cell therapy. *PMLive* [online] Retrieved from http://www.pmlive.com/pharma_news/takedas_alofisel_becomes_europes_first_allogenic_stem_cell_therapy_1229414 *Accessed 22 Jan 2020*

Jones, R. R., Hamley, I. W. & Connon, C. J. (2012). Ex vivo expansion of limbal stem cells is affected by substrate properties. *Stem Cell Research, 8*(3), 403-409.

Jurado, M., De La Mata, C., Ruiz-García, A., López-Fernández, E., Espinosa, O., Remigia, M. J., . . . & Solano, C. (2017). Adipose tissue-derived mesenchymal stromal cells as part of therapy for chronic graft-versus-host disease: A phase I/II study. *Cytotherapy, 19*(8), 927-936.

Karvinen, J., Koivisto, J. T., Jönkkäri, I. & Kellomäki, M. (2017). The production of injectable hydrazone crosslinked gellan gum-hyaluronan-hydrogels with tunable mechanical and physical properties. *Journal of the Mechanical Behavior of Biomedical Materials, 71*, 383-391.

Kawasaki, S., Tanioka, H., Yamasaki, K., Connon, C. J. & Kinoshita, S. (2006). Expression and tissue distribution of p63 isoforms in human ocular surface epithelia. *Experimental Eye Research, 82*(2), 293-299.

Kethiri, A. R., Basu, S., Shukla, S., Sangwan, V. S. & Singh, V. (2017). Optimizing the role of limbal explant size and source in determining the outcomes of limbal transplantation: An in vitro study. *PloS One, 12*(9), e0185623.

Khan, B. F. (2015). Boston keratoprosthesis: Design, materials, and manufacturing . In M. S. Cortina, & J. de la Cruz (Eds.), *Keratoprostheses and artifical corneas: Fundamentals and applications* (pp. 45-50). Berlin Heidelberg: Springer-Verlag.

Kim, J. I., Kim, J. Y. & Park, C. H. (2018). Fabrication of transparent hemispherical 3D nanofibrous scaffolds with radially aligned patterns via a novel electrospinning method. *Scientific Reports, 8*(1), 1-13.

Koch, L., Kuhn, S., Sorg, H., Gruene, M., Schlie, S., Gaebel, R., . . . & Chichkov, B. (2009). Laser printing of skin cells and human stem cells. *Tissue Engineering Part C: Methods, 16*(5), 847-854.

Kong, B., Chen, Y., Liu, R., Liu, X., Liu, C., Shao, Z., Xiong, L., Liu, X., Sun, W. & Mi, S. (2020). Fiber reinforced GelMA hydrogel to induce the regeneration of corneal stroma. *Nature Communications, 11*, 1435.

Kong, B., Sun, W., Chen, G., Tang, S., Li, M., Shao, Z. & Mi, S. (2017). Tissue-engineered cornea constructed with compressed collagen and laser-perforated electrospun mat. *Scientific Reports, 7*(1), 970-0.

Kong, B., & Mi, S. (2016). Electrospun scaffolds for corneal tissue engineering: A review. *Materials, 9*(8), 614.

Koulikovska, M., Rafat, M., Petrovski, G., Veréb, Z., Akhtar, S., Fagerholm, P. & Lagali, N. (2015). Enhanced regeneration of corneal tissue via a bioengineered collagen construct implanted by a nondisruptive surgical technique. *Tissue Engineering Part A, 21*(5-6), 1116-1130.

Ksander, B. R., Kolovou, P. E., Wilson, B. J., Saab, K. R., Guo, Q., Ma, J., McGuire, S. P., Gregory, M. S., Vincent, W. J. & Perez, V. L. (2014). ABCB5 is a limbal stem cell gene required for corneal development and repair. *Nature, 511*(7509), 353.

Kumar, P., Satyam, A., Fan, X., Rochev, Y., Rodriguez, B. J., Gorelov, A., Joshi, L., Raghunath, M., Pandit, A. & Zeugolis, D. I. (2015). Accelerated development of

supramolecular corneal stromal-like assemblies from corneal fibroblasts in the presence of macromolecular crowders. *Tissue Engineering Part C: Methods, 21*(7), 660-670.

Kureshi, A. K., Dziasko, M., Funderburgh, J. L. & Daniels, J. T. (2015). Human corneal stromal stem cells support limbal epithelial cells cultured on RAFT tissue equivalents. *Scientific Reports, 5*, 16186.

Lagali, N. (2020). Corneal Stromal Regeneration: Current Status and Future Therapeutic Potential. *Current Eye Research, 45*(3), 278-290.

Lee, A., Hudson, A. R., Shiwarski, D. J., Tashman, J. W., Hinton, T. J., Yerneni, S., Bliley, J. M., Campbell, P. G. & Feinberg, A. W. (2019). 3D bioprinting of collagen to rebuild components of the human heart. *Science, 365*(6452), 482-487.

Lee, H. J., Fernandes-Cunha, G. M., Na, K., Hull, S. M. & Myung, D. (2018). Bio-Orthogonally Crosslinked, In Situ Forming Corneal Stromal Tissue Substitute. *Advanced Healthcare Materials, 7*(19), 1800560.

Lee, S., & Tseng, S. C. (1997). Amniotic membrane transplantation for persistent epithelial defects with ulceration. *American Journal of Ophthalmology, 123*(3), 303-312.

Lee, W. B., Shtein, R. M., Kaufman, S. C., Deng, S. X. & Rosenblatt, M. I. (2015). Boston Keratoprosthesis: Outcomes and Complications: A Report by the American Academy of Ophthalmology. *Ophthalmology, 122*(7), 1504-1511.

Lee, Y., Chung, H. J., Yeo, S., Ahn, C., Lee, H., Messersmith, P. B. & Park, T. G. (2010). Thermo-sensitive, injectable, and tissue adhesive sol–gel transition hyaluronic acid/pluronic composite hydrogels prepared from bio-inspired catechol-thiol reaction. *Soft Matter, 6*(5), 977-983.

Levis, H. J., Kureshi, A. K., Massie, I., Morgan, L., Vernon, A. J. & Daniels, J. T. (2015). Tissue Engineering the Cornea: The Evolution of RAFT. *Journal of Functional Biomaterials, 6*(1), 50-65.

Levis, H. J., Brown, R. A. & Daniels, J. T. (2010). Plastic compressed collagen as a biomimetic substrate for human limbal epithelial cell culture. *Biomaterials, 31*(30), 7726-7737.

Li, J., Xiao, Y., Coursey, T. G., Chen, X., Deng, R., Lu, F., Pflugfelder, S. C. & Li, D. (2017). Identification for differential localization of putative corneal epithelial stem cells in mouse and human. *Scientific Reports, 7*(1), 5169.

Lindroos, B., Suuronen, R. & Miettinen, S. (2011). The potential of adipose stem cells in regenerative medicine. *Stem Cell Reviews and Reports, 7*(2), 269-291.

Lindroos, B., Boucher, S., Chase, L., Kuokkanen, H., Huhtala, H., Haataja, R., Vemuri, M., Suuronen, R. & Miettinen, S. (2009). Serum-free, xeno-free culture media maintain the proliferation rate and multipotentiality of adipose stem cells in vitro. *Cytotherapy, 11*(7), 958-972.

Listek, V. (2019, Jul 31). Poietis: Bioprinting With Their Innovative Laser-Assisted Technology. *3Dprint.com* [online] Retrieved from https://3dprint.com/249669/poietis-bioprinting-with-their-innovative-laser-assisted-technology/ *Accessed Mar 5 2020*

Liu, H., Zhang, J., Liu, C., Hayashi, Y. & Kao, W. W. (2012). Bone marrow mesenchymal stem cells can differentiate and assume corneal keratocyte phenotype. *Journal of Cellular and Molecular Medicine, 16*(5), 1114-1124.

Liu, H., Zhang, J., Liu, C., Wang, I., Sieber, M., Chang, J., Jester, J. V. & Kao, W. W. (2010). Cell therapy of congenital corneal diseases with umbilical mesenchymal stem cells: lumican null mice. *PloS One, 5*(5)

Liu, W., Deng, C., McLaughlin, C. R., Fagerholm, P., Lagali, N. S., Heyne, B., Scaiano, J. C., Watsky, M. A., Kato, Y. & Munger, R. (2009). Collagen–phosphorylcholine interpenetrating network hydrogels as corneal substitutes. *Biomaterials, 30*(8), 1551-1559.

Liu, W., Merrett, K., Griffith, M., Fagerholm, P., Dravida, S., Heyne, B., . . . & Li, F. (2008). Recombinant human collagen for tissue engineered corneal substitutes. *Biomaterials, 29*(9), 1147-1158.

Loebel, C., Mauck, R. L. & Burdick, J. A. (2019). Local nascent protein deposition and remodelling guide mesenchymal stromal cell mechanosensing and fate in three-dimensional hydrogels. *Nature Materials, 18*, 883-891.

Lynch, A. P., & Ahearne, M. (2017). Retinoic acid enhances the differentiation of adipose-derived stem cells to keratocytes in vitro. *Translational Vision Science & Technology, 6*(1), 6.

Lynn, A. K., Yannas, I. V. & Bonfield, W. (2004). Antigenicity and immunogenicity of collagen. *Journal of Biomedical Materials Research Part B: Applied Biomaterials, 71*(2), 343-354.

Majumdar, S., Wang, X., Sommerfeld, S. D., Chae, J. J., Athanasopoulou, E., Shores, L. S., Duan, X., Amzel, L. M., Stellacci, F. & Schein, O. (2018). Cyclodextrin Modulated Type I Collagen Self-Assembly to Engineer Biomimetic Cornea Implants. *Advanced Functional Materials, 28*(41), 1804076.

Malda, J., Visser, J., Melchels, F. P., Jüngst, T., Hennink, W. E., Dhert, W. J., Groll, J. & Hutmacher, D. W. (2013). 25th anniversary article: engineering hydrogels for biofabrication. *Advanced Materials, 25*(36), 5011-5028.

Mandrycky, C., Wang, Z., Kim, K. & Kim, D. (2016). 3D bioprinting for engineering complex tissues. *Biotechnology Advances, 34*(4), 422-434.

Maranchi, J. P., Trexler, M. M., Guo, Q. & Elisseeff, J. H. (2014). Fibre-reinforced hydrogels with high optical transparency. *International Materials Reviews, 59*(5), 264-296.

Massoudi, D., Malecaze, F. & Galiacy, S. D. (2016). Collagens and proteoglycans of the cornea: importance in transparency and visual disorders. *Cell and Tissue Research, 363*(2), 337-349.

Mathews, P. M., Lindsley, K., Aldave, A. J. & Akpek, E. K. (2018). Etiology of global corneal blindness and current practices of corneal transplantation: a focused review. *Cornea, 37*(9), 1198-1203.

Matthyssen, S., Van den Bogerd, B., Dhubhghaill, S. N., Koppen, C. & Zakaria, N. (2018). Corneal regeneration: A review of stromal replacements. *Acta Biomaterialia, 69*, 31-41.

Meek, K. M., & Knupp, C. (2015). Corneal structure and transparency. *Progress in Retinal and Eye Research, 49*, 1-16.

Meek, K. M., & Boote, C. (2009). The use of X-ray scattering techniques to quantify the orientation and distribution of collagen in the corneal stroma. *Progress in Retinal and Eye Research, 28*(5), 369-392.

Meek, K. M., Leonard, D. W., Connon, C. J., Dennis, S. & Khan, S. (2003). Transparency, swelling and scarring in the corneal stroma. *Eye, 17*(8), 927.

Mei, H., Gonzalez, S. & Deng, S. X. (2012). Extracellular matrix is an important component of limbal stem cell niche. *Journal of Functional Biomaterials, 3*(4), 879-894.

Meyer-Blazejewska, E. A., Call, M. K., Yamanaka, O., Liu, H., Schlötzer-Schrehardt, U., Kruse, F. E. & Kao, W. W. (2011). From hair to cornea: Toward the therapeutic use of hair follicle-derived stem cells in the treatment of limbal stem cell deficiency. *Stem Cells, 29*(1), 57-66.

Mi, S., Khutoryanskiy, V. V., Jones, R. R., Zhu, X., Hamley, I. W. & Connon, C. J. (2011). Photochemical cross-linking of plastically compressed collagen gel produces an optimal scaffold for corneal tissue engineering. *Journal of Biomedical Materials Research Part A, 99*(1), 1-8.

Mikhailova, A., Jylha, A., Rieck, J., Nattinen, J., Ilmarinen, T., Vereb, Z., . . . & Skottman, H. (2015). Comparative proteomics reveals human pluripotent stem cell-derived limbal epithelial stem cells are similar to native ocular surface epithelial cells. *Scientific Reports, 5*, 14684.

Mikhailova, A., Ilmarinen, T., Uusitalo, H. & Skottman, H. (2014). Small-Molecule Induction Promotes Corneal Epithelial Cell Differentiation from Human Induced Pluripotent Stem Cells. *Stem Cell Reports, 2*(2), 219-231.

Miotto, M., Gouveia, R. M., Ionescu, A. M., Figueiredo, F., Hamley, I. W. & Connon, C. J. (2019). 4D Corneal Tissue Engineering: Achieving Time-Dependent Tissue Self-Curvature through Localized Control of Cell Actuators. *Advanced Functional Materials, 29*(8), 1807334.

Miotto, M., Gouveia, R. M. & Connon, C. J. (2015). Peptide amphiphiles in corneal tissue engineering. *Journal of Functional Biomaterials, 6*(3), 687-707.

Mittal, S. K., Omoto, M., Amouzegar, A., Sahu, A., Rezazadeh, A., Katikireddy, K. R., Shah, D. I., Sahu, S. K. & Chauhan, S. K. (2016). Restoration of Corneal Transparency by Mesenchymal Stem Cells. *Stem Cell Reports, 7*(4), 583-590.

Murphy, S. V., & Atala, A. (2014). 3D bioprinting of tissues and organs. *Nature Biotechnology, 32*(8), 773-785.

Myung, D., Duhamel, P., Cochran, J. R., Noolandi, J., Ta, C. N. & Frank, C. W. (2008). Development of hydrogel-based keratoprostheses: A materials perspective. *Biotechnology Progress, 24*(3), 735-741.

Naylor, R. W., McGhee, C. N., Cowan, C. A., Davidson, A. J., Holm, T. M. & Sherwin, T. (2016). Derivation of corneal keratocyte-like cells from human induced pluripotent stem cells. *PloS One, 11*(10)

Nishida, K., Yamato, M., Hayashida, Y., Watanabe, K., Maeda, N., Watanabe, H., Yamamoto, K., Nagai, S., Kikuchi, A. & Tano, Y. (2004). Functional bioengineered corneal epithelial sheet grafts from corneal stem cells expanded ex vivo on a temperature-responsive cell culture surface. *Transplantation, 77*(3), 379-385.

Notara, M., Schrader, S. & Daniels, J. T. (2011). The porcine limbal epithelial stem cell niche as a new model for the study of transplanted tissue-engineered human limbal epithelial cells. *Tissue Engineering Part A, 17*(5-6), 741-750.

O'Callaghan, A. R., & Daniels, J. T. (2011). Concise review: limbal epithelial stem cell therapy: controversies and challenges. *Stem Cells, 29*(12), 1923-1932.

Oh, J. Y., Kim, M. K., Shin, M. S., Lee, H. J., Ko, J. H., Wee, W. R. & Lee, J. H. (2008). The anti-inflammatory and anti-angiogenic role of mesenchymal stem cells in corneal wound healing following chemical injury. *Stem Cells, 26*(4), 1047-1055.

Oommen, O. P., Wang, S., Kisiel, M., Sloff, M., Hilborn, J. & Varghese, O. P. (2013). Smart Design of Stable Extracellular Matrix Mimetic Hydrogel: Synthesis, Characterization, and In Vitro and In Vivo Evaluation for Tissue Engineering. *Advanced Functional Materials, 23*(10), 1273-1280.

Ortega, Í, Ryan, A. J., Deshpande, P., MacNeil, S. & Claeyssens, F. (2013). Combined microfabrication and electrospinning to produce 3-D architectures for corneal repair. *Acta Biomaterialia, 9*(3), 5511-5520.

Orwin, E. J., & Hubel, A. (2000). In vitro culture characteristics of corneal epithelial, endothelial, and keratocyte cells in a native collagen matrix. *Tissue Engineering, 6*(4), 307-319.

Osaka University, 29 Aug 2019 World's first transplant of cornea made from iPS cells http://www.med.osaka-u.ac.jp/eng/archives/5349 *Accessed 3 Apr 2020*

Oyen, M. L. (2014). Mechanical characterisation of hydrogel materials. *International Materials Reviews, 59*(1), 44-59.

Panda, A., Vanathi, M., Kumar, A., Dash, Y. & Priya, S. (2007). Corneal Graft Rejection. *Survey of Ophthalmology, 52*(4), 375-396.

Pascolini, D., & Mariotti, S. P. (2012). Global estimates of visual impairment: 2010. *British Journal of Ophthalmology, 96*(5), 614-618.

Patrikoski, M., Juntunen, M., Boucher, S., Campbell, A., Vemuri, M. C., Mannerström, B. & Miettinen, S. (2013). Development of fully defined xeno-free culture system for the preparation and propagation of cell therapy-compliant human adipose stem cells. *Stem Cell Research & Therapy, 4*(2), 27.

Pellegrini, G., Ranno, R., Stracuzzi, G., Bondanza, S., Guerra, L., Zambruno, G., Micali, G. & De Luca, M. (1999). The control of epidermal stem cells (holoclones) in the treatment of massive full-thickness burns with autologous keratinocytes cultured on fibrin. *Transplantation, 68*(6), 868-879.

Pellegrini, G., Traverso, C. E., Franzi, A. T., Zingirian, M., Cancedda, R. & De Luca, M. (1997). Long-term restoration of damaged corneal surfaces with autologous cultivated corneal epithelium. *The Lancet, 349*(9057), 990-993.

Petsch, C., Schlötzer-Schrehardt, U., Meyer-Blazejewska, E., Frey, M., Kruse, F. E. & Bachmann, B. O. (2014). Novel collagen membranes for the reconstruction of the corneal surface. *Tissue Engineering Part A, 20*(17-18), 2378-2389.

Petsche, S. J., Chernyak, D., Martiz, J., Levenston, M. E. & Pinsky, P. M. (2012). Depth-dependent transverse shear properties of the human corneal stroma. *Investigative Ophthalmology & Visual Science, 53*(2), 873-880.

Phu, D., Wray, L. S., Warren, R. V., Haskell, R. C. & Orwin, E. J. (2010). Effect of substrate composition and alignment on corneal cell phenotype. *Tissue Engineering Part A, 17*(5-6), 799-807.

Pinnamaneni, N., & Funderburgh, J. L. (2012). Concise review: Stem cells in the corneal stroma. *Stem Cells, 30*(6), 1059-1063.

Polisetti, N., Sorokin, L., Okumura, N., Koizumi, N., Kinoshita, S., Kruse, F. E. & Schlötzer-Schrehardt, U. (2017). Laminin-511 and-521-based matrices for efficient ex vivo-expansion of human limbal epithelial progenitor cells. *Scientific Reports, 7*, 5152.

Prabhasawat, P., Ekpo, P., Uiprasertkul, M., Chotikavanich, S., Tesavibul, N., Pornpanich, K. & Luemsamran, P. (2016). Long-term result of autologous cultivated oral mucosal epithelial transplantation for severe ocular surface disease. *Cell and Tissue Banking, 17*(3), 491-503.

Proulx, S., Uwamaliya, J. d., Carrier, P., Deschambeault, A., Audet, C., Giasson, C. J., Guérin, S. L., Auger, F. A. & Germain, L. (2010). Reconstruction of a human cornea by the self-assembly approach of tissue engineering using the three native cell types. *Molecular Vision, 16*, 2192.

Rafat, M., Xeroudaki, M., Koulikovska, M., Sherrell, P., Groth, F., Fagerholm, P. & Lagali, N. (2016). Composite core-and-skirt collagen hydrogels with differential degradation for corneal therapeutic applications. *Biomaterials, 83*, 142-155.

Rafat, M., Li, F., Fagerholm, P., Lagali, N. S., Watsky, M. A., Munger, R., Matsuura, T. & Griffith, M. (2008). PEG-stabilized carbodiimide crosslinked collagen–chitosan hydrogels for corneal tissue engineering. *Biomaterials, 29*(29), 3960-3972.

Rama, P., Matuska, S., Paganoni, G., Spinelli, A., De Luca, M. & Pellegrini, G. (2010). Limbal Stem-Cell Therapy and Long-Term Corneal Regeneration. *New England Journal of Medicine, 363*(2), 147-155.

Reinshagen, H., Auw-Haedrich, C., Sorg, R. V., Boehringer, D., Eberwein, P., Schwartzkopff, J., Sundmacher, R. & Reinhard, T. (2011). Corneal surface reconstruction using adult mesenchymal stem cells in experimental limbal stem cell deficiency in rabbits. *Acta Ophthalmologica, 89*(8), 741-748.

Ricardo, J. R. S., Cristovam, P. C., Pedro Filho, A. N., Farias, C. C., de Araujo, A. L., Loureiro, R. R., Covre, J. L., de Barros, J. N., Barreiro, T. P. & dos Santos, M. S. (2013). Transplantation of conjunctival epithelial cells cultivated ex vivo in patients with total limbal stem cell deficiency. *Cornea, 32*(3), 221-228.

Richardson, A., Wakefield, D. & Di Girolamo, N. (2016). Fate Mapping Mammalian Corneal Epithelia. *The Ocular Surface, 14*(2), 82-99.

Riestra, A. C., Vazquez, N., Chacon, M., Berisa, S., Sanchez-Avila, R. M., Orive, G., Anitua, E., Meana, A. & Merayo-Lloves, J. (2017). Autologous method for ex vivo expansion of human limbal epithelial progenitor cells based on plasma rich in growth factors technology. *The Ocular Surface, 15*(2), 248-256.

Romito, A., & Cobellis, G. (2016). Pluripotent stem cells: current understanding and future directions. *Stem Cells International, 2016*

Rose, J. B., Pacelli, S., Haj, A. J. E., Dua, H. S., Hopkinson, A., White, L. J. & Rose, F. R. (2014). Gelatin-based materials in ocular tissue engineering. *Materials, 7*(4), 3106-3135.

Rossen, J., Amram, A., Milani, B., Park, D., Harthan, J., Joslin, C., McMahon, T. & Djalilian, A. (2016). Contact lens-induced limbal stem cell deficiency. *The Ocular Surface, 14*(4), 419-434.

Samaeekia, R., Rabiee, B., Putra, I., Shen, X., Park, Y. J., Hematti, P., Eslani, M. & Djalilian, A. R. (2018). Effect of human corneal mesenchymal stromal cell-derived exosomes on corneal epithelial wound healing. *Investigative Ophthalmology & Visual Science, 59*(12), 5194-5200.

Sánchez-Abarca, L. I., Hernández-Galilea, E., Lorenzo, R., Herrero, C., Velasco, A., Carrancio, S., Caballero-Velázquez, T., Rodríguez-Barbosa, J. I., Parrilla, M. & Del Cañizo, C. (2015). Human bone marrow stromal cells differentiate into corneal tissue and prevent ocular graft-versus-host disease in mice. *Cell Transplantation, 24*(12), 2423-2433.

Sangwan, V. S., Basu, S., MacNeil, S. & Balasubramanian, D. (2012). Simple limbal epithelial transplantation (SLET): a novel surgical technique for the treatment of unilateral limbal stem cell deficiency. *British Journal of Ophthalmology, 96*(7), 931-934.

Sani, E. S., Kheirkhah, A., Rana, D., Sun, Z., Foulsham, W., Sheikhi, A., Khademhosseini, A., Dana, R. & Annabi, N. (2019). Sutureless repair of corneal injuries using naturally derived bioadhesive hydrogels. *Science Advances, 5*(3), eaav1281.

Satake, Y., Higa, K., Tsubota, K. & Shimazaki, J. (2011). Long-term outcome of cultivated oral mucosal epithelial sheet transplantation in treatment of total limbal stem cell deficiency. *Ophthalmology, 118*(8), 1524-1530.

Saunders, S. (2017, 17 Aug). Biomedical Research Team in Spain Working on 3D Printed Corneas to Make Up for Lack of Donors. *3Dprint.com* [online] Retrieved from https://3dprint.com/184469/spain-3d-printed-cornea-project/ *Accessed 31 Mar 2020*

Schlötzer-Schrehardt, U., Dietrich, T., Saito, K., Sorokin, L., Sasaki, T., Paulsson, M. & Kruse, F. E. (2007). Characterization of extracellular matrix components in the limbal epithelial stem cell compartment. *Experimental Eye Research, 85*(6), 845-860.

Schlötzer-Schrehardt, U., & Kruse, F. E. (2005). Identification and characterization of limbal stem cells. *Experimental Eye Research, 81*(3), 247-264.

Schmittgen, T. D., & Livak, K. J. (2008). Analyzing real-time PCR data by the comparative C T method. *Nature Protocols, 3*(6), 1101.

Shafiq, M. A., Gemeinhart, R. A., Yue, B. Y. & Djalilian, A. R. (2011). Decellularized human cornea for reconstructing the corneal epithelium and anterior stroma. *Tissue Engineering Part C: Methods, 18*(5), 340-348.

Shanbhag, S. S., Nikpoor, N., Donthineni, P. R., Singh, V., Chodosh, J. & Basu, S. (2020). Autologous limbal stem cell transplantation: a systematic review of clinical outcomes with different surgical techniques. *British Journal of Ophthalmology, 104*(2), 247-253.

Shin, J., Lee, J. S., Lee, C., Park, H., Yang, K., Jin, Y., . . . & Cho, S. (2015). Tissue Adhesive Catechol-Modified Hyaluronic Acid Hydrogel for Effective, Minimally Invasive Cell Therapy. *Advanced Functional Materials, 25*(25), 3814-3824.

Shojaati, G., Khandaker, I., Funderburgh, M. L., Mann, M. M., Basu, R., Stolz, D. B., Geary, M. L., Dos Santos, A., Deng, S. X. & Funderburgh, J. L. (2019). Mesenchymal Stem Cells Reduce Corneal Fibrosis and Inflammation via Extracellular Vesicle-Mediated Delivery of miRNA. *Stem Cells Translational Medicine, 8*(11), 1192-1201.

Shortt, A. J., Tuft, S. J. & Daniels, J. T. (2011). Corneal stem cells in the eye clinic. *British Medical Bulletin, 100*(1), 209-225.

Shortt, A. J., Secker, G. A., Munro, P. M., Khaw, P. T., Tuft, S. J. & Daniels, J. T. (2007a). Characterization of the limbal epithelial stem cell niche: novel imaging techniques permit in vivo observation and targeted biopsy of limbal epithelial stem cells. *Stem Cells, 25*(6), 1402-1409.

Shortt, A. J., Secker, G. A., Notara, M. D., Limb, G. A., Khaw, P. T., Tuft, S. J. & Daniels, J. T. (2007b). Transplantation of Ex Vivo Cultured Limbal Epithelial Stem Cells: A Review of Techniques and Clinical Results. *Survey of Ophthalmology, 52*(5), 483-502.

Sidney, L. E., Branch, M. J., Dua, H. S. & Hopkinson, A. (2015). Effect of culture medium on propagation and phenotype of corneal stroma–derived stem cells. *Cytotherapy, 17*(12), 1706-1722.

Skottman, H. (2010). Derivation and characterization of three new human embryonic stem cell lines in Finland. *In Vitro Cellular & Developmental Biology. Animal, 46*(3/4), 206-209.

Sommer, A. C., & Blumenthal, E. Z. (2019). Implementations of 3D printing in ophthalmology. *Graefe's Archive for Clinical and Experimental Ophthalmology,* , 1-8.

Stepp, M. A., Zhu, L., Sheppard, D. & Cranfill, R. L. (1995). Localized distribution of alpha 9 integrin in the cornea and changes in expression during corneal epithelial cell differentiation. *Journal of Histochemistry & Cytochemistry, 43*(4), 353-362.

Sutton, G., You, J., Cooper, S., Frazer, H., Hodge, C., Liu, X., Taylor, A., McColl, E. & Wallace, G. (2018). Development of iFixPen™–using 3D printing to treat corneal ulcers. *Investigative Ophthalmology & Visual Science, 59*(9), 4343.

Takahashi, K., Tanabe, K., Ohnuki, M., Narita, M., Ichisaka, T., Tomoda, K. & Yamanaka, S. (2007). Induction of pluripotent stem cells from adult human fibroblasts by defined factors. *Cell, 131*(5), 861-872.

Taylor, C. J., Peacock, S., Chaudhry, A. N., Bradley, J. A. & Bolton, E. M. (2012). Generating an iPSC bank for HLA-matched tissue transplantation based on known donor and recipient HLA types. *Cell Stem Cell, 11*(2), 147-152.

Taylor, C. J., Bolton, E. M., Pocock, S., Sharples, L. D., Pedersen, R. A. & Bradley, J. A. (2005). Banking on human embryonic stem cells: estimating the number of donor cell lines needed for HLA matching. *The Lancet, 366*(9502), 2019-2025.

Thomson, J. A., Itskovitz-Eldor, J., Shapiro, S. S., Waknitz, M. A., Swiergiel, J. J., Marshall, V. S. & Jones, J. M. (1998). Embryonic stem cell lines derived from human blastocysts. *Science, 282*(5391), 1145-1147.

Tonsomboon, K., & Oyen, M. L. (2013). Composite electrospun gelatin fiber-alginate gel scaffolds for mechanically robust tissue engineered cornea. *Journal of the Mechanical Behavior of Biomedical Materials, 21*, 185-194.

TrialSite News. (2019, 16 Jul). LV Prasad Eye Institute India Leads Regenerative Clinical Trials for Restoring Eyesight Acid Burn Victims. *TrialSite News* [online] Retrieved from https://www.trialsitenews.com/lv-prasad-eye-institute-india-leads-regenerative-clinical-trials-for-restoring-eyesight-acid-burn-victims/ *Accessed 30 Mar 2020*

Tuckey, K. (2017, 30 Sep). Scientists 3-D print new cornea for human transplant, from fish scales. *Stuff* [online] Retrieved from https://www.stuff.co.nz/national/health/97380731/scientists-3d-print-new-cornea-for-human-transplant-from-fish-scales *Accessed 31 Mar 2020*

Uzunalli, G., Soran, Z., Erkal, T. S., Dagdas, Y. S., Dinc, E., Hondur, A. M., Bilgihan, K., Aydin, B., Guler, M. O. & Tekinay, A. B. (2014). *Bioactive self-assembled peptide nanofibers for corneal stroma regeneration*

Vazirani, J., Nair, D., Shanbhag, S., Wurity, S., Ranjan, A. & Sangwan, V. (2018). Limbal Stem Cell Deficiency—Demography and Underlying Causes. *American Journal of Ophthalmology, 188*, 99-103.

Vemuganti, G. K., Kashyap, S., Sangwan, V. S. & Singh, S. (2004). Ex-vivo potential of cadaveric and fresh limbal tissues to regenerate cultured epithelium. *Indian Journal of Ophthalmology, 52*(2), 113.

Venugopal, B., Shenoy, S. J., Mohan, S., Anil Kumar, P. R. & Kumary, T. V. (2019). Bioengineered corneal epithelial cell sheet from mesenchymal stem cells—A functional alternative to limbal stem cells for ocular surface reconstruction. *Journal of Biomedical Materials Research Part B: Applied Biomaterials,*

Vrana, N. E., Builles, N., Justin, V., Bednarz, J., Pellegrini, G., Ferrari, B., Damour, O., Hulmes, D. J. & Hasirci, V. (2008). Development of a reconstructed cornea from collagen–chondroitin sulfate foams and human cell cultures. *Investigative Ophthalmology & Visual Science, 49*(12), 5325-5331.

Wade, R. J., & Burdick, J. A. (2014). Advances in nanofibrous scaffolds for biomedical applications: From electrospinning to self-assembly. *Nano Today, 9*(6), 722-742.

Wang, C., Varshney, R. R. & Wang, D. (2010). Therapeutic cell delivery and fate control in hydrogels and hydrogel hybrids. *Advanced Drug Delivery Reviews, 62*(7), 699-710.

Wang, Z., Abdulla, R., Parker, B., Samanipour, R., Ghosh, S. & Kim, K. (2015). A simple and high-resolution stereolithography-based 3D bioprinting system using visible light crosslinkable bioinks. *Biofabrication, 7*(4), 045009.

Watson, S. L., Marcal, H., Sarris, M., Di Girolamo, N., Coroneo, M. T. & Wakefield, D. (2010). The effect of mesenchymal stem cell conditioned media on corneal stromal fibroblast wound healing activities. *The British Journal of Ophthalmology, 94*(8), 1067-1073.

West, J. D., Dorà, N. J. & Collinson, J. M. (2015). Evaluating alternative stem cell hypotheses for adult corneal epithelial maintenance. *World Journal of Stem Cells, 7*(2), 281.

Whitcher, J. P., Srinivasan, M. & Upadhyay, M. P. (2001). Corneal blindness: a global perspective. *Bulletin of the World Health Organization, 79*, 214-221.

Wilmut, I., Leslie, S., Martin, N. G., Peschanski, M., Rao, M., Trounson, A., Turner, D., Turner, M. L., Yamanaka, S. & Taylor, C. J. (2015). Development of a global network of induced pluripotent stem cell haplobanks. *Regenerative Medicine, 10*(3), 235-238.

Wilson, S. L., El Haj, A. J. & Yang, Y. (2012a). Control of scar tissue formation in the cornea: strategies in clinical and corneal tissue engineering. *Journal of Functional Biomaterials, 3*(3), 642-687.

Wilson, S. L., Wimpenny, I., Ahearne, M., Rauz, S., El Haj, A. J. & Yang, Y. (2012b). Chemical and topographical effects on cell differentiation and matrix elasticity in a corneal stromal layer model. *Advanced Functional Materials, 22*(17), 3641-3649.

Wray, L. S., & Orwin, E. J. (2009). Recreating the microenvironment of the native cornea for tissue engineering applications. *Tissue Engineering Part A, 15*(7), 1463-1472.

Wu, J., Du, Y., Mann, M. M., Funderburgh, J. L. & Wagner, W. R. (2014a). Corneal stromal stem cells versus corneal fibroblasts in generating structurally appropriate corneal stromal tissue. *Experimental Eye Research, 120*, 71-81.

Wu, J., Rnjak-Kovacina, J., Du, Y., Funderburgh, M. L., Kaplan, D. L. & Funderburgh, J. L. (2014b). Corneal stromal bioequivalents secreted on patterned silk substrates. *Biomaterials, 35*(12), 3744-3755.

Wu, J., Du, Y., Watkins, S. C., Funderburgh, J. L. & Wagner, W. R. (2012). The engineering of organized human corneal tissue through the spatial guidance of corneal stromal stem cells. *Biomaterials, 33*(5), 1343-1352.

Wu, Z., Kong, B., Liu, R., Sun, W. & Mi, S. (2018). Engineering of corneal tissue through an aligned PVA/collagen composite nanofibrous electrospun scaffold. *Nanomaterials, 8*(2), 124.

Wu, Z., Su, X., Xu, Y., Kong, B., Sun, W. & Mi, S. (2016). Bioprinting three-dimensional cell-laden tissue constructs with controllable degradation. *Scientific Reports, 6*, 24474.

Yang, X., Moldovan, N. I., Zhao, Q., Mi, S., Zhou, Z., Chen, D., Gao, Z., Tong, D. & Dou, Z. (2008). Reconstruction of damaged cornea by autologous transplantation of epidermal adult stem cells. *Molecular Vision, 14*, 1064.

Yang, Y., Wimpenny, I. & Ahearne, M. (2011). Portable nanofiber meshes dictate cell orientation throughout three-dimensional hydrogels. *Nanomedicine: Nanotechnology, Biology and Medicine, 7*(2), 131-136.

Yao, L., Li, Z., Su, W., Li, Y., Lin, M., Zhang, W., Liu, Y., Wan, Q. & Liang, D. (2012). Role of mesenchymal stem cells on cornea wound healing induced by acute alkali burn. *PLoS One, 7*(2), e30842.

Yazdani, M., Shahdadfar, A., Jackson, C. J. & Utheim, T. P. (2019). Hyaluronan-Based Hydrogel Scaffolds for Limbal Stem Cell Transplantation: A Review. *Cells, 8*(3), 245.

Yazdanpanah, G., Haq, Z., Kang, K., Jabbehdari, S., Rosenblatt, M. l. & Djalilian, A. R. (2019). Strategies for reconstructing the limbal stem cell niche. *The Ocular Surface, 17*(2), 230-240.

Yazdanpanah, G., Jabbehdari, S. & Djalilian, A. R. (2017). Limbal and corneal epithelial homeostasis. *Current Opinion in Ophthalmology, 28*(4), 348.

Ye, J., Shi, X., Chen, X., Xie, J., Wang, C., Yao, K., Gao, C. & Gou, Z. (2014). Chitosan-modified, collagen-based biomimetic nanofibrous membranes as selective cell adhering wound dressings in the treatment of chemically burned corneas. *Journal of Materials Chemistry B, 2*(27), 4226-4236.

Yoeruek, E., Bayyoud, T., Maurus, C., Hofmann, J., Spitzer, M. S., Bartz-Schmidt, K. & Szurman, P. (2012). Decellularization of porcine corneas and repopulation with human corneal cells for tissue-engineered xenografts. *Acta Ophthalmologica, 90*(2)

Zakaria, N., Possemiers, T., Dhubhghaill, S. N., Leysen, I., Rozema, J., Koppen, C., Timmermans, J. P., Berneman, Z. & Tassignon, M. J. (2014). Results of a phase I/II clinical trial: standardized, non-xenogenic, cultivated limbal stem cell transplantation. *Journal of Translational Medicine, 12*, 58-58.

Zarembinski, T. I., Doty, N. J., Erickson, I. E., Srinivas, R., Wirostko, B. M. & Tew, W. P. (2014). *Thiolated hyaluronan-based hydrogels crosslinked using oxidized glutathione: An injectable matrix designed for ophthalmic applications*

Zhang, B., Xue, Q., Li, J., Ma, L., Yao, Y., Ye, H., Cui, Z. & Yang, H. (2019). 3D bioprinting for artificial cornea: Challenges and perspectives. *Medical Engineering & Physics, 71*, 68-78.

Zhang, C., Wen, J., Yan, J., Kao, Y., Ni, Z., Cui, X. & Wang, H. (2015a). In situ growth induction of the corneal stroma cells using uniaxially aligned composite fibrous scaffolds. *RSC Advances, 5*(16), 12123-12130.

Zhang, L., Coulson-Thomas, V. J., Ferreira, T. G. & Kao, W. W. Y. (2015b). Mesenchymal stem cells for treating ocular surface diseases. *BMC Ophthalmology, 15*(S1), 155.

Zhang, S., Espandar, L., Imhof, K. M. & Bunnell, B. A. (2013). Differentiation of Human Adipose-derived Stem Cells along the Keratocyte Lineage. *Journal of Clinical & Experimental Ophthalmology, 4*(270), 11435.

Zhu, J., & Marchant, R. E. (2011). Design properties of hydrogel tissue-engineering scaffolds. *Expert Review of Medical Devices, 8*(5), 607-626.

# PUBLICATIONS

# PUBLICATION I

**Hydrazone-crosslinked hyaluronan-based hydrogels for therapeutic delivery of adipose stem cells to treat corneal defects**

Laura Koivusalo, Jennika Karvinen, Eetu Sorsa, Ilari Jönkkäri, Jari Väliaho, Pasi Kallio, Tanja Ilmarinen, Susanna Miettinen, Heli Skottman, Minna Kellomäki

Materials Science and Engineering: C, 2018, vol 85, 68-78
https://doi.org/10.1016/j.msec.2017.12.013

Materials Science & Engineering C 85 (2018) 68–78

Contents lists available at ScienceDirect

Materials Science & Engineering C

journal homepage: www.elsevier.com/locate/msec

# Hydrazone crosslinked hyaluronan-based hydrogels for therapeutic delivery of adipose stem cells to treat corneal defects

Laura Koivusalo[a,*,1], Jennika Karvinen[b,1], Eetu Sorsa[b], Ilari Jönkkäri[c], Jari Väliaho[b], Pasi Kallio[b], Tanja Ilmarinen[a], Susanna Miettinen[a], Heli Skottman[a], Minna Kellomäki[a,b]

[a] BioMediTech Institute and Faculty of Medicine and Life Sciences, University of Tampere, Arvo Ylpön katu 34, FI-33520 Tampere, Finland
[b] BioMediTech Institute and Faculty of Biomedical Sciences and Engineering, Tampere University of Technology, Korkeakoulunkatu 3, FI-33101 Tampere, Finland
[c] Faculty of Engineering Sciences, Tampere University of Technology, Korkeakoulunkatu 6, FI-33101 Tampere, Finland

ARTICLE INFO

*Keywords:*
Hyaluronan
Hydrogel
Collagen I
Adipose stem cells
Cell delivery
Corneal stroma

ABSTRACT

Corneal blindness is a worldwide problem, plagued by insufficient amount of high-quality donor tissue. Cell therapy using human adipose stem cells (hASCs) has risen as an alternative to regenerate damaged corneal stromal tissue, the main structural and refractive layer of the cornea. Herein we propose a method to deliver hASCs into corneal defects in hyaluronan (HA)-based hydrogels, which form rapidly *in situ* by hydrazone crosslinking. We fabricated two different HA-based hydrazone-crosslinked hydrogels (HALD1-HACDH and HALD2-HAADH), and characterized their swelling, degradation, mechanical, rheological and optical properties and their ability to support hASC survival. To promote hASC attachment and survival, we incorporated collagen I (col I) to the more stable HALD1-HACDH hydrogel, since the HALD2-HAADH hydrogel suffered swift degradation in culture conditions. We then used an organ culture model with excised porcine corneas to study the delivery of hASCs in these three hydrogels for stromal defect repair. Although all hydrogels showed good hASC survival directly after encapsulation, only the collagen-containing HALD1-HACDH-col I hydrogel showed cells with elongated morphology, and significantly higher cell metabolic activity than the HALD1-HACDH gel. The addition of col I also increased the stiffness and reduced the swelling ratio of the resulting hydrogel. Most importantly, the corneal organ culture model demonstrated these hydrogels as clinically feasible cell delivery vehicles to corneal defects, allowing efficient hASC integration to the corneal stroma and overgrowth of corneal epithelial cells.

## 1. Introduction

Corneal blindness due to trauma, burns and various inherited or acquired diseases is a worldwide problem, with estimated 1.5 to 2 million new cases annually [1]. Currently these cases are only treatable by transplantation of a donor cornea; a procedure restricted by immune reactions and graft failure, as well as a continuous shortage of suitable donor tissue [2]. The limitations of corneal transplants have driven the search for alternative treatment options, particularly by means of tissue engineering and stem cell therapy. Mesenchymal stem cells (MSCs) have gained great interest in corneal regeneration due to their immunomodulatory and antiangiogenic properties [3], as well as for their capability to inhibit corneal scarring [4]. Human adipose stem cells (hASCs) are an abundant and accessible source of adult MSCs [5], which have also been shown to differentiate towards corneal stromal keratocytes *in vivo* when delivered to the corneal stroma [6,7]. However, simple stromal injection of hASCs in saline solution results in only low amount of integrated cells and insufficient new collagen production [6,8], whereas hydrogel delivery increases the survival of hASCs in the corneal stroma [7].

Collagen I (col I) and hyaluronan (HA) are natural extracellular matrix (ECM) components, present in varying abundance in different tissues. Col I is the main component of ECM in the corneal stroma, where it exists as highly regular fibrils for combined mechanical strength and high transparency [9]. HA is a high molecular weight polysaccharide, which has a high capacity to retain water and is degraded *in vivo* by hyaluronidase enzymes [10,11]. Rather than use HA in its native form, it can be modified through the carboxyl acid and hydroxyl groups in the D-glucuronic acid and *N*-acetyl-D-glucosamine sugar residues. HA-based hydrogels have also been previously suggested for corneal stromal repair, but to date they have required external crosslinkers and need to be preformed prior to implantation [7].

* Corresponding author.
*E-mail address:* laura.koivusalo@uta.fi (L. Koivusalo).
[1] Authors contributed equally.

https://doi.org/10.1016/j.msec.2017.12.013
Received 3 July 2017; Received in revised form 22 August 2017; Accepted 7 December 2017
Available online 18 December 2017
0928-4931/ 

Hydrogel components, which gel upon mixing without external crosslinking agents, have the added advantage that they can be injected directly to the defect site where they are able to fill even irregularly shaped defects.

Hydrazone crosslinking has been widely used to prepare hydrogels for tissue engineering applications. Hydrazone crosslinking is a reaction between aldehyde- and hydrazide-groups and belongs to the group of pseudo click reactions (pseudo refers to moderate orthogonality). These reactions have many favorable properties, i.a. high reactivity, simple reaction conditions, no toxic reagents or side products, and high yields [12]. HA can be modified with complementary reactive aldehyde and hydrazide groups to enable this crosslinking. Aldehyde groups can be generated from vicinal diol groups of HA using periodate oxidation [13], or by incorporating an amino-glycerol side chain *via* an amidation reaction and selective oxidation of the pendent group of HA [14]. The latter method provides a less invasive way to modify the polymer. Hydrazide groups can be produced *via* reaction with either adipic acid dihydrazide [15,16] or carbodihydrazide [17]. The polyanionic behavior of HA at physiological pH hinders the adhesion of proteins and cells, which can be overcome by addition of other ECM binding sites, such as collagen [18]. Collagen can be incorporated to the previously described hydrogels, for example through imine formation, although it should be noted, that neutralized collagen can also form a gel on its own at 37 °C.

The aim of the study was to create transparent HA-based hydrogels for the delivery of hASCs for regeneration of the corneal stroma. In this study, we fabricated two HA-based hydrazone crosslinked hydrogels, and characterized their swelling, degradation, mechanical, rheological and optical properties and their ability to support hASC survival. We then further incorporated human col I into the more stable hydrogel, with the aim to promote hASC attachment and survival. In order to demonstrate proof-of-concept, we used an organ culture model with excised porcine corneas to evaluate the clinical relevance of the HA-based hydrogels for hASC delivery to stromal defects.

## 2. Materials and methods

### 2.1. Materials and general methods

Hyaluronic acid sodium salt ($M_w$ = 1.5 × $10^5$ g/mol) was purchased from Lifecore (Chaska, MN, USA). Adipic acid dihydrazide (ADH), hyaluronidase from bovine testes (Type I−S, 400–1000 units/mg solid), hydroxylamine hydrochloride, acetic acid, sucrose, 1-hydroxybentzotriazole (HOBt), carbodihydrazide (CDH), 3-amino-1,2-propanediol, t-butyl carbazate (TBC), picrylsulfonic acid solution (5% (*w/v*) in $H_2O$, TNBS), sodium cyanoborohydride, sodium periodate, sodium acetate, ethylene glycol, 1-Ethyl-3-[3-(dimethylamino)propyl] carbodiimide (EDC), dimethyl sulphoxide (DMSO), and deuterium oxide (99.9 atom% D, contains 0.05 wt% 3-(trimethylsilyl)-propionic-2,2,3,3-d4 acid, sodium salt) and collagen type I from human placenta were purchased from Sigma-Aldrich (St. Louis, MO, USA). Sodium chloride was purchased from J.T. Baker (Holland). All solvents used were of analytical quality. Milli-Q water was used in synthesis and determinations. Dialysis membranes (Spectra/Por®cut-off 3500, 12–14,000 and 25,000 g/mol) were purchased from Spectrum Laboratories, Inc. (Rancho Dominguez, CA, USA).

NMR-spectra were measured with Varian Mercury 300 MHz NMR Spectrometer (Palo Alto, USA). Samples (5 mg) were dissolved in deuterium oxide (600 μL) containing internal standard (0.05 wt% 3-(trimethylsilyl)-propionic-2,2,3,3-d4 acid, sodium salt). FTIR-spectra from hyaluronan components and formed hydrogels were measured on a Perkin Elmer Spectrum One ATR-FTIR Spectrometer (Waltham, MA, USA) in the spectral range of 400 to 4000 $cm^{-1}$.

### 2.2. Synthesis of aldehyde-modified hyaluronans

Aldehyde groups were introduced to HA according to previously reported method [14]. Reaction scheme is shown in Fig. S1 (a). Briefly, HA (400 mg) was dissolved in deionized water (60 mL). 3-amino-1,2-propanediol (182 mg), and HOBt (153 mg) pre-dissolved in 1:1 (*v/v*) mixture of acetonitrile-water (2 mL) were added, and pH of the solution was adjusted to 6 (1 M HCl). EDC (58 mg) was added to the mixture under nitrogen and stirred overnight. Derivatized polymer was dialyzed with MW cutoff 3500 membrane against dilute HCl (pH 3) containing 0.1 M NaCl for 48 h and against dilute HCl (pH 3) for 24 h. Purified polymer was lyophilized to obtain a white cotton-like product (2,3-dihydroxypropyl amide derivative of HA). This product (200 mg) was dissolved in deionized water (25 mL). Sodium periodate (107 mg) pre-dissolved in deionized water (0.5 mL) was added to the solution in the dark at room temperature (RT) and stirred for 5 min. Ethylene glycol (0.06 mL) was added to inactivate unreacted periodate and solution was stirred for 2 h. Derivatized polymer was dialyzed with MW cutoff 3500 membrane against deionized water for 24 h. Purified polymer was lyophilized to obtain a white cotton-like product, HALD1. $^1$H NMR ($D_2O$, 300 MHz) 2,3-dihydroxypropyl amide derivative of HA: δ 4.53 (br s, 1H), 3.83–3.34 (m, 10H), 2.00 (s, 3H). HALD1 (Fig. S3 (a), $D_2O$, 300 MHz): δ 9.57 (s, 1H), 4.53 (br s, 1H), 3.65 (sharp s, 1H), 3.83–3.34 (m, 10H), 2.01 (s, 3H). FTIR (Fig. 1 (a), $cm^{-1}$): 1732 (ν(C═O) of −C(O)H), 1643 (ν(C═O) of *sec*. amide), 1617 (d(N−H) of −NHC(O)−), 1558 (d(N−H) of sec. amide).

Alternatively, a periodate oxidation was used to generate aldehyde groups from vicinal diol groups of HA according to previously reported method [13] with small modifications. Reaction scheme is shown in Fig. S1 (b). Briefly, sodium hyaluronate (0.500 g) was dissolved in deionized water (100 mL). Sodium periodate (0.30 g) was dissolved in deionized water (2.7 mL), added dropwise and stirred for 4 h in the dark at RT under nitrogen. Ethylene glycol (4 equivalents) was added to inactivate any unreacted periodate and the solution was then stirred for 1 h. Derivatized polymer was dialyzed with MW cutoff 25,000 membrane against deionized water for three days. Purified polymers were lyophilized to obtain white cotton-like product, HALD2. $^1$H NMR (Fig. S3 (b), $D_2O$, 300 MHz): HALD2: *δ* 4.47 (m, 1H, H1 of glucose unit), 3.84–3.34 (m, 5H, H2–5 of glucose unit), 2.02 (s, 3H, −NHC(O)CH3). FTIR (Fig. 1 (b), $cm^{-1}$): HALD2: 1721 (ν(C═O) of −C(O)H), 1633 (ν(C═O) of −NHC(O)− and −C(O)OH), 1618 (d(N−H) of −NHC(O)−).

Degree of substitution (DS%) of HALD components were determined with TNBS method similarly to [19,20]. Briefly, HALD (20 mg) was dissolved in acetate buffer (2 mL, 0.1 M, pH 5.2) and added to TBC solution in acetate buffer (1 mL, 0.0348 g, 10-fold excess per molar amount of sodium periodate used). The mixture was allowed to react for 1 h at RT. Sodium cyanoborohydride (1 mL, 0.0166 g, equimolar amount to TBC) in acetate buffer was added and allowed to react for 24 h at room temperature under nitrogen. The polymer was dialyzed with MW cutoff 25,000 membrane against 0.1 M NaCl for 24 h and for a further 24 h in deionized water. Purified polymer was lyophilized to obtain a white cotton-like product. The $^1$H NMR spectrum was measured and the DS% was determined from the integration of $^1$H NMR peaks. $^1$H NMR ($D_2O$, 300 MHz): δ 2.0 (3H, $NHCOCH_3$) and 1.4 (9H, t-Boc).

### 2.3. Synthesis of hydrazide-modified hyaluronans

Hydrazide groups were introduced to HA according to previously reported method [17]. Reaction scheme is shown in Fig. S1 (c). Briefly, HA (408 mg) was dissolved in deionized water (100 mL). Carbodihydrazide (90 mg) and HOBt (153 mg) were added to the solution and pH was adjusted to 4.7 (0.1 M NaOH). EDC (19.17 mg) was added under nitrogen and stirred for overnight. Derivatized polymer was dialyzed with MW cutoff 3500 membrane against dilute HCl (pH 3.5) containing 0.1 M NaCl for 48 h and against deionized water for 24 h. Purified

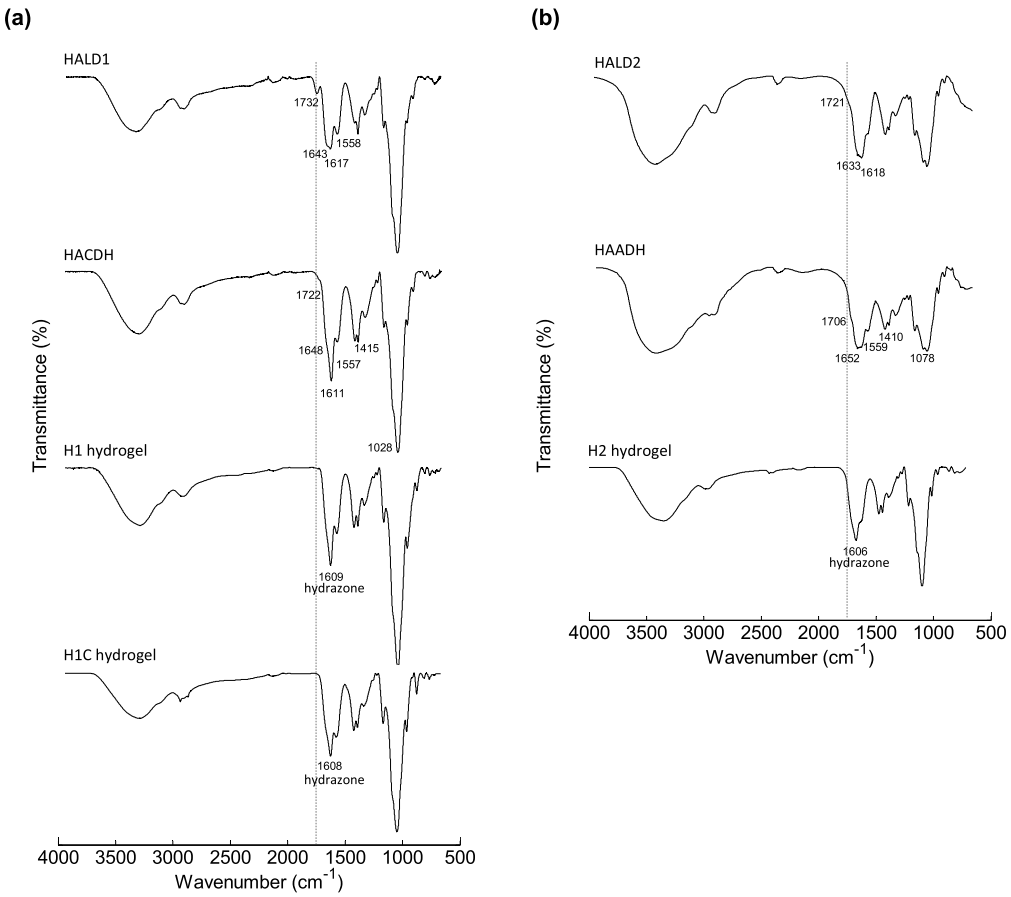


**Fig. 1.** Chemical structure analysis of polymer components and HA-based hydrogels. (a) FTIR spectra of HALD1 and HACDH components and hydrazone crosslinked HALD1-HACDH (− col I) hydrogels (H1 and H1C). (b) FTIR spectra of HALD2 and HAADH components and hydrazone crosslinked HALD2-HAADH (H2) hydrogel. The appearance of a hydrazone C═N stretching signal at 1609, 1608 and 1606 $cm^{-1}$ for H1, H1C and H2 hydrogels (respectively) and the disappearance of an aldehyde signal at 1732 $cm^{-1}$ for H1 and H1C hydrogels, and at 1721 $cm^{-1}$ for H2 hydrogel confirmed the presence of hydrazone crosslinking.

polymer was lyophilized to obtain a white cotton-like product, HACDH. $^1$H NMR (Fig. S4, $D_2O$, 300 MHz): δ 4.54 (br s, 1H), 3.84–3.34 (m, 10H), 2.02 (s, 3H). FTIR (Fig. 1 (a), $cm^{-1}$): 1722 and 1648 (νC═O) of *sec*. amide), 1611 (d(N−H) of prim. amine), 1557 (d(N−H) of prim. amide), 1415 (d(N−H) of sec. amide), 1028 (ν(C−N) of amine).

DS% of HACDH was determined with TNBS assay as described in [17].

Alternatively, HA was modified with hydrazide groups *via* reaction with adipic acid dihydrazide. The fabrication of the polymer product, HAADH, has been previously reported in [16]. $^1$H NMR and FTIR spectra are reported in the same article.

### 2.4. Formation of hydrazone crosslinked hyaluronan-based hydrogels

Hydrogels were fabricated according to Table 1 and Fig. S2. HALD1-HACDH hydrogel (H1) was prepared by dissolving the freeze-dried HALD1 and HACDH components in PBS (pH 7.4) and mixing them in equal volumes. The gelation was shown to occur at RT and at 37 °C; in this case the components were allowed to gel at 37 °C for at least 30 min. HALD2-HAADH hydrogel (H2) was prepared similarly, with the freeze dried HALD2 and HAADH components dissolved in 10% sucrose. For different characterizations, cut syringes were used as molds to ease pushing the sample out. For cell culture, circular polydimethyl siloxane (PDMS) molds with 10 mm inner diameter were used. Solutions were sterilized prior to gelation using Whatman FP 30/0.2 CA-s 0.2 μm (Whatman plc, Little Chalfont, UK) filters.

Additionally, human col I was introduced as a third gel component in H1-based hydrogel (H1C). Briefly, col. I solution (5 mg/mL in acetic acid, pH ≈ 3) was sonicated and then neutralized using 1 M NaOH. After neutralization, col I was mixed with HALD1 component followed by mixing with HACDH component.

The gelation time of hydrogels was determined using a tube tilt test [21], where the gel point can be determined simply by tilting a tube

**Table 1**
Compositions of hydrazone crosslinked HA-based hydrogels.

| Code | Gel components A-B-C | DS% A/B | Conc. mg/mL A/B/C | Volume ratio A:B:C |
|---|---|---|---|---|
| H1 | HALD1-HACDH | 15/17 | 30/30 | 1:1 |
| H1C | HALD1-HACDH-col I | 15/17 | 30/30/5 | 2:2:1 |
| H2 | HALD2-HAADH | 9/50 | 20/10 | 1:1 |

with gel solution and observing the time point where the system stops flowing.

### 2.5. Swelling kinetics

The swelling kinetics of the hydrogels were studied in cell culture medium (DMEM/F-12, Thermo Fisher Scientific, Waltham, MA, USA). Three parallel freshly made hydrogel samples (100 μL) were weighed and placed into medium at 37 °C. At different time points, the hydrogels were weighed and the swelling ratio (SR) was calculated from the following equation:

$$SR = \frac{W_{swollen} - W_{initial}}{W_{initial}} \times 100\%$$

where $W_{swollen}$ is the mass of swollen hydrogel and $W_{initial}$ is the mass of freshly made wet hydrogel.

### 2.6. Enzymatic degradation

The enzymatic degradation of the hydrogels was studied by incubating three parallel freshly made hydrogel samples (100 μL) in hyaluronidase (HAse)-solution (20–50 U/mL in PBS) at 37 °C until they were completely degraded. At specific time points, the samples were weighed and the residual mass (%) was calculated. Control samples, without hyaluronidase, were used to show that the degradation was not only due to hydrolysis.

### 2.7. Rheological measurements

The rheological measurements were performed using a rotational Haake RheoStress RS150 rheometer equipped with Rheowizard 4.3 software (ThermoHaake, Germany) with cone-plate geometry (20 mm diameter) and a gap of 0.8 mm. Three parallel hydrogel samples (500 μL, height 1 mm x diameter 20 mm) were prepared 24 h before measurements into molds and covered with Parafilm. All rheological experiments were performed at 37 °C in the oscillatory mode. Amplitude sweep ($\gamma$ = 0.01–10, $\omega$ = 1 Hz) and frequency sweep ($\omega$ = 0.1–10 Hz, $\gamma$ = 0.1) were used. Storage (G′), loss (G″) and complex moduli (G*) as well as the loss tangent ($\tan\delta = G''/G'$) indicating the overall viscoelasticity of material were determined [16].

### 2.8. Mechanical measurements

The compression measurements were conducted using a BOSE Electroforce Biodynamic 5100 machine equipped with a 225 N load sensor and Wintest 4.1 software (Bose Corporation, Eden Prairie, MN, USA). Five parallel hydrogel samples (875 μL, height 7 mm x diameter 12 mm) were prepared 24 h before measurements into molds and covered with Parafilm. To keep the sample from slipping, the platen surfaces were covered with Parafilm. Samples were compressed using unconfined compression at a rate of 10 mm/min to at least 65% strain in air at RT.

The stiffness of the materials was estimated based on the data obtained from a stress-strain curve. The determination was done similarly to [16]. Briefly, if the measured data is represented by a polynomial (6th order), the stiffness ($\Gamma$) may be defined as a derivative of stress ($\sigma$) with respect to strain ($\varepsilon$) according to the equation:

$$\frac{d\sigma}{d\varepsilon} \equiv \Gamma(\varepsilon) = \sum_{k=1}^{n} k c_k \varepsilon^{k-1}$$

where the coefficients of the polynomial $c_k$ are the so-called elastic constants. Here, $c_1$ is the second-order elastic constant, which is sometimes also called the elastic constant, Young's modulus or elastic stiffness constant [22–24]. Second-order elastic constants were estimated based on the means of stiffness polynomials of the five parallel samples at 0–0.15 strain with minimum standard deviations. It should be noted that the stiffness describes the same quantity as the second-order elastic constant, the latter being the stiffness at zero strain $\Gamma(0) = c_1$.

### 2.9. Optical measurements – refractive index and transparency

Refractive indices of the hydrogels were determined using surface plasmon resonance equipment Navi 210A (BioNavis, Tampere, Finland). The device's goniometer and light source were used to scan the critical angle of total internal reflection between glass and hydrogel. A glass slide (BK7 glass) with a known refractive index was used for device calibration and measurements. After calibration, the flow cell of the device was filled with a hydrogel sample. A curve showing the reflection coefficient as a function of the angle of incidence was obtained from the measurement. The refractive indices of the hydrogels were determined from the curves utilizing Snell's law with the critical angle condition:

$$n_{gel} = n_{glass} \sin(\alpha)$$

where $n_{gel}$ and $n_{glass}$ are the refractive indices of hydrogel and glass slide ($n_{glass}$ = 1.514, [25]), and $\alpha$ is the angle of incidence determined from the curve.

The optical transparency of hydrogels was evaluated using a spectrophotometer (UV–VIS–NIR Spectrophotometer UV-3600Plus, Shimadzu, Kyoto, Japan) operating at the visible wavelength range (400–700 nm). Hydrogel samples (900 μL, thickness 10 mm) were prepared directly into the 1.5 mL semi-micro cuvettes. The hydrogel films (diameter 10 mm × thickness 1 mm) were also photographed to show their optical clarity and transparency.

### 2.10. Cell experiments in hyaluronan-based hydrogels

#### 2.10.1. Cell encapsulation in hydrogels and in vitro cell culture

This study was conducted under approval of the Ethics Committee of the Pirkanmaa Hospital District (Tampere, Finland, approval number R15161). The hASCs were isolated from adipose tissue samples from a female donor undergoing elective plastic surgery at Tampere University Hospital (Tampere, Finland) with patient's written consent. hASCs were isolated mechanically and enzymatically from subcutaneous adipose tissue as described previously [26,27] and characterized for their surface marker expression by flow cytometry (FACSAria; BD Biosciences, Erembodegem, Belgium) as described in [27]. The cell characterization profile is shown in Table S1.

The hASCs were cultured in a medium containing Dulbecco's modified Eagle's medium/Ham's nutrient mixture F-12 (DMEM/F-12 1:1, Thermo Fisher Scientific, Waltham, MA, USA) supplemented with 5% human serum (type AB male, HIV tested from BioWest, Nuaillé, France), 1% L-glutamine (GlutaMAX™, Thermo Fisher Scientific) and 1% antibiotics (100 U/mL penicillin, 100 μg/mL streptomycin, Lonza, Basel, Switzerland). The cells were maintained in T175 cell culture flasks at 37 °C in 5% $CO_2$, and passaged at approximately 80% confluence using TrypLE™ Select (Thermo Fisher Scientific).

Cells were encapsulated in hydrogels at passages 4–6. Prior to encapsulation, hASCs were detached from cell culture flasks and collected by centrifugation. Cells were resuspended in cell culture medium, counted and the appropriate number of cells required for each hydrogel were centrifuged to a pellet. Supernatant was removed and cell pellets were mixed by thorough pipetting into the aldehyde-modified HA component at a concentration of $4 \times 10^6$ cells/mL, with final hydrogel volume of 100 μL. The hydrogels were then formed in PDMS molds as described in Section 2.3. The cell-laden hydrogels were transferred onto tissue culture plates for further *in vitro* culture, with fresh hASC medium changed three times a week.

*2.10.2. Cell viability measurements*

The viability of hydrogel-encapsulated hASCs was assessed at time points 1 day, 3 days, 7 days and 10 days after encapsulation. Resazurin-based measurement of metabolic activity was performed using PrestoBlue® Cell Viability Reagent and qualitative analysis of viable cells using LIVE/DEAD® viability/cytotoxicity kit for mammalian cells (both from Thermo Fisher Scientific).

For PrestoBlue® analysis, three samples of each hydrogel containing hASCs and one sample without cells were washed once with DPBS (Lonza) and PrestoBlue® reagent diluted 1:10 (*v*/v) in hASC medium was added to the samples. After a 4-h incubation at 37 °C, 100 μL aliquots of PrestoBlue® medium were collected in triplicate from each sample on a 96-well plate and their fluorescence was measured using Viktor 1420 Multilabel Counter (Wallac, Turku, Finland) at excitation and emission wavelengths of 544 nm and 590 nm, respectively.

For qualitative analysis of cell viability, hydrogel samples were incubated with Live/Dead staining solution containing 2 μM Calcein AM and 1 μM Ethidium homodimer diluted in DPBS in 37 °C for 45 min. The samples were washed with DPBS to reduce background fluorescence, and subsequently imaged using an Olympus IX51 fluorescence microscope equipped with a DP71 camera (Olympus Corporation, Tokyo, Japan).

*2.10.3. Cornea organ culture*

Whole porcine eyes were obtained from a local abattoir and kept on ice in AMES buffer (Sigma–Aldrich) containing 10 mM HEPES and 2% antibiotics for up to 4 h. Excess tissue was removed and the eyes were disinfected as described in [28]. The corneas were excised, moved to tissue culture plates, and cultured partially submerged in serum-free co-culture medium (CnT-Prime-CC, CellnTech, Bern, Switzerland) with 1% antibiotics, 0.25 μg/mL amphotericin B (Thermo Fisher Scientific) and 5 μg/mL Plasmocin (InvivoGen, Toulouse, France) at 37 °C in 5% $CO_2$ for up to two weeks. The culture medium was changed three times a week, with dropwise addition of new medium to wet the central cornea.

For implantation of hydrogels to porcine corneas, they were mounted on a Barron artificial anterior chamber (Katena products Inc., Denville, NJ, USA) where the operation was performed. First, the corneal epithelium was scraped off using the flat edge of a scalpel (Feather Safety Razor co,. ltd, Osaka, Japan). Then, a 5-mm trephine (Robbins Instruments, Chatham, NJ, USA) was used to make a partial depth incision in the center of the cornea, from which the stroma was removed with a crescent knife (Bausch&Lomb Inc., Rochester, NY, USA). In the formed stromal cavities, hydrogels with hASCs ($n$ = 5) and without any cells ($n$ = 2) were cast as described in Sections 2.3. and 2.10.1. with final hydrogel volume of 50 μL. After gelation, the corneas were removed from the artificial anterior chamber, placed back into culture plates and covered with silicone contact lenses (EyeQ One-Day Premium, Cooper Vision, Hamble, UK). The culture medium was changed to hASC medium, with the corneas partially submerged. The porcine corneas were cultured for 7 days with the hydrogels and subsequently fixed for 4 h in RT with either 4% PFA or acid-formalin/EtOH –fixative (10% formaldehyde in 70% ethanol and 5% glacial acetic acid, all *v*/v), as the acid-formalin/EtOH should preserve HA better than the standard formalin fixation [29]. The samples were dehydrated in an automated tissue processor (Tissue-Tek VIP, Sakura Finetek Europe) and embedded in paraffin.

To evaluate hASC incorporation into the corneal stroma, immunohistochemical staining for the pan-human marker TRA-1-85 was performed. 5-μm-thick sections of samples were mounted onto SuperFrost glass slides, conventionally deparaffinated and hydrated. Antigen retrieval was performed by placing slides in hot 0.01 M citrate buffer (pH 6.0) for 10 min. After cooling to RT, samples were washed with PBS, endogenic tissue peroxidases were inactivated with 3% $H_2O_2$ for 5 min, and unspecific binding sites were blocked by incubation with 2.5% normal horse serum (Vector ImmPress reagent, Vector Laboratories) at 37 °C for 45 min. Samples were subsequently incubated with anti-TRA-1-85 mouse IgG antibody (courtesy of Peter Andrews, University of Sheffield) in a 1:50 (*v*/v) dilution in 0.5% BSA at 37 °C for 60 min, and washed with PBS. Secondary labeling with the reporter enzyme was done by incubating samples with Vector ImmPress HRP Reagent (Vector Laboratories, Inc., Burlingame, CA, USA) for 30 min at RT. After subsequent washes in PBS, peroxidation was performed for 5 min at RT with Dako liquid DAB + chromogen system (Dako North America, Inc., Carpinteria, CA, USA). Finally, samples were counterstained with Harris hematoxylin (Millipore, Billerica, MA, USA) and mounted with Pertex (Histolab, Askim, Sweden). Samples were imaged with a Nikon Eclipse TE2000-S microscope equipped with a DS-Fi1 camera (Nikon Instruments, Amsterdam, Netherlands).

*2.11. Statistical data analysis*

Statistical data analyses were performed with MATLAB (Statistics and Machine Learning Toolbox™). All the quantitative data are presented as mean and standard deviation. A non-parametric Kruskal-Wallis test and a Wilcoxon rank sum test were used to determine whether there were statistically significant differences within the mechanical and rheological data set, and to analyze specific sample pairs, respectively. Due to a relatively low $n$, a non-parametric testing was chosen. Bonferroni correction was used when more than two groups were compared. A $p$-value $< 0.05$ was considered significant.

## 3. Results and discussion

*3.1. Synthesis of complementary reactive hyaluronan components*

Hyaluronans were modified with aldehyde groups either through periodate oxidation or through selective oxidation of diol-modified HA. The modifications were confirmed with $^1$H NMR and FTIR analysis. In the $^1$H NMR spectrum (Fig. S3 (a)) of HALD1, a barely observable aldehyde peak (9.57 ppm) was detected, whereas with HALD2 it was not visible (Fig. S3 (b)). The reason why the aldehyde peak is not usually observed, is due to a reversible hemiacetal formation [30]. The presence of aldehyde-groups was confirmed based on the FTIR-spectrum (Fig. 1), where the typical aldehyde shoulder (HALD1: 1732 $cm^{-1}$, HALD2: 1721 $cm^{-1}$) was detected. The benefit of using selective oxidation of diol-modified HA instead of periodate oxidation is that it keeps the ring-structure of HA intact and therefore HA is more easily recognized by the cells. Hyaluronans were also modified with hydrazide-groups using either CDH or ADH as a source of the hydrazide unit. The $^1$H NMR spectrum (Fig. S4) of HACDH hardly differed from that of non-modified HA (spectrum not shown), whereas in the FTIR-spectrum (Fig. 1 (a)) signals from the hydrazide unit were detected, including strong amide C=O stretching (1722 $cm^{-1}$) and amide N–H deformation (1611 and 1557 $cm^{-1}$) signals. The benefit of using CDH instead of ADH is discussed more deeply in the next section. The DS% of HALD1 and HACDH components were kept relatively low not to lose the favorable properties of original polymer (Table 1).

*3.2. Formation of hydrazone crosslinked hydrogels*

HA-based hydrazone crosslinked hydrogels were formed from complementary reactive HA components according to Table 1 and Fig. S2. Different aldehyde- and hydrazide-modified components were used for the two hydrogel types, H1 and H2. H1 hydrogel was composed of the HALD1 component formed by selective oxidation of diol-modified HA, and the HACDH component formed by reacting the carboxylic groups in HA with an excess of CDH in the presence of EDC and HOBt. H2 hydrogel, on the other hand, was composed of the periodate oxidized HALD2 component and the HAADH component formed by reacting the carboxylic groups in HA with an excess of ADH in the presence of EDC and HOBt. H1 hydrogel was considered more stable due to a resonance stabilization effect of CDH [17]. CDH has a neighboring

heteroatom ($N^3$) providing resonance stabilization to the developing $N^2$ positive charge. This type of linker ($C^1$═$N^1$–$N^2$H–(C═O)$N^3$H) allows the delocalization of $N^2$ positive charge due to its urea-type structure. There is no stabilization effect with ADH [17]. H1 hydrogel was preferred due to the more stable structure and the less invasive modification of HALD1 component, thus the effect of col I addition was only tested with the H1 hydrogel. The gelation of H1 hydrogels was successful only when PBS or cell culture medium solutions were used, whereas H2 hydrogel gelated only in deionized water or in 10% sucrose. Sucrose was used to make the osmotic pressure more suitable for the cells in cell culture experiments, therefore it was used in other experiments as well.

The hydrogels gelated in 3–5 min, therefore it was possible to mix the components, for example by pipetting the gel solution few times back and forth in the tip. Alternatively, a double syringe system could be used, making the hydrogel injectable. The gelation time is appropriate for clinical applications of the hydrogels as a cell delivery vehicle, as the gels can flow to fill the wound site, but gelate rapidly enough for a fast and simple implantation.

The chemical structure of the hydrogels was determined with FTIR. The FTIR spectra (Fig. 1) of hydrogels showed the appearance of a hydrazone C═N stretching signal at 1609, 1608 and 1606 $cm^{-1}$ for H1, H1C and H2 hydrogels and the disappearance of an aldehyde signal at 1732 $cm^{-1}$ for H1 and H1C hydrogels, and at 1721 $cm^{-1}$ for H2 hydrogel.

### 3.3. Swelling kinetics

The swelling tests were conducted in cell culture medium (DMEM/F-12) to determine hydrogel swelling behavior in the cell culture environment. The swelling ratios (SR, %) of the hydrogels are shown in Fig. 2 (a). The results revealed a difference in the stability of hydrogels. Both H1 and H1C hydrogels were stable even after 48 h, whereas H2 hydrogel degraded in hours, and after 24 h there was no gel left to weigh. Both H1 and H1C hydrogels swell considerably. After 48 h, the SR of H1 hydrogel was over 200%, whereas that of H1C hydrogel was approximately 150%. Although the SRs are quite high considering the final application, it is notable that the addition of col I lowered the SR approximately 20% at each data point. One possible explanation for this is that the imine formation between amino groups of collagen and the aldehyde groups of HA makes the structure of H1C hydrogel more crosslinked. Higher degree of crosslinking reduces the swelling ratio. There is also a marked difference in the swelling behavior of the components themselves; HA is susceptible to swelling whereas collagen is not. As expected, replacing some of the HA with collagen led to a lower swelling ratio.

Usually the swelling ratio is determined by studying the water uptake of dry hydrogels. In this case, it was more informative to study the swelling of freshly made wet hydrogels, because this form of gel was used in the cell culture experiments. It is also known that the drying methods, for example freeze-drying, affect the hydrogel structure [31] and therefore can distort the swelling results. We have also noticed this in our studies (data not shown).

### 3.4. Enzymatic degradation

Enzymatic degradation of the hydrogels was studied using HAse enzyme (20–50 U/mL in PBS). The degradation curves are shown in Fig. 2 (b). The results showed that the degradation behavior of H1 and H2 hydrogels was very different. H1 and H1C hydrogels remained relatively stable for 28 h, after which they were completely degraded by the enzyme by the 48-h time point. H1C hydrogel was slightly more stable than H1, but not significantly. The H1 and H1C control hydrogels did not exhibit significant degradation during the 48 h, indicating that the observed degradation is truly enzymatic rather than caused by simple hydrolysis. On the other hand, H2 hydrogel degraded in a matter of hours. After 24 h, there was no gel left to weigh. Even the control hydrogel started to degrade at the same time, which refers to its tendency to simple hydrolysis caused by the solution environment. Similar behavior was observed in the swelling tests. Different stability behavior between the H1, H1C and H2 hydrogels can be explained by the resonance stabilization effect of CDH described earlier (Section 3.2.).

Based on the results, HAse which degrades HA in biological systems, can recognize the modified HA components and therefore indicates that these hydrogels should be degradable also *in vivo*. HA degradation products are mainly metabolized in the lymph nodes and liver, or locally in alymphatic, densely structured tissues, such as the cornea [10]. As cultured tissue finally replaces the hydrogel scaffold material, the degradation rate of these hydrogels should be tested more thoroughly in actual conditions in order to see if it matches the regeneration rate of the receiving native tissue, as the true HAse enzyme concentration in the cornea may vary from the amount of enzyme used here. It should be noted that the remodeling process of the injured stroma can take months or even years to complete [32].

### 3.5. Rheological properties

The viscoelastic properties of the hydrogels were determined using rheological tests. The amplitude dependence of modulus for hydrogels is presented in Fig. 3 (a). The linear viscoelastic region (LVR) was

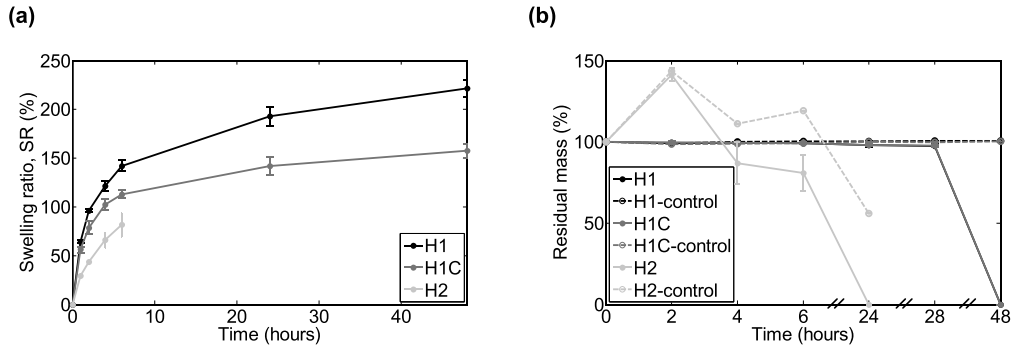


**Fig. 2.** Swelling kinetics and enzymatic degradability of HA-based hydrogels. (a) Swelling ratio (SR, %) as a function of time (hours) curves of HALD1-HACDH (H1), HALD1-HACDH-col I (H1C) and HAL2-HAADH (H2) hydrogels in cell culture medium (DMEM/F-12). (b) Enzymatic degradation profiles of H1, H1C and H2 hydrogels in HAse enzyme (20–50 U/mL in PBS). Both experiments showed the instability of H2 hydrogel, whereas H1 and H1C were shown to be more stable. The mean ($n$ = 3) and standard deviation bars are shown.

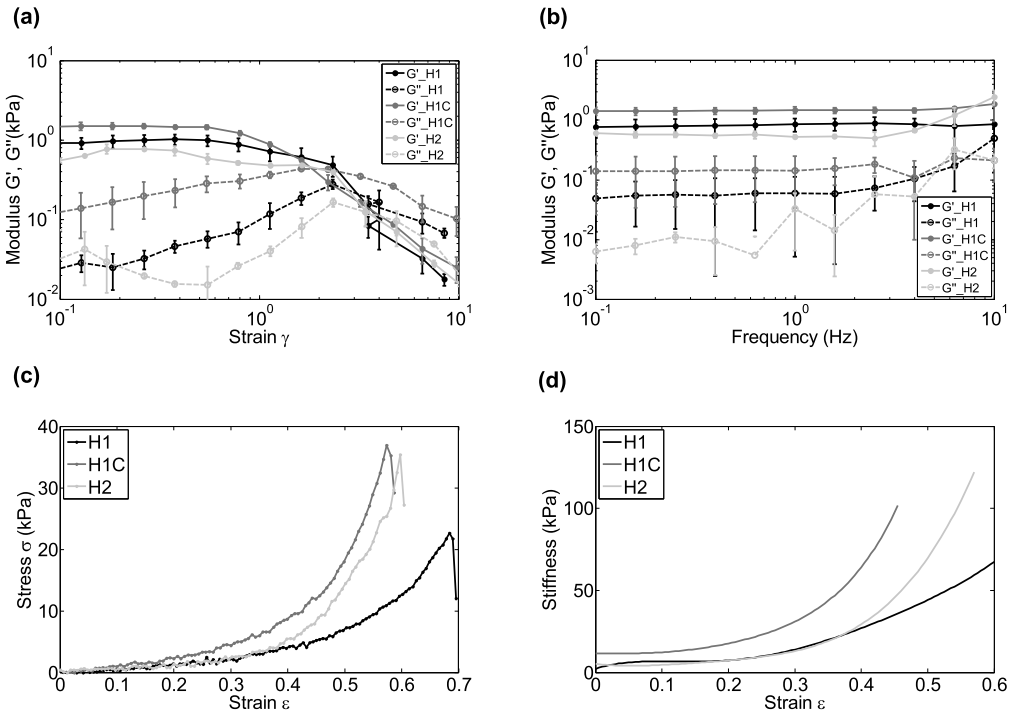


**Fig. 3.** Rheological and mechanical properties of HA-based hydrogels. (a) Amplitude dependence and (b) frequency dependence of modulus of HALD1-HACDH (H1), HALD1-HACDH-col I (H1C) and HALD2-HAADH (H2) hydrogels (measured with Haake RheoStress RS150 rheometer). The mean ($n$ = 3) and standard deviation are shown. (c) Stress as a function of strain (representative curves, measured with BOSE Electroforce Biodynamic 5100 machine equipped with a 225 N load sensor), and (d) stiffness as a function of strain (average curves, calculated similarly to [16]) curves of H1, H1C and H2 hydrogels.

determined for all the hydrogels. The hydrogels showed linear behavior of G′ up to about 10% strain. Outside this region, G′ dropped indicating a structure breakdown.

The frequency sweep measurements were performed based on the LVR. The frequency dependence of modulus is presented in Fig. 3 (b). A true gel structure was discovered, meaning that G′ was parallel to G″. Moreover, G′ was higher than G″ and independent of frequency, which is typical for ideal gels [33]. The H1 and H1C hydrogels showed more linear behavior of G′ and G″ than the H2 hydrogel. Especially, G″ of the H2 hydrogel was more non-linear, indicating possible non-homogeneity of the structure. This can cause changes in the structure during the measurement. For the H2 hydrogel, the G″ increased at higher strains. This means that there is less time for greater movement of the polymer chains and polymer chains fail to rearrange at a given time scale. This will lead to stiffening and more solid-like behavior [34].

The complex modulus (G*) values of the hydrogels are presented in Table 2. The G* of the H1 and H1C hydrogels were higher than with the H2 hydrogel, although there were no statistically significant differences between the gels. Higher G* indicates stiffer structure and higher resistance to deformation. It is also known that if the loss tangent is lower than 0.1, the hydrogels are considered as strong gels [35]. This was true for all the tested hydrogels (H1:tan δ = 0.084, H1C: tan δ = 0.096 and H2: tan δ = 0.014).

**Table 2**
The complex modulus, second-order elastic constant, and refractive index values of HALD1-HACDH (H1), HALD1-HACDH-col I (H1C) and HALD2-HAADH (H2) hydrogels. * $p < 0.05$ H1C with respect to H2. There were no statistically significant differences found between the complex modulus of hydrogels.

| Gel | Complex modulus, G* kPa | Second-order elastic constant kPa | Refractive index |
|---|---|---|---|
| H1 | 0.81 ± 0.23 | 6.7 ± 1.0 | 1.337 |
| H1C | 1.42 ± 0.16 | 11.6 ± 1.7* | 1.334 |
| H2 | 0.57 ± 0.06 | 5.4 ± 1.1 | 1.332 |

Rheological properties of the cornea have been studied previously by, for example, Ionescu et al. [36], Petsche et al. [37] and Hatami-–Marbini [38]. Due to the differences in the testing conditions, experimental procedures and samples, the results are not directly comparable with each other or with our results.

### 3.6. Mechanical properties

For tissues and hydrogels, the stress-strain curve is non-linear in the elastic portion even at small strains. For this reason, a polynomial fit, instead of a linear fit, was used for the data. Moreover, the stiffness as a function of strain was represented to illustrate the material behavior in a wider strain range. The representative compressive stress as a function of the deformation strain curves are shown in Fig. 3 (c). The results showed that the hydrogels were initially resistant to deformation, but became progressively stiffer as load increased. Finally, the hydrogels fractured at 55% to 70% strain range. Due to a higher fracture strain, the H1 hydrogel was considered to be more elastic compared to the H1C and H2 hydrogels, whereas the col I-containing H1C hydrogel was the least elastic.

The curves of average stiffness as a function of increasing strain are shown in Fig. 3 (d). The stiffness was shown to be strain dependent. At low strains (0% to 20%) the stiffness was quite constant, but increased after that more or less depending on the sample. This phenomenon is

called strain hardening and it indicates a non-linear deformation characteristic of hydrogels under compression [39].

The second-order elastic constants (stiffness at zero strain) of the hydrogels are shown in Table 2. The H1C hydrogel with highest second-order elastic constant showed significant difference ($p < 0.05$) with respect to the H2 hydrogel. Otherwise, there were no statistically significant differences between the hydrogels.

In the cornea, the predominant component for its mechanical strength is the stroma [40]. Although, the mechanical properties of the studied hydrogels were not close to the native tissue (0.1 to 57 MPa [41]), the hydrogel films were still fairly easy to handle during the cell culturing. This was also one of the main requirements for the material, more than just replicate the mechanical properties, which might be redundant for cell delivery applications.

### 3.7. Optical properties

The refractive index data of hydrogels was presented as the reflection coefficient, and it was plotted as a function of angle of incidence curves, which are shown in Fig. S5. The angle value was derived by drawing tangent lines on the vertical and horizontal parts of the curve and determining the angle at their intersection point. The calculated refractive indices are shown in Table 2. The refractive indices of all hydrogels were close to that of water ($n = 1.333$). The H1 hydrogel had the highest refractive index of the three, bringing it closest to that of the native corneal stroma ($n = 1.376$ [42]). The rays pass from the cornea into the aqueous humor having a lower refractive index ($n = 1.336$), so most of the reflection occurs at the cornea-air interface.

Although cornea represents the strongest part of the refracting power of the eye, the exact replication of its refractive capacity may not be necessary for clinically viable corneal biomaterials. As refractive errors can be easily adjusted with spectacles, the transparency of the material is more important than its correct refractive properties. This is especially true for degradable materials, which should promote the healing of healthy stromal tissue to ultimately regain the refraction power of the cornea.

The visible light transmission spectra of hydrogels are shown in Fig. 4 (a). The light transmittances for H1, H1C and H2 hydrogels were 85 ± 1, 82 ± 1 and 90 ± 1%, respectively in the 400–700 nm wavelength range. The transparency of the hydrogels was close to the native cornea (> 87%) [43]. The results showed that H2 hydrogel was slightly more transparent than H1-based hydrogels. Also, the addition of col I slightly lowered the transparency. The visible inspection of the samples (inside the cuvettes) also supported these findings. While H2 hydrogel looked visibly clear, the crosslinking was clearly seen inside the H1-based hydrogels. This can be explained with the higher polymer concentration and higher crosslinking density of H1-based hydrogels. The sample thickness used in the transparency measurements was significantly higher than the one intended for the final application. Therefore, thinner hydrogel films were photographed in order to show their optical clarity and transparency. As the photographic images presented in Fig. 4 (b) (and (c)) show, all hydrogels were visibly transparent, even with the addition of col. I.

We measured the optical properties from the hydrogel delivery vehicle alone. However, we note that encapsulating cells in the hydrogels causes light scattering, thus affecting their optical properties. Furthermore, both the refractive index and the transparency may change after implantation due to swelling and degradation, as well as the proliferation and differentiation of encapsulated cells.

### 3.8. In vitro cell culture

Human ASCs were encapsulated into the three HA-based hydrogels and their viability was assessed qualitatively using Live/Dead staining and the relative metabolic activity in different hydrogels was analyzed with PrestoBlue®. Both the Live/Dead staining (Fig. 5 (a)) and the PrestoBlue® results (Fig. 5 (b)) show that all HA-based hydrogels were capable of sustaining short-term cell survival. However, the more unstable H2 hydrogel samples degraded during the first three days of culture, making their handling for imaging and PrestoBlue® analysis difficult. For this reason, no images could be obtained after the first time point.

Live/Dead staining showed that the number of live cells seemed to decrease from the first time point onwards, although the number of dead cells did not increase. The major cause for this cell loss seems to be cell movement away from the hydrogels, which was observed during culture (Fig. 5 (c)). Additionally, hydrogel swelling, which pulls the cells further away from each other, and possible wash-out of unattached cells may contribute to apparent cell loss from the hydrogels. The col I-containing H1C hydrogel seemed to support hASC attachment better than the purely HA-based H1 hydrogel, based on the presence of more cells with elongated morphology in the Live/Dead images. Previous research has also shown, that the addition of ECM components, such as col I and laminin to hyaluronan hydrogels is required to support cellular attachment and elongated morphology for cardiomyocytes [44], vocal fold fibroblasts [13] and neural cells [18].

Cell metabolic activity seemed to decrease in all hydrogels after the first time point (Fig. 5 (b)). The trend was similar in all hydrogels, but

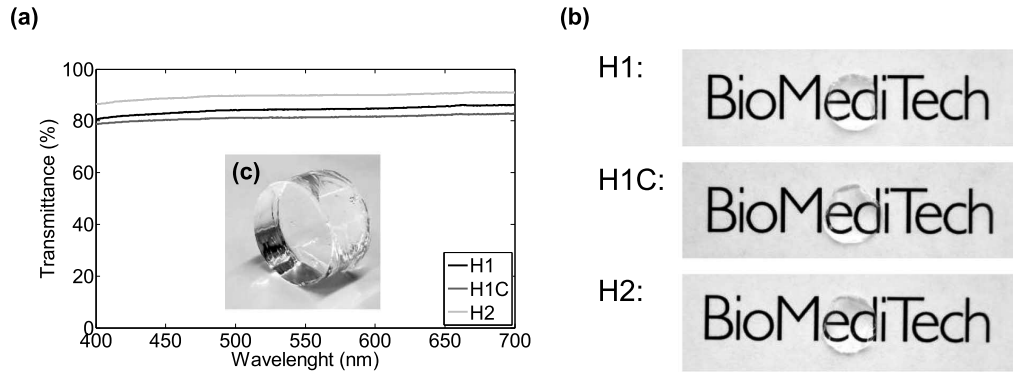


**Fig. 4.** Transparency of HA-based hydrogels. (a) Light transmission spectra of HALD1-HACDH (H1), HALD1-HACDH-col I (H1C) and HAL2-HAADH (H2) hydrogels. (b) Photographic images of H1, H1C and H2 hydrogels (diameter 10 mm × thickness 1 mm) showing their transparency. (c) Photographic image of H1-based hydrogel (diameter 12 mm × thickness 7 mm) prepared for the compression testing.

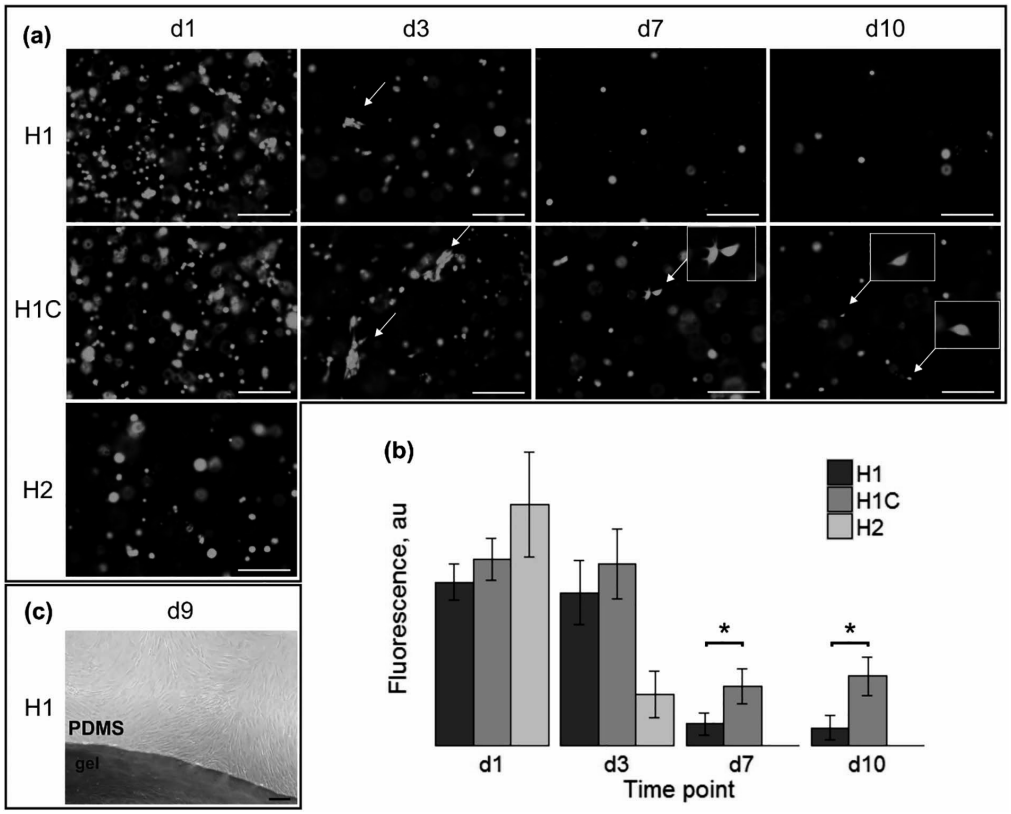


**Fig. 5.** Cell viability and metabolic activity in HA-based hydrogels. (a) Live-dead staining of hASCs encapsulated in HALD1-HACDH (H1), HALD1-HACDH-col I (H1C) and HALD2-HAADH (H2) hydrogels at different time points. Live cells are shown in green and dead cells in red, with arrows pointing at elongated cells. (b) Metabolic activity of hydrogel-encapsulated hASCs during *in vitro* culture as measured by PrestoBlue® analysis. The bars show the relative fluorescence values of cell-laden hydrogel samples with mean and standard deviation. The H2 hydrogel could not be handled for imaging any more at day 3, and the PrestoBlue® analysis could not be performed after that time point. *significant difference at $p < 0.05$ (c) Representative image of the observed cell growth out of the hydrogels and under the PDMS mold at day 9. Scale bars in the images are 200 μm. (For interpretation of the references to colour in this figure legend, the reader is referred to the web version of this article.)

the onset of the steep decline in metabolic activity varied; for the H2 hydrogel, the drop occurred between day 1 and day 3, whereas for H1 and H1C it occurred between day 3 and day 7. The decline in cell metabolic activity correlated with the observed decrease of cells in the Live/Dead images, also indicating that cells escaped from the hydrogels. However, the remaining cells maintained their metabolic activity at a steady level for the rest of the culture period. Importantly, the H1C hydrogel-encapsulated hASCs had significantly higher metabolic activity than those in the H1 hydrogel in the two last time points, which indicates that addition of col I has a significant effect on promoting active cell metabolism and survival.

The Live/Dead and PrestoBlue® results indicate that hASCs survive encapsulation into all of the HA-hydrogels, but the addition of col I is required for cell attachment to the hydrogel matrix. The efficient loss of cells from the hydrogels consisting of purely HA-components, suggests they could be suitable cell delivery vehicles, with either a rapid (H2) or more delayed delivery (H1) of hASCs to stromal defects. However, for long-term tissue integration of the hydrogel matrix, cell attachment may be required for efficient cell proliferation and ECM synthesis [45].

### 3.9. Implantation to corneal organ culture model

The corneal organ culture model is an excellent method to study cellular interactions at the organ level and to evaluate the clinical feasibility of biomaterials for corneal applications [46,47]. The corneal organ culture model has been previously used mainly to study re-epithelialization, since the organ-cultured corneas retain their capability for epithelial regeneration for as long as two months in culture [28]. Although the results obtained from the corneal organ culture model always require validation in an *in vivo* animal model, its use in fast and low-cost preliminary screening of corneal biomaterials can significantly reduce unnecessary animal testing.

We used excised porcine corneas to model the delivery of hASCs in the HA-based hydrogels into stromal defects. As a proof-of-concept, we inflicted large stromal wounds, into which the hydrogels were implanted with and without hASCs. The immunohistological evaluation of the porcine corneas with hydrogel-delivered hASCs revealed cell migration into the corneal stroma, after just one week of culture (Fig. 6). Successful integration of hASCs into the stroma was observed for all of the hydrogels, although H1C hydrogel samples seemed to show slightly less migrated hASCs in the stroma than H1 and H2. Possibly, collagen's effect on improving hASC attachment may have delayed their migration to the stroma from the H1C hydrogel. The integration of hASCs to the corneal stroma in the organ culture model demonstrates the clinical feasibility of the hydrogels for stromal delivery of hASCs.

Despite the predominant loss of the hydrogels themselves during

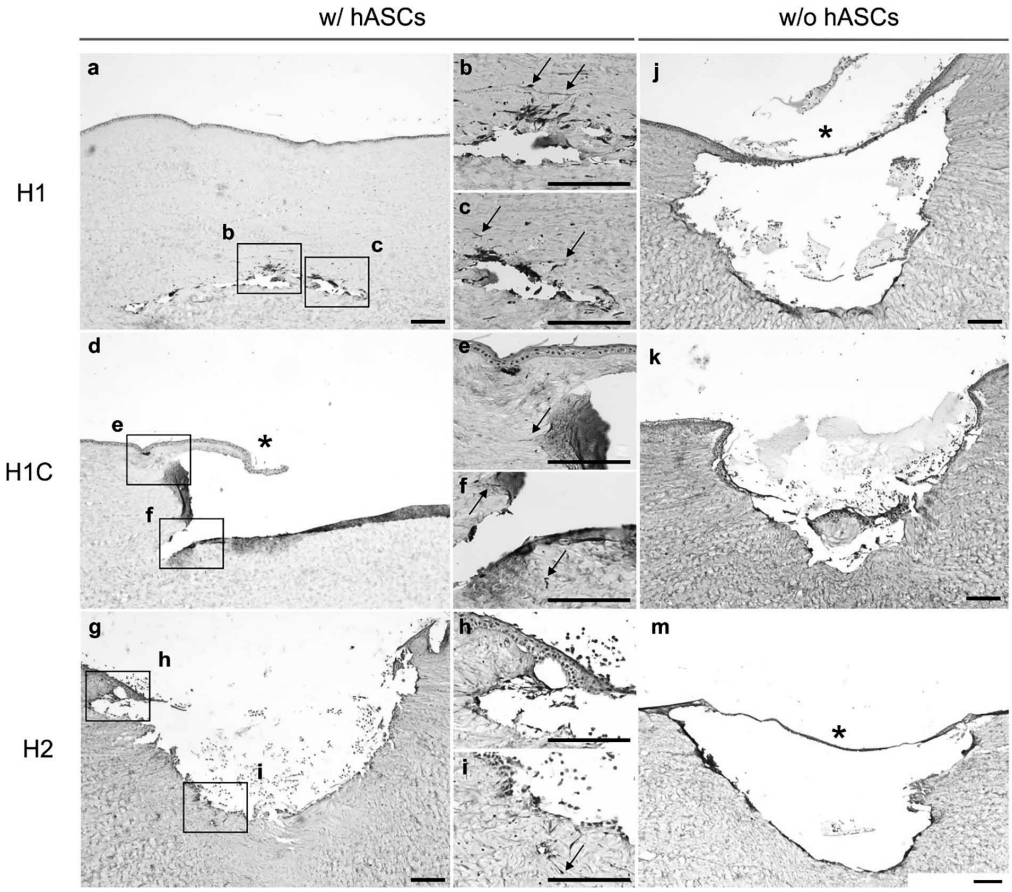


**Fig. 6.** Immunohistochemical detection of hydrogel-delivered hASCs after seven days in porcine corneal organ culture model using human cell marker TRA-1-85. Images on the left panel (a–i) describe hydrogels HALD1-HACDH (H1), HALD1-HACDH-col I (H1C) and HALD2-HAADH (H2) with encapsulated hASCs, and the images on the right (j–m) depict delivery of each gel vehicle only. All other sections depict the central wound area, except that of H1 w/hASCs, which was sectioned near the wound edge. Successful hASC integration into the corneal stroma was seen for all hydrogels (examples marked with arrows), and epithelium growth on top of the transplanted gels was observed with all gels, even without hASCs (denoted by * in images e, j and m). However, epithelial overgrowth could not be verified for all samples, as the gels were lost during histological processing. Scale bars in the images are 200 μm.

histological processing, re-epithelialization of the corneal surface was evident from the tissue sections. This was clearly seen in the vehicle-only controls of H1 and H2 in Fig. 6 (j) and (m), respectively. Fig. 6 (d) also implies epithelial outgrowth over the H1C hydrogel sample, although the complete epithelium is not visible in the section. Previous research has also reported that HA can support corneal epithelial cell growth [48], which further validates its use in the repair of the underlying stroma. However, some sections showed epithelial growth at the edges of the wound rather than on top of the hydrogel (shown in Fig. 6 (k)), indicating that the gels were not always in good contact with the underlying tissue.

The organ culture model also revealed that the degradation rate of the hydrogels on the corneal surface is not directly comparable to the dilute medium environment of the swelling tests or *in vitro* culture. For example, the complete re-epithelialization and shape retention of the corneal surface in Fig. 6 (m) indicates that the H2 hydrogel remained stable for the entire culture period of seven days, whereas during *in vitro* culture, the hydrogel could no longer be observed after three days.

## 4. Conclusions

In this study, we fabricated two types of hydrazone crosslinked HA-based hydrogels, with the addition of human collagen I. We characterized the physical and mechanical properties of these hydrogels and evaluated their potential as cell delivery vehicles to the corneal stroma. Based on the results, HALD1-HACDH hydrogels showed better stability and manageability compared to the HALD2-HAADH hydrogel, which degraded *in vitro* in three days. These hydrogels had also good optical properties, the refractive indices were close to the native cornea and they were visually transparent. Although all hydrogels showed good hASC survival directly after encapsulation, only the col I-containing HALD1-HACDH-col I hydrogel showed cells with elongated morphology, and significantly higher cell metabolic activity than the HALD1-HACDH gel. Corneal organ culture model suggests that these hydrogels could be used as injectable cell delivery vehicles to corneal stromal defects, allowing efficient cell integration to the stroma and overgrowth of epithelial cells. Biodegradability of the HA components and favorable properties of hydrazone crosslinking, such as short gelation time, lack of harmful reagents or side-products and mild reaction conditions, together with the results make these hydrogels a potential

material for hASC delivery to treat corneal stromal defects.

Supplementary data to this article can be found online at https://doi.org/10.1016/j.msec.2017.12.013.

## Acknowledgements

This work was funded by the Finnish Funding Agency for Innovation's (TEKES) Human Spare Parts project and the European COST Action BM-1302 (Joining forces in corneal regeneration research). The funding sources were not involved in conduction if the research or interpretation of the results. The authors would like to thank Ph.D. Alexandre Efimov and Laboratory Attendant Anne-Maarit Tikkanen (Faculty of Natural Sciences, Laboratory of Chemistry and Bioengineering, Tampere University of Technology, Tampere, Finland) for their help related to the NMR- and FTIR-measurements. We would also like to thank Ph.D. Maria Notara (University Hospital Cologne, Cologne, Germany) for expertise in the corneal organ culture method, Marja-Leena Koskinen for aiding with the histological analysis and Miia Juntunen for technical assistance and theTampere Imaging Facility, BioMediTech and Institute of Medicine and Life Sciences, University of Tampere for the tools and expertise in cell imaging.

## References

[1] WHO, Priority eye diseases, http://www.who.int/blindness/causes/priority/en/index8.html, (2016) (accessed 03.07.2017).
[2] C.E. Ghezzi, J. Rnjak-Kovacina, D.L. Kaplan, Corneal tissue engineering: recent advances and future perspectives, Tissue Eng. B Rev. 21 (2015) 278–287.
[3] Oh. JY, M.S. MK Kim, H.J. Shin, J.H. Lee, W.R. Ko, Wee, et al., The anti-inflammatory and anti-angiogenic role of mesenchymal stem cells in corneal wound healing following chemical injury, Stem Cells 26 (2008) 1047–1055.
[4] M. SK Mittal, A. Omoto, A. Amouzegar, A. Sahu, K.R. Rezazadeh, Katikireddy, et al., Restoration of corneal transparency by mesenchymal stem cells, Stem Cell Rep. 7 (2016) 583–590.
[5] B. Lindroos, R. Suuronen, S. Miettinen, The potential of adipose stem cells in regenerative medicine, Stem Cell Rev. Rep. 7 (2011) 269–291.
[6] F. Arnalich-Montiel, S. Pastor, A. Blazquez-Martinez, J. Fernandez-Delgado, M. Nistal, J.L. Alio del Barrio, et al., Adipose-derived stem cells are a source for cell therapy of the corneal stroma, Stem Cells 26 (2008) 570–579.
[7] L. Espandar, B. Bunnell, G.Y. Wang, P. Gregory, C. McBride, M. Moshirfar, Adipose-derived stem cells on hyaluronic acid–derived scaffold: a new horizon in bioengineered cornea, Arch.Ophthalmol. 130 (2012) 202–208.
[8] J. Alio del Barrio, M. Chiesa, N. Garagorri, N. Garcia-Urquia, J. Fernandez-Delgado, L. Bataille, et al., A cellular human corneal matrix sheets seeded with human adipose-derived mesenchymal stem cells integrate functionally in an experimental animal model, Exp.Eye Res 132 (2015) 91–100.
[9] K.M. Meek, C. Knupp, Corneal structure and transparency, Prog.Retin.Eye Res. 49 (2015) 1–16.
[10] J. Fraser, T. Laurent, U. Laurent, Hyaluronan: its nature, distribution, functions and turnover, J.Intern.Med. 242 (1997) 27–33.
[11] X. Xu, D.A. AK Jha, M.C. Harrington, X. Farach-Carson, Jia. Hyaluronic acid-based hydrogels: from a natural polysaccharide to complex networks, Soft Matter 8 (2012) 3280–3294.
[12] Y. Jiang, J. Chen, C. Deng, E.J. Suuronen, Z. Zhong, Click hydrogels, microgels and nanogels: emerging platforms for drug delivery and tissue engineering, Biomaterials 35 (2014) 4969–4985.
[13] X. Jia, Y. Yeo, R.J. Clifton, T. Jiao, D.S. Kohane, J.B. Kobler, et al., Hyaluronic acid-based microgels and microgel networks for vocal fold regeneration, Biomacromolecules 7 (2006) 3336–3344.
[14] E. Martínez-Sanz, D.A. Ossipov, J. Hilborn, S. Larsson, K.B. Jonsson, O.P. Varghese, Bone reservoir: injectable hyaluronic acid hydrogel for minimal invasive bone augmentation, J. Control. Release 152 (2011) 232–240.
[15] P. Bulpitt, D. Aeschlimann, New strategy for chemical modification of hyaluronic acid: preparation of functionalized derivatives and their use in the formation of novel biocompatible hydrogels, J. Biomed. Mater. Res. A 47 (1999) 152–169.
[16] J. Karvinen, J.T. Koivisto, I. Jönkkäri, M. Kellomäki, The production of injectable hydrazone crosslinked gellan gum-hyaluronan-hydrogels with tunable mechanical and physical properties, J. Mech. Behav. Biomed. Mater. 71 (2017) 383–391.
[17] O.P. Oommen, S. Wang, M. Kisiel, M. Sloff, J. Hilborn, O.P. Varghese, Smart design of stable extracellular matrix mimetic hydrogel: synthesis, characterization, and in vitro and in vivo evaluation for tissue engineering, Adv. Funct. Mater. 23 (2013) 1273–1280.
[18] S. Suri, C.E. Schmidt, Cell-laden hydrogel constructs of hyaluronic acid, collagen, and laminin for neural tissue engineering, Tissue Eng. A 16 (2010) 1703–1716.
[19] D.A. Ossipov, S. Piskounova, J. Hilborn, Poly (vinyl alcohol) cross-linkers for in vivo injectable hydrogels, Macromolecules 41 (2008) 3971–3982.
[20] K.H. Bouhadir, D.S. Hausman, D.J. Mooney, Synthesis of cross-linked poly (aldehyde guluronate) hydrogels, Polymer 40 (1999) 3575–3584.
[21] ASTM Standard F2900, Standard Guide for Characterization of Hydrogels used in Regenerative Medicine, ASTM International, West Conchoken, PA, USA, 2011, pp. 1–10.
[22] K. Brugger, Thermodynamic definition of higher order elastic coefficients, Phys. Rev. 133 (1964) A1611.
[23] J.F. Nye, Physical Properties of Crystals: Their Representation by Tensors and Matrices, Oxford University Press, 1985.
[24] W.D. Callister, D.G. Rethwich, Materials Science and Engineering: An Introduction, 7th ed., Wiley, New York, 2007.
[25] H. Nakajima, APPENDIX B: Table of Refractive Indices for BK7, Optical Design Using Excel: Practical Calculations for Laser Optical Systems, 1st ed., John Wiley & Sons Singapore Pte Ltd, 2015, pp. 277–278.
[26] J.M. Gimble, F. Guilak, Adipose-derived adult stem cells: isolation, characterization, and differentiation potential, Cytotherapy 5 (2003) 362–369.
[27] B. Lindroos, S. Boucher, L. Chase, H. Kuokkanen, H. Huhtala, R. Haataja, et al., Serum-free, xeno-free culture media maintain the proliferation rate and multipotentiality of adipose stem cells in vitro, Cytotherapy 11 (2009) 958–972.
[28] M. Notara, S. Schrader, J.T. Daniels, The porcine limbal epithelial stem cell niche as a new model for the study of transplanted tissue-engineered human limbal epithelial cells, Tissue Eng. A 17 (2011) 741–750.
[29] W. Lin, S. Shuster, H.I. Maibach, R. Stern, Patterns of hyaluronan staining are modified by fixation techniques, J. Histochem. Cytochem. 45 (1997) 1157–1163.
[30] D.A. Ossipov, S. Piskounova, O.P. Varghese, J. Hilborn, Functionalization of hyaluronic acid with chemoselective groups via a disulfide-based protection strategy for in situ formation of mechanically stable hydrogels, Biomacromolecules 11 (2010) 2247–2254.
[31] C. García-González, M. Alnaief, I. Smirnova, Polysaccharide-based aerogels—promising biodegradable carriers for drug delivery systems, Carbohydr. Polym. 86 (2011) 1425–1438.
[32] S.L. Wilson, A.J. El Haj, Y. Yang, Control of scar tissue formation in the cornea: strategies in clinical and corneal tissue engineering, J. Funct. Biomat. 3 (2012) 642–687.
[33] E.R. Morris, K. Nishinari, M. Rinaudo, Gelation of gellan–a review, Food Hydrocoll. 28 (2012) 373–411.
[34] M.J. Moura, M.M. Figueiredo, M.H. Gil, Rheological study of genipin cross-linked chitosan hydrogels, Biomacromolecules 8 (2007) 3823–3829.
[35] A. Borzacchiello, L. Ambrosio, Structure-Property Relationships in Hydrogels, Hydrogels, Springer, 2009, pp. 9–20.
[36] A. Ionescu, M. Alaminos, Juan de la Cruz Cardona, Durán, Juan de Dios García-López, M. González-Andrades, R. Ghinea, et al., Investigating a novel nanostructured fibrin–agarose biomaterial for human cornea tissue engineering: Rheological properties, J. Mech. Behav. Biomed. Mater. 4 (2011) 1963–1973.
[37] S.J. Petsche, D. Chernyak, J. Martiz, M.E. Levenston, P.M. Pinsky, Depth-dependent transverse shear properties of the human corneal stroma, Invest. Ophthalmol. Vis. Sci. 53 (2012) 873–880.
[38] H. Hatami-Marbini, Viscoelastic shear properties of the corneal stroma, J. Biochem. 47 (2014) 723–728.
[39] G. Lamouche, B.F. Kennedy, K.M. Kennedy, C. Bisaillon, A. Curatolo, G. Campbell, et al., Review of tissue simulating phantoms with controllable optical, mechanical and structural properties for use in optical coherence tomography, Biomed. Opt. Express 3 (2012) 1381–1398.
[40] W.J. Dupps, S.E. Wilson, Biomechanics and wound healing in the cornea, Exp. Eye Res. 83 (2006) 709–720.
[41] N. Garcia-Porta, P. Fernandes, A. Queiros, J. Salgado-Borges, M. Parafita-Mato, J.M. González-Méijome, Corneal biomechanical properties in different ocular conditions and new measurement techniques, ISRN Ophthalmol. 2014 (2014).
[42] K.M. Meek, S. Dennis, S. Khan, Changes in the refractive index of the stroma and its extrafibrillar matrix when the cornea swells, Biophys. J. 85 (2003) 2205–2212.
[43] W. Liu, C. Deng, C.R. McLaughlin, P. Fagerholm, N.S. Lagali, B. Heyne, et al., Collagen–phosphorylcholine interpenetrating network hydrogels as corneal substitutes, Biomaterials 30 (2009) 1551–1559.
[44] J. Dahlmann, A. Krause, L. Möller, G. Kensah, M. Möwes, A. Diekmann, et al., Fully defined in situ cross-linkable alginate and hyaluronic acid hydrogels for myocardial tissue engineering, Biomaterials 34 (2013) 940–951.
[45] J. Zhu, R.E. Marchant, Design properties of hydrogel tissue-engineering scaffolds, Expert Rev. Med. Devices 8 (2011) 607–626.
[46] M.D.M. Evans, G.A. McFarland, R.Z. Xie, S. Taylor, J.S. Wilkie, H. Chaouk, The use of corneal organ culture in biocompatibility studies, Biomaterials 23 (2002) 1359–1367.
[47] S. Sandeman, A. Lloyd, B. Tighe, V. Franklin, J. Li, F. Lydon, et al., A model for the preliminary biological screening of potential keratoprosthetic biomaterials, Biomaterials 24 (2003) 4729–4739.
[48] J.A. Gomes, R. Amankwah, A. Powell-Richards, H.S. Dua, Sodium hyaluronate (hyaluronic acid) promotes migration of human corneal epithelial cells in vitro, Br. J. Ophthalmol. 88 (2004) 821–825.

**APPENDIX A: Supplementary Material**

# Hydrazone crosslinked hyaluronan based hydrogels for therapeutic delivery of adipose stem cells to treat corneal defects

Laura Koivusalo, Jennika Karvinen, Eetu Sorsa, Ilari Jönkkäri, Jari Väliaho, Pasi Kallio, Tanja Ilmarinen, Susanna Miettinen, Heli Skottman, Minna Kellomäki

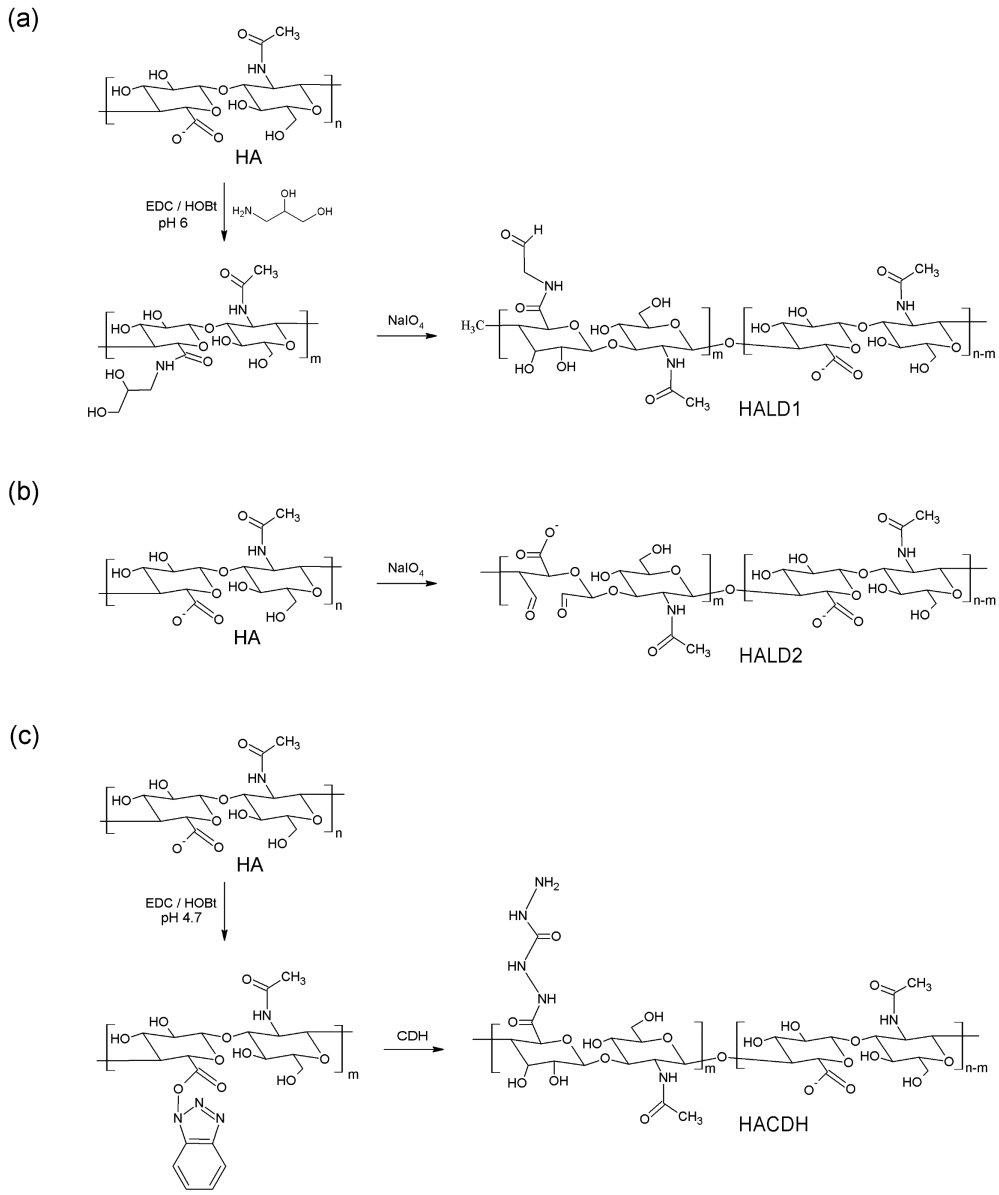


**Fig. S1.** Reaction schemes of (a) selective oxidation of diol-modified HA (HALD1), (b) periodate oxidation of HA (HALD2) and (c) hydrazide-modification of HA (HACDH). The reaction scheme of HAADH modification is shown in (Karvinen, Koivisto et al. 2017).

**APPENDIX A: Supplementary Material**

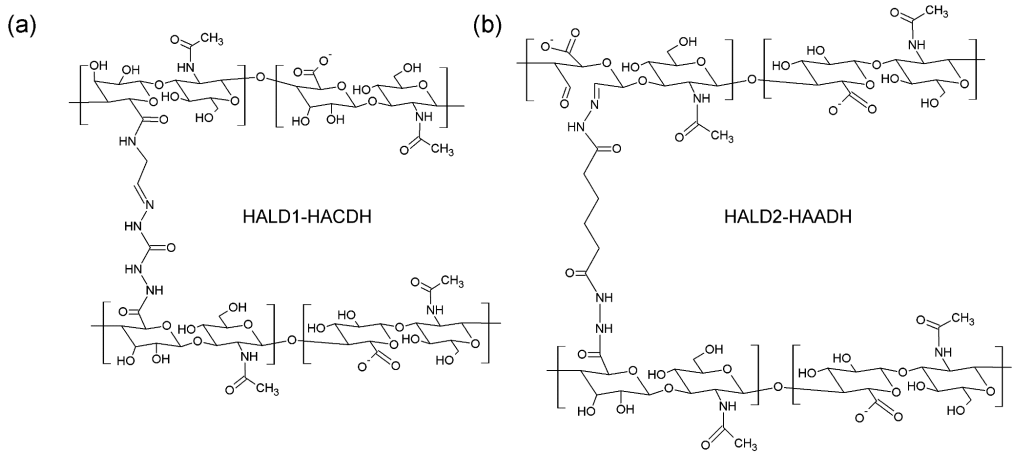


**Fig. S2.** The chemical structures of hydrazone crosslinked (c) HALD1-HACDH (H1) and (d) HALD2-HAADH (H2) hydrogels.

**APPENDIX A: Supplementary Material**

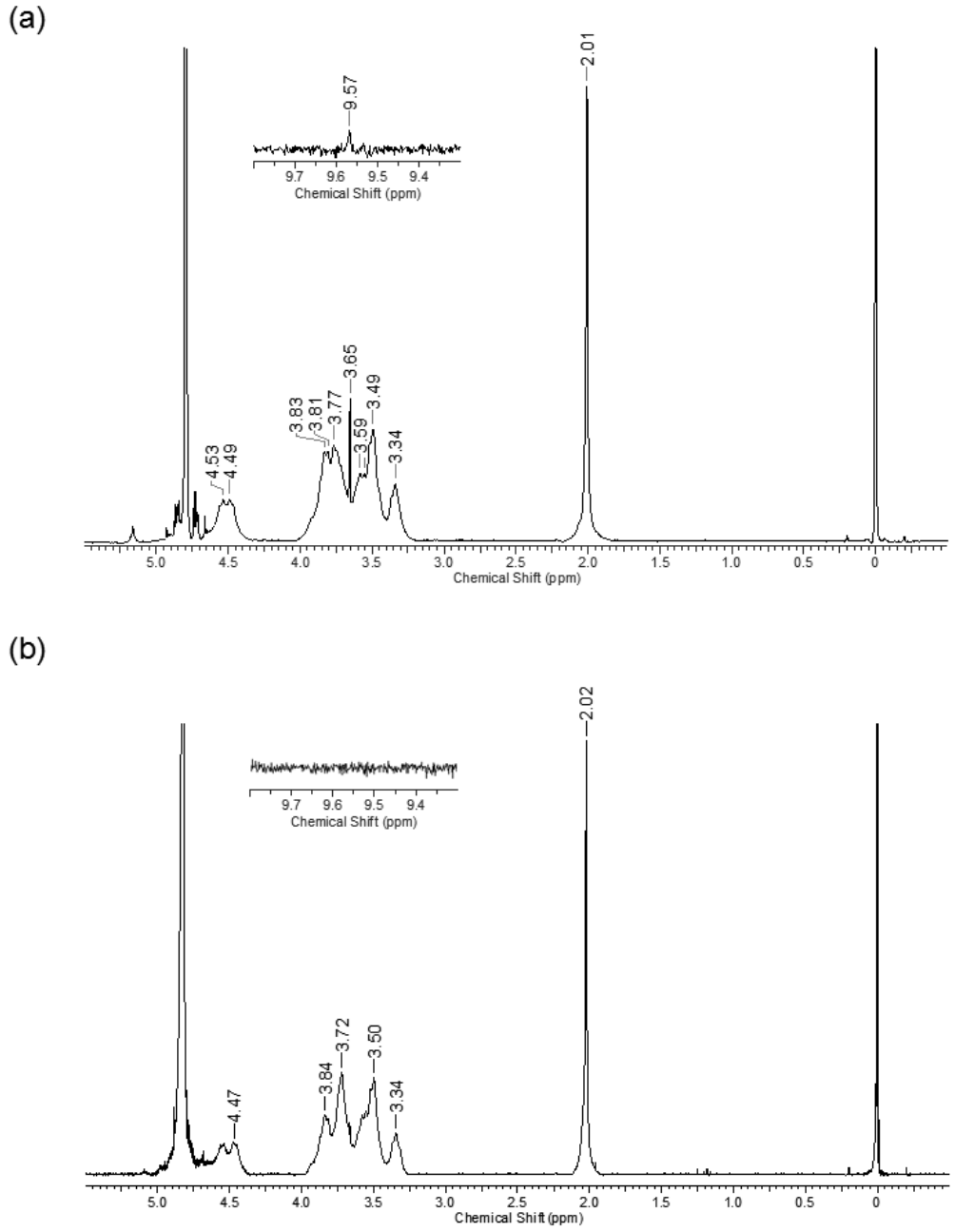


**Fig. S3.** $^{1}$H-NMR spectra of hydrogel components (a) HALD1 and (b) HALD2.

**APPENDIX A: Supplementary Material**

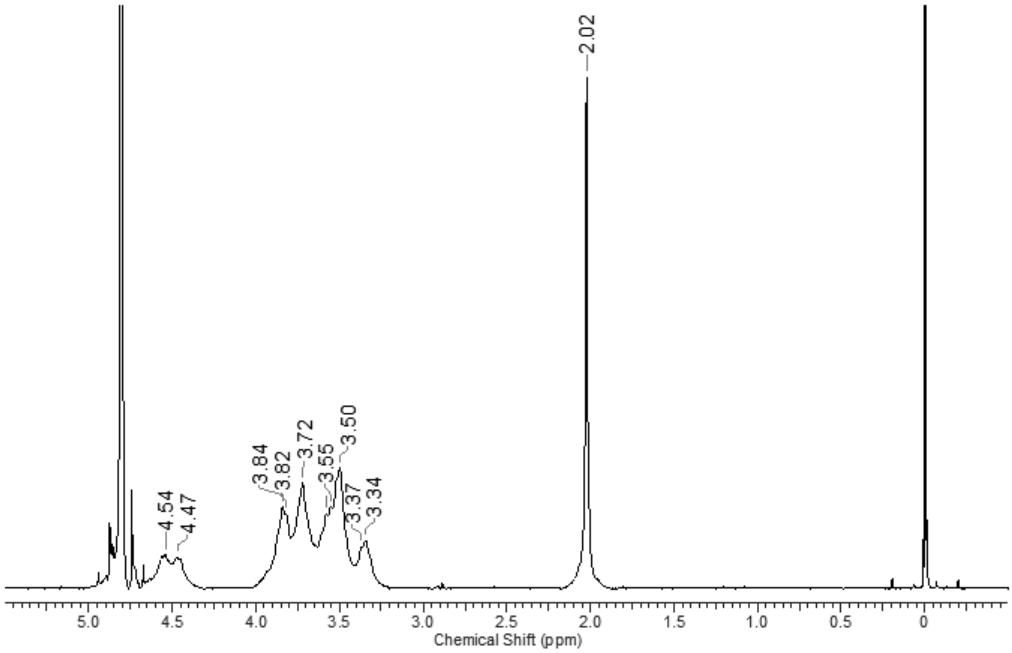


**Fig. S4.** $^{1}$H-NMR spectra of hydrogel component HACDH.

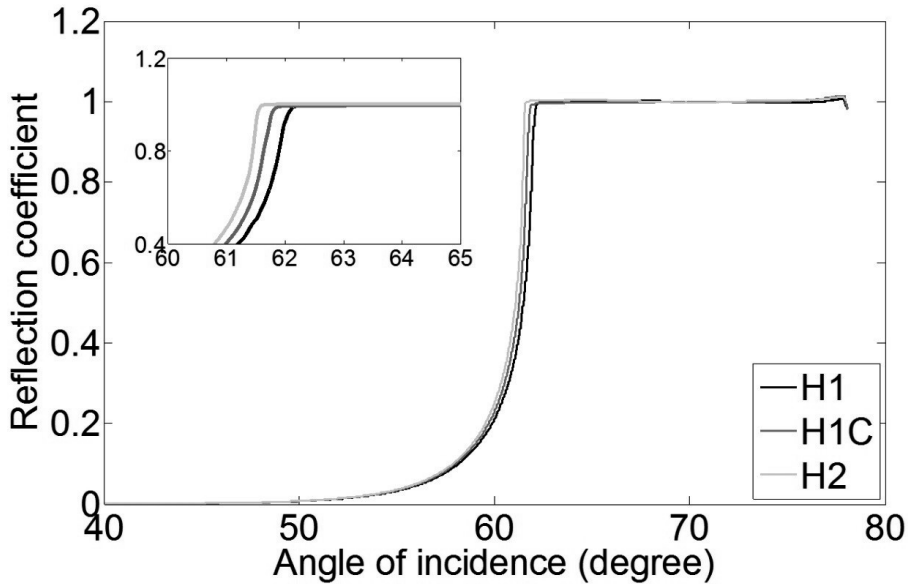


**Fig. S5.** Reflection coefficient as a function of angle of incidence curves of HALD1-HACDH (H1), HALD1-HACDH-colI (H1C) and HALD2-HAADH (H2) hydrogels.

**APPENDIX A: Supplementary Material**

**Table S1.** Cell surface marker profile of hASCs determined by flow cytometry.

| Marker | Amount of positive cells (%) |
|---|---|
| **CD73** | 95.8 |
| **CD90** | 99.2 |
| **CD105** | 98.7 |
| **CD14** | 0.7 |
| **CD19** | 0.9 |
| **CD45** | 2.0 |
| **HLA-DR** | 1.1 |
| **CD34** | 47.5 |

# PUBLICATION II

**Tissue adhesive hyaluronic acid hydrogels for sutureless stem cell delivery and regeneration of corneal epithelium and stroma**

Laura Koivusalo, Maija Kauppila, Sumanta Samanta, Vijay Singh Parihar, Tanja Ilmarinen, Susanna Miettinen, Oommen P. Oommen, Heli Skottman

Biomaterials, 2019, vol 225, 119156
https://doi.org/10.1016/j.biomaterials.2019.119516

Biomaterials 225 (2019) 119516

Contents lists available at ScienceDirect

Biomaterials

journal homepage: www.elsevier.com/locate/biomaterials

# Tissue adhesive hyaluronic acid hydrogels for sutureless stem cell delivery and regeneration of corneal epithelium and stroma

Laura Koivusalo[a], Maija Kauppila[a], Sumanta Samanta[b], Vijay Singh Parihar[b], Tanja Ilmarinen[a], Susanna Miettinen[c], Oommen P. Oommen[b,**], Heli Skottman[a,*]

[a] Eye Regeneration Group, Faculty of Medicine and Health Technology and BioMediTech Institute, Tampere University, Tampere, 33520, Finland
[b] Bioengineering and Nanomedicine Lab, Faculty of Medicine and Health Technology and BioMediTech Institute, Tampere University, Tampere, 33720, Finland
[c] Adult Stem Cell Group, Faculty of Medicine and Health Technology and BioMediTech Institute, Tampere University, Finland & Research, Development and Innovation Centre, Tampere University Hospital, Tampere, 33520, Finland

ARTICLE INFO

*Keywords:*
Hyaluronic acid
Hydrogel
Tissue adhesive
Cell delivery
Cornea regeneration

ABSTRACT

Regeneration of a severely damaged cornea necessitates the delivery of both epithelium-renewing limbal epithelial stem cells (LESCs) and stroma-repairing cells, such as human adipose-derived stem cells (hASCs). Currently, limited strategies exist for the delivery of these therapeutic cells with tissue-like cellular organization. With the added risks related to suturing of corneal implants, there is a pressing need to develop new tissue adhesive biomaterials for corneal regeneration. To address these issues, we grafted dopamine moieties into hydrazone-crosslinked hyaluronic acid (HA-DOPA) hydrogels to impart tissue adhesive properties and facilitate covalent surface modification of the gels with basement membrane proteins or peptides. We achieved tissue-like cellular compartmentalization in the implants by encapsulating hASCs inside the hydrogels, with subsequent conjugation of thiolated collagen IV or laminin peptides and LESC seeding on the hydrogel surface. The encapsulated hASCs in HA-DOPA gels exhibited good proliferation and cell elongation, while the LESCs expressed typical limbal epithelial progenitor markers. Importantly, the compartmentalized HA-DOPA implants displayed excellent tissue adhesion upon implantation in a porcine corneal organ culture model. These results encourage sutureless implantation of functional stem cells as the next generation of corneal regeneration.

## 1. Introduction

Millions of people worldwide suffer from corneal blindness [1,2]. Severe corneal blindness resulting from thermal or chemical burns, is characterized by the loss of limbal epithelial stem cells (LESCs), the tissue-resident stem cells of the cornea, which leads to chronic inflammation, overgrowth of blood vessels and conjunctival cells, as well as stromal scarring [3,4]. Currently, these is no treatment available for these patients, as they require the implantation of new functional stem cells for long-term regeneration of the cornea [3,5]. For restoring vision, controlled regeneration of both corneal epithelium and stroma is necessary. Although autologous and allogenic primary LESCs from healthy donor eyes have been widely studied for epithelial regeneration, the supply of isolated stem cells is scarce [6]. With the advancements in stem cell technologies, high quantities of clinically relevant LESCs can be obtained through differentiation from human embryonic stem cells (hESC-LESCs) or induced pluripotent stem cells (iPSCs) for corneal epithelial regeneration [7–10]. For stromal regeneration, one of the most promising cell sources are human adipose stem cells (hASCs), due to their capacity to mitigate inflammation and differentiate into corneal stromal cells post implantation [11–15]. However, delivery of two therapeutic stem cell populations compartmentalized in a tissue-specific arrangement is a daunting task, which we have previously sought to solve by using laser-assisted bioprinting [16]. So far, only few applications have emerged combining different cells to regenerate both the scarred stromal tissue as well as the surface epithelium [17,18], but their implantation requires suturing, which can increase inflammation and neovascularization of the cornea [2].

Hyaluronic acid (HA) is a naturally occurring polysaccharide, which can be chemically modified for many tissue engineering applications, while being enzymatically cleared *in vivo*. We have previously shown the formation of stable HA hydrogels by hydrazone crosslinking between aldehyde and carbodihydrazide derivatives of HA [19,20]. This two-component system allows fast gelation and encapsulation of living

* Corresponding author.
** Corresponding author.
*E-mail addresses:* oommen.oommen@tuni.fi (O.P. Oommen), heli.skottman@tuni.fi (H. Skottman).

https://doi.org/10.1016/j.biomaterials.2019.119516
Received 9 September 2019; Accepted 21 September 2019
Available online 23 September 2019

cells for efficient cell delivery [19–22]. In the cornea, native HA has been shown to induce epithelial cell migration and wound healing, and it has recently been identified as an important regulator of the LESC niche of the cornea, making it an ideal culture substrate for these cells [23,24]. Despite this, no HA based implantable materials for LESC transplantation have been previously reported, as corneal cell attachment to HA based films has been poor [25]. Injectable HA-based materials have previously been used for cell delivery to the corneal stroma [20,26], but these *in situ* forming hydrogels cannot be used to deliver an intact epithelial layer. Hence, new implant design is essential for efficient transplantation of distinctly compartmentalized cells to the cornea, as well as other epithelialized tissues, which require the combination of 3D and 2D cell arrangement.

Sutureless implantation of the hydrogel constructs takes advantage of the tissue adhesive capability of dopamine, a catecholamine derived from marine mussels (*Mytillus edulis*) that functions as a glue in wet conditions [27,28]. Several *in situ* forming tissue adhesive hydrogels based on this catechol chemistry have already been introduced for drug and cell delivery applications [28–30]. However, these hydrogels are formed either through self-polymerization of dopamine residues or metal-coordination polymerization, which both result in the formation of a strong brown coloration unsuitable for corneal applications [28–31]. Thus far, the only previously reported tissue adhesive material with a premade dopamine-containing hydrogel, includes a freeze-dried dopamine-alginate membrane for general surgery applications [32]. In corneal regeneration, dopamine residues can potentially have additional benefits for tissue innervation, as dopamine is a known neurotransmitter of corneal nerves [33].

Thus, our ambition was to develop a tissue adhesive scaffold for corneal regeneration with cellular compartmentalization of LESCs on the surface and hASCs in the hydrogel bulk, promoting regeneration of both the epithelial and stromal layers upon implantation at the defect site. We have successfully developed this compartmentalized scaffold and demonstrated the proof-of-concept of sutureless implantation in a porcine corneal organ culture model, which displayed efficient tissue integration while retaining the functional characteristics of these stem cells.

## 2. Materials and methods

Hyaluronic acid (MW 130 kDa) was purchased from LifeCore Biomedical (Chaska, USA). Dopamine hydrochloride, 1-ethyl-3-(3-dimethylaminopropyl)-carbodiimide hydrochloride (EDC), 1-hydroxybenzotriazole hydrate (HOBt), Carbodihydrazide (CDH), 3-amino-1,2-propanediol and sodium periodate, hyaluronidase (from bovine testes), collagen type IV from human placenta, and 5,5-Dithiobis(2-nitrobenzoic acid) (Ellman's reagent) were purchased from Sigma-Aldrich. Traut's reagent (2-iminothiolane), Zeba™ spin desalting column (7K MWCO), 0.5 M ethylenediaminetetraacetic acid (EDTA, UltraPure), Dulbecco's modified Eagle's medium/Ham's nutrient mixture F-12 (DMEM/F-12 1:1), Advanced DMEM, l-glutamine (GlutaMAX™), amphotericin B, TrypLE™ Select, LIVE/DEAD® viability/cytotoxicity kit, PrestoBlue® reagent, CyQUANT cell proliferation assay and Molecular Probes' secondary antibodies were purchased from Thermo Fisher Scientific. TaqMan primers for keratocan (KERA, Hs00559942_m1), lumican (LUM, Hs00929860_m1), aldehyde dehydrogenase 3A1 (ALDH3A1, Hs00964880_m1) and housekeeping gene GAPDH (Hs99999905_m1), cDNA reverse transcription kit and RNAse free DNase I for qRT-PCR were purchased from Thermo Fisher Scientific. For RNA isolation from hydrogel samples and controls, TRIreagent from Molecular Research Center Inc. (Cincinnati, OH) and RNeasy Mini Kit from Qiagen (Qiagen Sollentuna, Sweden) were used. Synthetic laminin-derived peptides CDPGYIGSR were obtained from Bachem (Bubendorf, Switzerland) and Calbiochem (UK). Antibiotics (100 U $mL^{-1}$ penicillin, 100 µg $mL^{-1}$ streptomycin) and Dulbecco's phosphate buffered saline (DPBS) were purchased from Lonza (Basel, Switzerland). Cell culture media CnT-30 and CnT-Prime-CC were purchased from CELLnTECH (Bern, Switzerland), and human serum (type AB male, HIV tested) from BioWest (Nuaillé, France). Spectra Por-3 dialysis membrane (MWCO 3500 g $mol^{-1}$) used for purification was purchased from Spectrum Lab, USA. All solvents were of analytical quality. Spectrophotometric analyses were carried out on Shimadzu UV-3600 plus UV-VIS-NIR spectrophotometer or PerkinElmer Lambda 35 UV/VIS spectrophotometer.

### 2.1. Synthesis and preparation of hydrogels

#### 2.1.1. Synthesis of dopamine modified hyaluronic acid (HA-DA)

1 mmol of HA (400 mg, 1 equivalent) was dissolved in 60 mL deionized water, to which 1 mmol HOBt (153 mg, 1 equivalent) and 1 mmol dopamine (190 mg, 1 equivalent) was then added. The pH of the reaction solution was adjusted to 5.5 with 1 M HCl and 1 M NaOH. Then 0.25 mmol EDC (48 mg, 0.25 equivalent) was added in 2 batches at 30 min interval. pH of the solution was maintained at 5.5 for 6 h, and then allowed to stir overnight. The reaction mixture was loaded into a dialysis bag and dialyzed against dilute HCl (pH = 3.5) containing 100 mM NaCl (4 × 2 L, 24 h) followed by dialysis in dilute HCl (pH 3.5, 2 × 2 L, 24 h) and then dialyzed against deionized water (2 × 2 L, 24 h). The solution was lyophilized to obtain HA-DA. Degree of dopamine conjugation was 14.4% (with respect to the disaccharide units of HA) as estimated by NMR spectroscopy ($^1$H NMR, 300 MHz). The degree of modification was estimated by calculating the ratio of the N-acetyl peak of HA at 2.0 ppm and the aliphatic protons from dopamine at 2.42 or 2.72 ppm. This estimation was in agreement with the aromatic protons of dopamine between 6.7 and 7.3 ppm (Fig. S1 in Supplementary Information).

#### 2.1.2. Synthesis of HA-CDH conjugate

The conjugation of carbodihydrazide (CDH) on hyaluronic acid was carried out by carbodiimide coupling chemistry following our previously reported protocol [19]. The degree of hydrazide modifications was found to be 10% (with respect to the disaccharide repeat units), as determined by trinitrobenzene sulfonic acid (TNBS) assay [34].

#### 2.1.3. Synthesis of HA-DA-CDH conjugate

The conjugation of carbodihydrazide (CDH) on dopamine-modified hyaluronic acid (HA-DA) was carried out following the same procedure as reported for the synthesis of HA-CDH conjugates. Briefly, 0.5 mmol of HA-DA (200 mg, 1 equivalent) was dissolved in 120 mL of deionized water. Thereafter, 0.375 mmol CDH (34 mg, 0.75 equivalent) and 0.5 mmol HOBt (76.5 mg, 1 equivalent) was added to the aqueous HA-DA solution. The pH of the reaction mixture was adjusted to 4.7. Finally, 0.1 mmol EDC·HCl (20 mg, 0.2 equivalent) was added and allowed to stir overnight. The reaction mixture was dialyzed and lyophilized, as described above. The degree of hydrazide modifications was found to be 10% (with respect to the disaccharide repeat units) as determined using TNBS assay [34].

#### 2.1.4. Synthesis of HA-Aldehyde (HA-Ald)

The HA-Ald was synthesized following our previously developed procedure, as described in Ref. [35]. The percentage of aldehyde modification in HA was found to be 10% (with respect to the disaccharide units) as determined by $^1$H NMR spectroscopy. The modification degree was estimated by treating HA-Ald with *tert*-butyl carbazate followed by NaCNBH3 reduction (Fig. S2 in Supplementary Infromation) [35].

### 2.2. Preparation of hydrogels

The hydrogels were prepared using conventional hydrazone crosslinking chemistry. The individual components were sterilized with UV for 30 min and dissolved to concentration 16 mg $mL^{-1}$ (w/v), HA-Ald

and HA-DA-CDH in sterile DPBS and HA-CDH in sterile 10 wt% sucrose solution. The hydrogels were prepared by mixing the hydrazide component (either HA-CDH or HA-DA-CDH) with HA-Ald in equal volumes. In cell-containing hydrogels, hASCs were suspended in the hydrazide component prior to mixing, at a concentration of $2 \times 10^6$ cells $mL^{-1}$.

### 2.3. Rheological studies

Rheological characterization of the hydrogels was performed to understand the structure-property relationship caused by hydrogel crosslinking chemistry using TA instruments' DHR-II rheometer. Both amplitude and frequency sweep tests were performed to analyze the mechanical properties of the hydrogels. During an amplitude sweep, the amplitude of the deformation was varied while the frequency was kept constant at 1 Hz, to determine the linear viscoelastic region (LVR). Subsequent frequency sweep tests were performed between 0.1 and 10 Hz using a constant strain within the LVR, which was 1% in HA-HA and HA-DOPA gels. For the analysis, the storage and loss modulus were plotted against the frequency (Hz).

The distance between two crosslinks or entanglement points, i.e. the average mesh size (ξ), and average molecular weight between crosslinks ($M_c$) were calculated based on rubber elastic theory that can be applied on hydrogels with elastic character. Average mesh size, ξ, was determined using Equation (1)

$$(\xi) = \left(\frac{G'N}{RT}\right)^{-1/3} \quad (1)$$

where $G'$ is storage modulus of the hydrogel, N is the Avogadro constant ($6.023 \times 10^{23}$ $mol^{-1}$), R is the molar gas constant (8.314 J $K^{-1}mol^{-1}$) and $T$ is the temperature (298 K). Average molecular weight between crosslinks, $M_c$, was calculated using Equation (2)

$$(M_c) = \frac{c\varphi RT}{G'_P} \quad (2)$$

where $c$ is the polymer concentration (1.6% w/v), ρ is the density of water at 298 K (997 kg $m^{-3}$), R is the molar gas constant (8.314 J $K^{-1}mol^{-1}$), $T$ is the temperature (298 K) and $G'_p$ is the peak value of $G'$.

DHR-II TA instruments' rheometer was also used to quantify the differences in adhesion properties between HA-HA gels and HA-DOPA gels using a tack adhesion test. We first glued a piece of porcine cornea on the top head of the 12 mm parallel plate and placed a fully cured gel of 2 mm thickness at the bottom parallel plate. Subsequently, the probe (cornea tissue) was placed in contact with the gel, with a holding period of 120 s where a constant force of 100 mN was applied. Thereafter, an axial force of 5 N was applied to separate the probe and the gel at a constant separation rate. The experiment was performed in triplicates and the same probe was used to eliminate the effect of surface roughness and a constant holding period was maintained to establish uniform molecular contacts between the probe and the gel.

### 2.4. Swelling and degradation analysis

To determine the swelling and degradation behavior of the hydrogels, 100 μL hydrogel samples were prepared into cut 1 mL syringes. The initial weight of the samples was recorded and the samples were then submerged in DPBS, hASC culture medium (DMEM/F-12 + 5% human serum) or 20–50 U $mL^{-1}$ hyaluronidase solution. The residual mass of the samples in hyaluronidase were recorded at time points 2 h, 4 h, 6 h, 24 h, 48 h (2 days), 72 h (3 days), and 96 h (4 days) until the samples had degraded. The degradation study was performed for three parallel samples. The hydrogel samples in DPBS and medium were weighed after 6 h, and on following days for a total of three weeks. The swelling measurement was conducted on four parallel samples. The swelling ratio (SR) for the samples was calculated from the recorded weight ($W$) based on Equation (3)

$$SR = \frac{W_{swollen} - W_{initial}}{W_{initial}} \times 100\% \quad (3)$$

### 2.5. Transparency analysis

The transparency of the hydrogels was analyzed based on transmittance properties as well as visual evaluation. The transmittance was measured by preparing the hydrogels in 550 μL micro-cuvettes (light path 10 mm) and measuring their transmittance using a UV/VIS spectrophotometer at wavelengths ranging from 380 to 900 nm, using an empty cuvette (air) as blank. Transmittance was measured from three independent samples. Visual transparency was evaluated from 150 μL hydrogel samples prepared in 10 mm diameter molds. The hydrogel samples were removed from their molds, placed on pieces of text, and photographed from above in natural lighting.

### 2.6. Conjugation of basement membrane proteins

Covalent surface modification of the hydrogels was performed using synthetic laminin-derived peptide CDPGYIGSR and collagen type IV (col IV). Prior to conjugation, the laminin-derived peptide was dissolved in 5% acetic acid at 1 mg $mL^{-1}$, and col IV in 0.25% acetic acid at 2 mg $mL^{-1}$. The final concentrations on hydrogel surfaces were 2 μg $cm^{-2}$ for the laminin peptide, and 5 μg $cm^{-2}$ for col IV. The acidic peptide and protein solutions were brought to pH 8 using 1 M NaOH right before conjugation. Based on the molar concentration of amine groups in col IV (148 μM as determined by TNBS assay), 10-fold molar concentration (1.48 mM) of Traut's reagent was used to convert amines in col IV to thiol groups according to manufacturer's instructions. The thiolated col IV (col IV-SH) was purified using a desalting column with 7K MWCO. The concentration of thiols in the final products was quantified using Ellman's reagent. Thiolated col IV and unmodified col IV were added to the HA-DOPA and HA-HA hydrogels at a concentration of 5 μg $cm^{-2}$, in PBS pH 8.5 containing 1 mM EDTA, and allowed to react at 37 °C for 2 h. Hydrogels without col IV were used as controls. The hydrogels were washed 5 × 5 min with DPBS prior to seeding hESC-LESCs on their surface.

### 2.7. Quantification of thiol groups

The reaction kinetics of the conjugation reaction and the quantification of thiol groups in thiolated col IV were measured using Ellman's reagent. Reaction kinetics were measured using the laminin-derived peptide CDPGYIGSR, which contains only one thiol group in the N-terminal cysteine residue per molecule. The reaction kinetics measurement was performed for the same peptide obtained from two different manufacturers, Bachem and Calbiochem. For quantitation of reaction kinetics, Ellman's reagent was added to the conjugation solution in equal molarity to the amount of peptide. The peptide solution (at a concentration of 2 μg $cm^{-2}$) was pipetted to the gels on a 96-well plate (100 μL per well) and allowed to react for 1 h at RT. The rest of the reaction solution was left as a control to account for the dimerization of the Cys-terminated peptides. Every 10 min, the absorbance of the sample from the hydrogels and from control solution at 412 nm was recorded using the UV/VIS spectrophotometer in 1 mL cuvettes (950 μL of PBS pH 8.5 + 50 μL sample). To calculate the progress of the reaction, the absorbance of the control solution was subtracted from the absorbance of the sample. Reaction kinetics measurement was performed once for each manufacturer's peptide.

The amount of thiol groups of the col IV-SH was quantified using the molar absorptivity of Ellman's reagent. 4 mg $mL^{-1}$ solution of Ellman's reagent was prepared in reaction buffer (0.1 M PBS, pH 8.0, containing 1 mM EDTA). Two tubes were prepared with 1.25 mL of reaction buffer and 25 μL of the Ellman's reagent, and added with 125 μL of either the col IV-SH sample or pure reaction buffer, which served as the blank.

After 15 min, the absorbance of the sample was measured at 412 nm against the blank using the UV/VIS spectrophotometer. The concentration of thiol groups was calculated based on the molar extinction coefficient of Ellman's reagent (14 150 $M^{-1}cm^{-1}$) and Equation (4)

$$c = \frac{A}{bE} \tag{4}$$

where $A$ is the absorbance of the sample at 412 nm, $b$ is the length of the light path (1 cm), and E is the molar extinction coefficient.

### 2.8. Cell culture and in vitro analysis

All cell studies were conducted with approval from the Ethics Committee of the Pirkanmaa Hospital District (Tampere, Finland) under the approval number R15161 for use of adipose stem cells in research and approval number R05116 to derive, culture, and differentiate hESC lines for research. The hASCs were isolated from adipose tissue samples from a female donor during elective plastic surgery at Tampere University Hospital (Tampere, Finland) under patient's written consent, as described previously [36,37]. The flow cytometric cell characterization profile of the hASCs used in this study is described elsewhere [20]. The hASCs were cultured in a medium containing DMEM/F-12 supplemented with 5% human serum, 1% GlutaMAX™ and 1% antibiotics. The cells were maintained in T175 cell culture flasks at 37 °C in 5% $CO_2$, and passaged using TrypLE™ Select. Cells were maintained up to passage 4 prior to encapsulation in hydrogels. For encapsulation, hASCs were detached from cell culture flasks, collected by centrifugation and counted. The required number of cells for each hydrogel was collected in Eppendorf tubes, and the cells were pelleted. Supernatant was removed and cell pellets were mixed by thorough pipetting into the hydrazide component (HA-CDH or HA-DA-CHD) at a concentration of $2 \times 10^6$ cells $mL^{-1}$. The hydrogels were then formed by mixing the cell-containing hydrazide component with an equal volume of HA-Ald in either 24-well cell culture inserts (Merck Millipore), total volume of 100 µL, or custom-made polydimethylsiloxane (PDMS) molds with 10 mm diameter wells, total volume of 200 µL. The hydrogels were allowed to gel for 2 h in a humid atmosphere at RT before adding medium. The cell-laden hydrogels were then cultured either in hASC medium (for 3D cell survival determination) or CnT-Prime-CC (for co-culture of hASCs and hESC-LESCs) at 37 °C in 5% $CO_2$. To create the compartmentalized stem cell implants, the hASCs were cultured alone for 24 h before conjugation of col IV-SH and seeding of hESC-LESCs.

The hESC-LESCs were differentiated from human embryonic stem cell line Regea08/017 cultured in feeder-free conditions, according to our previously published protocols [38,39]. The hESC-LESCs were thawed from cryostorage to the basement membrane protein-conjugated hydrogels in a concentration of 0.9–1.5 $\times 10^6$ cells $cm^{-2}$, with further culture of the cell-laden hydrogel in CnT-30 medium containing 0.5% antibiotics. For surface attachment study, hESC-LESCs were cultured on the hydrogels for seven days. The hydrogel scaffolds containing both hASCs and hESC-LESCs were cultured in CnT-30 medium for two to five days before transplantation in the porcine organ culture model or fixation for histological evaluation.

The viability of hESC-LESCs on the surface-modified hydrogels was evaluated based on cell morphology, with light microscope images taken with Zeiss Axio Vert A1 (Carl Zeiss AG, Jena, Germany), and compared quantitatively using PrestoBlue® reagent. For PrestoBlue® analysis of cell metabolism, three parallel samples were analyzed for each condition. The samples were washed once with DPBS, and the PrestoBlue® reagent, diluted 1:10 (v/v) in CnT-30 medium, was added to the samples. The samples were incubated for 30 min at 37 °C, after which 2 × 100 µL samples of the medium were collected on a 96-well plate. The fluorescence values for the medium samples were measured using Viktor 1420 Multilabel Counter (Wallac, Turku, Finland) at 544 nm excitation and 590 emission wavelengths.

For hASCs encapsulated into the hydrogels, viability was evaluated qualitatively using LIVE/DEAD® viability/cytotoxicity kit, and quantitatively with CyQUANT cell proliferation kit and PrestoBlue® after 1, 3, 7 and 10 days. For Live/Dead staining, the hydrogels were removed from their molds, washed with DPBS and incubated with Live/Dead staining solution containing 2 µM Calcein AM and 1 µM Ethidium homodimer diluted in DPBS in 37 °C for 30–45 min. The samples were washed once, and imaged using Olympus IX51 fluorescence microscope equipped with a DP71 camera (Olympus Corporation, Tokyo, Japan). For CyQUANT analysis of hydrogel DNA content, three gels with hASCs and one blank gel were collected in each time point to 2 mL Eppendorf tubes and frozen in −80 °C. After thawing, 100 µL of the CyQUANT lysis buffer was added to the samples, which were then mechanically homogenized using an Ultra-Turrax disperser (IKA Labortechnik, Staufen, Germany). Samples were centrifuged at 8000 g for 30 s to remove any remaining hydrogel, with the final sample diluted 1:10 in CyQUANT lysis buffer. The diluted samples were then pipetted to 96-well plates with CyQUANT Dye, and the fluorescence was read at 480/520 nm with Victor 1420 Multilabel Counter microplate reader. For cell number quantitation, the measured fluorescence values were compared to a reference standard curve created from 2D cultured hASCs. PrestoBlue® analysis from encapsulated hASCs was conducted as described previously in Ref. [20]. Statistical testing of the cell viability results was performed by two-way ANOVA between HA-DOPA and HA-HA gels using GraphPad Prism v5.02.

### 2.9. Porcine corneal organ culture

Porcine eyes were obtained from a local abattoir. The eyes were kept in cold DPBS containing 2% antibiotics for up to 4 h before dissection and transfer to the organ culture. The eyes were processed as previously described, and cultured partially submerged in CnT-Prime-CC medium with 1% antibiotics and 0.1% amphotericin B [20]. Prior to implantation of the cell-laden hydrogels, an epithelium defect was induced by applying a circular Whatman paper impregnated with 1 M NaOH on the cornea surface for 40 s, followed by rinsing with DPBS and epithelial scraping. For hydrogel implantation, the organ-cultured corneas were immobilized on a Barron artificial anterior chamber (Katena products Inc., Denville, NJ, USA), where a partial depth incision was made to the stroma using a 5-mm trephine, from which the stromal button was excised. The hydrogel implant containing hASCs and hESC-LESCs was cut to size using a 5-mm trephine, and the implant was transferred to the stromal wound using a flat spatula. After hydrogel implantation, the corneas were transferred to 6-well plates, covered with soft contact lenses and cultured for additional seven days in CnT-30 medium at 37 °C, 5% $CO_2$.

To determine the differentiation potential of implanted hASCs in the corneal organ culture, 50 µL HA-HA and HA-DOPA gels with encapsulated hASCs (300 000 cells/gel) were made directly into the stromal wounds, with four replicates of each gel. The corneas were cultured for 10 days in keratocyte differentiation medium (KDM) containing Advanced DMEM supplemented with 10 ng $mL^{-1}$ basic fibroblast growth factor (bFGF), 0.1 mM ascorbic acid-2-phosphate and 1 µM retinoic acid, as described previously in Refs. [11,40]. The gels with cells were collected from the corneal wounds after the culture period into TRIreagent, and the samples were homogenized using Bioruptor sonicator (Diagenode SA, Belgium) (30 s ON, 30 s OFF, 2 cycles). RNA from the samples was isolated by adding chloroform to the TRIreagent solution, vortexing and centrifugation (12 000 g for 10 min). The upper chloroform phase was collected to a new tube and isopropanol was added, followed by vortex and centrifugation (12 000 g, 10 min). The supernatant was removed, and the RNA pellet was eluted into 70% ethanol, vortexed and centrifuged (12 000 g, 10 min). The supernatant was removed and remaining pellet was air-dried and eluted into 30 µl RNAse free water. The amount of RNA was quantitated using NanoDrop spectrophotometer (Thermo Fisher Scientific). Enough RNA to perform

qRT-PCR was obtained from three replicates for both gels, and the RNA was treated with DNAse I and transcribed to cDNA using High capacity cDNA reverse transcription kit (Applied Biosystems, Thermo Fisher Scientific). As a control, 2D differentiation of hASCs was performed on standard tissue culture plastic 6-well plates, culturing them in KDM for 10 days. Control samples of undifferentiated hASCs and 2D differentiation were collected for quantitative real-time polymerase chain reaction (qRT-PCR) with Qiagen RNeasy Mini Kit according to manufacturer's instructions, and transcribed to cDNA together with RNA from the gel samples. qRT-PCR analysis for three corneal keratocyte markers, keratocan (KERA), lumican (LUM) and aldehyde dehydrogenase 3A1 (ALDH3A1) was run with Applied Biosystems real time PCR instrument. The relative fold change of gene expression was analyzed using the $2^{-\Delta\Delta Ct}$ method.

### 2.10. Histological analysis and immunofluorescence

For histological analysis, the porcine organ culture corneas were fixed using 4% paraformaldehyde (PFA) for 3 h at RT, submerged in Tissue-Tek OCT (Sakura Finetek Europe) at 4 °C overnight, and snap-frozen in liquid nitrogen. 8 mm thick sections were cut from the samples and air dried for 1 h at RT. Cell-laden hydrogel samples were similarly processed, with 30 min fixation in 4% PFA. Sections from the porcine corneas were then immunohistochemically stained against human cell surface marker TRA-1-85 to detect implanted human cells. 2.5% normal horse serum (Vector ImmPress reagent, Vector Laboratories Inc.) was used to block unspecific binding. Samples were then labeled overnight at 4 °C with primary mouse IgG antibody TRA-1-85 (courtesy of Peter Andrews, University of Sheffield) diluted 1:100 (v/v) in 0.5% bovine serum albumin (BSA). Intrinsic peroxide activity was blocked by incubating the samples with 3% $H_2O_2$ for 10 min at RT, followed by labelling with Vector ImmPress horse anti-mouse IgG (containing horseradish peroxidase) for 30 min at RT. The antibody labelling was visualized by peroxidation reaction using DAB + chromogen system (Dako North America, Inc., Carpinteria, CA, USA), which was performed for 30 s at RT. The tissue was counterstained using Mayer's hematoxylin, followed by dehydration, and mounting using Coverquick mounting medium (VWR, Helsinki, Finland). Samples were imaged using Hamamatsu NanoZoomer S60 (Hamamatsu Photonics Norden, Kista, Sweden) whole slide scanner, and images were obtained using NDP.view2 viewing software.

Immunofluorescence staining, for hESC-LESCs on top of hydrogels and the transverse cryosections of the cell-laden hydrogels, was carried out using primary antibodies against p63α, p40, cytokeratin 12 (CK12), and col IV. Details of the antibodies are listed in Table 1. The hydrogel samples on well plates were fixed with 4% PFA for 30 min at RT, followed by washing with DPBS. The samples were then permeabilized using 0.1% Triton X-100 for 15 min, followed by blocking with 3% BSA and incubation with primary antibodies diluted in 1% BSA overnight at 4 °C. After washing with DPBS, the samples were incubated with fluorescently labeled secondary antibodies (Table 1) diluted in 1% BSA, for 1 h at RT. The samples were then washed and mounted under coverslips using mounting medium containing 4′,6-Diamidino-2-Phenylindole (DAPI) (Vectashield® from Vector Laboratories or ProLong™ Gold from Thermo Fisher Scientific) and imaged using Olympus IX51 fluorescence microscope. Fluorescent images were converted to color images and adjusted for contrast and brightness using Photoshop.

## 3. Results and discussion

### 3.1. Synthesis and characterization of dopamine-functionalized HA hydrogel

We have previously developed hydrazone-based robust hydrogels using HA-aldehyde (HA-Ald) and HA-carbodihydrazide (HA-CDH) with exceptional enzymatic stability and swelling characteristics [19]. We used this two-component biorthogonal system for fabricating the compartmentalized cellular scaffold for corneal applications. In order to introduce the tissue adhesive properties to facilitate sutureless implantation of the scaffold, we conjugated L-dopamine moiety in the polymer. The degree of dopamine functionalization was 14%, as determined by $^1$H NMR (Fig. S1 in Supplementary Information). The aldehyde and CDH groups were grafted on HA following our previously optimized carbodiimide protocol [19] and the percentage of aldehyde and CDH functionalization was around 10% (with respect to the disaccharide repeat units), which was quantified by $^1$H NMR (Fig. S2 in Supporting Information) and UV/VIS spectroscopy. We utilized HA gels with similar aldehyde and CDH modification without dopamine units as the control group. The dopamine-functionalized HA-gels were designated as HA-DOPA, while the control gel was designated as HA-HA. Their structures are presented in Fig. 1.

### 3.2. HA-HA and HA-DOPA gels display highly elastic character

We performed rheological evaluation to estimate the viscoelastic properties of HA-HA and HA-DOPA gels by measuring the gel deformation following the frequency sweep method. The gels were subjected to strain sweep to determine the linear viscoelastic region (LVR) of the hydrogel, followed by a frequency sweep test at 0.1–10 Hz using a constant strain within the LVR (Fig. 2a). The gels showed storage moduli ($G'$) of 898.81 ± 16.46 Pa and 619.57 ± 13.02 Pa and loss moduli ($G''$) of 3.046 ± 0.07 Pa and 1.88 ± 0.624 Pa respectively for HA-HA and HA-DOPA gels. The storage modulus $G'$ was consistently higher than the loss modulus $G''$ throughout the screened frequency range suggesting that both the hydrogels were stable and possessed viscoelastic properties. The tan δ, which represents the ratio of storage and loss moduli, was found to be significantly less than 1 (0.0034 and 0.0030 for HA-HA and HA-DOPA gels respectively) suggesting a highly elastic character for these gels. By using the modulus data, we estimated the average mesh size ξ (representing the distance between the entanglement points or probable pore size) and the average molecular weight between the crosslinks $M_c$ by using the rubber elastic theory that can be applied to highly elastic hydrogels [41]. These calculations revealed that average mesh size ξ was 16.6 nm and 18.8 nm while the $M_c$ was 41.46 kg mol$^{-1}$ and 56.96 kg mol$^{-1}$ for HA-HA and HA-DOPA gels respectively. Thus, HA-HA gel was stiffer and more compact than the HA-DOPA gel, with smaller ξ and $M_c$.

Next, we investigated the effect of encapsulated stem cells on the

**Table 1**
Antibodies used for immunofluorescence staining.

| Antibody | Host | Supplier | catalog no. | dilution [v/v] |
|---|---|---|---|---|
| p63α | rabbit | Cell Signaling Technology | 4892 | 1:200 |
| p40 | mouse | Biocare Medical | 3066 | 1:100 |
| CK12 | goat | Santa Cruz Biotechnology | sc-17099 | 1:200 |
| collagen IV | goat | Millipore | AB769 | 1:200 |
| anti-rabbit Alexa-488 | donkey | Molecular Probes | A21206 | 1:800 |
| anti-goat Alexa-568 | donkey | Molecular Probes | A11057 | 1:800 |
| anti-mouse Alexa-647 | donkey | Molecular Probes | A31571 | 1:800 |

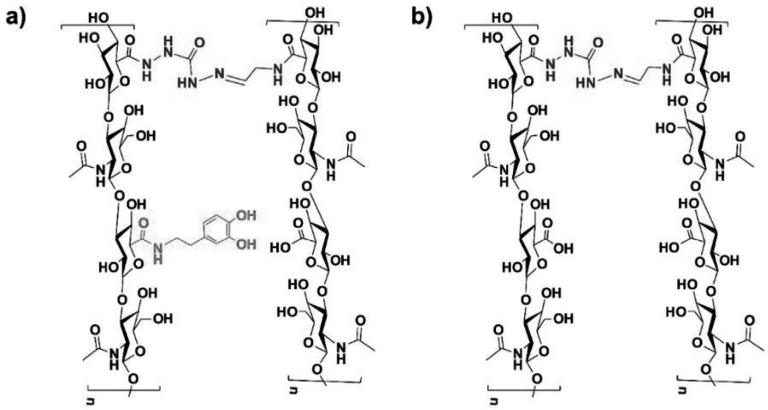


**Fig. 1.** Chemical structures of hydrazone-crosslinked HA-DOPA (a) and HA-HA (b) hydrogels.

viscoelastic properties of the scaffold (Fig. 2b). We cultured hASCs in HA-HA and HA-DOPA gels ($2 \times 10^6$ cells $mL^{-1}$) for 24 h as described in section 2.8. After that, the cell-laden hydrogels were extracted from their molds and we performed the rheological measurements as described in section 2.3. We found that the encapsulation of cells within the hydrogel resulted in the reduction of storage modulus ($G'$) for both HA-HA and HA-DOPA gels. This could be attributed to two factors, the presence of different serum proteins and biomolecules in the cell culture medium and the cell surface proteins. The gels showed storage moduli $G'$ of 309.15 ± 5.63 Pa and 483.70 ± 7.35 Pa and loss moduli $G''$ of 6.94 ± 1.71 Pa and 11.00 ± 1.69 Pa respectively for HA-HA and HA-DOPA gels at the frequency of 1 Hz. Interestingly, when we compare the two gels formulated in PBS to the gels formulated with cells in cell culture medium we observed that the change in $G'$ was smaller in

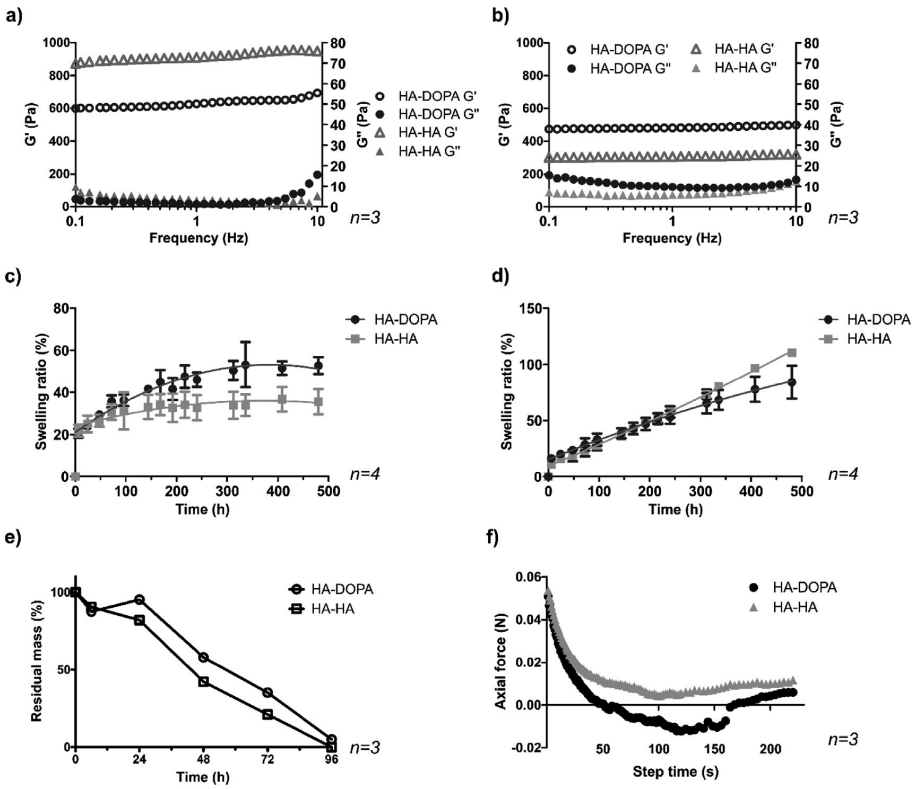


**Fig. 2.** Material characterization of HA-DOPA and HA-HA gels. a) Rheological measurement of $G'$ and $G''$ in the frequency sweep mode. b) Frequency sweep of $G'$ and $G''$ of hydrogels with encapsulated hASCs. c) Hydrogel swelling ratios in PBS. d) Hydrogel swelling ratios in cell culture medium. e) Enzymatic degradation of the hydrogels in the presence of hyaluronidase. f) Adhesion force measurement of the hydrogels to corneal surface.

**Table 2**
Material properties of HA-DOPA and HA-HA gels.

| Hydrogel | n | $G'$ [Pa] | G″[Pa] | tan δ[G′/G″] | $\xi$ [nm] | $M_C$ [kg mol$^{-1}$] |
|---|---|---|---|---|---|---|
| HA-HA | 3 | 898.81 ± 16.46 | 3.046 ± 0.07 | 0.0034 | 16.6 | 41.46 |
| HA-DOPA | 3 | 619.57 ± 13.02 | 1.88 ± 0.624 | 0.0030 | 18.8 | 56.96 |
| HA-HA with cells | 3 | 309.15 ± 5.63 | 6.94 ± 1.71 | 0.0224 | 23.7 | 123.27 |
| HA-DOPA with cells | 3 | 483.70 ± 7.35 | 11.00 ± 1.69 | 0.0227 | 20.41 | 79.38 |

HA-DOPA gels when compared to HA-HA gels. The $G'$ decreased with the incorporation of cells in HA-HA gels from 898.81 ± 16.46 Pa to 309.15 ± 5.63 Pa, and in HA-DOPA from 619.57 ± 13.02 Pa to 483.70 ± 7.35 Pa. This observation indicates that the dopamine units form some kind of interpenetrating network or exert adhesive forces that prevent the swelling and disruption of molecular crosslinks. This is further evidenced by the average mesh size ξ values for both gels. In the presence of cells, HA-DOPA and HA-HA had average mesh size 20.41 nm and 23.7 nm respectively, while without cells the values were 18.8 nm and 16.6 nm, respectively. This means that the HA-DOPA gel had a larger pore size in PBS, whereas in the presence of cells, the average mesh size was reduced, presumably due to adhesive forces exerted by the dopamine moiety. The tan δ was found to be less than 1 (0.0224 and 0.0227 for HA-HA and HA-DOPA gels respectively) suggesting elastic characteristics for these gels, but the degree of elasticity was much lower in the presence of cells compared to the gels without encapsulated cells (tan δ 0.0034 and 0.0030 for HA-HA and HA-DOPA gels respectively). Thus, in the presence of cells, HA-DOPA gels were stiffer and more compact with smaller $\xi$ and $M_c$ than HA-HA gels. The material characteristics are summarized in Table 2.

For the cornea, the material property most often described is the shear modulus. The shear modulus of the native cornea varies with depth, with the anterior stroma having a higher modulus (7.71 kPa) than the deeper parts of the cornea (1.31–1.99 kPa) [42]. Although our application focuses on replacing the anterior stromal part of the cornea with the hydrogel scaffold, we consider the mismatch of the initial mechanical properties of the material to the cornea to be inconsequential for the final regenerative target. For stable corneal regeneration and integration, the stromal cells should secrete their own extracellular matrix (ECM) and remodel their environment. This has been previously shown during a 4-year follow-up of cell-free stromal implants composed of densely crosslinked collagen hydrogels, where surrounding stromal cells were seen to slowly replace the implant with stromal tissue [43]. Our approach aims at faster remodeling and integration of the scaffold to the corneal tissue through encapsulation of hASCs.

### 3.3. HA-DOPA gel shows good swelling stability in physiological conditions

To evaluate the swelling property of the HA-HA and HA-DOPA gels, we measured their weight increase in phosphate buffered saline (PBS, pH 7.4) and cell culture medium at 37 °C (Fig. 2c and d). Both gels showed similar swelling behavior, but the swelling kinetics differed in PBS compared to cell culture medium. In PBS, the hydrogels reached an equilibrium swelling state after 1 week, whereas in medium, the hydrogels continued to swell in a linear manner throughout the measurement period. In PBS, both gels displayed an initial 20% burst in swelling upon hydration, after which the swelling slowed down and subsequently leveled at approximately 34% for HA-HA and 50% for HA-DOPA during three weeks. The higher swelling ratio of HA-DOPA gel may be associated with the larger average mesh size, which allows more water permeability inside the hydrogel network. Interestingly, in medium, the swelling ratio for HA-HA surpassed that of HA-DOPA after the 1-week time point, ultimately reaching 110% for HA-HA and 85% for HA-DOPA in three weeks. We believe the sustained swelling properties of the two hydrogels in cell culture medium are attributed to the dynamic nature of the hydrazone bond, which may undergo exchange with proteins present in the medium. Lower swelling in medium observed for HA-DOPA may indicate that the hydrazone bond dynamics are complemented by additional interpenetrating crosslinks introduced by dopamine self-polymerization or adhesive forces exerted by dopamine, which was supported by a slight increase in intensity of the slight brown hue of HA-DOPA gels during prolonged exposure to cell culture medium, as discussed in detail in Section 3.5.

Hydrazone crosslinking using CDH-derived hydrazones has been shown to be considerably more stable than hydrazone crosslinks from other hydrazides, due to the resonance stabilization effect across the hydrazone bond [19]. The engraftment of dopamine residues to HA increased the PBS swelling capacity of the gels, indicating that the incorporation of dopamine slightly hindered the crosslinking efficacy of the gels. Conversely, the HA-DOPA gels were more stable in medium, which arguably resembles the *in vivo* environment more closely than PBS, indicating their overall suitability for tissue engineering applications. However, in the cornea, the tissue environment is not as dilute as the conditions of the swelling study. *In vivo*, the hydration of corneal tissue is maintained by the pumping mechanism of the endothelium, and the surface of the cornea is wetted by tear fluid secreted by the lacrimal and Meibomian glands and the goblet cells of the conjunctiva, with its varying composition of lipids, proteins and small molecules [44]. The actual swelling of the implants in the intended application should hence be studied in a more tissue-specific environment.

We studied the *in vitro* degradation kinetics of the hydrogels in the presence of hyaluronidase (HAse), a ubiquitous enzyme known for the *in vivo* degradation of HA. At a concentration of 20–50 U mL$^{-1}$ of HAse, both HA-HA and HA-DOPA gels displayed complete digestion in 96 h (Fig. 2e). Although, the concentration of HAse used in this experiment is not directly comparable to that in the eye, the enzymatic degradation of the scaffold implies that the chemical modifications on the HA-HA and HA-DOPA gels did not disrupt the native bioactivity and the biodegradability of the polymer. For final applications, the rate of degradation *in vivo* should be studied further to match the regeneration of the replaced corneal tissue, which can take from months to even years to complete [45].

### 3.4. HA-DOPA adheres strongly to the corneal surface

Adhesion of biomaterial scaffold to the defect site is of paramount importance for successful tissue regeneration. Scaffolds bearing aldehyde functional groups are known to display tissue adhesive properties [46]. However, as the aldehyde functional groups are utilized for hydrazone crosslinking, the free aldehyde residues are not sufficient enough to provide the adhesiveness required for scaffold integration. We anticipated that incorporation of dopamine groups would further augment the adhesive properties of the scaffold. We conjugated 14.4% dopamine units on the HA backbone, as the overall HA modification (hydrazide and dopamine moiety) must not exceed 25% [47] in order to preserve the biodegradability and activity of the biopolymer.

We performed a rheometric tack adhesion test to quantify the adhesion properties of HA-HA gels and HA-DOPA gels with the corneal surface. Although both HA-HA and HA-DOPA gels displayed some adhesion properties, HA-DOPA clearly showed greater adhesion to the cornea with cohesive failure between the probe and the gel. This can be

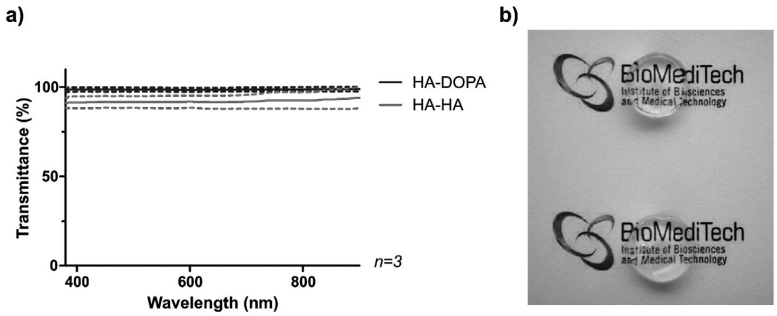


**Fig. 3.** Transmittance and transparency HA-DOPA and HA-HA gels. a) Transmittance of light at different wavelengths through the hydrogels. b) Transparency of the hydrogels illustrated by photography of HA-DOPA (upper) and HA-HA (lower) gels on text.

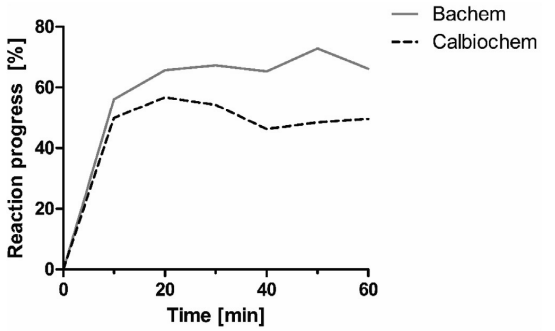


**Fig. 4.** Reaction kinetics measurement of surface conjugation of Cys-terminated laminin-derived peptide. The reaction progress was calculated based on the presence of free thiol groups in the reaction solution at different time points.

seen from Fig. 2f, as more negative force was required to separate the probe and the gel surface.

### *3.5. Hydrogels display excellent transparency for corneal applications*

Transparency is a key property of any biomaterial used for corneal applications. The native cornea exhibits light transmission of 90–95% in wavelengths ranging from 600 to 1000 nm [48]. To analyze the transparency of the hydrogels, we measured the transmittance of light over the visible light spectrum (380–900 nm), shown in Fig. 3a. Both hydrogels showed over 90% light transmittance over the whole visible spectrum. Interestingly, transmittance values for HA-DOPA (98 ± 2.39%) measured even higher than for HA-HA (95 ± 4.64%). This indicates that the slight brown hue caused by the DOPA residues, seen in Fig. 3b, did not seem to hinder the transmittance of light through the HA-DOPA gel, whereas the lower transmittance of HA-HA might be caused by minute inhomogeneity of the gel occurring through mixing of the sucrose-dissolved HA-CDH component and HA-Ald dissolved in PBS.

The brown coloration is a distinct trait of dopamine-containing materials. As dopamine residues self-polymerize, they display an intense brown color [49]. Dopamine-functionalized hydrogels reported so far generally rely on self-polymerization reaction or metal-coordination for effective crosslinking [28–31]. However, in our hydrogel implants, the dopamine residues are not responsible for the crosslinking, leaving them free to participate in the surface modification and tissue-adhesion of the preformed hydrogel implant. This results in a transparent hydrogel, which is suitable for corneal applications. Further *in vivo* studies are warranted to assess the impact of dopamine functionalization and transparency on the regenerated corneal tissue.

### *3.6. Immobilization of cell adhesive factors enables cellular compartmentalization in tissue adhesive hydrogels*

One major limitation of HA-based hydrogels for 3D cell culture is the poor cell adhesion due to the lack of binding sites for integrins, the major mediators of cell adhesion to the ECM. However, the encapsulated cells can probe their microenvironment and secrete ECM making it conducive for cell growth and differentiation [50,51]. To achieve cellular compartmentalization of the two stem cell populations, we conjugated cell adhesive peptides and proteins on the surface, exploiting the Michael acceptor characteristics of the dopamine residue. Our first choice of cell adhesive molecule was a cysteine-terminated laminin-derived synthetic peptide (CDPGYIGSR) which could be covalently grafted to the surface of the hASC-encapsulated hydrogel. This laminin-derived peptide contains the cell adhesion motif YIGSR, which has been previously shown to have significant potential for improving primary corneal epithelial cell adhesion to biomaterial surfaces [52]. Furthermore, recombinant laminin is an integral component of the culture substrate for the differentiation and culture of hESC-LESCs [38]. Ellman's quantitation of free thiols (Fig. 4) revealed that the conjugation reaction initially progressed rapidly, and reached a plateau after 10–20 min. Comparison of the same peptide from different manufacturers produced similar reaction kinetics, while the Bachem peptide conjugation reaction progressed further until approximately 70% of the peptide were bound to the surface, and was thus selected for the cell attachment study. Although we could achieve excellent conjugation of the laminin peptide on to the preformed hydrogels by Michael addition reaction, we could obtain only sparsely distributed hESC-LESCs on these peptide-modified surfaces (Fig. 5h). Subsequently, another component of hESC-LESC culture substrate, human collagen type IV (col IV) was chosen as the preferential basement membrane protein. Col IV was thiolated using 2-iminothiolane (Traut's reagent) to col IV-SH with the necessary reactive groups for Michael addition. The conversion of primary amines in col IV to thiol groups, as determined by Ellman quantitation assay, was found to be 57 ± 4.2% in this study.

The hESC-LESCs cultured on col IV-SH conjugated HA-DOPA surfaces displayed efficient cell adhesion and better long-term cell viability than on similarly treated HA-HA (Fig. 5). Interestingly, we observed some degree of hESC-LESCs attachment even when unmodified col IV was coated on the HA-DOPA gels (Fig. 5e-g) indicating the adhesive tendency of dopamine-functionalized surfaces. Also the HA-HA control gel also displayed some binding of col IV-SH (Fig. 5i-k). This may be attributed to the dynamic nature of the hydrazone bond, allowing the thiol-containing peptides or proteins to undergo thiazolidine crosslinking with aldehyde groups available on the scaffolds [53]. The microscopic evaluation of cell morphology was supported by the PrestoBlue® cell viability measurement (Fig. 5q-r), which shows that initially the hESC-LESCs attach on both gel types, but there is a gradual

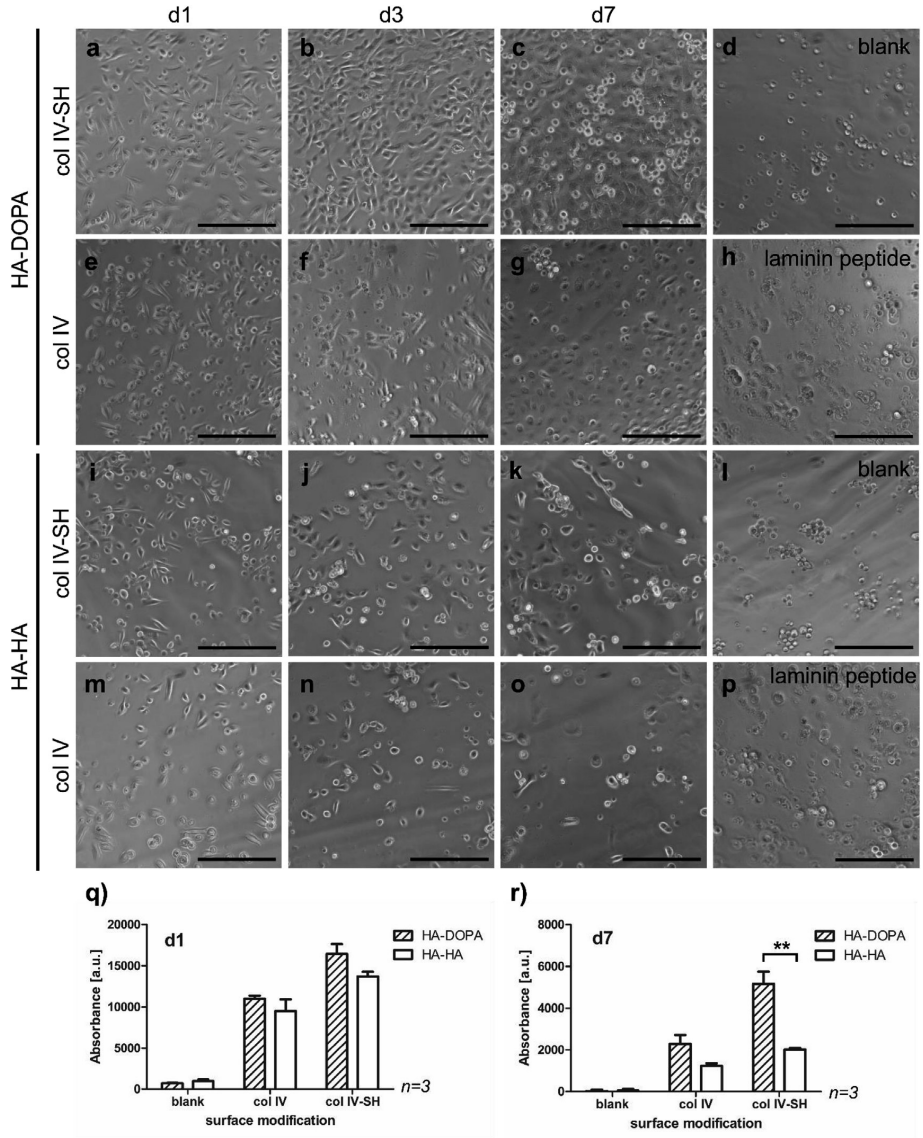


**Fig. 5.** Morphology and viability of hESC-LESCs on surface-modified hydrogels. a-c) hESC-LESCs seeded on thiolated col IV (col IV-SH)-immobilized HA-DOPA after 1 day, 3 days and 7 days of culture, respectively. The same time points are also shown for HA-DOPA with non-thiolated col IV (e–g) and col IV-SH on HA-HA (i–k) and non-thiolated col IV on HA-HA (m–o). Images d) and l) represent hESC-LESC morphology observed on unmodified HA-DOPA and HA-HA surfaces, respectively. Images h) and p) are representative images of hESC-LESCs 2 days after plating on laminin-derived peptide –immobilized HA-DOPA and HA-HA, respectively. Graphs q) and r) show the PrestoBlue® viability measurements of hESC-LESCs on col IV –modified hydrogel surfaces at day 1 and day 7, respectively. Scale bars in images are 200 μm ** denotes statistical significance at $p < 0.01$.

loss of cells from the HA-HA gels, resulting in a significantly higher cell viability on HA-DOPA at day 7. The immunofluorescence staining for col IV in hydrogel cross-sections, shown in Fig. 6a, verified the presence of high amounts of col IV on the col IV-SH-conjugated HA-DOPA, but only very little on HA-HA at 2 days after conjugation.

The cells grown on the HA-DOPA gels for 7 days showed appropriate protein expression for progenitor-type hESC-LESCs, as shown in Fig. 6b. The continued expression of the limbal stem cell marker ΔNp63α, which was confirmed by the co-labelling of p63α and p40 in cell nuclei, together with the low expression levels of epithelial maturation marker cytokeratin 12 (CK12) indicated that the hESC-LESCs retained their progenitor-like phenotype after 1 week of culture on these substrates. The hESC-LESCs still present on col IV-SH-conjugated HA-HA gels after 7 days also retained similar marker expression, although the portion of ΔNp63α-positive cells was smaller than on HA-DOPA. This suggests that covalent conjugation of the protein is indispensable on the hydrogel surface for the continued growth and maintenance of hESC-LESCs.

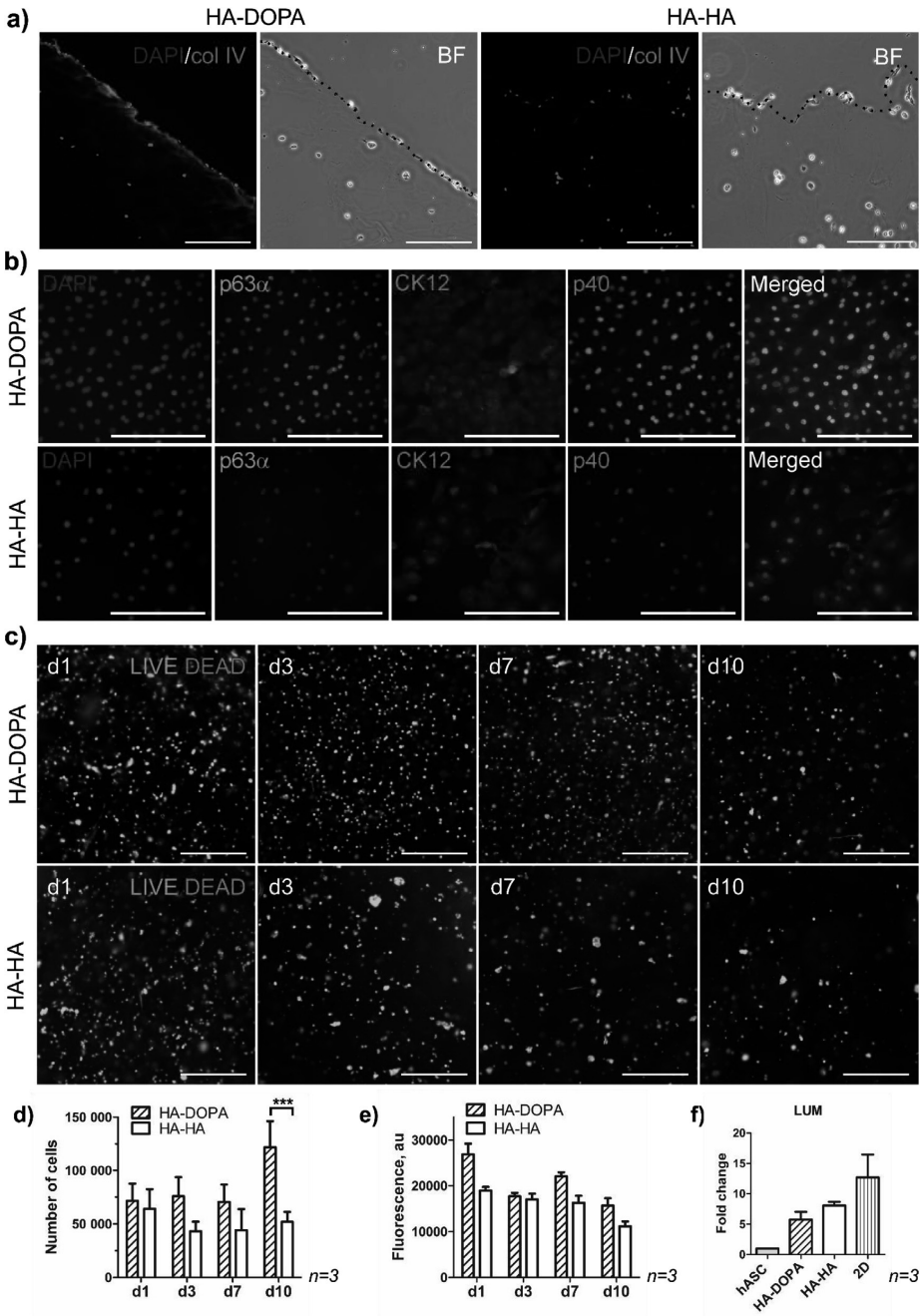


**Fig. 6.** Covalent surface conjugation of col IV-SH enables the existence of two distinctly organized human stem cell types in the hydrogels. a) Fluorescent staining of col IV at the surface of HA-DOPA and HA-HA gels 2 days after conjugation, the dotted line represents the surface of the hydrogel. b) hESC-LESCs cultured on col IV-SH-conjugated HA-DOPA and HA-HA for 7 days express the limbal stem cell markers p63α and p40, with low expression of epithelial differentiation marker CK12. c) Live/Dead staining of hASCs inside hydrogels at different time points, live cells are shown in green, and dead cells in red. d) CyQUANT results representing the number of hASCs in the gels during culture. e) PrestoBlue® quantitation metabolic activity of hASCs inside gels during culture. f) Relative gene expression of hASCs 10 days after implantation to *ex vivo* corneal model and 2D control condition showed increased expression of lumican, an extracellular matrix component of the cornea. Values reflect fold changes in mRNA expression over undifferentiated hASCs. Scale bars in images a) and b) are 200 μm, in c) 500 μm *** denotes statistical significance at $p < 0.001$. (For interpretation of the references to color in this figure legend, the reader is referred to the Web version of this article.)

The encapsulated hASCs remained viable within the HA-DOPA and HA-HA gels for 2 weeks of culture, as presented in Fig. 6c. The Live/Dead staining shows only few dead cells, whereas the amount of live cells remains high throughout the culture period, with slightly more cells in the HA-DOPA gels than the HA-HA. Furthermore, within the HA-DOPA gels hASCs occurred mostly as single cells or small groups of cells with some apparent elongation, whereas in HA-HA more rounded cell clustering was observed. This observation is interesting as HA gels lack integrin binding sites and the cells cultured in these gels traditionally show rounded morphology. We hypothesize that the adhesive nature of the DOPA residues in HA-DOPA gels may promote entrapment of the endogenous ECM produced by the cells, thus promoting cell elongation within these gels. In accordance with our results, mesenchymal stem cells within hydrogels have been shown to produce very rapidly a cell-type specific ECM around themselves, through which they interact with the surrounding hydrogel [51].

The CyQUANT results, shown in Fig. 6d, for assessing the number of cells within the HA-DOPA and HA-HA gels also indicate higher hASC viability and proliferation within the HA-DOPA gels than in HA-HA in all time points, with significantly higher number of cells on day 10. However, the PrestoBlue® results (Fig. 6e) of cells' metabolic activity within the gels show less pronounced difference between the groups. Overall, the HA-DOPA gels were superior to HA-HA gels in terms of cell growth of both hESC-LESCs and hASCs.

### *3.7. HA-DOPA gels support sutureless implantation in porcine corneal organ culture*

As a proof-of-concept in using the tissue adhesive hydrogel implants for delivering epithelial and stromal regenerating cells to the cornea, we performed an anterior lamellar keratoplasty procedure (i.e. removal of part of the outer stroma) in an *ex vivo* cornea organ culture model with excised porcine corneas. We transplanted the approximately 2 mm thick hydrogel implants into the created stromal wounds, without utilizing additional means of securing the implants in place. Due to the fitted trephination of both the wound and the implant, as well as the static nature of the subsequent organ culture, all implants remained in place for the duration of the culture. However, during manipulation of the corneas for fixation and histology, some HA-HA implants were extruded from the wounds (example shown in Fig. S3 in Supplementary Information). All HA-DOPA implants remained well attached, and in tight contact with the surrounding stromal tissue. After 7 days of culture, immunohistochemical staining against the human cell surface marker TRA-1-85 showed the presence of human cells both on the surface of the hydrogels as well as inside them (Fig. 7). However, we did not observe significant outgrowth of hASCs to the corneal stroma or migration of the hESC-LESCs out from the implant during this 1-week culture period. This outcome could be improved with further optimization of the implantation techniques to achieve better alignment of the implant surface with the surface of the cornea. However, we anticipate that the remodeling of the implant by the encapsulated and surrounding cells during stromal regeneration would ultimately take care of small mismatches in surface alignment between the implant and the corneal surface.

To investigate the differentiation potential of implanted hASCs in the corneal organ culture model, we adapted a method used previously for implantation of hASCs to corneal stromal wounds with HA-hydrogels, as described in Ref. [20], with known *in vitro* differentiation methods of hASCs to corneal keratocytes [11,40]. By culturing the porcine corneas with hASCs delivered in HA-DOPA or HA-HA in keratocyte differentiation medium for 10 days, we analyzed the expression of three marker genes of corneal keratocyte differentiation by qRT-PCR compared to undifferentiated hASCs. However, only one of the studied genes, lumican, was detected in satisfactory amounts after this culture period in *ex vivo* cultured hASCs as well as the 2D differentiation control (Fig. 6f). The expression of lumican in the *ex vivo* differentiated hASCs was similarly increased in HA-DOPA and HA-HA, while the expression in both gels was slightly lower than that in the 2D condition. Lumican is a small leucine rich proteoglycan aiding in ECM organization, abundantly expressed by corneal keratocytes. However, as lumican is not solely expressed by corneal cells, the differentiation of hASCs towards corneal keratocytes was not conclusively verified in this study. Despite the inconclusive keratocyte differentiation, the results suggest the 3D *ex vivo* differentiation capacity of these cells to be similar to the 2D control condition. This further strengthens the rationale behind this work, as the scope of our research focuses on the delivery of these undifferentiated cells to the corneal stroma, where their therapeutic capacity *in vivo* has been clinically demonstrated [14,15].

Based on these results, the corneal organ culture method provides the practical utility of the HA-DOPA gels as a sutureless stem cell delivery method for corneal regeneration and encourages to proceed towards *in vivo* studies for further evaluation of the therapeutic functionality of these stem cell-containing tissue adhesive implants.

## 4. Conclusions

In this study, we fabricated an implantable tissue adhesive hydrogel scaffold for the delivery of spatially compartmentalized therapeutic stem cells for simultaneous regeneration of the corneal stroma and epithelium, with encapsulated hASCs in the hydrogel bulk and hESC-LESCs on the surface. Dopamine moieties grafted to the hyaluronic acid hydrogel imparted the tissue adhesive function, facilitated the conjugation of cell-adhesive proteins to the hydrogel surface and supported hASC culture. Furthermore, incorporation of dopamine moieties augmented the cell viability, improved the mechanical properties and reduced hydrogel swelling in presence of cell culture medium. Using this sophisticated delivery system, we established the proof-of-concept of implanting two regenerative stem cell types in the cornea using a porcine corneal organ culture model, demonstrating its potential as an implantable tissue-engineered construct for corneal applications. We believe that our study represents the first sutureless delivery of any cells to the surface of the eye, as well as the first sutureless delivery system of two differentially localized cell populations to any tissue.

## Author contributions

L.K., T.I., H.S. and O.P.O. conceived the study, L.K. and M.K. designed and performed the swelling study, *in vitro* materials characterization, and cell studies and analyzed the data. S.S. and V.S.P. synthesized and characterized the hyaluronic acid derivatives, developed and characterized hydrogels, performed the rheological studies and corneal adhesion studies. S.M. contributed reagents and cell material for use in this study. L.K. and O.P.O. wrote the manuscript. M.K., T.I., S.M., and H.S. participated in critical evaluation of the manuscript.

## Conflicts of interest

The authors declare no conflict of interest.

## Data availability

All of the data reported in this work are available upon request.

## Acknowledgements

The authors would like to thank Outi Melin and Hanna Pekkanen for their assistance in producing the hESC-LESCs, and Miia Juntunen for assistance with the hASCs. We also thank the Tampere Imaging Facility (BioMediTech and Faculty of Medicine and Health Technology, Tampere University) for the imaging facilities, and Paijan Tilateurastamo for the porcine eyes. The authors thank the Graduate School of Faculty of Medicine and Life Sciences, University of Tampere,

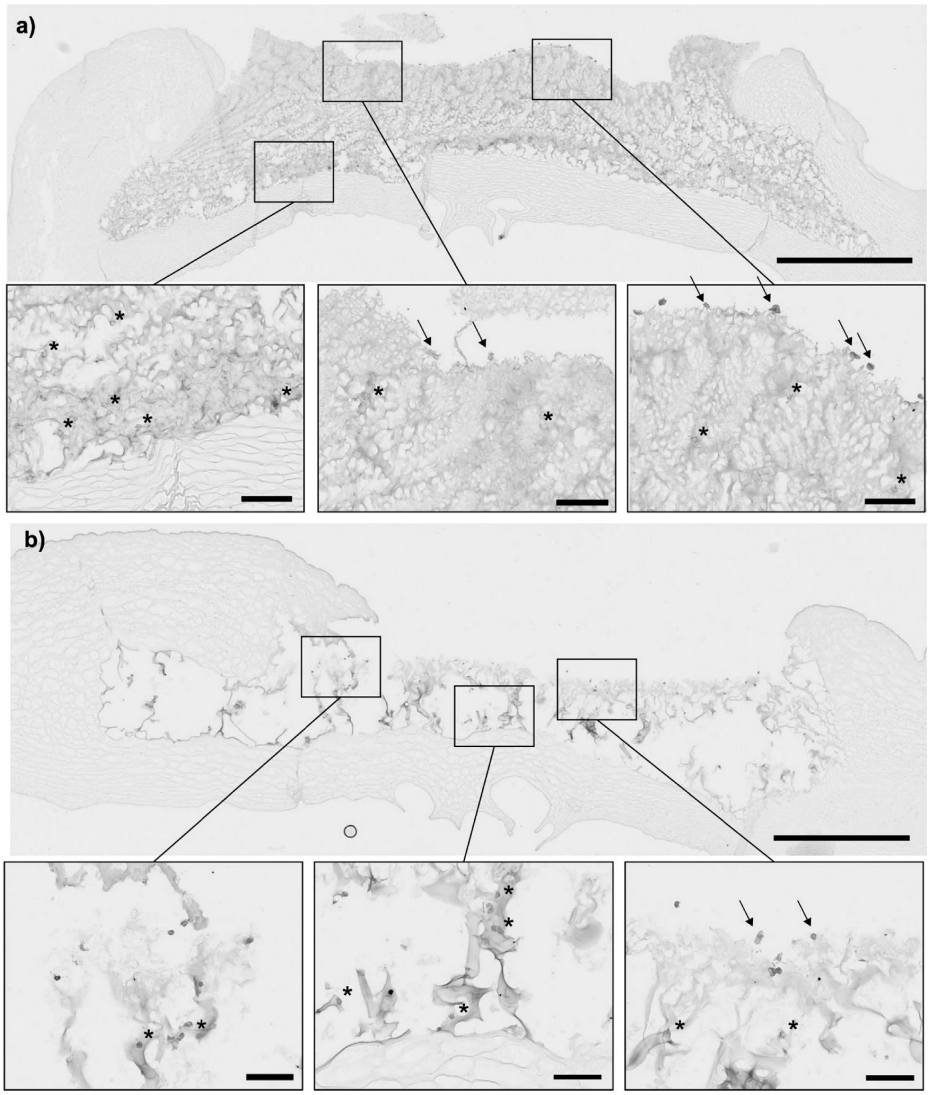


**Fig. 7.** Histological evaluation of the hASC and hESC-LESC containing HA-DOPA (a) and HA-HA (b) hydrogel implants in porcine corneal organ culture for 7 days. The presence of human cells was detected using TRA-1-85 cell surface marker (in brown). The higher magnification images show encapsulated cells (*) and cells on the surface of the implant (arrows). Scale bars in the whole cornea images are 1 mm, and 100 μm in the insets. (For interpretation of the references to color in this figure legend, the reader is referred to the Web version of this article.)

Instrumentarium Science Foundation, Academy of Finland and Business Finland for their funding for this research. This study was partly supported by the Competitive State Research Financing of the Expert Responsibility area of Tampere University Hospital.

## Appendix A. Supplementary data

Supplementary data to this article can be found online at https://doi.org/10.1016/j.biomaterials.2019.119516.

## References

[1] D. Pascolini, S.P. Mariotti, Global estimates of visual impairment: 2010, Br. J. Ophthalmol. 96 (2012) 614–618.
[2] M. Griffith, E.I. Alarcon, I. Brunette, Regenerative approaches for the cornea, J. Intern. Med. 280 (2016) 276–286.
[3] T. Nakamura, T. Inatomi, C. Sotozono, N. Koizumi, S. Kinoshita, Ocular surface reconstruction using stem cell and tissue engineering, Prog. Retin. Eye Res. 51 (2016) 187–207.
[4] G. Pellegrini, C.E. Traverso, A.T. Franzi, M. Zingirian, R. Cancedda, M. De Luca, Long-term restoration of damaged corneal surfaces with autologous cultivated corneal epithelium, Lancet 349 (1997) 990–993.
[5] S. Kolli, S. Ahmad, M. Lako, F. Figueiredo, Successful clinical implementation of corneal epithelial stem cell therapy for treatment of unilateral limbal stem cell deficiency, Stem Cells 28 (2010) 597–610.
[6] G.K. Vemuganti, S. Kashyap, V.S. Sangwan, S. Singh, Ex-vivo potential of cadaveric and fresh limbal tissues to regenerate cultured epithelium, Indian J. Ophthalmol. 52 (2004) 113.
[7] A. Mikhailova, T. Ilmarinen, H. Uusitalo, H. Skottman, Small-molecule induction promotes corneal epithelial cell differentiation from human induced pluripotent

stem cells, Stem Cell Rep. 2 (2014) 219–231.
[8] A. Mikhailova, T. Ilmarinen, A. Ratnayake, G. Petrovski, H. Uusitalo, H. Skottman, et al., Human pluripotent stem cell-derived limbal epithelial stem cells on bioengineered matrices for corneal reconstruction, Exp. Eye Res. 146 (2016) 26–34.
[9] H. Miyashita, H. Niwano, S. Yoshida, S. Hatou, E. Inagaki, K. Tsubota, et al., Long-term homeostasis and wound healing in an in vitro epithelial stem cell niche model, Sci. Rep. 7 (2017) 43557 report.
[10] J. Yang, J.W. Park, D. Zheng, R. Xu, Universal corneal epithelial-like cells derived from human embryonic stem cells for cellularization of a corneal scaffold, Transl. Vis. Sci. Technol. 7 (2018) 23.
[11] Y. Du, D.S. Roh, M.L. Funderburgh, M.M. Mann, K.G. Marra, J.P. Rubin, et al., Adipose-derived stem cells differentiate to keratocytes in vitro, Mol. Vis. 16 (2010) 2680–2689.
[12] L. Zhang, V.J. Coulson-Thomas, T.G. Ferreira, W.W.Y. Kao, Mesenchymal stem cells for treating ocular surface diseases, BMC Ophthalmol. 15 (2015) 155.
[13] S. Zhang, L. Espandar, K.M. Imhof, B.A. Bunnell, Differentiation of human adipose-derived stem cells along the keratocyte lineage, J. Clin. Exp. Ophthalmol. 4 (2013) 11435.
[14] F. Arnalich-Montiel, S. Pastor, A. Blazquez-Martinez, J. Fernandez-Delgado, M. Nistal, Alio del Barrio, L. Jorge, et al., Adipose-derived stem cells are a source for cell therapy of the corneal stroma, Stem Cells 26 (2008) 570–579.
[15] Alió del Barrio, L. Jorge, M. El Zarif, M.P. de Miguel, A. Azaar, N. Makdissy, W. Harb, et al., Cellular therapy with human autologous adipose-derived adult stem cells for advanced keratoconus, Cornea 36 (2017) 952–960.
[16] A. Sorkio, L. Koch, L. Koivusalo, A. Deiwick, S. Miettinen, B. Chichkov, et al., Human stem cell based corneal tissue mimicking structures using laser-assisted 3D bioprinting and functional bioinks, Biomaterials 171 (2018) 57–71.
[17] L.J. Bray, K.A. George, S. Suzuki, T.V. Chirila, D.G. Harkin, Fabrication of a corneal-limbal tissue substitute using silk fibroin, in: B. Wright, C. Connon (Eds.), Corneal Regenerative Medicine, Springer, 2013, pp. 165–178.
[18] M. González-Andrades, R. Mata, M. del Carmen González-Gallardo, S. Medialdea, S. Arias-Santiago, J. Martínez-Atienza, et al., A study protocol for a multicentre randomised clinical trial evaluating the safety and feasibility of a bioengineered human allogeneic nanostructured anterior cornea in patients with advanced corneal trophic ulcers refractory to conventional treatment, BMJ open 7 (2017) e016487.
[19] O.P. Oommen, S. Wang, M. Kisiel, M. Sloff, J. Hilborn, O.P. Varghese, Smart design of stable extracellular matrix mimetic hydrogel: synthesis, characterization, and in vitro and in vivo evaluation for tissue engineering, Adv. Funct. Mater. 23 (2013) 1273–1280.
[20] L. Koivusalo, J. Karvinen, E. Sorsa, I. Jönkkäri, J. Väliaho, P. Kallio, et al., Hydrazone crosslinked hyaluronan-based hydrogels for therapeutic delivery of adipose stem cells to treat corneal defects, Mater. Sci. Eng. C 85 (2018) 68.
[21] E. Martínez-Sanz, D.A. Ossipov, J. Hilborn, S. Larsson, K.B. Jonsson, O.P. Varghese, Bone reservoir: injectable hyaluronic acid hydrogel for minimal invasive bone augmentation, J. Control. Release 152 (2011) 232–240.
[22] D.A. Ossipov, S. Piskounova, O.P. Varghese, J. Hilborn, Functionalization of hyaluronic acid with chemoselective groups via a disulfide-based protection strategy for in situ formation of mechanically stable hydrogels, Biomacromolecules 11 (2010) 2247–2254.
[23] T.F. Gesteira, M. Sun, Y.M. Coulson-Thomas, Y. Yamaguchi, L. Yeh, V. Hascall, et al., Hyaluronan rich microenvironment in the limbal stem cell niche regulates limbal stem cell differentiation, Investig. Ophthalmol. Vis. Sci. 58 (2017) 4407–4421.
[24] J.A. Gomes, R. Amankwah, A. Powell-Richards, H.S. Dua, Sodium hyaluronate (hyaluronic acid) promotes migration of human corneal epithelial cells in vitro, Br. J. Ophthalmol. 88 (2004) 821–825.
[25] C. Fiorica, R.A. Senior, G. Pitarresi, F.S. Palumbo, G. Giammona, P. Deshpande, et al., Biocompatible hydrogels based on hyaluronic acid cross-linked with a polyaspartamide derivative as delivery systems for epithelial limbal cells, Int. J. Pharm. 414 (2011) 104–111.
[26] L. Espandar, B. Bunnell, G.Y. Wang, P. Gregory, C. McBride, M. Moshirfar, Adipose-derived stem cells on hyaluronic acid–derived scaffold: a new horizon in bioengineered cornea, Arch. Ophthalmol. 130 (2012) 202–208.
[27] P.J.M. Bouten, M. Zonjee, J. Bender, S.T.K. Yauw, H. van Goor, Hest van, C.M. Jan, et al., The chemistry of tissue adhesive materials, Prog. Polym. Sci. 39 (2014) 1375–1405.
[28] J. Shin, J.S. Lee, C. Lee, H. Park, K. Yang, Y. Jin, et al., Tissue adhesive catechol-modified hyaluronic acid hydrogel for effective, minimally invasive cell therapy, Adv. Funct. Mater. 25 (2015) 3814–3824.
[29] C.E. Brubaker, H. Kissler, L. Wang, D.B. Kaufman, P.B. Messersmith, Biological performance of mussel-inspired adhesive in extrahepatic islet transplantation, Biomaterials 31 (2010) 420–427.
[30] Y. Lee, H.J. Chung, S. Yeo, C. Ahn, H. Lee, P.B. Messersmith, et al., Thermo-sensitive, injectable, and tissue adhesive sol–gel transition hyaluronic acid/pluronic composite hydrogels prepared from bio-inspired catechol-thiol reaction, Soft Matter 6 (2010) 977–983.
[31] Y. Chan Choi, J.S. Choi, Y.J. Jung, Y.W. Cho, Human gelatin tissue-adhesive hydrogels prepared by enzyme-mediated biosynthesis of DOPA and Fe3+ion cross-linking, J. Mater. Chem. B 2 (2014) 201–209.
[32] F. Scognamiglio, A. Travan, M. Borgogna, I. Donati, E. Marsich, J.W.A.M. Bosmans, et al., Enhanced bioadhesivity of dopamine-functionalized polysaccharidic membranes for general surgery applications, Acta Biomater. 44 (2016) 232–242.
[33] L. Figueira, C. Ferreira, C. Janeiro, P. Serrao, F. Falcao-Reis, D. Moura, Concentration gradient of noradrenaline from the periphery to the centre of the cornea - a clue to its origin, Exp. Eye Res. 168 (2018) 107–114.
[34] O.P. Varghese, M. Kisiel, E. Martínez-Sanz, D.A. Ossipov, J. Hilborn, Synthesis of guanidinium-modified hyaluronic Acid hydrogel, Macromol. Rapid Commun. 31 (2010) 1175–1180.
[35] S. Wang, O.P. Oommen, H. Yan, O.P. Varghese, Mild and efficient strategy for site-selective aldehyde modification of glycosaminoglycans: tailoring hydrogels with tunable release of growth factor, Biomacromolecules 14 (2013) 2427–2432.
[36] J.M. Gimble, F. Guilak, Adipose-derived adult stem cells: isolation, characterization, and differentiation potential, Cytotherapy 5 (2003) 362–369.
[37] B. Lindroos, S. Boucher, L. Chase, H. Kuokkanen, H. Huhtala, R. Haataja, et al., Serum-free, xeno-free culture media maintain the proliferation rate and multipotentiality of adipose stem cells in vitro, Cytotherapy 11 (2009) 958–972.
[38] H. Hongisto, T. Ilmarinen, M. Vattulainen, A. Mikhailova, H. Skottman, Xeno- and feeder-free differentiation of human pluripotent stem cells to two distinct ocular epithelial cell types using simple modifications of one method, Stem Cell Res. Ther. 8 (2017) 291.
[39] Heli Skottman, Derivation and characterization of three new human embryonic stem cell lines in Finland, Vitro Cell Dev Biol : Anim, vol. 46, 2010, pp. 206–209.
[40] A.P. Lynch, M. Ahearne, Retinoic acid enhances the differentiation of adipose-derived stem cells to keratocytes in vitro, Transl. Vis. Sci. Technol. 6 (2017) 6.
[41] P.B. Welzel, S. Prokoph, A. Zieris, M. Grimmer, S. Zschoche, U. Freudenberg, et al., Modulating biofunctional starPEG heparin hydrogels by varying size and ratio of the constituents, Polymers 3 (2011) 602–620.
[42] S.J. Petsche, D. Chernyak, J. Martiz, M.E. Levenston, P.M. Pinsky, Depth-dependent transverse shear properties of the human corneal stroma, Investig. Ophthalmol. Vis. Sci. 53 (2012) 873–880.
[43] P. Fagerholm, N.S. Lagali, J.A. Ong, K. Merrett, W.B. Jackson, J.W. Polarek, et al., Stable corneal regeneration four years after implantation of a cell-free recombinant human collagen scaffold, Biomaterials 35 (2014) 2420–2427.
[44] S.M. Lam, L. Tong, X. Duan, A. Petznick, M.R. Wenk, G. Shui, Extensive characterization of human tear fluid collected using different techniques unravels the presence of novel lipid amphiphiles, J. Lipid Res. 55 (2014) 289–298.
[45] S.L. Wilson, I. Wimpenny, M. Ahearne, S. Rauz, A.J. El Haj, Y. Yang, Chemical and topographical effects on cell differentiation and matrix elasticity in a corneal stromal layer model, Adv. Funct. Mater. 22 (2012) 3641–3649.
[46] D. Wang, S. Varghese, B. Sharma, I. Strehin, S. Fermanian, J. Gorham, et al., Multifunctional chondroitin sulphate for cartilage tissue–biomaterial integration, Nat. Mater. 6 (2007) 385.
[47] O.P. Oommen, J. Garousi, M. Sloff, O.P. Varghese, Tailored doxorubicin-H yaluronan conjugate as a potent anticancer glyco-D rug: an alternative to prodrug approach, Macromol. Biosci. 14 (2014) 327–333.
[48] K.M. Meek, C. Knupp, Corneal structure and transparency, Prog. Retin. Eye Res. 49 (2015) 1–16.
[49] Y. Liu, K. Ai, L. Lu, Polydopamine and its derivative materials: synthesis and promising applications in energy, environmental, and biomedical fields, Chem. Rev. 114 (2014) 5057–5115.
[50] Silvia A. Ferreira, Meghna S. Motwani, Peter A. Faull, Alexis J. Seymour, Tracy T.L. Yu, Marjan Enayati, et al., Bi-directional cell-pericellular matrix interactions direct stem cell fate, Nat. Commun. 9 (2018) 1–12.
[51] C. Loebel, R.L. Mauck, J.A. Burdick, Local nascent protein deposition and remodelling guide mesenchymal stromal cell mechanosensing and fate in three-dimensional hydrogels, Nat. Mater. 1 (2019).
[52] K. Merrett, C.M. Griffith, Y. Deslandes, G. Pleizier, H. Sheardown, Adhesion of corneal epithelial cells to cell adhesion peptide modified pHEMA surfaces, J. Biomater. Sci. Polym. Ed. 12 (2001) 647–671.
[53] D. Bermejo-Velasco, G.N. Nawale, O.P. Oommen, J. Hilborn, O.P. Varghese, Thiazolidine chemistry revisited: a fast, efficient and stable click-type reaction at physiological pH, Chem. Commun. 54 (2018) 12507–12510.

# Supplementary Information

## Tissue Adhesive Hyaluronic Acid Hydrogels for Sutureless Stem Cell Delivery and Regeneration of Corneal Epithelium and Stroma

Laura Koivusalo, Maija Kauppila, Sumanta Samanta, Vijay Singh Parihar, Tanja Ilmarinen

Susanna Miettinen, Oommen P. Oommen, Heli Skottman

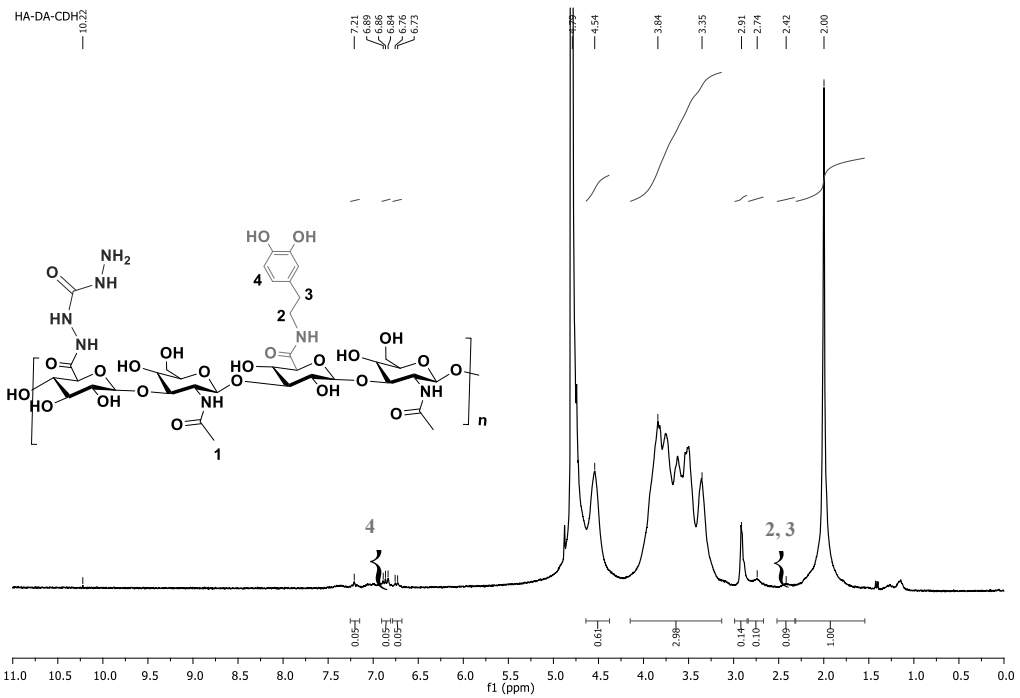


**Figure S1. $^{1}$H NMR spectrum of HA-DOPA-CDH in $D_2O$.**

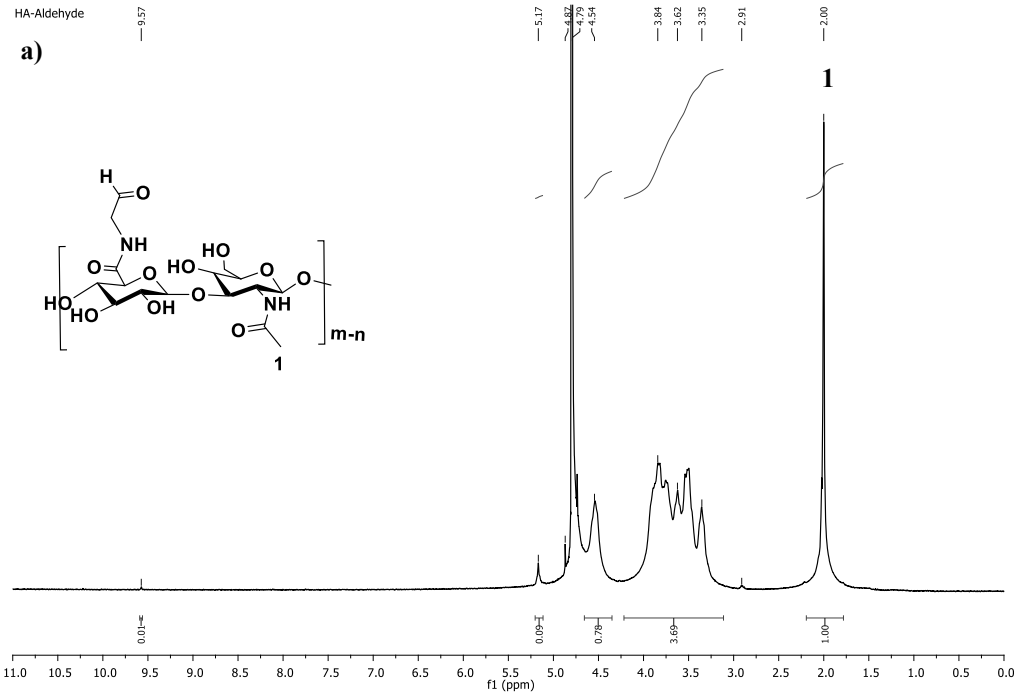
HA-Aldehyde
a)
9.57
5.17
4.87
4.79
4.54
3.84
3.62
3.35
2.91
2.00
1
m-n
1
0.01
0.09
0.78
3.69
1.00
f1 (ppm)

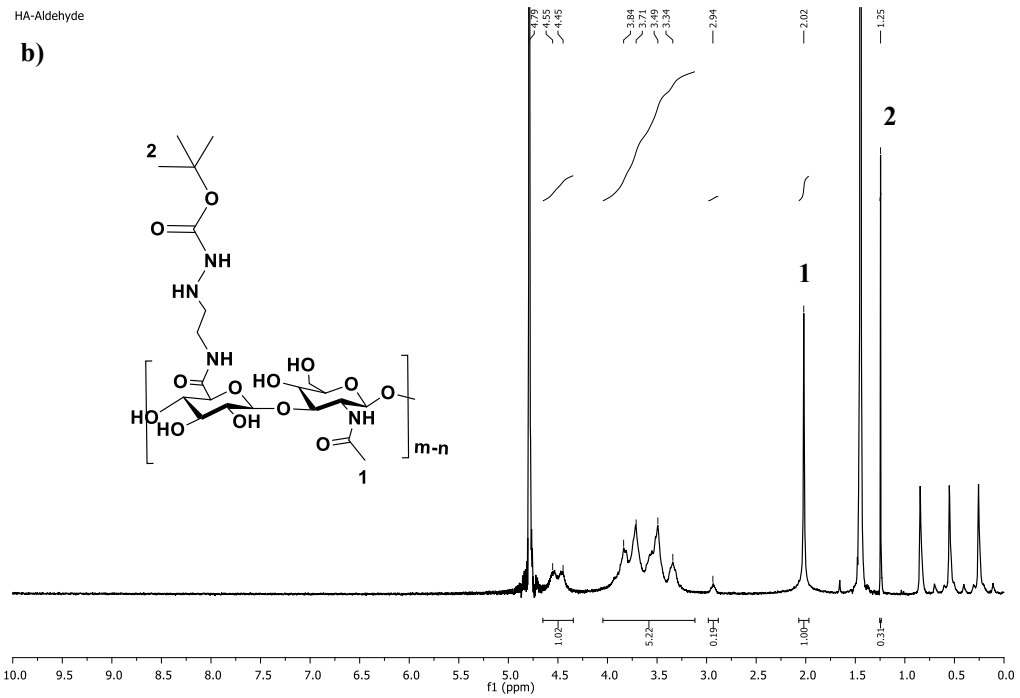
HA-Aldehyde
b)
4.79
4.55
4.45
3.84
3.71
3.49
3.34
2.94
2.02
1.25
2
1
m-n
1
1.02
5.22
0.19
1.00
0.31
f1 (ppm)

**Figure S2.** a) $^{1}H$ NMR spectrum of HA-Ald in $D_2O$ and b) HA- *t*-butyl carbazate derivative formed by the reaction of HA-Ald with *t*-butyl carbazate followed by $NaCNBH_3$ reduction in $D_2O$. The excess *t*-butyl carbazate appears at 1.48 ppm. The percentage of aldehyde functionalization was calculated by estimating the ratio of the *t*-butyl signal at 1.4 ppm and the *N*-acetyl signal at 2.0 ppm.

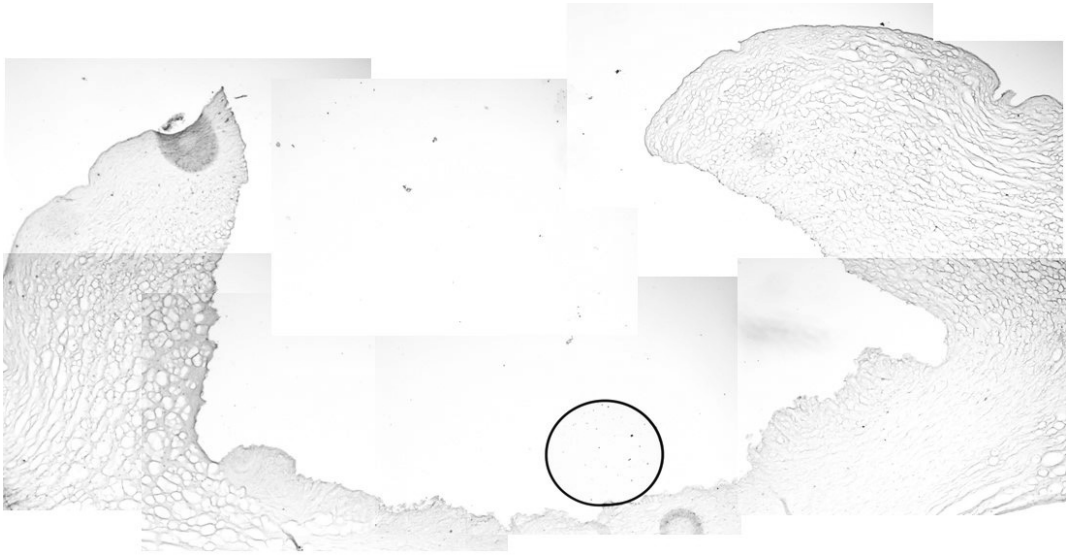

**Figure S3.** Ex vivo porcine cornea organ culture with extruded HA-HA implant after 7 days of culture showing no signs of tissue adhesion.

# PUBLICATION III

**Human stem cell based corneal tissue mimicking structures using laser-assisted bioprinting and functional bioinks**

Anni Sorkio, Lothar Koch, Laura Koivusalo, Andrea Deiwick, Susanna Miettinen, Boris Chichkov, Heli Skottman

Biomaterials, 2018, vol 171, 57-71.
https://doi.org/10.1016/j.biomaterials.2018.04.034

Biomaterials 171 (2018) 57–71

Contents lists available at ScienceDirect

Biomaterials

journal homepage: www.elsevier.com/locate/biomaterials

# Human stem cell based corneal tissue mimicking structures using laser-assisted 3D bioprinting and functional bioinks

Anni Sorkio [a, b], Lothar Koch [b], Laura Koivusalo [a], Andrea Deiwick [b], Susanna Miettinen [a, d], Boris Chichkov [b, c, 1], Heli Skottman [a, *, 1]

[a] BioMediTech Institute and Faculty of Medicine and Life Sciences, University of Tampere, Arvo Ylpön katu 34, FI-33520 Tampere, Finland
[b] Laser Zentrum Hannover e.V., Hollerithallee 8, 30419 Hannover, Germany
[c] Institute for Quantum Optics, Leibniz Universität Hannover, Welfengarten 1, 30167 Hannover, Germany
[d] Science Center, Tampere University Hospital, P.O. BOX 2000, FI-33521 Tampere, Finland

ARTICLE INFO

*Article history:*
Received 21 December 2017
Received in revised form
11 April 2018
Accepted 14 April 2018
Available online 16 April 2018

*Keywords:*
3D bioprinting
Laser-assisted bioprinting
Cornea
Human pluripotent stem cells
Limbal epithelial stem cells
Adipose stem cells
Human collagen I
Recombinant human laminin

ABSTRACT

There is a high demand for developing methods to produce more native-like 3D corneal structures. In the present study, we produced 3D cornea-mimicking tissues using human stem cells and laser-assisted bioprinting (LaBP). Human embryonic stem cell derived limbal epithelial stem cells (hESC-LESC) were used as a cell source for printing epithelium-mimicking structures, whereas human adipose tissue derived stem cells (hASCs) were used for constructing layered stroma-mimicking structures.

The development and optimization of functional bioinks was a crucial step towards successful bioprinting of 3D corneal structures. Recombinant human laminin and human sourced collagen I served as the bases for the functional bioinks. We used two previously established LaBP setups based on laser induced forward transfer, with different laser wavelengths and appropriate absorption layers. We bioprinted three types of corneal structures: stratified corneal epithelium using hESC-LESCs, lamellar corneal stroma using alternating acellular layers of bioink and layers with hASCs, and finally structures with both a stromal and epithelial part. The printed constructs were evaluated for their microstructure, cell viability and proliferation, and key protein expression (Ki67, p63α, p40, CK3, CK15, collagen type I, VWF). The 3D printed stromal constructs were also implanted into porcine corneal organ cultures.

Both cell types maintained good viability after printing. Laser-printed hESC-LESCs showed epithelial cell morphology, expression of Ki67 proliferation marker and co-expression of corneal progenitor markers p63α and p40. Importantly, the printed hESC-LESCs formed a stratified epithelium with apical expression of CK3 and basal expression of the progenitor markers. The structure of the 3D bioprinted stroma demonstrated that the hASCs had organized horizontally as in the native corneal stroma and showed positive labeling for collagen I. After 7 days in porcine organ cultures, the 3D bioprinted stromal structures attached to the host tissue with signs of hASCs migration from the printed structure. This is the first study to demonstrate the feasibility of 3D LaBP for corneal applications using human stem cells and successful fabrication of layered 3D bioprinted tissues mimicking the structure of the native corneal tissue.



## 1. Introduction

The cornea is the transparent anterior part of the eye, which is essential for vision. Corneal blindness due to trauma or diseases affects millions of people worldwide. In the most severe cases, the limbus, a niche for epithelium-renewing limbal epithelial stem cells (LESCs), is destroyed, resulting in limbal stem cell deficiency (LSCD) with overgrowth of the conjunctiva and blood vessels, severe pain and photophobia [1]. In these patients, the traditional corneal transplants from deceased donors have poor long-term success due to lack of epithelial renewal [2,3]. Delivery of *in vitro* expanded autologous LESCs to the corneal surface has been introduced as is a possible treatment for patients suffering from unilateral or partially bilateral LSCD [4,5]. Even more advanced

* Corresponding author.
*E-mail address:* heli.skottman@uta.fi (H. Skottman).
[1] Authors contributed equally.

https://doi.org/10.1016/j.biomaterials.2018.04.034

techniques are required to produce allogeneic LESCs or LESC-like equivalents for bilateral LSCD. Furthermore, the underlying corneal stroma is often damaged especially in cases of traumatic corneal blindness, and requires a replacement to restore visual function. Thus, there is an increased demand for developing methods to produce more native-like 3D corneal structures using human stem cells and functional biomaterials. Tissue engineering has sought to answer this ever-increasing demand by creating chemically defined cell and biomaterial based products to treat and cure corneal blindness.

Biomaterials for corneal stromal reconstruction are required to integrate with the host tissue, be functionally transparent and mechanically stable. For biologically functional corneal tissue equivalents, these materials require a cell density and 3D organization similar to that of the native cornea. Functional corneal stromal tissue has previously been fabricated by seeding human cells into decellularized porcine [6] or human cornea stromal tissue [7] or stimulating human cells to secrete their own extracellular matrix and produce corneal tissue equivalents [8]. However, use of decellularized tissue still lacks established methods for complete removal of antigenic moieties while maintaining proper tissue integrity [9], whereas the tissue equivalents secreted by human cells are slow to manufacture and limited to only thin or stacked constructs [10].

Corneal tissue in general is an optimal target for tissue engineering and 3D bioprinting technology due to its relatively low thickness [11] and lack of vascularization, which has limited the use of 3D printing technology in many other applications, such as bone, heart or skin tissue [12,13]. 3D bioprinting is a promising technique for fast production of thick corneal constructs, but previous work in the field has been conducted with immortalized corneal epithelial cells without any epithelial organization [14]. The applied nozzle-free laser-assisted bioprinting (LaBP) method allows high resolution printing of bioinks with high viscosity and high cell density without affecting the viability of the cells, while being capable of high printing resolution (<10 pL droplets) [15–17]. To reach high resolution with nozzle-based printing techniques, such as extrusion or ink jet printing, small nozzles (<100 μm diameter) are needed, which prevent the use of high cell density due to high shear stress to the cells. Furthermore, with LaBP, we can achieve precise spatial organization of cells and use different cell types in the same engineered structure. In any 3D bioprinting application, a suitable bioink is needed to produce shape-retaining multilayered corneal structures. For production of clinically relevant corneal structures, it is crucial to develop new functional bioinks based on xeno-free components, as well as suitable regenerative cell types.

Human pluripotent stem cells (hPSCs) can provide almost limitless amounts of LESC-like cells, with gene and protein expression similar to native LESCs [18,19]. With our recently established feeder-cell free hPSC culture and differentiation protocol [20], we have further brought our LESC differentiation towards a clinically relevant method for regeneration of the ocular surface. For reconstruction of the corneal stroma, human adipose tissue derived stem cells (hASCs) have gathered wide attention due to their high availability from healthy adult donors, as well as their capability to differentiate towards corneal keratocytes, which has been demonstrated in both *in vitro* [21–23] and *in vivo* [24,25] studies. Furthermore, autologous hASCs have already reached clinical pilots for treating corneal stromal disorders [26]. In addition, hASCs have excellent immunomodulatory properties, reducing inflammation at the site of implantation [27] as well as anti-scarring properties [28,29]. With these two different stem cell types, we can produce a tissue engineered corneal structure, which could simultaneously replace the damaged corneal stroma and regenerate the corneal epithelium.

In the present study, we produced 3D corneal mimicking tissues using human stem cells, functional bioinks and LaBP. Human embryonic stem cell (hESC) derived LESCs were the cell source for printing corneal epithelium-mimicking structures, whereas hASCs were the cellular component in lamellar corneal stromal tissues. We chose human sourced collagen I and recombinant human laminin as bases for the bioinks to develop clinically suitable techniques for corneal tissue engineering. Here, we demonstrate the feasibility of 3D LaBP for corneal applications and show successful fabrication of layered 3D bioprinted tissues from both investigated cell types that resemble the structure of the native corneal tissues.

## 2. Experimental methods

### 2.1. Bioinks

For hESC-LESCs, bioink containing human recombinant laminin-521 (LN521; Biolamina, Sweden) was chosen, as laminin is a major component in LESC basement membrane in the native cornea [30]. The hESC-LESC bioink consisted of 33% of 0.1 mg/ml LN521, 50% of defined and serum-free CnT-30 medium (CELLnTEC Advanced Cell Systems AG, Bern, Switzerland) supplemented with RevitaCell™ (100x) (Gibco, Life technologies) at a 1X final concentration, and 17% of 1 w/v% Hyaluronic acid sodium salt (HA) from *Streptococcus equi saline* ($M_w = 1.5–1.8 \times 10^6$ Da) (Sigma Aldrich, Deisenhofen, Germany) in Tris-buffered saline (TBS).

Human collagen I (Col I) was used as a base of the bioink for hASCs as it is the primary component of the human corneal stroma [31]. OptiCol™ Human Collagen Type I (3 mg/ml) (Cell Guidance Systems Ltd, Cambridge, UK) was neutralized to a pH of 7.4 with 0.25 N sodium hydroxide (NaOH) in the presence of 10X Dulbecco's Phosphate Buffered Saline (DPBS, Carl Roth, Karlsruhe, Germany). The bioink for hASCs included 44.4% of neutralized human Col I, 22.2% of ethylenediaminetetraacetic acid (EDTA) human female AB blood plasma, 22.2% of 40 IU/ml Thrombin from human plasma (Sigma Aldrich, Deisenhofen, Germany) in 0.1 M TBS and 11.1% of 10x DBPS. The human plasma was extracted with EDTA tubes, from blood collected from venipunctures and centrifuged at 4500 U/min for 30 min. Thereafter, human plasma was collected and sterile filtrated.

For 3D structures, acellular layers without hASCs were printed between hASCs in order to establish corneal stromal mimicking structures. There, a bioink with 40% of neutralized human Col I, 20% of human plasma, 20% of thrombin, 10% of 1 w/v% HA and 10% of 10x DBPS was used. The specific concentrations for the used reagents are listed above.

### 2.2. In vitro degradation

Degradation kinetics of the collagen-based hASC bioink in both cell culture medium and varying concentrations of collagenase were determined by weighing the gelled acellular bioink at different time points. For this purpose, the acellular bioink was prepared, as described in Section 2.1, by mixing bioink components to a total volume of 200 μl into 48-wells and allowed to gel for 2–3 h. The gels were then transferred to larger wells for degradation studies in either EBM-2 medium (Lonza, Basel, Switzerland) or in 0.1 M Tris-HCl buffer, pH 7.4, supplemented with 5 mM $CaCl_2$ and 0.005 (w/v) $NaN_3$, containing 0 U/ml, 5 U/ml, 50 U/ml, or 250 U/ml of collagenase (collagenase type I, CLS I, from *Clostridium histolyticum*; Biochrom, Berlin, Germany) and stored in an incubator at 37 °C. The initial weight of the gels was recorded and they were subsequently weighed at different time points up to 8 days (in medium) or 6 h (in collagenase), respectively. Degradation studies

were performed on four parallel samples at each condition.

### 2.3. Human embryonic stem cell derived limbal epithelial stem cells

Previously established hESC line Regea08/017 (XX) [32] was used for LESC differentiation as previously described [20]. In brief, undifferentiated hESCs were maintained on well-plates coated with 1.09 μg/cm$^2$ LN521 in Essential 8™ Flex Medium (E8, Thermo Fisher Scientific) supplemented with 50 U/ml Penicillin-Streptomycin (Gibco, Thermo Fisher Scientific). For LESC differentiation, hESCs were enzymatically detached and transferred to Corning® Costar® Ultra-Low attachment plates in XF-ko-SR medium (KnockOut™ DMEM supplemented with 15% KnockOut™ SR XenoFree CTS™ (XF-ko-SR), 2 mM GlutaMAX™, 0.1 mM 2-Mercaptoethanol, 1% MEM Non-Essential Amino Acids, and 50 U/ml Penicillin-Streptomycin (all from Gibco, Thermo Fisher Scientific)) supplemented with 5 μM blebbistatin (Sigma-Aldrich) overnight to induce embryoid body formation. The following day, the embryoid bodies were guided towards surface ectoderm with one day in XF-ko-SR medium supplemented with 10 μM SB-505124 and 50 ng/ml human basic fibroblast growth factor (PeproTech Inc., Rocky Hill, NJ) followed by two days in XF-ko-SR medium supplemented with 25 ng/ml bone morphogenetic protein 4 (PeproTech Inc.). Subsequently, the embryoid bodies were seeded onto 0.75 μg/cm$^2$ LN521 and 5 μg/cm$^2$ collagen IV coated well-plates in CnT-30 medium and cultured for 22–24 days. Finally, differentiated hESC-LESCs were cryopreserved in PSC Cryopreservation Medium (Thermo Fisher Scientific).

For printing, the cryopreserved hESC-LESCs were thawed onto 0.75 μg/cm$^2$ LN521 and 5 μg/cm$^2$ human collagen IV coated well plates in CnT-30 medium supplemented with RevitaCell™ (100X) (Gibco, Life technologies) at a 1X final concentration and cultured overnight. The following day, the medium was replaced with CnT-30, and hESC-LESCs were cultured for six to seven days before enzymatically detaching cells with TrypLE™ for printing. After 4 min incubation in TrypLE™, the enzyme was removed, and Defined Trypsin Inhibitor (DTI) (Thermo Fischer Scientific) was added to inactivate any remaining enzyme. Human ESC-LESCs were gently detached with a cell scraper in DTI and centrifuged. Subsequently, the supernatant was removed and cells counted in CnT-30 medium. Appropriate amount of cells was aliquoted in Eppendorf tubes, and centrifuged. The supernatant was removed, and hESC-LESCs were resuspended in LN521 containing bioink and used for LaBP with cell density of $30 \times 10^6$ cells/ml.

### 2.4. Human adipose derived stem cells

Human ASCs were isolated mechanically and enzymatically from subcutaneous adipose tissue samples of a female donor undergoing elective plastic surgery at Tampere University Hospital (Tampere, Finland) according to previously published protocols [33,34]. The isolated hASCs were characterized for their surface marker expression by flow cytometry (FACSAria; BD Biosciences, Erembodegem, Belgium) as previously described [34] (Supplementary Table S1).

The hASCs were cultured in EBM-2 Medium (Lonza, Basel, Switzerland) devoid of fetal bovine serum and supplemented with 2% human serum (type AB male, HIV tested from BioWest, Nuaillé, France Human). This medium was selected to maintain hASC in their undifferentiated state during *in vitro* culture. Human ASCs were passaged upon confluency using TrypLE™ and used for LaBP at passages 3–5. For printing, hASCs were enzymatically detached with TrypLE™, centrifuged and resuspended in culture medium for counting. Thereafter, hASCs were centrifuged in Eppendorf tubes, supernatant was removed and the cells were resuspended in human Col I based bioink with a cell density of $30 \times 10^6$ cells/ml for LaBP.

### 2.5. Laser-assisted bioprinting of human stem cells

Here, we used laser-assisted bioprinting (LaBP) based on laser induced forward transfer (LIFT). A detailed description of the LaBP setup has been previously published [15]. In brief, the setup consists of a pulsed laser source and two horizontal co-planar glass slides ($26 \times 26$ mm$^2$). The upper one, referred to as donor slide, is coated with a thin laser-absorbing layer (two different laser absorbing materials were used in this study) and, subsequently, with a thicker layer of the bioink to be printed. This bioink is usually a sol (the non-gelled precursor of a hydrogel) with embedded cells. The donor slide is mounted upside-down in the printing setup (Supplementary Fig. S1) and laser pulses are focused through the donor slide into the absorption layer, which is evaporated in the laser focus. An expanding vapor bubble is generated at the immobile donor slide surface that propels the subjacent biomaterial towards the second glass slide, referred to as collector slide, or an arbitrary object to print onto. Due to the collapsing of the vapor bubble after a few microseconds and inertia, the bioink forms a jet that lasts for a few hundred microseconds. This jet impinges on the collector slide and deposits as a small droplet in the picoliter volume range (a few ten to a few hundred microns in diameter) on the collector slide. By moving the laser focus, the donor and collector slides relative to each other, bioink droplets are positioned in specific patterns. Thus, 3D structures from the bioink can be produced by repeating this procedure layer-by-layer [35]. The deposition of the bioink is controlled via computerized scanning setup [15]. In this study, we used two laser-based printing systems with different laser wavelengths and appropriate absorption layer material. In the first setup, a Nd:YAG-laser (DIVA II; Thales Laser, Orsay, France) with 1064 nm wavelength, 10 ns pulse duration and 20 Hz repetition rate was combined with a 60 nm thin gold absorption layer. The second system applied an Er:YAG-laser (DPM-15, Pantec Engineering AG, Ruggell, Liechtenstein) with 2940 nm wavelength, 3 μs pulse duration, and up to 1 kHz repetition rate (500 Hz was used within this study); this wavelength fits into an absorption maximum of water making it optimal for hydrogel absorption layers. The first printing setup was applied for printing hESC-LESCs, and hASCs in both 2D and 3D structures, whereas the latter was used for constructing 3D cornea-mimicking structures with both cell types. The laser pulse energy was adjusted for both cell types under investigation. All printing experiments were carried out at room temperature (RT) under humid environment.

For hESC-LESC printing, an additional transparent polyethylene terephthalate (PET) film with 0.4 μm pores (Sarstedt, Nümbrecht, Germany) coated with 0.75 μg/cm$^2$ LN521 and 5 μg/cm$^2$ human Collagen IV (Col IV) was placed on the collector glass slide. 50 μl of laminin-containing bioink with hESC-LESCs was spread on the donor layer, resulting in approximate layer thickness of 74 μm. 7 mm × 7 mm samples were printed with a speed of 5000 μm/s. Three layers of hESC-LESCs were printed on top of each other, using laser pulse energy of 18 μJ. The samples were allowed to stabilize at +37 °C for 30 min before adding CnT-30 medium supplemented with 1X RevitaCell™. The following day, the medium was replaced with fresh CnT-30 medium without RevitaCell™. The printed hESC-LESCs were cultured for up to 12 days and the culture medium was changed three times a week.

Human ASCs were printed in 2D patterns in order to evaluate the viability of the cells after LaBP. Collector slides were coated with Corning® Matrigel® Basement Membrane Matrix (Fisher Scientific GmbH, Schwerte, Germany). The Matrigel® was diluted in 2:1 ratio in EBM-2 cell culture medium. 75 μl of diluted Matrigel® was

spread on the collector-slides, and allowed to gel for 10 min at +37 °C. 45 μl of the human Col I containing bioink with hASCs was spread on the donor slide resulting in approximate layer thickness of 67 μm. First, hASCs were printed in lines (with 500 μm spacing), or in spots (with 400 μm spacing) with the speed of 2000 μm/s and laser pulse energy of 20 μJ. The printed samples were allowed to stabilize for 10 min at +37 °C before submerging them in cell culture medium.

For creating 3D corneal stromal mimicking structures, alternating layers of hASCs and acellular layers 7 mm × 7 mm in size were printed with a speed of 5000 μm/s. Laser pulse energy of 20 μJ was used for hASC-containing bioink, while acellular layers were printed with higher laser pulse energy of 25 μJ. 45 μl of the hASC-containing bioink was applied on the donor slide resulting in approximate layer thickness of 67 μm, and 65 μl of the acellular bioink yielded a 96 μm thin layer on the donor slide. Two consecutive layers of hASC-containing bioink were laser-printed, followed by four acellular layers. All cell-containing layers in the 3D bioprinted stromal structures were printed in the same orientation. In total, 10 alternating layers of hASCs and acellular bioink were printed in layer-by-layer manner to create a thick 3D structure, as illustrated in Fig. 1. In total, the 3D laser-printed stromal mimicking structures consisted of 60 printed layers. The 3D stromal mimicking structures were printed on a stabilizing matrix, Matriderm® (Dr. Suwelack Skin & Health Care, Billerbeck, Germany). Matriderm® sheets are nontransparent collagen-elastin matrixes with 1 mm thickness. Matriderm® sheets have been previously used as a stabilizing matrix for Col-based bioinks and hASCs in skin applications [15]. The structures were allowed to stabilize at +37 °C in humid environment for 1 h before submerging them in the EBM-2 culture medium. Thereafter, the printed stromal structures were cultured for 14 days and fresh medium was changed three times a week.

Finally, we combined the two cell types to establish a proof-of-concept for 3D bioprinting human corneal mimicking structures from human stem cells. For this, the second bioprinting system based on LaBP was used in combination with a laser absorption layer composed of 18 μl Matrigel® and 2 μl glycerol, blade coated on a glass donor slide. Matrigel® was chosen, since Matrigel® gels relatively quickly at +37 °C, possess a hydrophilic surface and is biocompatible, while glycerol avoids fast drying of the layer before the bioink is applied on top. The applied human Col I-based bioink gelates very slowly and is thus not optimal as laser absorption layer. The concentration of Matrigel® in the final printed construct was approximately 0.4 μl/cm$^2$. On top of the absorption layer, 50 μl of bioink with suspended cells was spread (for printing, the donor slide was turned upside-down). Laser pulse energies of 150 μJ were applied, which are not directly comparable to those of the first bioprinting setup due to the different wavelength, laser pulse duration, and absorption material. Again, 7 × 7 mm$^2$ samples were printed, here with a speed of 7000 μm/s and 100 μm line spacing. The same cell densities and bioinks described above were used for both hESC-LESCs and hASCs. The 3D corneal mimicking structures were allowed to stabilize at +37 °C for 1 h before submerging them in culture medium. For these samples, a medium consisting of 1:1 ratio of CnT-30 with 1X RevitaCell™ and EBM-2 with 2% HS was used. Both PET and Matriderm® sheets were used as stabilizing substrates. The next day, same medium without RevitaCell™ was changed, and the structures were cultured for up to 3 days.

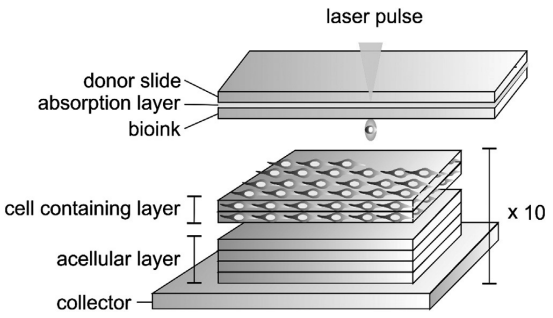


**Fig. 1.** Schematic diagram of the laser-assisted bioprinting system and printing of the 3D stromal mimicking structures. Stromal mimics comprised 10 alternating layers of hASCs and acellular bioink, with each individual cell-containing layer consisting of two layers of hASCs and the acellular layer consisting of four printed layers.

### 2.6. Cell viability

Cell viability and proliferation of both hESC-LESCs and hASCs after LaBP were assessed with two commercially available assays – LIVE/DEAD® Viability/Cytotoxicity Kit for mammalian cells and PrestoBlue™ cell viability reagent (both from Thermo Fischer Scientific), according to manufacturer's instructions. The hESC-LESC viability with LIVE/DEAD® kit was determined after 3 and 7 days of printing, whereas cell viability of hASCs was analyzed the following day. PrestoBlue™ viability assay was performed at days 1 and 7 for hESC-LESCs, at days 1 and 4 for hASCs printed in 2D patterns, and at days 1, 4 and 7 for hASCs printed in 3D stromal mimicking structures. For hESC-LESCs, eight samples with four technical replicates were analyzed in each time point. For hASCs printed in 2D patterns, in total 20 samples with four technical replicates were analyzed in both time points. Finally, four to six 3D bioprinted stromas with hASCs with four technical replicates were included in cell proliferation analysis at each time point. Moreover, cell morphology was inspected daily with phase contrast microscope.

### 2.7. Indirect immunofluorescence staining

The cell migration, cell morphology, expression of cell specific markers and tissue structure after LaBP were investigated with immunofluorescence (IF) stainings. For hESC-LESCs and hASCs printed in 2D patterns, the IF staining was done as previously described [36]. Primary antibodies rabbit anti-Ki67 1:200 (Millipore), rabbit anti-p63α 1:200 (Cell Signaling Tech), mouse anti-p40 1:200 (Biocare Medical), mouse anti-CK3 1:200 (Abcam) and mouse anti-CK15 (Thermo Fischer Scientific) were investigated for hESC-LESCs. Primary antibody detection was done with Alexa-Fluor conjugated 488 donkey anti-mouse IgG, 488 donkey anti-rabbit IgG and 568 donkey anti-rabbit IgG (all from Molecular Probes, Life Technologies). All secondary antibodies were diluted 1:400. Phalloidin-Atto 550 1:100 (Sigma Aldrich) was used for visualizing the filamentous actin cytoskeleton of the cells and mounting medium containing 4′,6-diamidino-2-phenylindole (DAPI; Vecta-Shield, Vector Laboratories Inc., Burlingame, CA) was used for staining the nuclei.

The 3D bioprinted structures as well as human corneal samples were rinsed twice with DPBS, and fixed in 4% PFA for 1 h at RT. Subsequently, the 3D samples were rinsed with PBS and incubated in 20% sucrose solution overnight at +4 °C. The next day, the samples were embedded in Tissue-Tek OCT (Science Services, Munich, Germany) and snap frozen at −80 °C. For IF and other histological stainings, cryosections of 7 μm were prepared and air dried for 1 h at RT. Thereafter, the cryosections were incubated in 3% BSA-PBS and 0.1% Triton-X-100 for 1.5 h at +37 °C. Primary antibody dilutions were prepared in 3% BSA-PBS and incubated overnight at +4 °C under humid conditions: rabbit anti-Ki67 1:200

(Millipore), mouse anti-collagen type I 1:200 (Abcam), rabbit anti-von Willebrand Factor (VWF) 1:200 (Dako Cytomation) and mouse anti-p40 1:200 were used. Primary antibody detection was done with the same secondary antibodies as described above 1:400 in 3% BSA-DPBS for 1.5 h at +37 °C. In addition, filamentous actin was stained with Phalloidin Tetramethylrhodamine B isothiocyanate 1:400 (Sigma Aldrich). Finally, the samples were thoroughly washed with PBS and mounted with ProLong™ Gold Antifade Mountant (Thermo Fischer Scientific) with DAPI to stain the nuclei.

The IF samples were imaged with AxioScope A1 fluorescence microscope (Carl Zeiss) or LSM 700 confocal microscope (Carl Zeiss, Jena, Germany) and images edited using ZEN 2011 Light Edition (Carl Zeiss) and Corel® Photo-Paint X8.

### 2.8. Hematoxylin and eosin staining

Hematoxylin and eosin (HE) staining was carried out for sections from the 3D bioprinted structures as well as corneal samples. HE staining was carried out following standard procedures for cryosections and paraffin embedded sections, and observed under a Nikon Eclipse TE200S microscope (Nikon Instruments Europe B.V., Amstelveen, Netherlands).

### 2.9. Corneal organ cultures

The corneal organ culture using excised porcine corneas was conducted as previously described [37–39]. Briefly, fresh porcine eyes were stripped of excess tissue and disinfected with 2% povidone iodine (Betadine®, Leiras, Helsinki, Finland), and the corneas were dissected from the eyes in aseptic conditions. The corneas were cultured partially submerged in CnT-Prime-CC medium (CELLnTECH Advanced Cell Systems AG) supplemented with 1% Penicillin-Streptomycin, 0.25 μg/ml amphotericin B (Thermo Fisher Scientific) and 5 μg/ml Plasmocin (InvivoGen, Toulouse, France) at +37 °C in 5% $CO_2$ for two weeks prior to implantation of the 3D bioprinted stromal constructs.

Two-day-old 3D printed stromal structures on the Matriderm® substrate were shipped from Germany to Finland overnight at +37 °C in EBM-2 medium containing 20 mM HEPES, and implanted into the corneal organ cultures 4 days after printing. Implantation was performed on a Barron artificial anterior chamber (Katena products Inc., Denville, NJ, USA), to allow handling of the cornea during the operation. Corneal epithelium was scraped off using a scalpel (Feather Safety Razor co., ltd, Osaka, Japan), and a 5 mm trephine (Robbins Instruments, Chatham, NJ, USA) was used to make a partial thickness cut to the center of the cornea. The stromal tissue was removed from the trephined area using a crescent knife (Bauch&Lomb Inc., Rochester, NY, USA). The trephine was also used to punch out a 5 mm diameter piece from the 3D printed stromal construct, which was placed into the stromal wound bed with the bioprinted stromal side facing downwards. Matriderm® substrate alone and acellular bulk-formed bioink gels were implanted as negative controls. Although constructs did not withstand suturing in place, it was deemed unnecessary due to the static culture conditions and the fitted trephination of the implant and the wound site. After implantation, the corneas were moved from the artificial anterior chamber back into culture plates, covered with soft contact lenses (EyeQ One-Day Premium, Cooper Vision, Hamble, UK), and cultured partially submerged in EBM-2 medium with 2% HS for 7 days, at +37 °C in 5% $CO_2$.

One week after implantation, the corneal organ cultures were fixed in 4% PFA for 4 h at RT, dehydrated in Tissue-Tek VIP 5 (Sakura Finetek Europe) automatic tissue processor overnight, and embedded in paraffin. The paraffin blocks were sectioned into 6-μm-thick slices using a microtome, and the sections were mounted on TOMO® adhesion microscope slides (Matsunami Glass Ind., Ltd., Osaka, Japan).

### 2.10. Immunohistochemical staining

The corneal organ cultures containing 3D bioprinted stromal constructs and their Matriderm® controls, were analyzed using immunohistochemical staining against the human cell marker TRA-1-85 to detect hASCs in the samples. The staining was performed similarly as in Ref. [40], with slight modifications. Briefly, samples were deparaffinized and hydrated, followed by antigen retrieval in hot 0.01 M citrate buffer (pH 6.0) for 10 min. Tissue intrinsic peroxide activity was blocked by incubation in 0.3% H2O2 for 30 min at RT. Ready-to-use 2.5% normal horse serum (Vector ImmPress reagent, Vector Laboratories Inc.) was used to block unspecific binding. Samples were then labeled with anti-TRA-1-85 mouse IgG antibody (courtesy of Peter Andrews, University of Sheffield) in a 1:100 (v/v) dilution in 0.5% BSA overnight at +4 °C, and labeled with Vector ImmPress horse anti-mouse IgG (containing horseradish peroxidase) (Vector Laboratories Inc.) for 30 min at RT. Staining was visualized by peroxidation reaction with DAB+ chromogen system (Dako North America, Inc., Carpinteria, CA, USA), which was performed for 30 s at RT. The tissue was counterstained using Harris' hematoxylin, followed by dehydration, and mounting using Pertex (Histolab, Askim, Sweden). Samples were imaged using Nikon Eclipse TE200S microscope.

### 2.11. Statistical analysis

The statistical significance of PrestoBlue™ cell proliferation data was determined with Mann–Whitney *U* test. The mean values of cell proliferation data for all printed tissues are presented ±standard error. *p*-values $\leq 0.05$ were considered statistically significant. The statistical data analysis was carried out with IBM SPSS Statistics software.

### 2.12. Ethical issues

This study was carried out under an approval from the local ethics committee of the Pirkanmaa hospital district Finland that allows us to derive and expand hESC lines from surplus embryos donated by couples undergoing infertility treatments, and to use these cell lines for research purposes (R05116). In addition, we have ethical approvals to extract and use hASC for research purposes (R15161) and to use human donor corneas unsuitable for transplantation for research purposes (R11134). New cell lines were not derived for this study.

## 3. Results

### 3.1. Laser-printed hESC-LESCs remain viable, express key markers and form mature 3D cornea-like tissue

Initially, laser-printed hESC-LESCs were spherical in morphology (Supplementary Fig. S2) but recovered their normal polygonal morphology during culture. The viability of hESC-LESCs was analyzed with LIVE/DEAD® after 1 and 7 days of printing. In both investigated time points, the laser-printed hESC-LESCs were viable in LN521 containing bioink, with only a few dead cells after 7 days of culture (Fig. 2A). In addition, laser-printed hESC-LESCs showed polygonal epithelial cell morphology at day 7 (Fig. 2B). Significantly higher cell proliferation ($p < 0.05$) was detected at day 7 after printing compared to cell proliferation at day 1 (Fig. 2C), as confirmed with PrestoBlue™ assay. To verify the cell phenotype and organization, IF staining was carried out at day 7. Phalloidin

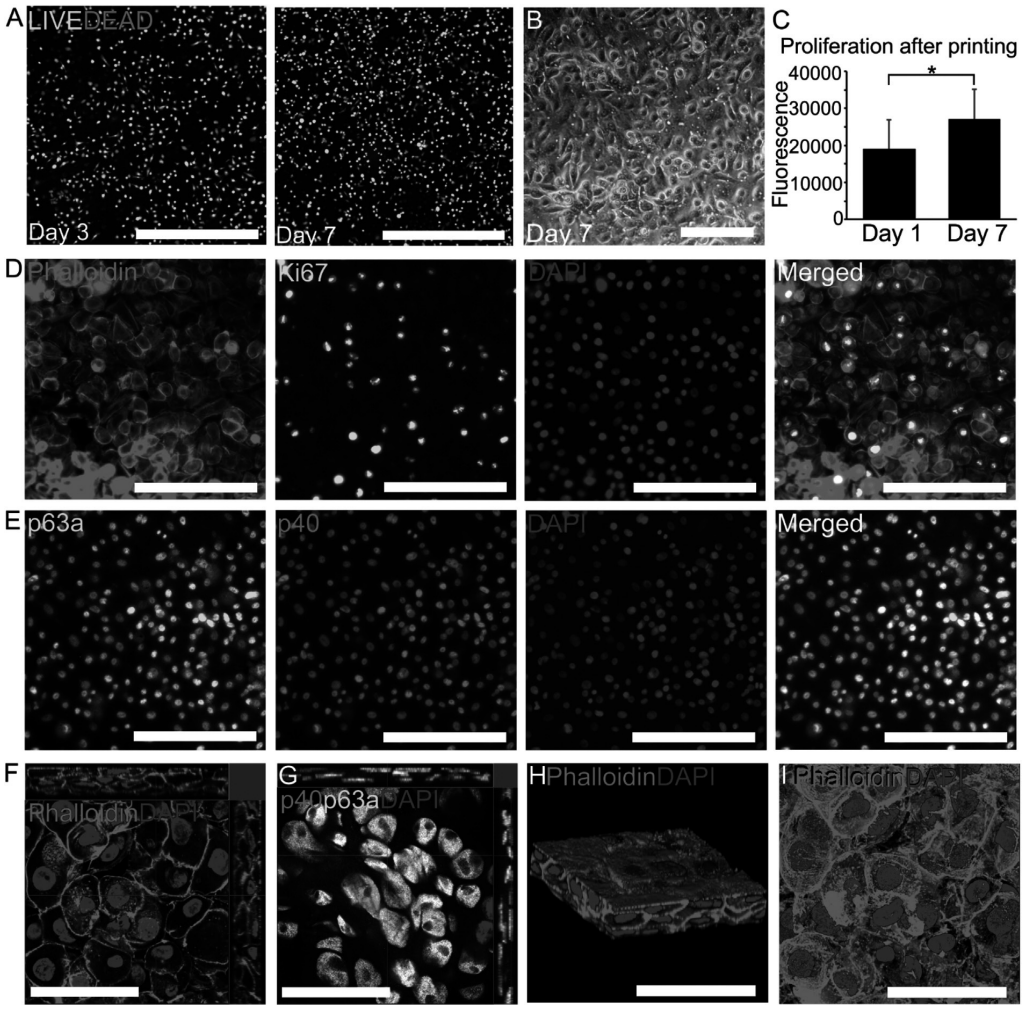


**Fig. 2.** 3D laser-assisted bioprinting of hESC-LESCs. Cell viability of hESC-LESCs three and seven days after printing shown with live-dead-staining (**A**). Live cells are visualized with green and dead cells with red. Scale bars 1 mm. Phase microscope image of printed hESC-LESCs (**B**). Scale bar 200 μm. Human ESC-LESC proliferation after printing (*$p < 0.01$) (**C**). Immunofluorescence staining of phalloidin (red) and Ki67 (green) illustrating hESC-LESC cell morphology and proliferating cells after seven days of printing (**D**). Protein expression of corneal epithelial progenitor markers p63α (green) and p40 (red) in 3D bioprinted hESC-LESCs at day seven (**E**). Representative vertical confocal image of layered hESC-LESCs (**F**). Localization of corneal progenitor markers p63α (green) and p40 (red) in layered hESC-LESCs (**G**). 3D rotated (**H**) and top view (**I**) transparency rendering mode confocal images of the layered hESC-LESCs. Scale bars 200 μm (**D-E**) and 50 μm (**F-I**). The nuclei are visualized with DAPI (blue). (For interpretation of the references to colour in this figure legend, the reader is referred to the Web version of this article.)

staining of the actin cytoskeleton confirmed the polygonal epithelial cell morphology of the printed cells seen in phase contrast microscopy (Fig. 2D). Moreover, the printed hESC-LESCs expressed the proliferation marker Ki67 (Fig. 2D) and co-expressed corneal progenitor markers p63α and p40 (Fig. 2E). Importantly, the printed layers of hESC-LESCs retained epithelium-like structure with 3–4 cell layers (Fig. 2F) and with p63α and p40 expressed throughout the layered epithelium (Fig. 2G). Finally, 3D confocal imaging of the day 7 IF samples demonstrated that the hESC-LESCs retained the 3D epithelial tissue after printing (Fig. 2H and I). Conversely, stratified epithelial tissue formation was not observed for non-bioprinted hESC-LESCs seeded in suspension on PET substrates after 7 days (Supplementary Fig. S3).

The 3D bioprinted hESC-LESCs were further cultured up to 12 days, and subsequently analyzed for maturation with IF. At this time point, the 3D bioprinted hESC-LESCs demonstrated epithelial cell morphology (Fig. 3A). Only a few of the printed cells expressed the proliferation marker Ki67 (Fig. 3A), but expression of corneal progenitor markers p63α, p40 and CK15 was strong (Fig. 3B and C). Epithelial cell morphology was also seen in phase contrast microscopy (Fig. 3D). Notably, hESC-LESCs showed maturation towards corneal epithelial cells, with expression of CK3, a marker for terminally differentiated corneal epithelium (Fig. 3E). After 12 days, the printed cells retained a stratified epithelium with four distinguishable cell layers (Fig. 3F–J). The stratified structure of the printed epithelium also demonstrated signs of further maturation

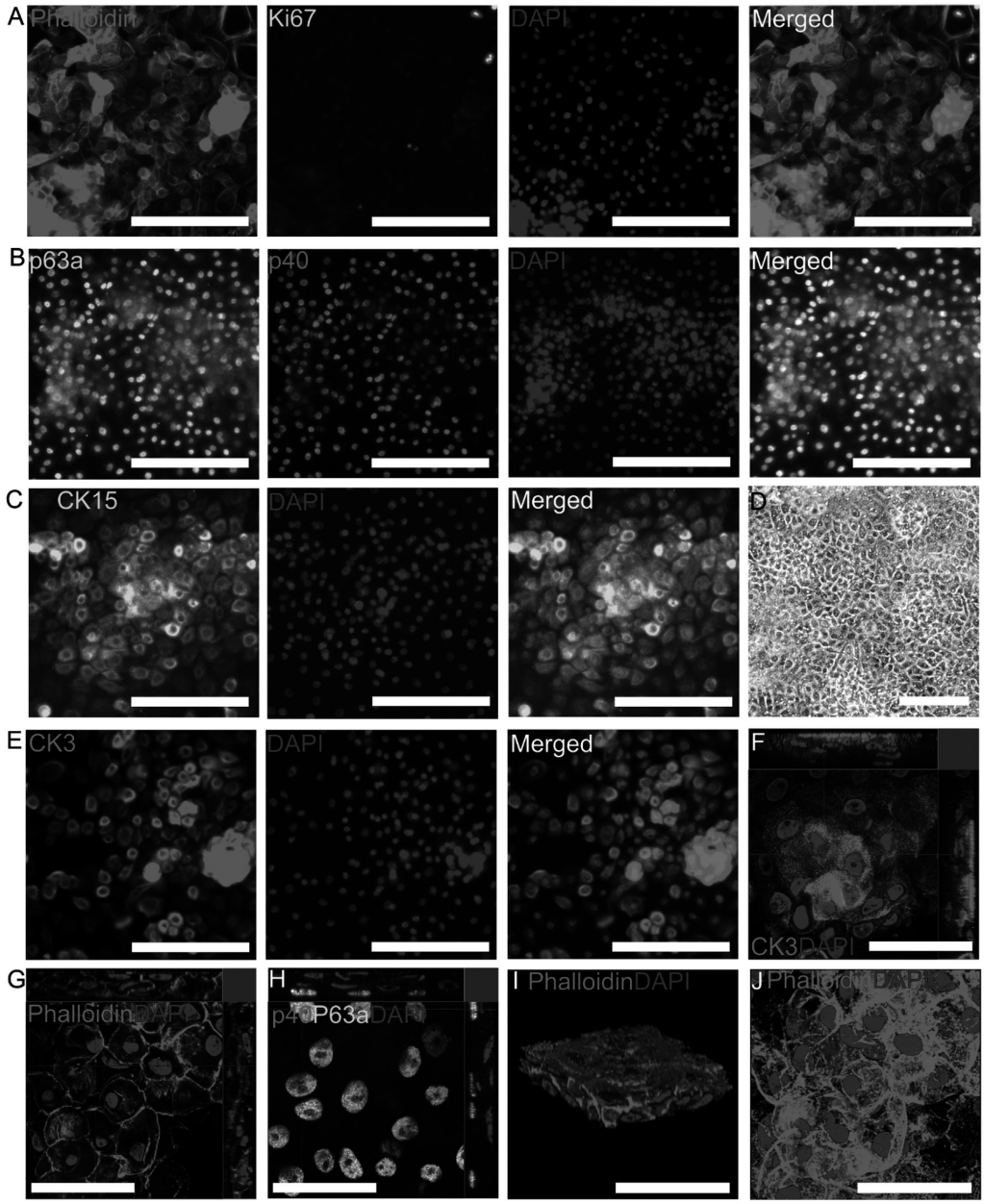


**Fig. 3.** The maturation of 3D bioprinted hESC-LESCs after 12 days demonstrated with immunofluorescence stainings. **A**. Cell morphology (phalloidin = red) and proliferating cells (Ki67 = green). Expression of corneal progenitor markers p63α (green), p40 (red) (**B**) and CK15 (green) (**C**). Phase microscope image of hESC-LESCs (**D**). Expression (**E**) and apical localization (**F**) of CK3 (red), a marker of terminally differentiated corneal epithelium. Representative vertical confocal sections of the layered hESC-LESCs (**G**) and the basal localization of the corneal progenitor markers p63α and p40 (**H**). 3D rotated (**I**) and top view (**J**) transparency rendering mode confocal images of the layered hESC-LESCs. Scale bars 200 μm (**A-E**) and 50 μm (**F-J**). (DAPI = blue). (For interpretation of the references to colour in this figure legend, the reader is referred to the Web version of this article.)

when analyzed with confocal microscopy, with apical expression of CK3 (Fig. 3F) and basal expression of p63α and p40 (Fig. 3H). The 3D confocal imaging confirmed the 3D epithelial tissue-like structure 12 days after printing (Fig. 3I and J).

### *3.2. hASCs in human Col I based bioink remain viable and proliferate after LaBP*

The biocompatibility of human Col I-containing bioink after

LaBP was first investigated by printing hASC in organized 2D patterns of aligned lines and spots. The human Col I containing bioink with hASCs demonstrated good printability and biocompatibility. The cells demonstrated excellent viability 1 day after printing: hardly any dead cells were detected in LIVE/DEAD® analysis of hASCs printed in lines (Fig. 4A) and spots (Fig. 4B). Cell viability was further confirmed with PrestoBlue™ and IF. The hASCs printed in line pattern showed significantly higher cell proliferation ($p < 0.001$) at day 4 compared to day 1. Both printed patterns were clearly visible on day 1 after printing, with elongated cells migrating from both patterns (Fig. 4D and E). By day 4, the initial printed patterns were not visible anymore, as the cells had proliferated and migrated extensively. However, hASCs printed in 2D lines clearly organized in a uniformly aligned fashion by day 4. Finally, hASCs printed in both patterns expressed cell proliferation marker Ki67 at both time points (Fig. 4D and E).

### 3.3. Laser-printed hASCs form organized corneal stromal mimicking structures

LaBP was used for fabricating thicker 3D stromal structures from hASCs and human Col I-containing bioink. Alternating layers of hASC-containing bioink and acellular bioink were printed to mimic the lamellar structure of the human corneal stroma, with each layer printed with the same orientation (Fig. 1). Initially, the 3D structures had an approximate thickness of 500 μm in a base area of 7 mm × 7 mm. The viability of the 3D printed structures was studied with PrestoBlue™ and LIVE/DEAD® staining. Human ASCs in 3D structures showed significantly higher cell proliferation ($p < 0.001$) after 4 and 7 days of culture compared to day 1 (Fig. 5A). Moreover, cell proliferation increased significantly ($p < 0.05$) between 4 and 7 days of culture. LIVE/DEAD® analysis of the 3D bioprinted structures demonstrated high cell viability after printing, with the majority of the cells viable throughout the structures (Fig. 5B and C). Only a few dead cells were detected when viewing the structures from the top (Fig. 5B), although slightly more dead cells were seen in the lower part of the structure when examining the cross-section (Fig. 5C). After 4 days of culture, Ki67 expressing cells were detected in IF analysis of the frozen sections (Fig. 5D), confirming the survival and viability of hASCs in 3D bioprinted structures. Without Matriderm® supportive sheets as a printing substrate, the printed structures showed extensive shrinkage and lost their printed form after a few days of culture.

The structure and cellular organization of the 3D bioprinted grafts were visualized from frozen sections with IF stainings (Fig. 5E–I) and compared to the structure of the native human corneal stroma (Fig. 5J and L). In all investigated time points, the hASCs had organized sparsely throughout the 3D structure. Moreover, some lamellar structures had formed, and hASCs showed elongated cell morphology. Even though the 3D bioprinted structures had higher cell density, the cell organization in 3D printed structures resembled the native human corneal stroma. Furthermore, high-magnification confocal images demonstrated that the hASCs had organized horizontally (Fig. 5K) as in the native corneal stroma (Fig. 5L). The thickness of the printed structures decreased slightly in culture: after 14 days, structures with thickness of 300 μm remained. When analyzing the cell organization in the printed structures from the top, a clear orientation of the cells was detected (Fig. 5M and N). The hASCs in the outermost layer were organized as an aligned cell layer (Fig. 5M), with almost perpendicular orientation to the layer directly underneath (Fig. 5N). 3D confocal images of the printed corneal stromal mimicking structures also confirmed the cellular organization into lamellae (Fig. 5O) with aligned cells (Fig. 5P). In addition, HE staining of the frozen cross-section of 3D bioprinted grafts after 7 days (Fig. 5Q) demonstrated the lamellar structure of the matrix and cells similar to the human corneal stroma (Fig. 5R).

The slight decrease in thickness of the bioprinted stromal constructs can be related to the loss of mass from the bioinks observed in the *in vitro* degradation data, which indicated that the bioink lost roughly half of its mass after 8 days in medium (Supplementary Fig. S4A). In the presence of 250 U/ml collagenase, the bioink degraded completely in only 4 h, but degradation was slower in more dilute collagenase concentrations (Supplementary Fig. S4B).

Finally, the matrix organization and composition of the 3D bioprinted structures were studied from the frozen cross-sections with IF staining and confocal imaging 7 days after printing. The 3D bioprinted structures showed positive labeling for collagen I and VWF, indicating that the surrounding matrix of the hASCs is mainly composed of human Col I and human plasma (Fig. 6A). High magnification confocal images from the frozen cross-sections showed horizontal and fibrillary alignment of these matrix proteins in the printed structures (Fig. 6B).

### 3.4. 3D bioprinted stromal structures show interaction and attachment to host tissue in corneal organ culture

The functionality of 3D bioprinted corneal stroma mimicking structures with hASCs was assessed using excised porcine corneas. Large stromal wounds were inflicted, where 3D bioprinted structures were implanted 4 days after printing. Matriderm® supportive sheets without hASCs were used as a control. In addition, the effect of acellular bioink alone was studied in the corneal organ culture. After 7 days in porcine corneal organ cultures, the 3D bioprinted structures showed interaction and attachment to the host tissue (Fig. 7A). Moreover, TRA-1-85 positive cells were detected in the host stromal tissue, indicating possible cell migration of hASCs from the printed structure (Fig. 7B). Strong adhesion of the printed tissue to the host corneal stroma was also revealed (Fig. 7C). The Matriderm® sheets alone and acellular bioink without hASCs showed only minor interaction with the host stroma (Fig. 7D–G). In contrast to the Matriderm-containing bioprinted constructs, the acellular bioink showed evidence of porcine epithelium overgrowth (Fig. 7G–I).

### 3.5. Laser-printed corneas from human stem cells resemble the structure of native corneal tissue

Finally, we tested a proof-of-concept to fabricate tissue-engineered cornea using both investigated human stem cell types. Multiple layers of hESC-LESCs were printed on top of the thicker 3D stromal structures containing hASCs. The corneal structure printed using the Matrigel™ absorption layer showed moderate transparency when printed on transparent PET substrate (Fig. 8A). However, printing on non-transparent Matriderm® supportive sheets was required to prevent the structure from shrinking during culture (Fig. 8B). After 3 days of co-culture, the hESC-LESCs showed a stratified, corneal progenitor marker p40 positive, layer on the surface of the laser-printed structures (Fig. 8C). The transparency of the constructs did not change during culture. The thickness and structure of the printed epithelium in tissue-engineered corneas resembled the structure of the uppermost part of the native human cornea used as a control.

## 4. Discussion

3D bioprinting is a promising method for efficient fabrication of the layered cornea-mimicking structures. To our best knowledge, only one previous study has assessed 3D bioprinting for corneal tissue engineering, by using pressure-assisted bioprinting of

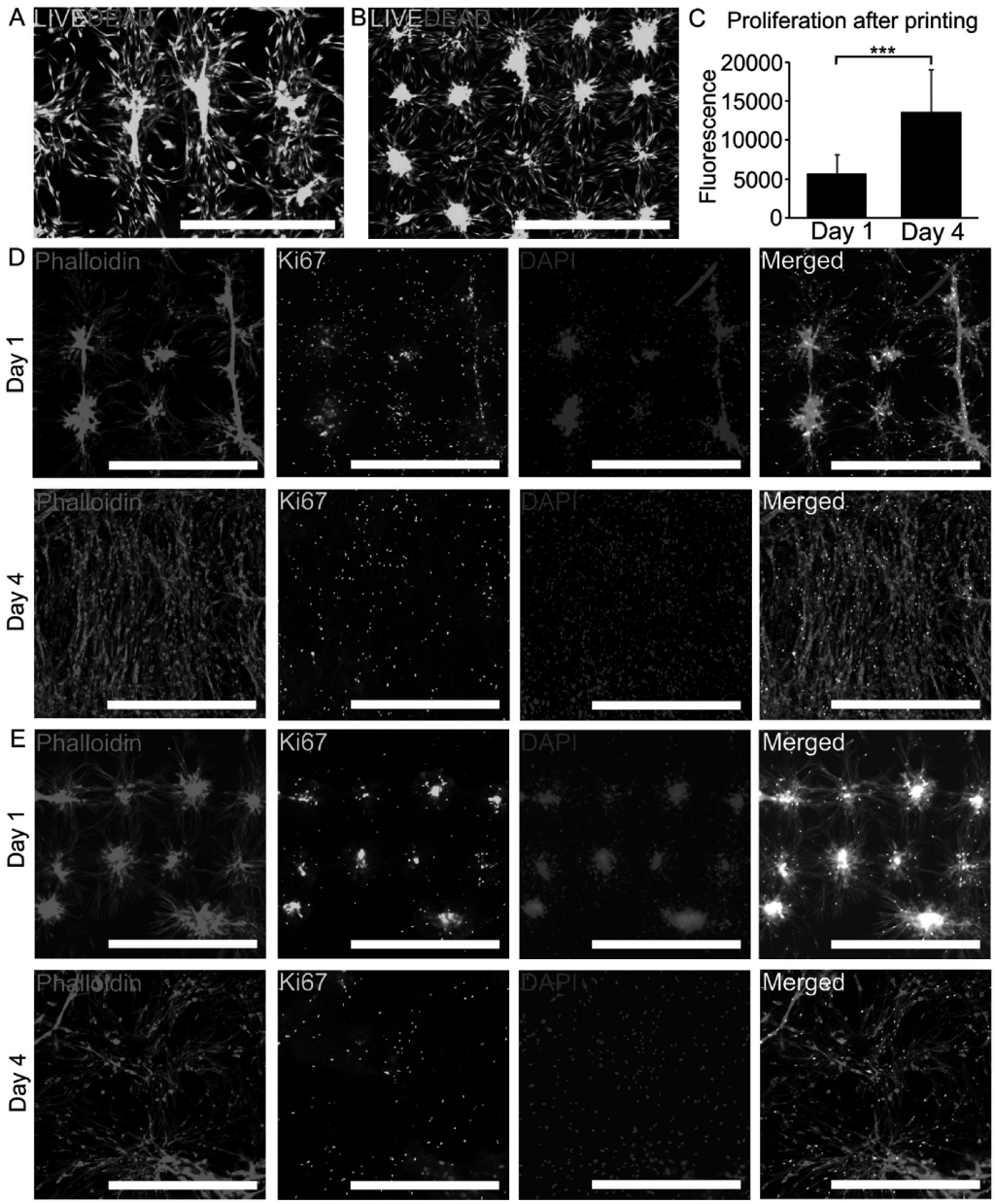


**Fig. 4.** Laser-assisted bioprinting of hASCs. Viability of hASCs printed as lines (**A**) and spots (**B**) after 1 day of printing. Live cells are shown in green and dead cells with red. Cell proliferation of hASCs printed in lines after one and four days of printing (**C**). Cell morphology and migration (phalloidin = red) and proliferating cells (Ki67 = green) of hASCs printed in lines (**D**) and spots (**E**) at one and four days. Scale bars 1 mm. The nuclei are visualized with DAPI (blue). (For interpretation of the references to colour in this figure legend, the reader is referred to the Web version of this article.)

immortalized human corneal epithelial cells in bioink containing rat-tail Col I, gelatin and alginate [14]. In contrast, our approach utilizes clinically relevant bioinks and two different human stem cell types with potential for corneal regeneration. In this study, we demonstrate the use of LaBP for producing native-like 3D cornea-mimicking structures using human stem cells and functional biomaterials. We developed novel bioinks from recombinant and human sourced materials for constructing 3D bioprinted corneal epithelium-mimicking structures from hESC-LESCs and stroma-mimicking structures from hASCs. Finally, we also tested a proof-of-concept to fabricate a tissue-engineered cornea using both stem cell types. To our knowledge, this is the first study to exploit

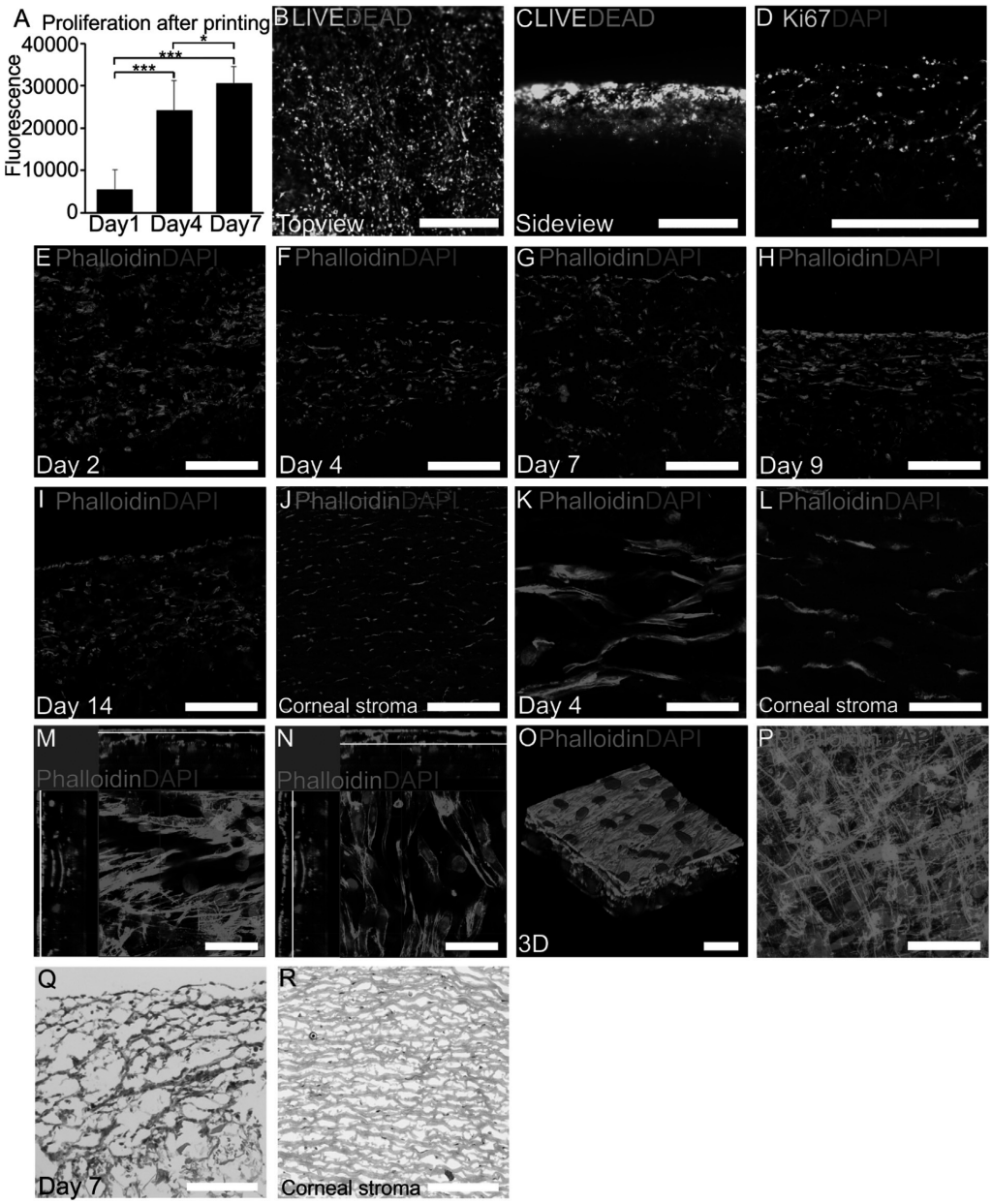


**Fig. 5.** Constructing 3D corneal stroma mimicking structures using hASCs and laser-assisted bioprinting. Cell proliferation of hASCs in 3D bioprinted structure 1, 4 and 7 days after printing (**A**) (***$p < 0.001$ and *$p < 0.01$). Top-view (**B**) and cross-section (**C**) of the live/dead-staining demonstrating the cell viability of hASCs in 3D the following day after printing (live cells = green, dead cells = red). Proliferating cells (Ki67 = green) visualized with immunofluorescence staining from cryosection after four days of printing (**D**). Scale bars 500 μm (**B-D**). Human ASC distribution, morphology and orientation in 3D bioprinted structures visualized with phalloidin (red) from cryocross-Sections 2 days (**E**), 4 days (**F**), 7 days (**G**), 9 days (**H**) and 14 days (**I**) after printing. The human corneal stroma is shown as a control (**J**). Scale bars 200 μm (**E-J**). High-magnification confocal images of the cell orientation in 3D bioprinted stroma after four days since printing (**K**) and in human corneal stroma (**L**). Vertical confocal sections of hASC in 3D bioprinted layered structure: cell orientation in the 1st layer (**M**) and 2nd layer (**N**). 3D rotated confocal image (**O**) and confocal maximum intensity projection image (**P**) of the top-layers in the 3D bioprinted stroma 7 days after printing. Scale bars 50 μm (**K-P**). Hematoxylin and eosin staining of 3D bioprinted stroma at 7 days (**Q**) and central human corneal stroma (**R**). Scale bars 200 μm (**Q-R**). (DAPI = blue). (For interpretation of the references to colour in this figure legend, the reader is referred to the Web version of this article.)

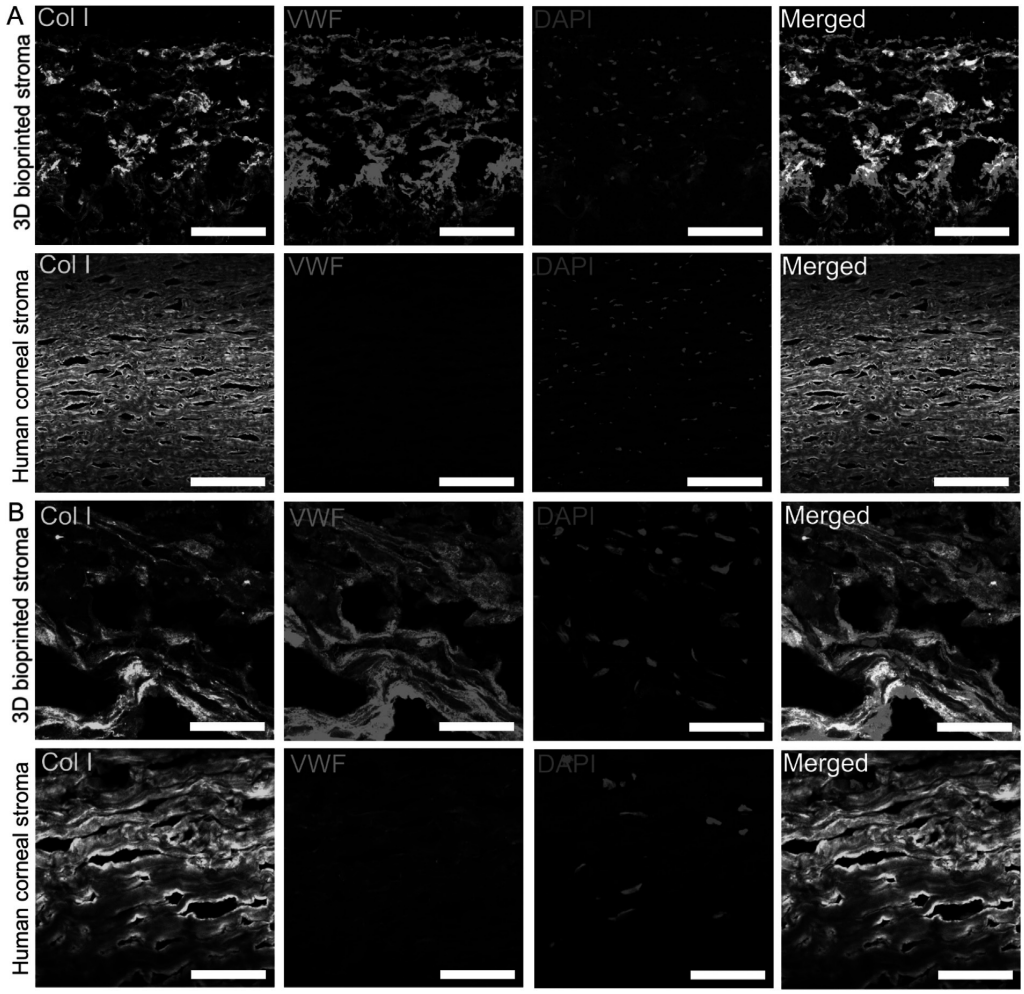


**Fig. 6.** Matrix composition of 3D bioprinted stroma 7 days after printing. Immunofluorescence staining of cryocross-sections against human collagen I (Col I, green) and Von Willebrandt factor (VWF, red) with low (**A**) and high (**B**) magnification confocal images. Human corneal stroma was used as a control. Scale bars 200 μm. (For interpretation of the references to colour in this figure legend, the reader is referred to the Web version of this article.)

LaBP for corneal tissue engineering applications.

LaBP with LIFT offers advantages over many other 3D bioprinting technologies, such as printing high-resolution 3D structures from viscous bioinks [41,42]. With LaBP, we can also achieve precise spatial organization of cells and use different cell types in the same engineered construct. Previous studies have shown successful bioprinting of both human induced pluripotent stem cells (hiPSC) and hESCs using extrusion-based bioprinting platforms [43–45]. These studies have shown that undifferentiated hPSCs can be bioprinted without adversely affecting their biological functions such as viability, proliferation, and pluripotency [44,45]. The results presented in this study are also among the first to describe successful 3D bioprinting of hPSC-derived cells, as only one previous work has presented printing of hPSC-derived hepatocyte-like cells using a valve-based bioprinting process [44].

In this study, we introduced novel bioinks for 3D bioprinting that show biocompatibility with human stem cells. For the basis of these bioinks, we chose natural components of the LESC basement membrane and corneal extracellular matrix: human recombinant laminin for printing hESC-LESCs, and human Col I for hASCs. Neither recombinant laminin nor human collagen have been previously used as major components of bioinks in 3D bioprinting. However, recombinant laminin-511 (LN511) and LN521 in the form of protein coatings have been shown to enhance the *in vitro* adhesion, migration, and proliferation of human limbal epithelial cells [46], and LN521 is used in combination with Col IV for differentiation of hESC-LESCs [20]. Col I is the major structural protein of the corneal stroma, where it exists as highly arranged fibrils [47]. Due to its major structural role in the native human corneal stroma, collagen has been vigorously investigated for corneal bioengineering [31]. Recently, human Col I and medical grade Col I bioengineered matrices have shown some promise in corneal tissue engineering applications [48,49]. In addition, porcine Col I has been investigated for use in corneal implants [19,50–52] In general, Col I

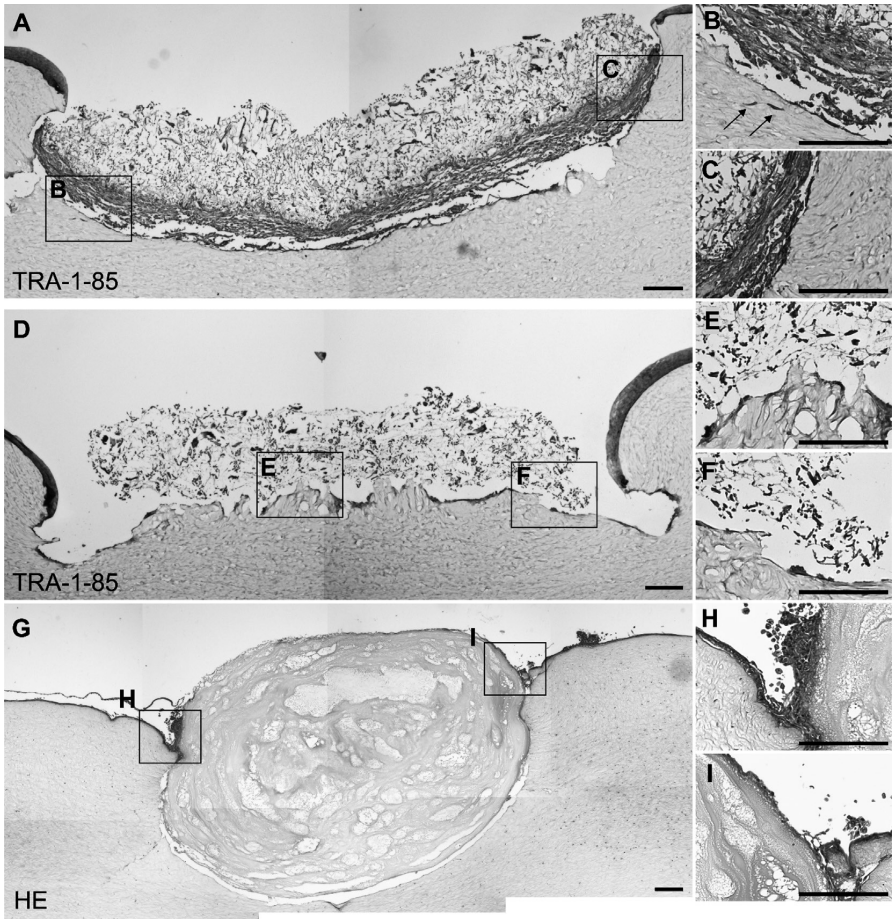


**Fig. 7.** 3D bioprinted stroma in porcine corneal organ culture model after 7 days (**A-C**). Blank Matriderm® sheets (**D-F**) and acellular bioink were used as control (**G-I**). Immunohistochemical staining of human cell marker TRA-1-85 (brown) demonstrated successful hASC integration into the porcine corneal stroma from the 3D bioprinted stromal mimicking structures, whereas for Matriderm® and acellular bioink only minor interaction with the stroma were observed. HE staining of the acellular bioink in organ culture showed evidence of overgrowth of the porcine epithelium. Scale bars 200 μm. (For interpretation of the references to colour in this figure legend, the reader is referred to the Web version of this article.)

from animal sources, such as rat tail and bovine, have been extensively used in 3D bioprinting in various applications (reviewed in Refs. [35,53–55]). However, it has been previously demonstrated that Col I from different sources show different ultrastructure and biomaterial properties and that the human Col I requires special handling upon biomaterial fabrication compared to bovine Col I [56]. Thus, results and fabrication parameters gained with animal-derived Col I in 3D bioprinting applications are not directly transferrable to use with the more clinically relevant human Col I. Here, we demonstrated the printability and biocompatibility of both LN521 and Col I based bioinks in LaBP.

Usually, bioinks require rapid crosslinking after 3D bioprinting to develop self-supporting structures that maintain their desired shape upon fabrication and in further culture [57]. In this study, we produced stable 3D cornea-mimicking structures without further crosslinking. For printing of hESC-LESCs, we utilized high viscosity bioinks achieved through mixing of HA and cell culture medium to LN521. The structures maintained their shape due to high viscosity caused by the presence of HA as well as high cell density. Despite the lack of further crosslinking, the printed hESC-LESCs formed 3D epithelium-mimicking tissue, which maintained its structure in culture. Sufficient stability for 3D bioprinted stromal structure from Col I bioink and hASCs was established with human blood plasma and thrombin coagulation during printing. Previously, the fibrin-thrombin coagulation reaction has been utilized for production of biomaterials for primary LESC culture and transplantation [58], and stabilization of 3D bioprinted skin [55,59]. In addition, gelatin/fibrin composite scaffolds stabilized in thrombin solution have been shown to sustain 14 days of culture, although both gelatin and fibrin are bioresorbable and degrade enzymatically [60]. Notably, the printed stromal mimicking structures showed extensive shrinkage and lost their original form after a few days of culture, unless printed on a Matriderm® supportive sheet. Even with the Matriderm® supportive sheets, the thickness of the printed structures decreased in culture: after 14 days, structures with thickness of 300 μm remained suggesting that further crosslinking of the Col I

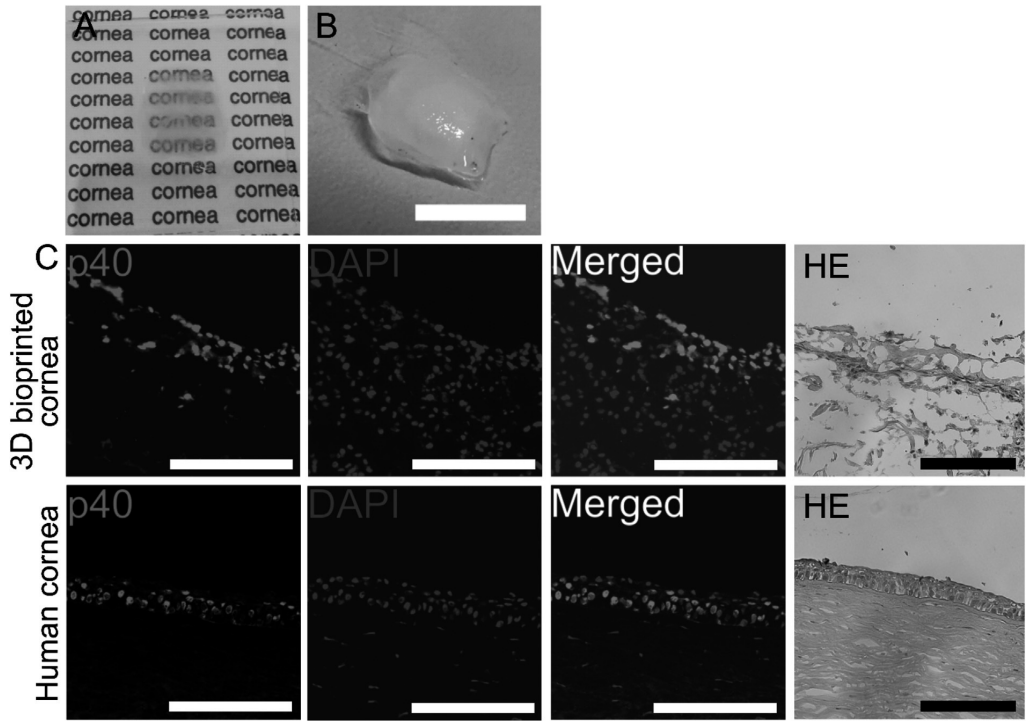


**Fig. 8.** 3D cornea from hESC-LESCs and hASCs fabricated using laser-assisted bioprinting. The bioprinted 3D cornea fabricated on PET substrate (**A**) shows moderate transparency, however printing on non-transparent Matriderm® substrate (**B**) was required to avoid shrinkage of the structure during culture. **C** shows comparison between the 3D bioprinted corneal tissue and the native human cornea. Immunofluorescence staining of cryocross-sections show multilayered structure of corneal progenitor marker p40 (red) positive hESC-LESCs on top of 3D scaffold after two days since printing. Hematoxylin and eosin (HE)-staining shows the structure of the bioprinted tissue. Cryosections of human cornea were used as a control. Scale bars in **B** 10 mm and in **C** 200 μm. (For interpretation of the references to colour in this figure legend, the reader is referred to the Web version of this article.)

bioink after LaBP might be needed to gain sufficient stability and mechanical stiffness. In order for the crosslinking not to obstruct the LaBP, the crosslinking should be induced after suspending cells. Photo-crosslinking of the printed corneal construct is one option to increase the mechanical stiffness of the printed grafts. However, it should be noted that these crosslinking methods require the addition of a photo-initiators or chemical crosslinkers that could be cytotoxic and may reduce cell survival in the 3D printed grafts [61,62].

The structures fabricated by LaBP showed high resolution after printing as well as functional cell maturation during culture. Initial printability and biocompatibility studies of human Col I containing bioink for printing hASC revealed cell organization in clearly visible 2D patterns with good cell viability. By day 4 in culture, the initial printed patterns were not visible anymore, and cells showed high proliferation marker expression, elongated cell morphology with some degree of alignment. In the bioprinted epithelium-mimicking structures, hESC-LESCs also maintained high viability and proliferation after printing, and showed typical polygonal epithelial cell morphology, and high expression of corneal progenitor markers p63α and p40. Importantly, the printed hESC-LESCs maintained their bioprinted 3D epithelial tissue structure with 3–4 cell layers and showed notable maturation towards corneal epithelium with apical expression of CK3 and basal expression of p63α and p40 within 12 days of culture. However, further studies are required to fully address the functionality of the hESC-LESC formed epithelium after 3D bioprinting.

Formation of the corneal stromal mimicking structures was achieved by bioprinting alternating layers of hASC-containing bioink and acellular bioink. Human ASCs had organized uniformly throughout the 3D structures and showed high proliferation and viability after printing. Although the 3D bioprinted structures had higher cell density than the native corneal stroma, the achieved cell organization in 3D printed structures was similar. In future studies, achieving more native like cell densities of corneal stroma could be realized through optimization of bioprinting parameters such as layer organization and thickness. The high-magnification confocal images revealed that the hASCs had organized in layers with alternating alignment, as in the native corneal stroma. Furthermore, these structures showed positive labeling for collagen I and VWF, indicating horizontal and fibrillar alignment of human Col I and plasma in the printed structures. Interestingly, these fibers demonstrated some organization and arrangement in the 3D environment, indicating that 3D bioprinting with LaBP is a promising fabrication method for corneal stromal mimicking structures. Previously, lamellar collagen organization has been achieved by culturing primary corneal stromal cells on aligned templates, but these methods are time-consuming and resulting structures limited in thickness [8,10,63]. As we did not crosslink the Col I matrix during fabrication, the fiber-like Col I seen after printing was likely produced or remodeled by the printed hASCs in the 3D structure. This could indicate functionality of these cells, as one of the key functions of corneal stromal cells is to produce and modify collagen fibers to maintain the fine stromal architecture [31].

However, further studies are needed to fully address the functionality of the hASCs, their collagen production and ECM remodeling with respect to the printed layer thickness in the 3D structure.

To assess the functionality of the 3D bioprinted stromal mimicking structures with hASC, we implanted them into organ-cultured porcine corneas. 7 days after implantation, the 3D bioprinted stromal structures showed interaction and attachment to the host tissue. Moreover, TRA-1-85 positive human cells were detected in the host stromal tissue, indicating potential cell migration of hASCs from the printed structure. In contrast, the Matridem® sheet alone showed only modest interaction with the stroma. Acellular bioink, on the other hand, showed evidence of overgrowth of host epithelium indicating good biocompatibility of the bioink. Importantly, successful implantation to the corneal organ culture model demonstrated good mechanical robustness of the 3D bioprinted structures, as they could withstand shipping from Germany to Finland, as well as mechanical handling during the implantation operation. Although additional means of fixing the implants in place were not used, the implanted hASCs showed attachment to the stromal wound bed. However, further development is required to achieve better surgically feasible structures, focusing on finding suitable transfer substrates instead of the Matriderm® sheets.

In the final stage, we tested a proof-of-concept to fabricate tissue-engineered cornea using both investigated human stem cell types. We bioprinted layers of hESC-LESCs on top of the thicker 3D stromal structures containing hASCs, and the resulting structures resembled the uppermost part of the native cornea. After 3 days of culture, the hESC-LESCs retained a corneal progenitor marker p40 positive layered epithelium, with four to six cell layers. However, the co-culture conditions of these two cell types need to be developed further [64,65] to enable longer culture periods *in vitro*, while maintaining the corneal regenerative properties of both cell types. For advanced *in vitro* functionality studies, such as barrier properties and mechanical studies of the bioprinted corneal structures, controlled differentiation and maturation towards corneal stroma and epithelium in different layers of the printed constructs are required. Importantly, new substrates for the bioprinted corneal structures are needed for optimizing both transparency and stability of the structures for proper realization of clinically feasible bioprinted corneal grafts.

## 5. Conclusions

With this study, we demonstrate for the first time the feasibility of 3D LaBP for corneal applications using human stem cells, and show successful fabrication of layered 3D bioprinted tissues mimicking the structure of native corneal tissues. In addition, we introduce novel human protein based bioinks for 3D bioprinting that show biocompatibility with human stem cells. The fabricated 3D corneal structures also demonstrated good mechanical properties without additional bioink crosslinking after LaBP. The *in vitro* and *in vivo* functionality of the 3D structures requires further studies but feasibility of the approach shows promise in porcine corneal organ culture.

## Roles for all authors

**AS**: Conceived and designed the experiments, performed the experiments, analyzed and interpreted the data, wrote the manuscript; **LKoc**: Conceived, designed, and performed experiments, contributed to the writing of the manuscript and its critical revision and final approval; **LKoi**: Conceived and designed the experiments, performed the experiments, analyzed and interpreted the data, wrote the manuscript; **AD:** Contributed regents/materials/analysis tools, performed experiments, participated in the critical revision of the manuscript; **SM**: Contributed regents/materials/analysis tools, participated in the critical revision of the manuscript; **BC**: Organized and supervised laser printing experiments, participated in the critical revision of the manuscript and final approval of the article; **HS**: Acquired the funding, conceived and designed the experiments, interpreted the data; participated in the critical revision of the manuscript and final approval of the article.

## Data availability statement

The raw/processed data required to reproduce these findings cannot be shared at this time due to technical or time limitations but will be available to download from http://www.biomeditech.fi/research/eye-regeneration-group/

## Acknowledgements

This study was financially supported by the Finnish Funding Agency for Innovation (Tekes), the Competitive State Research Financing of the Expert Responsibility area of Tampere University Hospital, Finland and the Academy of Finland. The authors further acknowledge financial support from Deutsche Forschungsgemeinschaft (DFG), the Cluster of Excellence REBIRTH, and Biofabrication for NIFE project (Land Niedersachsen/Volkswagenstiftung). The authors alone are responsible for preparing the manuscript: the funders had no role in experiment planning, data collection and analysis as well as decision to publish. The authors also wish to thank Outi Melin, Hanna Pekkanen, Sari Kalliokoski, Anna-Maija Honkala and Emma Vikstedt for technical assistance and Pantec Engineering AG, (Ruggell, Liechtenstein) for supporting us with the Er:YAG Laser.

## Appendix A. Supplementary data

Supplementary data related to this article can be found at https://doi.org/10.1016/j.biomaterials.2018.04.034.

## References

[1] M. Haagdorens, S.I. Van Acker, V. Van Gerwen, S.N. Dhubhghaill, C. Koppen, M. Tassignon, et al., Limbal stem cell deficiency, current treatment options and emerging therapies, In Vivo 11 (2015) 14.
[2] Y. Oie, K. Nishida, Corneal regenerative medicine, Regen. Ther. 5 (2016) 40–45.
[3] G. Pellegrini, P. Rama, S. Matuska, A. Lambiase, S. Bonini, A. Pocobelli, et al., Biological parameters determining the clinical outcome of autologous cultures of limbal stem cells, Regen. Med. 8 (2013) 553–567.
[4] P. Rama, S. Matuska, G. Paganoni, A. Spinelli, M. De Luca, G. Pellegrini, Limbal stem-cell therapy and long-term corneal regeneration, N. Engl. J. Med. 363 (2010) 147–155.
[5] G. Pellegrini, A. Lambiase, C. Macaluso, A. Pocobelli, S. Deng, G.M. Cavallini, et al., From discovery to approval of an advanced therapy medicinal product-containing stem cells, in the EU, Regen. Med. 11 (2016) 407–420.
[6] E. Yoeruek, T. Bayyoud, C. Maurus, J. Hofmann, M.S. Spitzer, K. Bartz-Schmidt, et al., Decellularization of porcine corneas and repopulation with human corneal cells for tissue-engineered xenografts, Acta Ophthalmol. 90 (2012).
[7] M.A. Shafiq, R.A. Gemeinhart, B.Y. Yue, A.R. Djalilian, Decellularized human cornea for reconstructing the corneal epithelium and anterior stroma, Tissue Eng. C Meth. 18 (2011) 340–348.
[8] R.M. Gouveia, V. Castelletto, I.W. Hamley, C.J. Connon, New self-assembling multifunctional templates for the biofabrication and controlled self-release of cultured tissue, Tissue Eng. A 21 (2015) 1772–1784.
[9] A.P. Lynch, M. Ahearne, Strategies for developing decellularized corneal scaffolds, Exp. Eye Res. 108 (2013) 42–47.
[10] R.M. Gouveia, E. González-Andrades, J.C. Cardona, C. González-Gallardo, A.M. Ionescu, I. Garzon, et al., Controlling the 3D architecture of Self-Lifting Auto-generated Tissue Equivalents (SLATEs) for optimized corneal graft composition and stability, Biomaterials 121 (2017) 205–219.
[11] C.E. Ghezzi, J. Rnjak-Kovacina, D.L. Kaplan, Corneal tissue engineering: recent advances and future perspectives, Tissue Eng. B Rev. 21 (2015) 278–287.
[12] N. Hong, G. Yang, J. Lee, G. Kim, 3D bioprinting and its in vivo applications,

J. Biomed. Mater. Res. Part B Appl. Biomater. 106B (2018) 444–459.
[13] C.S. Ong, P. Yesantharao, C.Y. Huang, G. Mattson, J. Boktor, T. Fukunishi, et al., 3D bioprinting using stem cells, Pediatr. Res. 83 (2018) 223–231, https://doi.org/10.1038/pr.2017.252.
[14] Z. Wu, X. Su, Y. Xu, B. Kong, W. Sun, S. Mi, Bioprinting three-dimensional cell-laden tissue constructs with controllable degradation, Sci. Rep. 6 (2016) 24474.
[15] L. Koch, S. Kuhn, H. Sorg, M. Gruene, S. Schlie, R. Gaebel, et al., Laser printing of skin cells and human stem cells, Tissue Eng. C Meth. 16 (2009) 847–854.
[16] Y. Lin, Y. Huang, D.B. Chrisey, Droplet formation in matrix-assisted pulsed-laser evaporation direct writing of glycerol-water solution, J. Appl. Phys. 105 (2009), 093111.
[17] H. Jian, M. Wang, S. Wang, A. Wang, S. Bai, 3D bioprinting for cell culture and tissue fabrication, Bio. Des. Manuf. (2018) 1–17.
[18] A. Mikhailova, T. Ilmarinen, H. Uusitalo, H. Skottman, Small-molecule induction promotes corneal epithelial cell differentiation from human induced pluripotent stem cells, Stem Cell Rep. 2 (2014) 219–231.
[19] A. Mikhailova, A. Jylha, J. Rieck, J. Nattinen, T. Ilmarinen, Z. Vereb, et al., Comparative proteomics reveals human pluripotent stem cell-derived limbal epithelial stem cells are similar to native ocular surface epithelial cells, Sci. Rep. 5 (2015) 14684.
[20] H. Hongisto, T. Ilmarinen, M. Vattulainen, A. Mikhailova, H. Skottman, Xeno- and feeder-free differentiation of human pluripotent stem cells to two distinct ocular epithelial cell types using simple modifications of one method, Stem Cell Res. Ther. 8 (2017) 291.
[21] Y. Du, D.S. Roh, M.L. Funderburgh, M.M. Mann, K.G. Marra, J.P. Rubin, et al., Adipose-derived stem cells differentiate to keratocytes in vitro, Mol. Vis. 16 (2010) 2680–2689.
[22] S. Zhang, L. Espandar, K.M. Imhof, B.A. Bunnell, Differentiation of human adipose-derived stem cells along the keratocyte lineage, J. Clin. Exp. Ophthalmol. 4 (2013) 11435.
[23] M. Ahearne, J. Lysaght, A.P. Lynch, Combined influence of basal media and fibroblast growth factor on the expansion and differentiation capabilities of adipose-derived stem cells, Cell Regen. 3 (2014), 13–9769-3-13. eCollection 2014.
[24] F. Arnalich-Montiel, S. Pastor, A. Blazquez-Martinez, J. Fernandez-Delgado, M. Nistal, J.L. Alio del Barrio, et al., Adipose-derived stem cells are a source for cell therapy of the corneal stroma, Stem Cell. 26 (2008) 570–579.
[25] J. Alio del Barrio, M. Chiesa, N. Garagorri, N. Garcia-Urquia, J. Fernandez-Delgado, L. Bataille, et al., Acellular human corneal matrix sheets seeded with human adipose-derived mesenchymal stem cells integrate functionally in an experimental animal model, Exp. Eye Res. 132 (2015) 91–100.
[26] J.L. Alio Del Barrio, M. El Zarif, M.P. de Miguel, A. Azaar, N. Makdissy, W. Harb, et al., Cellular therapy with human autologous adipose-derived adult stem cells for advanced Keratoconus, Cornea 36 (2017) 952–960.
[27] M. Patrikoski, J. Sivula, H. Huhtala, M. Helminen, F. Salo, B. Mannerstrom, et al., Different culture conditions modulate the immunological properties of adipose stem cells, Stem Cells Transl. Med. 3 (2014) 1220–1230.
[28] L. Wang, L. Hu, X. Zhou, Z. Xiong, C. Zhang, H.M. Shehada, et al., Exosomes secreted by human adipose mesenchymal stem cells promote scarless cutaneous repair by regulating extracellular matrix remodelling, Sci. Rep. 7 (2017) 13321.
[29] J. Deng, Y. Shi, Z. Gao, W. Zhang, X. Wu, W. Cao, et al., Inhibition of pathological phenotype of hypertrophic scar fibroblasts via coculture with adipose-derived stem cells, Tissue Eng. A 24 (2018) 382–393.
[30] T. Dietrich-Ntoukas, C. Hofmann-Rummelt, F.E. Kruse, U. Schlotzer-Schrehardt, Comparative analysis of the basement membrane composition of the human limbus epithelium and amniotic membrane epithelium, Cornea 31 (2012) 564–569.
[31] S. Chen, M.J. Mienaltowski, D.E. Birk, Regulation of corneal stroma extracellular matrix assembly, Exp. Eye Res. 133 (2015) 69–80.
[32] H. Skottman, Derivation and characterization of three new human embryonic stem cell lines in Finland, In Vitro Cell. Dev. Biol. Anim. 46 (2010) 206–209.
[33] J.M. Gimble, F. Guilak, Adipose-derived adult stem cells: isolation, characterization, and differentiation potential, Cytotherapy 5 (2003) 362–369.
[34] B. Lindroos, S. Boucher, L. Chase, H. Kuokkanen, H. Huhtala, R. Haataja, et al., Serum-free, xeno-free culture media maintain the proliferation rate and multipotentiality of adipose stem cells in vitro, Cytotherapy 11 (2009) 958–972.
[35] S. Michael, H. Sorg, C. Peck, L. Koch, A. Deiwick, B. Chichkov, et al., Tissue engineered skin substitutes created by laser-assisted bioprinting form skin-like structures in the dorsal skin fold chamber in mice, PLoS One 8 (2013), e57741.
[36] A.E. Sorkio, E.P. Vuorimaa-Laukkanen, H.M. Hakola, H. Liang, T.A. Ujula, J.J. Valle-Delgado, et al., Biomimetic collagen I and IV double layer Langmuir–Schaefer films as microenvironment for human pluripotent stem cell derived retinal pigment epithelial cells, Biomaterials 51 (2015) 257–269.
[37] L. Koivusalo, J. Karvinen, E. Sorsa, I. Jönkkäri, J. Väliaho, P. Kallio, et al., Hydrazone crosslinked hyaluronan-based hydrogels for therapeutic delivery of adipose stem cells to treat corneal defects, Mater. Sci. Eng. C 85 (1 April 2018) 68–78.
[38] C.S. Kamma-Lorger, C. Boote, S. Hayes, J. Albon, M.E. Boulton, K.M. Meek, Collagen ultrastructural changes during stromal wound healing in organ cultured bovine corneas, Exp. Eye Res. 88 (2009) 953–959.
[39] S. Mi, E.P. Dooley, J. Albon, M.E. Boulton, K.M. Meek, C.S. Kamma-Lorger, Adhesion of laser in situ keratomileusis-like flaps in the cornea: effects of crosslinking, stromal fibroblasts, and cytokine treatment, J. Cataract Refract. Surg. 37 (2011) 166–172.
[40] L. Koivusalo, J. Karvinen, E. Sorsa, I. Jönkkäri, J. Väliaho, P. Kallio, et al., Hydrazone crosslinked hyaluronan-based hydrogels for therapeutic delivery of adipose stem cells to treat corneal defects, Mater. Sci. Eng. C 85 (1 April 2018) 68–78.
[41] W. Zhu, X. Ma, M. Gou, D. Mei, K. Zhang, S. Chen, 3D printing of functional biomaterials for tissue engineering, Curr. Opin. Biotechnol. 40 (2016) 103–112.
[42] S.V. Murphy, A. Atala, 3D bioprinting of tissues and organs, Nat. Biotechnol. 32 (2014) 773–785.
[43] A. Faulkner-Jones, S. Greenhough, J.A. King, J. Gardner, A. Courtney, W. Shu, Development of a valve-based cell printer for the formation of human embryonic stem cell spheroid aggregates, Biofabrication 5 (2013), 015013.
[44] A. Faulkner-Jones, C. Fyfe, D. Cornelissen, J. Gardner, J. King, A. Courtney, et al., Bioprinting of human pluripotent stem cells and their directed differentiation into hepatocyte-like cells for the generation of mini-livers in 3D, Biofabrication 7 (2015), 044102.
[45] Q. Gu, E. Tomaskovic-Crook, G.G. Wallace, J.M. Crook, Bioprinting: 3D bioprinting human induced pluripotent stem cell constructs for in situ cell proliferation and successive multilineage differentiation (Adv. Healthcare mater. 17/2017), Adv. Healthc. Mater. 6 (2017).
[46] N. Polisetti, L. Sorokin, N. Okumura, N. Koizumi, S. Kinoshita, F.E. Kruse, et al., Laminin-511 and-521-based matrices for efficient ex vivo-expansion of human limbal epithelial progenitor cells, Sci. Rep. 7 (2017) 5152.
[47] K.M. Meek, C. Knupp, Corneal structure and transparency, Prog. Retin. Eye Res. 49 (2015) 1–16.
[48] N. Vázquez, M. Chacón, C.A. Rodríguez-Barrientos, J. Merayo-Lloves, M. Naveiras, B. Baamonde, et al., Human bone derived collagen for the development of an artificial corneal endothelial graft. In vivo results in a rabbit model, PLoS One 11 (2016), e0167578.
[49] W. Liu, K. Merrett, M. Griffith, P. Fagerholm, S. Dravida, B. Heyne, et al., Recombinant human collagen for tissue engineered corneal substitutes, Biomaterials 29 (2008) 1147–1158.
[50] M. Koulikovska, M. Rafat, G. Petrovski, Z. Veréb, S. Akhtar, P. Fagerholm, et al., Enhanced regeneration of corneal tissue via a bioengineered collagen construct implanted by a nondisruptive surgical technique, Tissue Eng. A 21 (2015) 1116–1130.
[51] M. Rafat, F. Li, P. Fagerholm, N.S. Lagali, M.A. Watsky, R. Munger, et al., PEG-stabilized carbodiimide crosslinked collagen–chitosan hydrogels for corneal tissue engineering, Biomaterials 29 (2008) 3960–3972.
[52] M. Rafat, M. Xeroudaki, M. Koulikovska, P. Sherrell, F. Groth, P. Fagerholm, et al., Composite core-and-skirt collagen hydrogels with differential degradation for corneal therapeutic applications, Biomaterials 83 (2016) 142–155.
[53] M.K. Włodarczyk-Biegun, A. del Campo, 3D bioprinting of structural proteins, Biomaterials 134 (2017) 180–201.
[54] M. Yeo, J. Lee, W. Chun, G.H. Kim, An innovative collagen-based cell-printing method for obtaining human adipose stem cell-laden structures consisting of core–sheath structures for tissue engineering, Biomacromolecules 17 (2016) 1365–1375.
[55] L. Koch, A. Deiwick, S. Schlie, S. Michael, M. Gruene, V. Coger, et al., Skin tissue generation by laser cell printing, Biotechnol. Bioeng. 109 (2012) 1855–1863.
[56] S. Majumdar, Q. Guo, M. Garza-Madrid, X. Calderon-Colon, D. Duan, P. Carbajal, et al., Influence of collagen source on fibrillar architecture and properties of vitrified collagen membranes, J. Biomed. Mater. Res. B Appl. Biomater. 104 (2016) 300–307.
[57] S. Ji, M. Guvendiren, Recent advances in bioink design for 3D bioprinting of tissues and organs, Front. Bioeng. Biotechnol. 5 (2017).
[58] G. Milazzo, D. Ardigo, M. Toschi, S. Matuska, P. Rama, M. De Luca, et al., Holoclar: first of its kind in more ways than one, Cell Gene Ther. Insights 2 (2016) 183–197.
[59] N. Cubo, M. Garcia, J.F. del Cañizo, D. Velasco, J.L. Jorcano, 3D bioprinting of functional human skin: production and in vivo analysis, Biofabrication 9 (2016), 015006.
[60] W. Xu, X. Wang, Y. Yan, W. Zheng, Z. Xiong, F. Lin, et al., Rapid prototyping three-dimensional cell/gelatin/fibrinogen constructs for medical regeneration, J. Bioact. Compat. Polym. 22 (2007) 363–377.
[61] C.G. Williams, A.N. Malik, T.K. Kim, P.N. Manson, J.H. Elisseeff, Variable cytocompatibility of six cell lines with photoinitiators used for polymerizing hydrogels and cell encapsulation, Biomaterials 26 (2005) 1211–1218.
[62] H. Liang, W. Chang, H. Liang, M. Lee, H. Sung, Crosslinking structures of gelatin hydrogels crosslinked with genipin or a water-soluble carbodiimide, J. Appl. Polym. Sci. 91 (2004) 4017–4026.
[63] D. Karamichos, M.L. Funderburgh, A.E. Hutcheon, J.D. Zieske, Y. Du, J. Wu, et al., A role for topographic cues in the organization of collagenous matrix by corneal fibroblasts and stem cells, PLoS One 9 (2014), e86260.
[64] E.A. Gosselin, T. Torregrosa, C.E. Ghezzi, A.C. Mendelsohn, R. Gomes, J.L. Funderburgh, et al., Multi-layered silk film co-culture system for human corneal epithelial and stromal stem cells, J. Tissue Eng. Regen. Med. 12 (1) (January 2018) 285–295.
[65] A.K. Kureshi, M. Dziasko, J.L. Funderburgh, J.T. Daniels, Human corneal stromal stem cells support limbal epithelial cells cultured on RAFT tissue equivalents, Sci. Rep. 5 (2015) 16186.